THE ROLE OF COBALT SPECIES IN FISCHER TROPSCH SYNTHESIS: EFFECT OF SUPPORT CHARACTERISTICS AND REDUCING CONDITIONS

by

NOTHANDO CYNTHIA SHIBA

submitted in accordance with the requirements for
the degree of

DOCTOR OF PHILOSOPHY

in the subject

of ENGINEERING

at the

UNIVERSITY OF SOUTH AFRICA

SUPERVISOR: Yali Yao

CO-SUPERVISOR: Diane Hildebrandt, Liu Xinying

(Submitted 20 July 2021).

Declaration

Name: Nothando Shiba

Student number: 58563784

Degree: Doctor of Philosophy in Engineering

Exact wording of the title of the thesis as appearing on the electronic copy submitted for examination:

THE ROLE OF COBALT SPECIES IN FISCHER TROPSCH SYNTHESIS: EFFECT OF SUPPORT CHARACTERISTICS AND REDUCING CONDITIONS.

I declare that the above thesis is my own work and that all the sources that I have used or quoted have been indicated and acknowledged by means of complete references.

I further declare that I submitted the thesis to originality checking software and that it falls within the accepted requirements for originality.

I further declare that I have not previously submitted this work, or part of it, for examination at Unisa for another qualification or at any other higher education institution.

_____ _____20/07/2021_____

SIGNATURE DATE

I would like to express my sincere gratitude to the following individuals and institutions who have played a major role in my PhD process and in making this possible:

- ✓ My supervisors, Dr Yali Yao, Professor Diane Hildebrandt and Professor Liu Xinying for their continued support, guidance, and inspiration. It has been quite an honour and a privilege to have worked with these great-minded people. They taught me how to be a great leader, researcher, article writer and to be resilient on every aspect of my life.
- ✓ Our IDEAS research group members, a special thanks goes to the laboratory technicians Humphrey Mbatha, Katu Ramutsindela, and Mandla Mngomezulu for their technical support in the laboratory, daily running's and troubleshooting and for creating a friendly and welcoming working environment for us. Furthermore, I would like to send a special thanks to my laboratory-mates and colleagues George Okoye-Chine and Olive Mbuya for their continued support, assistance, and friendship.
- ✓ The University of South Africa and the South Africa National Research Foundation (NRF UID 95445 and 117793) for the financial support.

Finally, I would like to dedicate this work to my family (my parents, my siblings, my husband and the twins) who have been a pillar of strength, who always supported my work and showed great sympathy and encouragement during hard times.

Abstract

The industry's great interest is to intensify the cobalt-based Fischer-Tropsch synthesis (FTS) process by increasing the per-pass conversion and the production of long chain hydrocarbons. To achieve this goal, it is imperative to understand the effect of pre-treatment conditions on the resulting cobalt species, their reactivity and selectivity for FTS. Herein, we focused on the surface phase transformations during the reduction of cobalt catalysts supported on SiO_2, TiO_2 and Al_2O_3 and their influence on the catalytic performance during FTS by either varying the reduction temperature or reduction agent (H_2/CO/syngas). We conducted in-situ PXRD and additional TPR measurements during H_2 activation, using special temperature programs which proved that the abundances of the cobalt species i.e., Co_3O_4, CoO and Co^0 could be controlled by the reduction atmosphere. A multiphase Co-CoO/SiO_2 was obtained when the catalyst was reduced in H_2 at a lower temperature (250 ˚C). This Co-CoO multiphase demonstrated a high activity for both Fischer-Tropsch (FT) and water gas shift (WGS) reactions. From the experimental data, we postulated that the Co-CoO interface dispersed on the SiO_2 support assisted the CO dissociation and the hydrogenation of the R-CHx intermediates. A new mechanism, called "CoO-Co H-assisted CO dissociation" was hypothesised to explain the high FT activity and selectivity of paraffinic products. Furthermore, the experimental data also proved that pure CoO, which was obtained from the partial reduction of the Co/TiO_2 catalyst reduced by H_2 at both 220 and 250 ˚C, was found to be active for the FT reaction rather than for the WGS reaction. In addition, an increase in the reduction temperature led to a shift in the product distribution in favor of paraffinic products. This was attributed to an increase in the secondary hydrogenation of olefins due to the surface restructuring of cobalt phases from CoO to Co^0. For syngas reduction, the Co_2C phase was detected by both PXRD and XPS analysis. The formation of the Co_2C phase suppressed the hydrogenation reaction, and this resulted in the high selectivity of olefins. Based on the experimental results, it is postulated that a synergistic effect between Co^0 and Co_2C species promotes the production of the long chain hydrocarbons (C_{5+}) and suppresses the formation of CH_4. In addition, the effect of Ru promotion and the activation by hydrogenation-carburisation-hydrogenation (H-C-H) method was also studied and found to have a positive influence on the activity of the supported cobalt catalysts. It is worth noting that the use of the syngas reduction could potentially replace the high temperature H_2 reduction step, which is a benefit for a cost-effective FT process, such as for small scale biomass (waste) to liquid plant.

Key words: Activation, CoO-Co multiphase, Co_xC, Fischer-Tropsch synthesis, H assisted CO dissociation, H_2 reduction, Olefin hydrogenation, Syngas reduction, Support, Reduction temperature, Water gas shift.

Publications:

1. Shiba NC, Yao Y, Forbes RP, Okoye-Chine CG, Liu X, Hildebrandt D. Role of CoO-Co nanoparticles supported on SiO_2 in Fischer-Tropsch synthesis: Evidence for enhanced CO dissociation and olefin hydrogenation. Fuel Proc. Tech. 2021; 216: 106781. https://doi.org/10.1016/j.fuproc.2021.106781.
2. Shiba NC, Yao Y, Liu X, Hildebrandt D. Recent developments in catalyst pretreatment technologies for cobalt-based Fisher–Tropsch synthesis. Rev. Chem. Eng. 2021. https://doi.org/10.1515/revce-2020-0023.
3. Shiba NC, Yao Y, Liu X, Hildebrandt D. The effect of pre-treatments conditions on the activity and selectivity of Co-based catalysts for CO hydrogenation. Reactions. 2021; 2: 258-274. https://doi.org/10.3390/reactions2030016.

Local conference proceedings:

1. Nothando C. Shiba, Yali Yao, Liu Xinying and Diane Hildebrandt, the effect of reducing agents on cobalt catalysts for Fischer-Tropsch synthesis**,** Catalysis Society of South Africa (CATSA) 2018 Conference, Northwest, South Africa, November 8-11, 2018. (Poster Presentation).
2. Nothando C. Shiba, Yali Yao, Liu Xinying and Diane Hildebrandt, the effect of reducing agents (H_2, CO and Syngas) on cobalt-based catalysts, Catalysis Society of South Africa (CATSA) 2019 Conference, Cape Town, South Africa, November 8-11, 2019. (Poster Presentation).

International conference proceedings:

1. Nothando C. Shiba, Yali Yao, Liu Xinying and Diane Hildebrandt, the effect of reducing agents on a cobalt commercial catalyst for Fischer Tropsch synthesis, the 10th International Conference on Environmental Catalysis & the 3rd International Symposium on Catalytic Science and Technology in Sustainable Energy and Environment 2018 (ICEC&EECAT2018), Tianjin, China, September 22-26, 2018. (Oral presentation).
2. Nothando C. Shiba, Yali Yao, Liu Xinying and Diane Hildebrandt, the effect of reducing agents on cobalt-based catalysts for Fischer Tropsch synthesis, Advanced Energy Materials 2018 (AEM 2018), University of Surrey, Guildford, UK, 10-12 September 2018. (Oral presentation).

TABLE OF CONTENTS

ASF :Anderson-Schulz-Flory

BET :Brunauer-Emmet-Teller

C_n :Hydrocarbon with carbon number n

C_{5+} :Hydrocarbons with carbon number greater than 5, C%

CO :Carbon monoxide

CO_2 :Carbon dioxide

F_{in} :Total molar flow rate of the inlet gas, mol/min

F_{out} :Total molar flow rate of the outlet gas, mol/min

FID :Flame ionization detector

FTS :Fischer-Tropsch synthesis

g :Gram

gcat :Mass of catalyst used in grams

GC :Gas Chromatography

H_2 :Hydrogen

N_2 : Nitrogen

O :Olefins

P :Paraffins

P/O :Molar paraffin to Olefin ratio

P_{H2} :Partial pressure of hydrogen, bar

P_{CO} :Partial pressure of carbon monoxide, bar

PXRD :*in-situ* Powder X-ray Diffraction

r_{CO} :Rate of CO consumption, mol/(min.gcat)

r_{CO2} :Rate of carbon dioxide consumption, mol/(min.gcat)

Syngas :A mixture of H_2 and CO

TCD :Thermal conductivity detector

TPR :Temperature programmed reduction

WGS :Water gas shift

wt% :Weight percentage, %

x :Constant

$X_{CO,in}$:The molar fraction of CO in the inlet gas, mol

$X_{CO,out}$:The molar fraction of CO in the outlet gas, mol

$X_{N2,in}$:The molar fraction of N_2 in the inlet gas, mol

$X_{N2,out}$:The molar fraction of N_2 in the outlet gas, mol

XRD :X-ray Diffraction

Greek symbols:

α :Chain growth probability factor

β : Variation of the vapour pressure coefficient

θi :A gas product

CHAPTER 1: INTRODUCTION

1.1 Motivation

The uncertain and volatile price of crude oil and the involvement of potentially environmentally damaging processes have shifted the world's attention towards the currently favored approach, Fischer-Tropsch synthesis (FTS). FTS converts syngas (H_2/CO) over the surface of a catalyst material to produce various chains of hydrocarbons. These hydrocarbons can be further processed into high quality products such as gasoline and diesel [1,2]. The commonly used catalysts for FTS are the transition metals, with cobalt (Co) and iron (Fe) being the most preferred catalysts for industrial use. Supported cobalt catalysts are shown to be highly active, especially when natural gas is used as feedstock, highly stable and selective to long chain hydrocarbons and have a low water gas shift (WGS) activity compared to iron. Currently, the primary objective of the FTS industry is to maximize the production of C_{5+} fractions and the use of Co-based catalysts seem to achieve this goal [3,4].

The FTS industry faces many challenges and limitations which include the use of expensive hydrogen as a reducing gas, strong metal-support interactions which are formed during pre-treatment, and the unpredictable C_{5+} selectivity which is influenced by cobalt particle size and dispersion obtained during preparation and pretreatment. The pre-treatment steps (preparation and reduction) play a major role in the catalyst performance. Previous studies indicate that: (I) strong metal-support interactions inhibit the reduction of cobalt at industrial relevant conditions thus leads to low FT activity [5], (II) small cobalt particles (<5 nm) can be oxidized at high water partial pressures which can induce pre-mature catalyst deactivation [6], (III) bigger Co particles (>12nm) may lead to a low metal dispersion and consequently, low FT activity due to lower Co site density [7]. A number of strategies have been brought forward to attend to these limitations such as: (I) the use of noble metals such as ruthenium (Ru) with high surface area binders such as silica (SiO_2), titania (TiO_2) and alumina (Al_2O_3) to minimize the interactions between cobalt and the support and to improve the dispersion of Co over the support surface [8]and (II) the use of adjustable-pore-size supports such as mesoporous silica can control the cobalt particle size for maximum dispersion and catalytic activity [9]. The elevated price of noble metals due

to the scarcity of these materials in the world and the increased costs of waste-handling from the FTS plant makes the use of these promoters unattractive and they escalate the overall operation costs of the plant. This calls for cheaper and simpler ways to control the Co-support interactions to improve Co dispersion in order to improve overall activity and selectivity of the FT catalyst.

An investigation of the effect of the reducing temperature and support characteristics on the nature of cobalt species formed, focusing on the extent of metal-support interactions, the cobalt dispersion, and their reactivity in FTS has been carried out with the aim to provide a great avenue for future FTS catalyst design systems. Furthermore, we investigated the use of syngas, which is readily available in an FTS plant, as both reducing and reaction gas to modify the surface orientation of the cobalt species to the most active cobalt phase (Co-hcp) to enhance the activity of the catalyst. Additional benefits to using syngas instead of hydrogen for reduction, include the potential to minimize the operational and start-up costs for smaller/pilot FT plants, where the cost of expensive hydrogen purification can be neglected. A few studies report the use of syngas as a reducing agent, and positive results on the catalyst activity and stability as well as C_{5+} selectivity have been reported with syngas-treatment compared to H_2 [10,11]. However, some reports show that the use of syngas as a reducing agent produces inactive cobalt carbides and carbon deposits which have a detrimental effect on the activity of the catalysts [12,13]. There are currently not enough studies available to settle the consensus in literature on syngas activation. Therefore, we demonstrated the effect of syngas activation on activity and selectivity of the FTS products and compared it to the conventional hydrogen gas treatment results, at similar reduction and reaction conditions.

1.2 Objective

The main aim of this thesis is to investigate the effect of the reduction atmosphere and support identity on the catalytic performance of cobalt FTS catalysts. It entails detailed research into the influence of reducing different supported materials at low and high temperatures, as well as the use of syngas as a reducing agent compared to conventional

hydrogen. It looks at the effect of metal support interactions, metal-metal oxide interactions on the FTS and WGS reactions as well as the product selectivity. While the effect of the reduction temperature on FTS has been studied extensively, there is currently only a limited number of studies showing the effect of syngas reduction at different temperature. Furthermore, the effect of support-metal or metal-metal oxide interactions on the activity of Co-based FTS catalysts have been seldomly addressed. Most researchers do mention that some supports have a strong binding effect to the base metal, or metal-oxide (i.e CoO, Co_3O_4) resulting in the formation of inactive species for FTS. This research present proof that some of the overlooked cobalt phases might be active for FTS and can play a major role in the reactivity of the cobalt species in FTS.

The results of this investigation are intended to provide valuable information, such as (1) whether to use H_2 or syngas to attain a high C_{5+} selectivity and which reducing agent provides great stability for practical sustainable industrial processes; (2) which reduction temperature is suitable for each support, the optimum conditions for syngas activation of cobalt catalysts; (3) the effect of support identity on the reactivity of cobalt, the support pore size effect on the crystallite size and the effect on the support interactions with the base metal, which interactions work and which interactions are inactive for FTS. In addition, the use of the syngas system could potentially cut-down the start-up and operating costs of an FTS plant, especially pilot plants. With an attempt to find suitable operation conditions for syngas reduction for Co catalysts, this research will compare the results obtained by syngas pre-treatment on different supports at different temperatures, which will provide an avenue for future FTS plants.

Furthermore, we focus on the use of readily available syngas as both reducing and reaction agent to modify the surface cobalt phases to the most active cobalt phase (Co-hcp) with the aim of improving the catalyst performance. With few exceptions, the effect of pre-treatment conditions on the full range hydrocarbon selectivity (C_{5+}, C_2-C_4, olefin/paraffin content and chain growth probability) is not widely explored in literature. A general review on C_{5+} selectivity, by far the most frequently reported, has shown that C_{5+} increases upon increasing conversion, however little information is reported on the other hydrocarbons.

We report the behavioural changes in olefin/paraffin selectivity and chain growth probability with different pre-treatment with the aim of providing new insights for FTS cobalt catalyst's design for targeted products. A comparison of the product distribution (C_{5+}, CH_4, CO_2, Paraffin/Olefin ratio) obtained at different reduction temperatures or under different reducing atmospheres is made at similar pre-treatment and reaction conditions which might explain the deviations from the Anderson-Schulz-Flory (ASF) distribution model observed experimentally and could reveal potential pathways to attain better selectivity to targeted products and for better FTS activity.

1.3 Approach

We conducted a large number of experiments in a fixed bed (FB) reactor using various supported cobalt catalysts on SiO_2, TiO_2 and Al_2O_3 under similar reaction conditions. The supported cobalt catalysts were prepared via incipient wetness impregnation. In order to give more reliable data about the effect of catalyst pretreatment on the catalytic activity and selectivity, this research is going to use new characterization techniques such as the in-situ PXRD coupled with external characterization techniques such as BET and TEM to study their physical properties prior to the FT reaction and stipulate the changes that occur during pre-treatment, reduction and reaction, which are detrimental to the catalyst's overall performance. *in-situ* PXRD was used to monitor the surface changes during the catalyst reduction to understand the evolution of cobalt species under different conditions and their effect on activity. While most studies focus on external surface characterization such as BET and TEM, we rely on both external and internal characterization to come up with a rational explanation of the observed deviations from the normal ASF distribution. We varied the reduction atmosphere either by changing the reduction temperature or the reducing gas (H_2/syngas) to investigate the effect of temperature or gas on each support and the effect of support characteristics at similar operating temperatures. Thereafter, we analyzed the product gas and liquid streams from the reactors using an online and offline gas chromatography (GC) to calculate the amount of CO and H_2 that have reacted to hydrocarbon products. We then compared the experimental results for each catalyst at

different operation conditions before applying theoretical models to find possible explanations of the behaviors obtained.

1.4 Thesis outline

The thesis is composed of eight chapters, which have been prepared or submitted as papers for publication in a journal. Therefore, there is a degree of repetition in the experimental section in each chapter, where similar experimental work is described. Nevertheless, this repetition should serve to increase the reader's understanding while moving from one chapter to another. The eight chapters include the following:

Chapter 1: Covers the introduction, the basis of the study and preliminary information.

Chapter 2: This chapter gives a review of previous published studies related to Fischer-Tropsch synthesis (FTS). This review covers traditional and new methods that have been adopted to scale-up the FTS process to maximise production of targeted products at a cost-effective scale.

Chapter 3: Describes the experimental procedure and equipment employed in carrying out the study. It entails details on the actual steps taken to evaluate the effect of temperature, reducing gas and support on the reactivity of the cobalt-based models under study to obtain the results that are discussed in Chapters 4-7.

Chapter 4: Entails an attempt to study the effect of reduction temperature on the activity of SiO_2-supported catalysts, reduced in H_2. The changes observed were due to the formation of different Co phases and compounds with the support oxide atoms. Furthermore, we deduced that the Co valent state determines reaction route and the product selectivity. TiO_2- and Al_2O_3-supported catalysts were used for comparison and as a reference to form a basis of the SiO_2 study.

Chapter 5: Includes a series of experiments using syngas as a reducing agent on SiO_2-supported catalysts. The reduction temperature was varied between 250-350 ˚C and the results were compared to the results obtained when H_2 was used to activate the catalysts. In addition, the use of H_2 and CO in series was explored to compare the use of a mixed syngas

(H_2/CO) or to use these gases separately in series which could benefit large commercial FTS plants.

Chapter 6: Covers the effect of the reduction temperature on TiO_2-supported catalysts when reduced in H_2. It provides further insight into the effect of support identity on the reducibility and activity of the catalysts at different reduction temperatures by comparing the resulting catalyst activity, product selectivity and olefin/paraffin distribution. We look to focus on the surface changes under H_2-reduction and compare them to the ones obtainable via SiO_2 or Al_2O_3 support.

Chapter 7: Combines FTS experiments performed with TiO_2- and Al_2O_3-supported catalysts, pre-treated in syngas at different temperatures. It investigates the effect of the support identity, metal-support interactions in syngas treatment compared to H_2-treatment. The catalyst activity, product selectivity and olefin/paraffin ratios of the catalysts measured from the syngas treatment were calculated and compare with the H_2-treatment as well as the interactions between FT and WGS reactions.

Chapter 8: Gives the overall conclusions comparing the use of H_2 vs syngas, the different reduction temperatures for each support and the different supports at similar operating conditions.

1.5 References

[1] Hao X, Djatmiko ME, Xu YY, Wang YI, Chang J, Li YW. Simulation analysis of a GTL process using ASPEN plus. Chem. Eng. & Tech. 2008; 31: 188-96. https://doi.org/10.1002/ceat.200700336.

[2] Surgenor AD, Klettlinger JL, Yen CH, Nakley LM. Alternative fuel research in Fischer-Tropsch synthesis. Energy Tech 2011; 1-7. https://doi.org/10.1109/EnergyTech.2011.5948546.

[3] Hu J, Yu F, Lu Y. Application of Fischer–Tropsch synthesis in biomass to liquid conversion. Catal. 2012; 2: 303-26. https://doi.org/10.3390/catal2020303.

[4] Hoek A, Post MF, Minderhoud JK, Lednor PW, inventors; Shell Oil Co, assignee. Process for the preparation of a Fischer-Tropsch catalyst and preparation of hydrocarbons from syngas. United States patent US 4,499,209. 1985.

[5] Zhang J, Chen J, Ren J, Li Y, Sun Y. Support effect of Co/Al_2O_3 catalysts for Fischer–Tropsch synthesis. Fuel. 2003; 82: 581-6. https://doi.org/10.1016/S0016-2361(02)00331-9.

[6] Jacobs G, Ma W, Davis BH. Influence of reduction promoters on stability of cobalt/g-alumina Fischer-Tropsch synthesis catalysts. Catal. 2014; 4: 49-76. https://doi.org/10.3390/catal4010049.

[7] Borg Ø, Blekkan EA, Eri S, Akporiaye D, Vigerust B, Rytter E, Holmen A. Effect of calcination atmosphere and temperature on γ-Al_2O_3 supported cobalt Fischer-Tropsch catalysts. Top. Catal. 2007; 45: 39-43. https://doi.org/10.1007/s11244-007-0237-4.

[8] Diehl F, Khodakov AY. Promotion of cobalt Fischer-Tropsch catalysts with noble metals: a review. Oil & Gas Sci. Tech. 2009; 64: 11-24. https://doi.org/10.2516/ogst:2008040.

[9] Loedolff MJ, Goh BM, Koutsantonis GA, Fuller RO. Supported heterogeneous catalysts: what controls cobalt nanoparticle dispersion on alumina. New J. Chem. 2018; 42: 14894-900. DOI: 10.1039/C8NJ03076F.

[10] Jalama K, Kabuba J, Xiong H, Jewell LL. Co/TiO_2 Fischer–Tropsch catalyst activation by synthesis gas. Catal. Comm. 2012; 17: 154-9. https://doi.org/10.1016/j.catcom.2011.10.029.

[11] De la Peña O'Shea VA, Campos-Martin JM, Fierro JL. Strong enhancement of the Fischer–Tropsch synthesis on a Co/SiO_2 catalyst activate in syngas mixture. Catal. Comm. 2004; 5: 635-8. https://doi.org/10.1016/j.catcom.2004.08.005.

[12] Withers Jr HP, Eliezer KF, Mitchell JW. Slurry-phase Fischer-Tropsch synthesis and kinetic studies over supported cobalt carbonyl derived catalysts. Ind. Eng. Chem. 1990; 29: 1807-14. doi/10.1021/ie00105a011.

[13] Dalai AK, Davis BH. Fischer–Tropsch synthesis: a review of water effects on the performances of unsupported and supported Co catalysts. Appl. Catal. A: Gen. 2008; 348: 1-5. https://doi.org/10.1016/j.apcata.2008.06.021.

CHAPTER 2: LITERATURE REVIEW

RECENT DEVELOPMENTS IN CATALYST PRETREATMENT TECHNOLOGIES FOR COBALT BASED FISCHER-TROPSCH SYNTHESIS

This work has been published in the Reviews in Chemical Engineering Journal. Reference: Shiba NC, Yao Y, Liu X, Hildebrandt D. Recent developments in catalyst pretreatment technologies for cobalt based Fisher–Tropsch synthesis. Rev. Chem. Eng. 2021. https://doi.org/10.1515/revce-2020-0023.

Abstract

Stringent environmental regulations and energy insecurity necessitate the development of an integrated process to produce high-quality fuels from renewable resources and to reduce dependency on fossil fuels, in this case Fischer-Tropsch synthesis (FTS). The FT activity and selectivity are significantly influenced by the pretreatment of the catalyst. This article reviews traditional and developing processes for pretreatment of cobalt catalysts with reference to their application in FTS. The activation atmosphere, drying, calcination, reduction conditions and type of support are critical factors that govern the reducibility, dispersion and crystallite size of the active phase. Compared to traditional high temperature H_2 activation, both Hydrogenation-Carbidisation-Hydrogenation and Reduction-Oxidation-Reduction pretreatment cycles result in improved metal dispersion and exhibit much higher FTS activity. Cobalt carbide (Co_2C) formed by CO treatment has the potential to provide a simpler and more effective way of producing lower olefins, and higher alcohols directly from syngas. Syngas activation or direct synthesis of the metallic cobalt catalyst has the potential to remove the expensive H_2 pretreatment procedure, and consequently, simplify the pretreatment process, which would make it more economical and thus more attractive to industry.

2.1 Introduction

Growing concern about the limited supply of fossil fuels and serious environmental problems has sparked a global interest in producing green fuel [1,2]. Given the increasing amount of waste worldwide, interesting options to pursue, in terms of full-scale plant development, include upgrading solid waste to high density and green materials via gasification and the Fischer-Tropsch Synthesis (FTS) processes [3,4,5,6]. FTS is a process

used for reductive polymerization of carbon monoxide by hydrogen to form organic products that contain mainly hydrocarbons, as well as some oxygenated products in smaller amounts [7,8,9]. Typical transition metals for catalyzing the Fischer-Tropsch (FT) reaction include iron (Fe), cobalt (Co), nickel (Ni) and ruthenium (Ru) [10-12], with activity increasing in the order Fe<Co<Ni<Ru. Ru is too expensive and non-sustainable for industrial processes, while it can be used as a promoter to improve the performance of the Co-based FT catalyst [13,14]. Ni is generally recognized as a methanation catalyst [15], and it results in a large amount of methane and light hydrocarbons [13]. However, it can produce long chain hydrocarbons in FTS [16] or work as a reduction promoter to enhance the Co catalyst activity [17,18]. Co and Fe are therefore the preferred metals for industrial FTS processes [11]. The FTS companies in South Africa currently use Fe-based catalysts, while Shell's Malaysian plant, Shell-Pearl GTL Chevron-Sasol and Sasol-QP use Co-based catalysts [19,20].

Despite cobalt catalysts being more expensive than iron [9], they are reported to be more active and highly selective towards long chain hydrocarbon products. Iron catalysts have both FT reaction and WGS reaction activity. As via WGS reaction more H_2 is produced ($CO+H_2O \rightarrow CO_2 + H_2$), therefore, iron catalysts are typically used to convert hydrogen lean syngas to hydrocarbons. However, cobalt catalysts have high activity for CO hydrogenation with low WGS activity, therefor they're suitable to convert natural gas derived syngas (with a higher H_2/CO ratio) to liquid fuels [21-22]. The FTS catalysts are prepared by impregnation, precipitation, pyrolysis or melting. Impregnation is the preferred route, since it is not time-consuming or costly, and it is often used for preparing cobalt catalyst for FTS [21-25]. FTS proceeds on the surface of the metal; however, Co is present as oxides in a freshly calcined catalyst. Therefore, catalysts are activated by means of a reductive treatment using either hydrogen (H_2), carbon monoxide (CO) or synthesis gas (syngas:H_2/CO), before the FT reaction, in order to convert the oxides to metallic cobalt [26-31].

Catalyst pretreatment is one of the key factors for: increased activity; improved selectivity to targeted product classes, such as long-chain hydrocarbons; and extended catalyst lifetime [32]. The key objective with the catalyst pre-treatments is to deliver a high surface density

of the active sites, and thereby increase the catalyst performance during FTS. High surface area supports are used for cobalt-based catalysts, and this influence the nature of the metal species formed and the role that these metal species play in FTS. Compounds formed between the metal and the support inhibits the reduction of cobalt oxides, which results in low metal dispersion and consequently in low FTS activity [33-35]. Promoters can be used to enhance the reducibility and dispersion of the metal by decreasing the metal-support interaction and the temperature required to reduce the metal oxide to the metal [36,37].

Catalyst activation is conducted under different conditions for each reducing agent (H_2, CO and syngas), which results in a unique activity and a unique product spectrum [20]. New pretreatment procedures, such as carburization-hydrogenation (C-H) [38], hydrogenation-carburization- hydrogenation (H-C-H) [39], and reduction-oxidation-reduction (R-O-R) [33], have been reported to enhance the catalytic performance of cobalt-based catalysts, by ensuring the formation of the active phase and maximum metal dispersion. The direct synthesis of the Co metal eliminates the reduction step, thus decreasing the complexity and cost of FTS [40]. While many of these procedures have been extensively and systematically examined for Fe catalysts, not much information is available for the Co catalysts with different pre-treatment procedures.

Catalyst preparation and pre-treatment conditions strongly affect the particle size, dispersion and reducibility of the metal on a support surface of correct geometry [38,41,42]. Optimization of the dispersion, the particle size and C_{5+} hydrocarbons selectivity seems to be the most obvious goal in the design of effective cobalt catalysts [40,43,44]. Cobalt based catalysts supported on metal oxides or carbon materials with a cobalt crystallite size range of 4-10 nm are preferred for: obtaining a higher turnover frequency (TOF), a higher C_{5+} selectivity and a low yield of unwanted products, in particular, CH_4 and CO_2 [37,45-47]. The cobalt crystallite size and phase (fcc, hcp) are determined by the pretreatment steps and are closely related to the catalyst activity and product selectivity in FTS [37, 45, 48].

Most reviews on cobalt-based FTS focus on the support materials, promoters, catalyst deactivation and regeneration, reaction mechanisms, and kinetics [21,23,32,37,49-54]. There are a few review papers available on the effect of cobalt pretreatment for FTS.

Arsalanfar et al. [21] published a review paper on cobalt-based FTS, which also gave a general view of the traditional pre-treatments, but research on the new pre-treatment methods were not presented. Diehl and Khodakov [32] published a review on the effect of noble metal promoters for cobalt-based FTS, which summarized the promoter effect on catalyst reducibility. To the best of our knowledge, no attempt has been made to compare all the reduction procedures available to enhance cobalt performance in FTS.

With the aim of identifying the pre-treatment synthesis variables that can optimize the effectiveness of the cobalt catalysts, this review focuses on both traditional methods and new developments in cobalt pre-treatment technologies and their effect on the catalyst metal structure, particle size, dispersion reducibility, and the impact that these variables have on the performance of cobalt-based FT catalysts. The review starts with an introduction to the one-step pretreatment method, including the effect of the activation agent (H_2, CO and syngas) and the reduction conditions on the performance in cobalt-based FTS. Thereafter, a summary of the recently developed two-step and three-step activation methods, as well as direct synthesis the reduced cobalt catalyst (zero-step activation) is provided, and these are compared to the traditional pretreatment approaches. The effect of other key factors, including cobalt precursors, promoters, support pore size and preparation conditions on the reducibility, dispersion and crystallite size of the active phase, has also been addressed. Finally, concluding remarks are provided, together with some thoughts on potentially interesting and important emerging areas of research.

2.2 One-step activation methods for cobalt-based catalysts

2.2.1 H_2 activation

H_2 is the conventional reducing agent for cobalt-based catalysts, when converting the oxide into metallic cobalt [48, 55-58]. Cobalt metal exists in two crystallographic structures after reduction, namely: face centered cubic (fcc) phase; and hexagonal closed packed (hcp) phase. The hcp is more stable at a low temperature, whilst the fcc phase becomes more stable when the crystalline size of the cobalt is less than 20 nm and at temperatures above 450 °C [59-60]. Different bulk symmetries and atomic packing sequences exist for Co(fcc) and Co(hcp), which result in diversity of the exposed facets with distinct surface topologies.

These differences are the deciding factor for the catalytic activity and selectivity of each catalyst [61]. The experiments conducted by Lyu et al. [62] showed that the rate determining step for the FT reaction is CO dissociation and that Co(hcp) has a lower intrinsic activation barrier for CO dissociation (about 40 kJ/mol less) than Co(fcc). This makes Co(hcp) preferable for the FT reaction (see Figure 2.1). Figure 2.1B shows a superior catalytic activity of the Co(hcp) phase compared to the Co(fcc) phase.

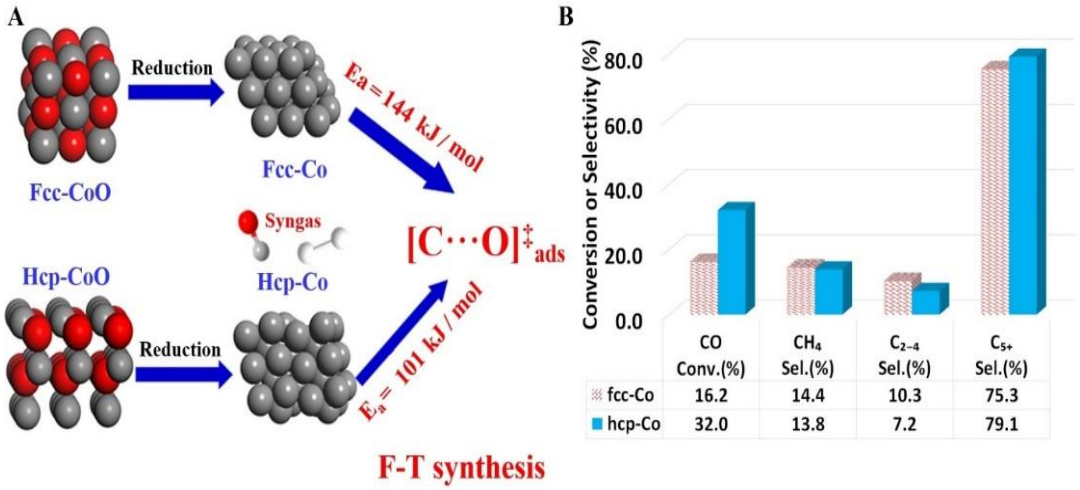

Figure 2. 1: (A) Schematic diagram of the reduction of CoO(fcc) and CoO(hcp), and the energy levels of the CO dissociation transition state over Co(hcp) and Co(fcc) (reproduced from Lyu et al. [62]) with permission from the American Chemical Society) (B) FTS activity and product selectivity over Co(hcp) and Co(fcc) catalysts with reaction conditions: 0.1 g of catalyst, $H_2/CO/N_2$ = 6/3/1 (mol/mol), 2.0 L/gcat/h), p = 10 bar, 210 °C (data from Lyu et al. [62]).

2.2.1.1 Activation temperature

Activation temperature has a significant effect on the catalytic performance of cobalt-based catalysts [30,14,63-65]. A typical hydrogen reduction is normally carried out at around 350 °C and atmospheric pressure [66-68]. However, this may differ according to the reducibility of each catalyst. Table 2.1 lists the effect of the reduction temperature on the activity and selectivity of the cobalt catalyst. The data in Table 2.1 indicate that each of the catalysts has an optimal reduction temperature and time. Dai and Yu [30] and Bian et al. [69] found that the catalyst's specific activity increased with a reduction temperature up to 500 ˚C. A further increase in the reduction temperature (>500 ˚C) led to a decline in CO conversion, C_{5+} selectivity and high CH_4 selectivity due to the formation of an overlayer (from the

support compounds) shielding the active sites and metal sintering [69,30]. Different trends were observed when using a TiO_2 support compared to those found for either Al_2O_3 or SiO_2.The highest catalyst activity was obtained when the reduction was done at 350 ^oC in H_2, while reduction at 250 ˚C produced the highest C_{5+} selectivity, as indicated in Table 2.1 [70]. The activity trend observed over the TiO_2 catalyst reflects on the effect of metal support interaction, the TiO_2 support might be strongly binded to the Co metal which led to a decrease in the catalyst's activity at temperatures beyond 350 ˚C.

The effect of reduction time was investigated by Dai and Yu [30], who found similar activity and selectivity when extending the reduction time from 2 h to 8 h at 330 ˚C. However, at a higher reduction temperature (415-500 ˚C), the activity and C_{5+} selectivity increased slightly with an increase in the reduction time (see Table 2.1). Bian et al. [69] reported that cobalt precursors, such as cobalt nitrate (Co(N)), cobalt acetate (Co(A)) and mixed cobalt acetate and nitrate (Co(A+N)), influenced the metal-support interactions, which led to different optimal reduction temperatures, i.e.: for Co(N) it is 300 ˚C; for Co(A) it is 500 ˚C; and for Co(A) it is 600 ˚C. A strong interaction between the Co precursor and the support results in high cobalt dispersion, but a low degree of reduction and FT activity [69]. The data shown in Table 2.1 indicate that the strong interactions between the SiO_2 support and cobalt precursors are in the order of Co(A) > Co(A+N)) > Co(N) [69]. For further discussion about the effect of the cobalt precursors, please refer to Section 2.6.

Poor catalyst reducibility and activity are usually reported to be due to metal-support interactions. Studies on how to minimize these interactions include the use of carbon supports and/or promoters, which have a positive effect on the reducibility of the catalyst at the expense of higher hydrocarbon products [47, 71-76]. In addition, comparison between the catalyst activity and selectivity should be made under similar operating conditions, as indicated in each group of experiments listed in the tables, in order to clearly note the effect of the pretreatment processes used. Furthermore, given that water has a strong impact on the product selectivity [53], the product selectivity needs to be compared at a similar reaction conversion, so as to avoid the influence of the water partial pressure on product selectivity.

Table 2. 1: Effect of reduction temperature on catalyst activity and selectivity.

Catalyst	Reduction T and time		Reduction degree	Dispersion	FT activity and selectivity			Reduction conditions	Reaction conditions	Ref.
	T	Time			CO conv	CH_4 sel	C_{5+} sel			
	°C	h	%	%	%	%	%			
11.6% Co(N)/Al_2O_3	295	5			0	0	0	H_2, at 295-535 °C, 500 h^{-1}	H_2/CO = 1.83 at 25 bar, 220°C	[30]
	330	2			10.8	10.4	71.4			
	330	8			10.7	11.8	70.9			
	415	0.8			58.7	13	75.8			
	415	5			66.8	15.9	72.6			
	415	9.2			67.4	15.6	73.7			
	500	2			69	13.9	74			
	500	8			73.3	12.2	75.7			
	535	5			71.8	12	73.1			
20%Co(N)/SiO_2	300	6	95	3.3	42.8	2.9	95	H_2, 300-600 °C , 1.8 L/gcat/h	H_2/CO = 1.88 at 10 bar, 220 °C	[69]
	400				42.3	2.9	94.9			
	500				37.9	2.9	95			
	600				29.2	2.9	94.2			
20%Co(A+N)/SiO_2	300	6	71	7.3	37.4	2.9	94.9			
	400				54.2	4.6	91.6			
	450				63.6	4.5	91.9			
	500				64.9	4.7	91.9			
	550				61	4.8	91.3			
	600				57.7	5.2	90.6			
20%Co(A)/SiO_2	400	6	55	8.5	41.2	4	92.8			
	500				51.3	5.2	90.5			
	600				57	5.9	89.5			
	700				54	5.8	89.6			
10%Co(N)/TiO_2	250	16	35	1.5	39	12	79.1	H_2, 250-450 °C, 1 bar, 2000 h^{-1} for 16 h	H_2/CO = 2, at 250 °C, 8 bar, 350 h^{-1} for TOS[a] > 400 h	[70]
	300		42.5	1.71	43	11.5	79.1			
	350		40.5	1.65	43.5	13	76			
	400		43.3	1.41	33	14.9	74.5			
	450		45.6	1.2	29	12	77.6			
10%Co(N)/TiO_2	250	2			15	3.8	92.2	H_2, 250-400 °C , 6 NL/gcat/h	H_2/CO = 2 at 20 bar, 220 °C, 3 NL/gcat/h	[28]
	350	2			30	19.8	67.5			
	400	2			23	26.7	59.6			

Co(N)= cobalt nitrate; Co(A) = cobalt acetate; Co(A+N) = cobalt nitrate + cobalt acetate

[a] TOS: time on stream

Figure 2.2 shows how a difference in the reduction temperature and support material could alter the dispersion, crystallite size and composition of the Co species, which further affects the activity of the catalyst. Complete reduction of CoO to Co° is obtained at temperatures up to 450 °C. a further increase in temperature (>700) results in a decrease in the Co metal dispersion for both porous and nonporous silica supports and is accompanied significant growth of the cobalt mean particle size. This was attributed to the formation of a thick SiO_2 or SiO_x layer shielding the Co-particles.

Figure 2.2 also shows the amounts of Co(fcc) and Co(hcp) phases obtained at temperatures below 700 ˚C. Only Co(fcc) was reported for the nonporous silica support at temperatures beyond 700 °C, which suggests that Co(hcp) may not be stable at a higher pretreatment temperature. Garces et al. [35] reduced an alumina supported cobalt catalyst at 350 ˚C and obtained only the Co(fcc) phase, whilst Co(hcp) was formed during the reduction of unpromoted Co_3O_4 under similar conditions. A further increase in the reduction temperature (>400 ˚C) resulted in the formation of Co(fcc) only for the unpromoted catalyst. Nevertheless, different compositions of Co(fcc) and Co(hcp) were obtained using a stepwise reduction process of the catalyst at 450 ˚C.

These results suggest that the operating conditions and the support determines the type of cobalt phase achievable, which further affects the activity of the catalyst. A number of studies confirmed that the Co(hcp) structure is preferentially formed at a low temperature, while Co(fcc) is dominant at a relatively high temperature [39, 59, 60, 63,75]. The number of active sites on the surface determines the activity of cobalt-based catalysts [30]; therefore, it is of interest to control the reduction environment for maximum dispersion of cobalt metal, preferably Co(hcp). In addition, the structure of the cobalt might be rearranged according to the process conditions for a long-term operation. More research work may be needed to trace the phase changes of the cobalt during long term FTS, i.e. the use of in-situ characterization.

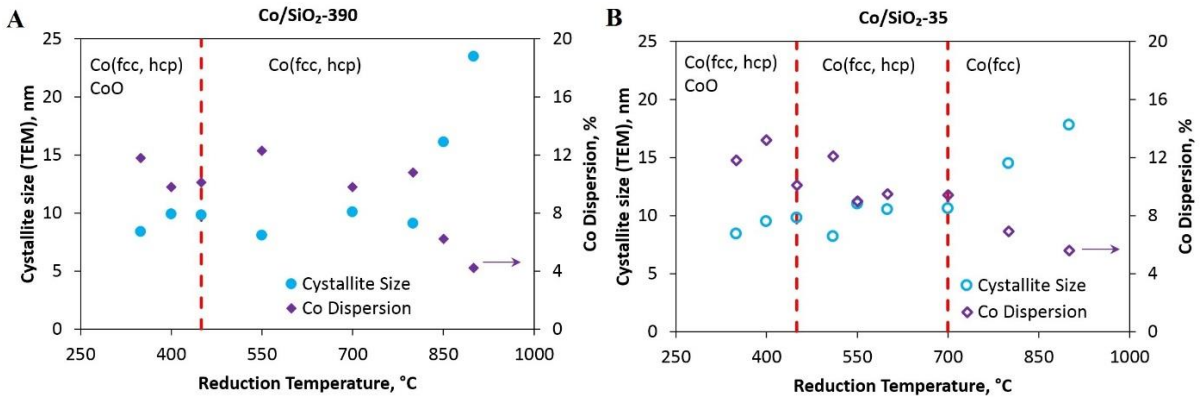

Figure 2. 2: Influence of the reduction temperature on the morphology and phase composition of Co/SiO_2 catalysts (data from Jabłonski et al. [63] (A) Co/SiO_2-390 prepared from cobalt nitrate and porous (390.6 m^2/g) silica (B) Co/SiO_2-35 prepared from cobalt nitrate and nonporous (35.1 m^2/g) silica. The crystallite size and phase were identified from TEM analysis.

2.2.1.2 Effect of water partial pressure

Water produced during the activation ($Co_3O_4+4H_2=3Co+4H_2O$) and reaction stages ($CO+2H_2 = CH_2+H_2O$) may cause catalyst deactivation, due to oxidation of the dispersed metal. Therefore, catalyst reduction is normally carried out at atmospheric pressure with diluted H_2 in order to maintain low partial pressure of water in the catalyst bed [59, 76].

Extensive investigations have been conducted on water co-feeding during FTS (after catalyst activation) [77-82]. However, studies on the effect of water during the reduction of Co species are relatively scarce. If the catalyst reduction is conducted in a large deep-bed reactor, a high concentration of water may be produced by the reduction of cobalt oxide with H_2. Zhang et al. [83] reported that the addition of water (up to 3%) led to a decrease in the degree of reduction for a ruthenium doped Co/Al_2O_3 catalyst. Hilmen et al. [78] found that the addition of water decreases the energy barrier and accelerates the diffusion of hydrogen spillover, which results in a shift in the reduction temperature for the $CoRe/Al_2O_3$ catalyst. However, a high-water concentration leads to oxidation of the dispersed particles. The cobalt-support compounds may be formed in the presence of water during the standard reduction procedure, which may result in poor catalyst activity, since they are not reducible under these conditions [83,84].

2.2.2 CO activation

Carbide has been identified in both cobalt-based and iron-based catalysts during FTS [75,85,86]. With a Co-based catalyst, treatment with H_2/CO or CO results in the formation of Co_2C and Co_3C, which are very stable under FTS reaction conditions [75,85,87]. In-situ XRD studies have confirmed the formation of bulk carbide together with metallic Co during CO and syngas reduction [48,88-90,75]. Unlike iron carbides, which have a positive effect on FTS, Co_xC is catalytically inactive for FTS, and is considered to be one of the deactivation mechanisms in Co-FTS [66,89,39, 91].

Positive effects of CO activation for CO hydrogenation were reported by Jalama et al. [92] and Khangale et al. [93] with cobalt catalysts supported on TiO_2 and Al_2O_3, respectively, which exhibited higher FTS activity when treated in 5%CO/He than 5%H_2/Ar. Contradictory effects on FT activity were observed by Li et al. [91] and Pan et al. [94] when using pure CO to reduce the catalyst, as per the results seen in Table 2.2. Table 2.2 lists the effect of the activation atmosphere and steps on catalyst performance, when the same reaction conditions are applied to all groups of catalysts. Some of these results are discussed in Section 2.2.3.

Reducing the catalyst in diluted CO is reported to inhibit the formation of cobalt carbides resulting in better metal dispersion, with CoO and Co˚ as the major phases (studied via XPS) [92]. However, pure CO promoted the formation of carbides, which led to a low surface site density and FT activity [94]. Beuther et al. [95] indicated that gaseous mixtures such as 5%H_2/Ar are used to slowly reduce the catalyst to avoid an exothermic reaction, that gives off nitrates which were introduced via the impregnation step. The concentration of gas can be increased gradually, until a pure gas stream is achieved [95]. The partial pressure of the reducing agents might be the key factor to improved catalytic activity with CO and syngas reduction; therefore, more research is needed in this area.

De la Pena O'Shea et al. [96] observed rapid deposition of nonreactive carbon species and the formation of carbon nanostructures with CO activation of a silica-supported cobalt catalyst, which resulted in poor performance during FTS. Li et al. [91] reported lower activity and better stability for a CO-reduced Co/Ru/TiO_2 catalyst, compared to H_2-activation. The H_2-reduced catalyst reached steady state at 40 h and started deactivating

with time on stream (TOS), whilst the CO-reduced catalyst conversion increased slightly after 40 h and then remained almost constant [91]. The slight increase in the conversion could be due to decomposition of the carbides to metallic cobalt. A few research studies indicate that prolonged TOS may cause partial decomposition of the bulk Co_2C to Co, which results in a significant increase in CO conversion and heavier product selectivity [66, 28, 97,98].

Experimental data has proven the low activity of Co_2C for CO hydrogenation to long chain hydrocarbon products [88, 42, 90, 99,100]. However, some of the experimental results suggest that the formation of Co_2C during FTS could promote the production of oxygenates, especially higher alcohols, through a CO insertion mechanism [42, 90, 99,100]. These results are in line with the findings reported by Volkova et al. [101] who noted an increase in alcohol productivity with an increase in the formation of the cobalt carbide phase, with it reaching maximum productivity at temperatures around 330-350 ˚C. The cobalt carbide phase resulted from CO activation, but more productivity was observed due to the presence of Cu in the catalyst [101].

Figure 2.3A shows the carburization of a 15%Co/Ce/Mn/Si catalyst, followed by a H_2-treatment. The CO-treated catalyst showed a very low CO conversion but exhibited higher selectivity for oxygenates (8%). An H_2-treatment was then done, which resulted in a significant increase in CO conversion from 10% to 65% and a sharp decrease in the selectivity of the oxygenates [88]. The conversion then slowly decreased with TOS and eventually reverted to the initial conversion seen before the H_2 treatment. This indicates that Co_2C is easily decomposed in H_2, forms again when syngas is reintroduced to the system, and is active for the conversion of syngas to oxygenates [88].

Gnanamani et al. [42] investigated the effect of CO and H_2 reduction on the catalytic activity for CO_2 hydrogenation over a 1%Na/20%Co-SiO_2 catalyst. The results are shown in Figure 2.3B. At the same reduction temperature (250 ˚C), higher activity was observed for the CO-reduced catalyst compared to the H_2-reduced catalyst (Figure 2.3B). The selectivity of alcohols is much higher than that of other products, due to the presence of the Co_2C phase, while the dominant product for the H_2-treated catalyst was found to be CH_4.

The authors explained that Na and Co_2C work together to favor the reverse water-gas shift reaction and that it shifted the selectivity towards alcohols [42]. Jiang et al. [102] reported that an ideal catalyst for direct hydrogenation of CO_2 to oxygenates or hydrocarbons should possess high activity for both subsequent C-C coupling and CO/CH_3OH formation.

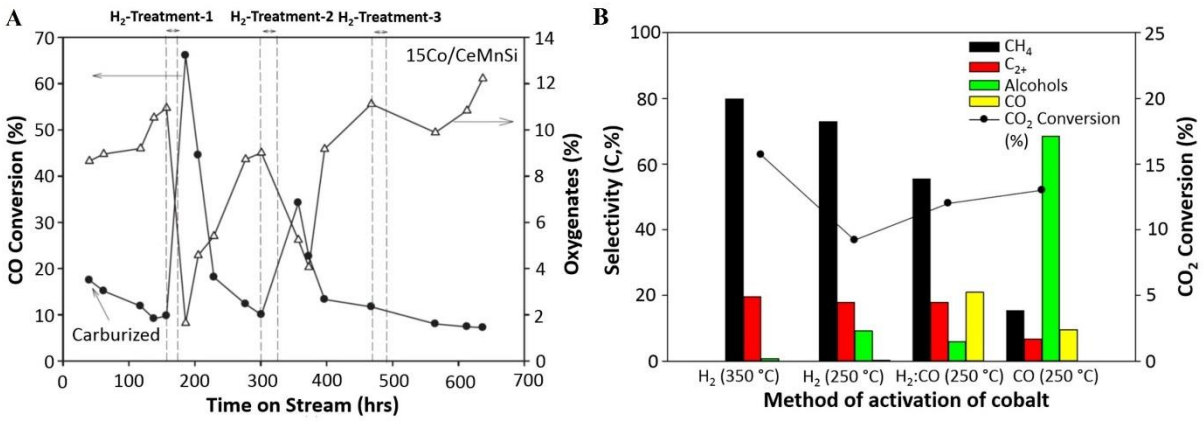

Figure 2. 3: Effect of CO and H_2 treatment on catalyst activity and product selectivity for FTS: (A) for CO hydrogenation, with reaction conditions: 230 ˚C, 18.9 bar, H_2/CO=1.86 [88]; (B) for CO_2 hydrogenation, with reaction conditions: 220 ˚C, 18.9 bar, H_2/CO_2=3 [42]. Reproduced with permission from Elsevier.

The results shown in Figure 2.3 suggest that cobalt carbide is active for both CO (Figure 2.3A) and CO_2 (Figure 2.3B) hydrogenation to produce oxygenates. One explanation might be that there are two distinct mechanisms of CO hydrogenation: 1) CO carbide mechanism (C-O bond dissociative adsorption and alkyl formation); 2) CO insertion mechanism (CO* associative adsorption) [103]. It was proposed that metallic Co catalyzes the former and Co_2C is responsible for the latter which follows the hydroformylation reaction to form (R-CO*) [103].

The experimental results indicate that it is possible to tune the adsorption sites when aiming for specific products, such as Co for wax production and Co_2C for high alcohols, by activating the cobalt catalyst with different reducing agents, which promotes different cobalt phases. Emerging research work has focused on the use of Co_2C as a catalyst to produce lower olefins and/or oxygenates [104,105,100,106,99]. The role of Co_3C on the FT activity and selectivity is complex and not well understood. More comparisons on the

effect of activation agents (H_2, CO, syngas) on catalyst activity are discussed in the next section.

2.2.3 Syngas activation

There is scant literature on the reduction of cobalt catalysts with syngas, because it promotes the formation of inactive carbon species and causes catalyst deactivation. However, using a low reduction temperature limits the formation of these species, and allows for the achievement of good catalyst activity, which has led to renewed research interest in the subject. Although most of the results found in the literature show negative effects for syngas activation of cobalt catalysts [66, 91], such as low activity with high methane selectivity, some positive effects for syngas activation of cobalt catalysts have been reported [28, 31,96, 84].

De la Pena O'Shea et al. [96] studied the reduction of a Co/SiO_2 catalyst in syngas (H_2/CO=1) compared to reduction in either H_2 or CO, via in-situ XRD and TEM. The results are shown in Figure 2.4. The XRD diffraction patterns indicate almost complete reduction of Co_3O_4 to CoO at 300 ℃ with the syngas pretreatment, and a slightly lower temperature for H_2-reduction (275 °C), whilst CO pretreatment resulted in the transformation of the oxide occurring at a slightly higher temperature (325 °C). Increasing the temperature further resulted in a homogeneous dispersed Co(hcp) on carbon nanostructures (Figure 2.4E) for the syngas reduced catalyst and a heterogeneous size distribution of Co(fcc) (Figure 2.4D) for hydrogen reduction; and a mixture of Co(fcc) and Co(hcp) for CO reduction. The syngas reduced catalyst performed better than either H_2 or CO-reduced catalysts, due to the formation of carbon nanostructures, which inhibits sintering of the metal particles. With reduction temperatures above 400 °C, the syngas reduced catalyst showed rapid formation of non-reactive carbon deposits, which resulted in a decline in activity [96].

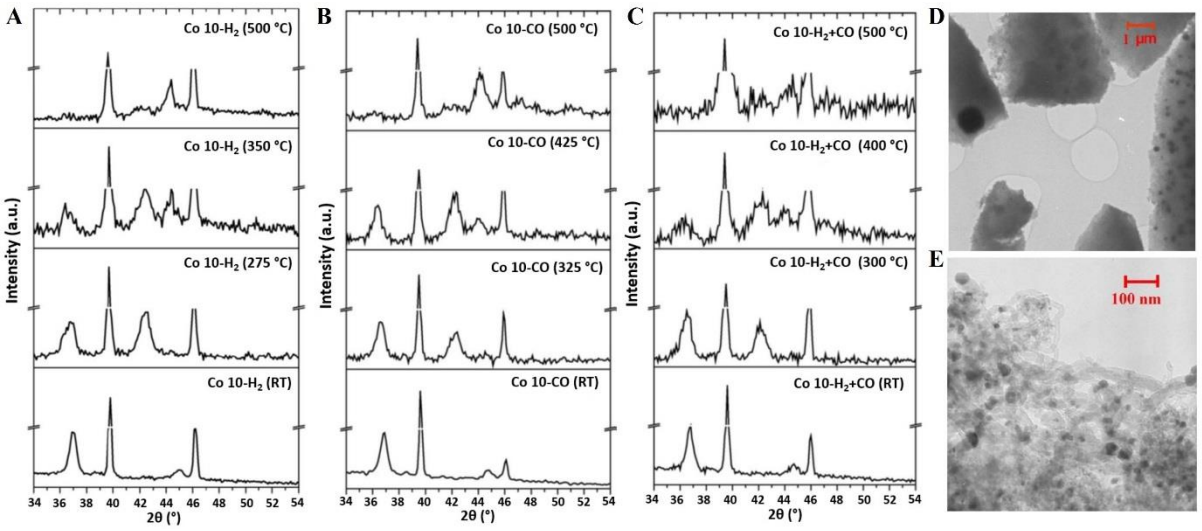

Figure 2. 4: In situ XRD patterns and TEM micrograph of Co 10-c catalyst (calcined 10 wt.% Co/SiO_2): (A) XRD results reduced by H_2; (B) XRD results reduced by CO; (C) XRD results reduced by syngas at different temperatures, with peaks at 39.68 and 46.18 due to the platinum holder; (D) TEM micrograph of Co 10–H_2 (500 °C); (E) TEM micrograph of Co 10–(H_2+CO) (500 °C). Reproduced from De la Pena O'shea et al. [96] with permission from Elsevier.

The effect of syngas activation on the catalytic performance of cobalt FTS is controversial. Table 2.2 summarizes the effect of reducing agents (CO, H_2 and syngas) on the activity and selectivity of the catalyst. De la Pena O'Shea et al. [31] studied the effect of reducing agents on the FT activity of a Co/SiO_2 catalyst, and found that syngas reduction resulted in strong enhancement in CO conversion, i.e. about 5 times higher than that obtained with standard activation in H_2 (see Table 2.2). The simultaneous presence of H_2 and CO was found to prevent the formation of graphitic carbon, resulting in improved reducibility and high metal dispersion. CO activation resulted in deposition of graphitic carbon structures via the Boudouard reaction which was attributed to the low CO conversion recorded. Jalama et al. [28] reported superior activity for Co/TiO_2 reduced in syngas compared to H_2 under similar operating conditions (see Table 2.2). The CO conversion and methane selectivity both increased sharply with an increase in the reduction temperature (250-400 ˚C) for the syngas-treated catalysts, whereas the C_{5+} production selectivity decreased. On the other hand, H_2-reduced samples showed low FT activity, C_{5+} selectivity and a high CH_4 selectivity at reduction temperatures higher than 350 ˚C [28]. The authors [28] reported that the presence of low partial pressure of CO in the reducing gas resulted in a different reducing mechanism

and promoted the reduction to some extent by preventing the formation of Co-support compounds. Furthermore, the carbides that were formed during the reduction with syngas were further reduced to more active and stable metallic Co under reaction conditions, which led to enhanced FT activity [28]. Contrarily, Dai et al. [30] reported that, the catalyst was much more active after H_2 activation compared to the catalyst reduced by syngas. In addition, the syngas reduced catalyst showed lower activity and higher methane selectivity due to the presence of carbides [30].

Studies on the effect of the reduction syngas molar ratio (H_2/CO) on the activity of Co-based catalysts are scarce, which points to the gap in literature that is yet to be filled. Some researchers have focused on the effect of the H_2/CO ratio on the performance of the reduced catalyst during FTS. Sadeqzadeh et al. [107] investigated the effect of the H_2/CO ratio on reduced $CoPt/Al_2O_3$ catalysts (reduced by H_2 at 400 °C for 16 h) and reported that the amount of both the amorphous phases and liquids formed during FTS increased at low H_2/CO=0.5, whereas under methanation conditions (H_2/CO $\geq$4), these phases diminish due to hydrocarbon evaporation and sintering of the cobalt metal particles. The concentration of the liquid hydrocarbons was found to be more significant at syngas ratios of about 2. Tristantini et al. [108] reported a high C_{5+} selectivity, low selectivity of methane and no water gas shift (WGS) activity for a feed gas with a molar H_2/CO ratio of 1. A further increase in the H_2/CO molar ratio led to a drop in the hydrocarbon production rate. Even though these results are based on the FT reaction, they provide insights into the effect of the syngas ratio on hydrocarbon selectivity and the surface phase changes.

Extensive research has been done on the effect of the H_2/CO ratio on the performance of iron-based catalysts [109-111], and it was reported that: iron carbides are more active in FT synthesis than the iron metal; the formation of the carbides is more favorable at a low syngas ratios ($\leq$1). It would be interesting to investigate the effect of the H_2/CO ratio on the formation of the cobalt phases as metallic Co is preferred for C_{5+} hydrocarbon production, while Co_2C promotes the production of olefins and oxygenates.

Overall, syngas reduction is a promising method that provides the most cost-competitive means of reducing the catalyst by eliminating the use of pure H_2. This is especially

applicable to small-scale plants, as the process could be simplified, and therefore, the capital and operation costs could be reduced. According to the results obtained by Jalama et al. [28], Gnanamani et al. [42] and De la Pena O'Shea et al. [31], synthetic gas has the potential to replace H_2 as a reducing agent, as it showed better activity and stability compared to either the standard activation procedure with H_2 or activation with CO. However, attention should be given when deciding on operating conditions as contradictory results on syngas activation for CO hydrogenation are reported. These are summarized in Table 2.2. The optimum operating conditions for syngas reduction to deliver comparable or better catalytic activity compared to H_2-reduced catalysts has not yet been established. More research in this area is required to fill the gap in the literature, which will lead to optimization of the standardized reduction method using syngas as both reaction and reduction gas.

Table 2. 2: Effect of reducing agents on the catalytic performance of cobalt-based catalysts.

Catalyst	Reduction conditions					Reducibility	Dispersion	FT activity and selectivity			Reaction conditions	Refs.
	Reducing agent	T °C	Time h	P bar	FR NL/gcat/h	%	%	CO conv %	CH_4 sel %	C_{5+} sel %		
10%Co/TiO_2	H_2	250	2	1	6	___	___	15	3.8	92.2	H_2/CO = 2 at 20 bar, 220 °C, 3 NL/gcat/h	[28]
	H_2/CO=2:1							15	5.3	89.5		
	H_2	350						30	19.8	67.5		
	H_2/CO=2:1							35	16.7	72.2		
	H_2	400						23	26.7	59.6		
	H_2/CO=2:1							42	20.7	67.2		
11.6%Co/Al_2O_3	H_2	483	___	1	[a]	___	___	72.1	14.5	76.8	H_2/CO = 1.83 at 25 bar, 220 °C, 500 h^{-1}	[30]
	H_2/CO= 1.83:1							39.8	18.2	65.1		
10%Co/SiO_2	H_2/N_2=2:8	500	2	1	___	___	___	28	24.5	62.9	H_2/CO = 2 at 40 bar, 230 °C, 12.7 NL/gcat/h	[31]
	CO/N_2=2:8							10	25.3	61.7		
	$H_2/CO/N_2$=1:1:8							90	31.8	58.4		
10%Co/TiO_2	H_2	280	24	10	2	___	___	73.5	10	77.8	H_2/CO = 2 at 23.5 bar, 230 °C, 2 NL/gcat/h	[91]
	CO	250		16				34	20	63.2		
10%Co/ZnO	H_2	320	10	1	0.5	90.7	3.5	19.3	6.3	83.4	H_2/CO = 2 at 25 bar, 205 °C, 0.64 NL/gcat/h	[94]
	CO	250				___	___	17.5	12.1	78.7		
	H_2	320				90.7	3.5	29.3	10.2	79.1	H_2/CO = 2 at 25 bar, 215 °C, 0.64 NL/gcat/h	
	CO	250				___	___	22.7	16.5	71.8		
15%Co/Al_2O_3	5% H_2/Ar	300	17	1	1.8	___	___	11.6	3.3	95.9	H_2/CO = 2 (reaction temperature and flow rate etc.were not reported)	[93]
	5% CO/He							14.9	8.3	70.2		
	5% H_2/Ar	350						12	5.7	93.5		
	5% CO/He							18.8	15	78.6		
10%Co/TiO_2	5% H_2/Ar	350	14	1	3.6	___	___	17.6	13.5	61.7	H_2/CO = 2 at 20 bar, 220 °C, 1.2 NL/gcat/h	[92]
	5% CO/He							21.1	14.6	69		
Co(A+N)/0.2%Ru/SiO_2 [b]	H_2/CO=2:1	200	1	1	1.8	41.7		30.2	___	___	H_2/CO=2:1, 240 °C, 1.0 Mpa, W/F (CO+H_2+Ar)=5 g h/mol	[64]
		300				70.2		50.9				
		400				99.8	6.91	72.3				
		500				99.9		69.2				

[a]: GHSV = 500 h^{-1}, [b]: The catalyst with total cobalt loading of 10 wt% was activated with H_2 at 400 °C for 10 h and then passivated in 1% O_2

2.3 Two-step activation of cobalt-based catalyst

Activation is the key step in generating the active phase and it impacts the crystallographic structure of the cobalt metal and crystallite size. The crystallographic orientation of the cobalt metal has a huge impact on the catalytic activity. Co(hcp) is known to result in better catalytic performance than Co(fcc) [107, 94, 55, 48]. Non-traditional activation procedures are aimed at increasing the dispersion of the Co(hcp) phase, in order to improve the activity and selectivity towards higher molecular mass products. The two-step procedure involves using different reducing agents in series, for example: (1) treatment with CO to carburize the catalyst followed by either H_2 or syngas (SG) to decarburize the carbides (CO-H_2 or CO-SG); (2) treatment in air to oxidize the cobalt at elevated temperatures, followed by reduction in H_2 or CO (air-H_2 or air-CO), to enrich the catalyst with Co(hcp) stacking which has a high intrinsic activity for FTS. These methods are discussed further below.

2.3.1 Carbidisation-hydrogenation (C-H) route

Crystallographic modification can be induced by means of carbidisation of cobalt under CO activation followed by decarbidisation in an H_2 atmosphere (C-H route), in order to improve the metal dispersion and catalytic activity of cobalt catalysts [94,55,112]. Braconnier et al. [113] reported that the carbidisation step involves adsorption and dissociation of CO, followed by diffusion of carbon into the metal particles. The decarbidisation step consists of carbon diffusion, followed by hydrogenation of surface carbon to methane. The authors suggested that the decarbidisation step proceeds faster than the carbidisation step since the Co_2C structure is close to that of Co(hcp), while the carbidisation step depends on both the rate of carbon diffusion and CO dissociation, which in turn is affected by the metal-support interactions.

Pan et al. [94 & 112] studied the effect of pretreatment procedures on the activity of Co/ZnO and Co/Al_2O_3 catalysts. It was found that CO reduction at 230 ˚C followed by syngas at 250 ˚C (CO-SG) and 26.9 bar, improved the catalytic performance (higher CO conversion and better hydrocarbon selectivity) compared to pure CO activation, see Table 2.3. The CO-SG catalyst afforded a 7.5 %CH_4 and 88.6 %C_{5+} and the CO-reduced catalyst produced about 17.2 %CH_4 and 73.7 %C_{5+}. The latter produced both Co(fcc) and Co(hcp) phases,

whereas the major phases in the CO activated catalyst were found to be CoO, Co_3C, Co_2C and minimal amounts of Co˚. Li et al. [91] suggested that hydrocarbon products are produced on metallic sites, whereas methane is produced on surface carbides. Therefore, the methane selectivity on the syngas reduced catalyst can be assigned to the surface Co_xC, which is found in small quantities after CO-SG reduction. Furthermore, the CO-SG reduction method was reported to produce significant amounts of deposited carbon (both polymeric and graphitic) which had an adverse effect on catalyst selectivity [112].

Carbon deposited during two-step activation (CO-SG) may limit the hydrogenation of 1-olefin and the difference in the catalytic behavior of Co/ZnO and Co/Al_2O_3 catalysts might be due to the different metal-support interactions, which are not entirely elucidated [112]. See Table 2.3. Furthermore, the second syngas reduction step was done at elevated temperatures and pressures (250 ˚C, 20 bar) which led to a pronounced and superior effect on the catalytic activity and selectivity. It should be noted that the single syngas reduction step (at 350 ˚C) on Co/Al_2O_3 exhibited a higher FT activity compared to the CO-SG reduced catalyst but had the least desirable selectivity (high CH_4 and lower C_{5+} hydrocarbons), due to relatively high amounts of deposited surface carbon.

Rebmann et al. [55] reported lower FT activity (low C_{5+} hydrocarbons and high CH_4 activity) for a Co/Al_2O_3 catalyst reduced in CO-H_2 at 230 ˚C compared to H_2 reduction at 500 ˚C. CO activation was found to promote carbon deposition, which blocked the support pores and led to low availability of active sites. Furthermore, reactive carbon promoted the formation of CH_4 [55]. Pan et al. [112] suggested that surface carbon has a significant effect on the strength of adsorption and dissociation rates, which may lead to an increase in the production of low molecular hydrocarbons. However, it is hard to compare the experimental results and draw conclusions, as the reduction temperatures were so different (CO-H_2 at 230 °C, and H_2 at 500 °C); however, the conversion data indicate that reducing at 230 °C in H_2 may be too low to get enough active sites for FTS. The two-step activation method is discussed further in section 2.3.2.

2.3.2 Oxidation-reduction (O-R) route

The effect of cyclic oxidation-reduction (O-R) treatments was first reported by Kobylinski et al. [114] who demonstrated that the activity of alumina supported catalysts could be increased by a factor of two when subjected to repeated O-R treatments (oxidation was done at 350 ˚C in air). Saib et al. [115] restored the activity of a spent $Co/Pt/Al_2O_3$ catalyst to that of a fresh catalyst by means of O-R treatment. Oxidation (at 300 ˚C in air) of the $Co/Pt/Al_2O_3$ catalyst re-dispersed the cobalt metal and removed most of the deleterious carbon. Excessive oxidation (>400 ˚C) was reported to promote the formation of Co/Al_2O_4 [115]. In addition, using the flat model system on a $Co/SiO_2/Si$ (100) catalyst led to the formation of hollow spheres by the Kirkendall effect resulting in the spread of cobalt crystallites that may undergo multi-nucleation under reduction to produce smaller cobalt crystallites. The O-R activation method can be used to improve the catalytic performance of cobalt-based catalysts as well as regenerate the catalysts and it is able to reverse the major deactivation mechanisms such as carbon deposition. However, caution should be used in selecting the oxidation temperature.

Table 2.3 lists the effect of the activation atmospheres and steps on the catalyst performance when the same reaction conditions were conducted for each group of the catalysts. British Petroleum (BP) researchers conducted experiments using a two-step activation method over a Co/ZnO catalyst: air followed by H_2 activation (air-H_2) and air followed by CO activation (air-CO), see Table 2.3 [116]. The two-step activation resulted in superior catalytic performance (high activity, high C_{5+} selectivity and low CH_4 selectivity) compared to a single step activation procedure using either H_2 or CO. The catalyst reduced in air at 500 ˚C for 50 h, followed by CO reduction at 250 ˚C for 3h, exhibited the highest activity, and selectivity towards C_{5+} hydrocarbon products. The air-CO activation results in superior catalytic performance compared to the catalyst with air-H_2; it promoted the formation of Co(hcp), whilst air-H_2 formed mainly Co(fcc), which is less active than Co(hcp) [116,113]. The success of the two-step activation method seems to be strongly dependent on the cobalt phase change occurring on the catalyst surface during reduction which in turn depends on the reduction conditions.

The two-step reduction methods (C-H and O-R) provide a guide on how to lower the methane selectivity associated with cobalt-based catalysts. The O-R treatment could be used to regenerate industrial catalysts, by restoring their activity and reversing carbon deposition. The C_{5+} selectivity is inhibited due to surface carbon deposited during reduction with CO which limits chain propagation and favors methanation. The reduction conditions for the two-step reduction method need to be tailored, in order to: minimize the deposition of polymeric and graphitic carbon; promote secondary reactions, such as hydrogenation of olefins and olefin chain growth reactions.

Table 2. 3: Comparison of the one-step and two-step activation routes for FTS.

Catalyst	Two-step Activation		FT activity and selectivity						Activation conditions	Reaction conditions	Ref
	Agent 1-T[a]	Agent 2-T	TOS h	T °C	CO conv %	CH_4 Sel %	C_{5+} Sel %	CO_2 Sel %			
10%Co/ZnO	H_2-320	N/A	24	205	19.3	6.3	83.4	0.3	H_2 reduction (320 °C for 10 h),	Feed gas (H_2:CO = 2 containing 5% Ar), 205 °C and 215 °C, 26.2 bar, 0.64 NL/g-cat/h	[112]
			45	215	29	9.3	80	0.5			
	CO-250	N/A	20	205	17.5	11	79.8	0.4	CO reduction (250 °C for 3 h),		
			44	215	22.7	15.5	72.5	0.7			
	CO-250	Syngas-250	26	205	28.3	6.1	82.8	0.9	Two steps: pretreatment in CO (250 °C for 3 h, 0.5NL/gcat/h) followed by syngas (H_2:CO = 2 containing 15% N_2 and 5% Ar, 0.69 NL/gcat/h, 29.6 bar, 250 °C for 1 h)		
			66	215	36.6	7.9	79.2	1.8			
15%Co/Al_2O_3	H_2-375	N/A	30-40	220	58.8	7.9	85.4		H_2 reduction (375 °C, 12.4 NL/g-cat/h for 12 h)	Feed gas: (H_2:CO = 2 containing 5% Ar), 220 °C, 20bar, SV = 3.65 NL/g-cat/h.	[94]
	Syngas-350	N/A			35.4	17.1	75.6		Syngas reduction ((H_2:CO = 2 plus 70% He), 350 °C, 12.4 NL/g-cat/h for 12 h)		
	CO-350	N/A			4.6	19.7	74.6		CO reduction (350 °C for 12 h)		
	CO-250	N/A			6.3	17.2	73.7		CO reduction (250 °C for 3 h)		
	CO-250	Syngas-250			7.3	7.1	88.6		Two steps: pretreatment in CO (250 °C for 3 h) followed by syngas ((H_2:CO = 2 containing 15% N_2), 250 °C, 7.7 NL/g-cat/h, 20 bar for 2 h)		
13.4%Co/Al_2O_3	H_2-375	N/A	150	220	6.3	23	50		500 °C for 16 h. a flow of CO followed by a flow of H_2 at 230 °C	H_2:CO = 2, 1.6 bar, 220 °C	[55]
	CO-230	H_2-230		220	3.7	25	45				
10%Co/ZnO	H_2-320	N/A	54	214	73.9	8	80.9		H_2 reduction (320 °C for 10 h)	H_2/CO = 2, 30bar, 206-216 °C	[115]
			149	216	74.2	7.8	82.6				
	CO-250	N/A	26	202	78.7	5.9	88.8		CO reduction (250 °C for 3 h)		
			77	209	83.9	7.1	87.8				
			149	210	86.4	7	88				
	Air-500	CO-250	26	204	90.4	7.6	86.8		Two steps: pretreatment in air (500 °C for 44 h) followed by CO (250 °C for 3 h)		
			94	205	84.2	5.5	80.6				
			144	205	79.8	6.2	89				
	Air-500	H_2-320	214	214	87	7.5	76.8		Two steps: pretreatment in air (500 °C for 6 h) followed by H_2 (320 °C for 9 h)		
	Air-500	CO-250	213	212	87	4.6	91		Two steps: pretreatment in air (500 °C for 50 h) followed by CO (250 °C for 3 h)		

[a] "Agent 1-T" refers to the first reduction agent and reduction temperature at T °C.

2.4 Three-step activation of a cobalt catalyst

2.4.1 Activation using the hydrogenation-carbidisation-hydrogenation (H-C-H) route

The cobalt species on the catalyst surface are strongly dependent on the gas compositions in the catalyst bed [75,85]. Recent studies indicate that Co_2C can be formed under CO treatment and transformed back to Co (hcp) at a relatively low temperature (about 150 °C) via hydrogenation [81]. Kwak et al. [85] reported that the optimum hydrogenation conditions for transitioning Co_2C to Co(hcp) after carburization in CO are 20 bars and 220 °C. The selective formation of Co(hcp) under the H-C-H cycle results in improved catalytic activity, due to the nature of the adsorption sites, i.e., Co(hcp) has a higher intrinsic activity, than Co(fcc) [75,85].

Claeys and co-workers [75] investigated the phase change of cobalt species (such as CoO, Co(fcc), Co(hcp) or Co_2C) by introducing H_2, CO and H_2 in series (H-C-H) in an in-situ magnetometer. The results reported by Claeys et al. [75] are plotted in Figure 2.5, which shows that Co(fcc) is predominantly produced with only a small amount of Co(hcp) present, after the first hydrogenation step; during carburization in CO, the amount of Co_2C increases with TOS, while the amount of both Co(fcc) and Co(hcp) decreases, but Co(hcp), in particular, is predominantly converted to Co_2C and decomposition of Co_2C starts at a temperature around 130 °C. The highest amount of Co(hcp) was obtained at a very low temperature of about 170 °C.

Braconnier et al. [113] studied the evolution of cobalt phases on silica and alumina supported catalysts when subjected to H-C-H treatment. The authors reported that the Co(fcc) phase in Co/SiO_2 easily transformed to carbides under CO treatment, and rapidly reduced to Co(hcp) in H_2, due to weaker cobalt-silica interactions and surface deformity. However, Co(fcc) remained after the full reduction (H-C-H) cycle of Co/Al_2O_3, which suggests that the CO treatment did not cause the Co(fcc) to fully transform to cobalt carbide. It has been reported that cobalt supported on silica has a faultier surface than cobalt supported on alumina and faulty/deformed surfaces are preferential sites for CO dissociation [113]. These results suggest that the type of support used plays a vital role in reducing cobalt oxide to metallic cobalt, and that the CO treatment results in surface carbon, which leads to a high methane production.

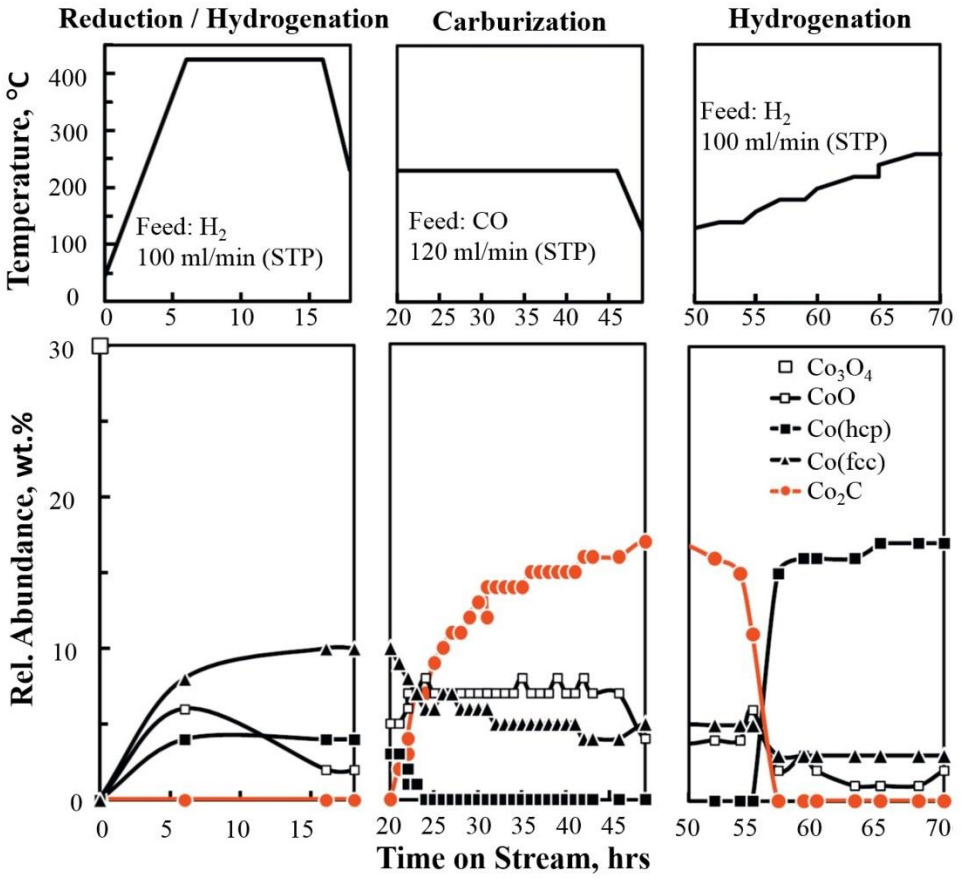

Figure 2. 5: In situ XRD data of reduction (hydrogenation), carburization, and temperature-programmed hydrogenation (TPH) of carbide in a 20%Co/0.05%Pt/Al_2O_3 catalyst. Reproduced from Claeys et al. [75] with permission from Elsevier.

Figure 2.6 shows the CO conversion for both Co/Al_2O_3 and Co-Ru/SiO_2 catalysts activated using a H-C-H method and a two-step reduction method, compared to the standard H_2 reduction method. With both catalysts, the catalyst reduced using the H-C-H method showed superior catalytic activity in comparison to both the single step H_2 reduction method and the two-step reduction method. Ducreux et al. [39] reported that the H-C-H method promoted the dispersion of Co(hcp) in both Co/Al_2O_3 and Co-Ru/SiO_2. The Co-Ru/SiO_2 catalyst treated in an inert gas followed by H_2 reduction exhibited the lowest catalytic activity (low CO conversion and C_{5+} selectivity) compared to those treated with H_2 and H-C-H reduction methods.

The data shown in Figures 2.5 and 2.6 provide insight on how structural changes can be induced on the cobalt surface in order to produce Co(hcp) stacking, which enhances the catalyst activity during FTS. Modification of the crystallographic structure of cobalt seems to be dependent on the support-metal interactions and reduction atmosphere. The H-C-H reduction method is more complicated than the one step activation method, and it could be beneficial in FT commercial plants, where the cost of reduction is relatively insignificant. However, the H-C-H activation cycle may not be suitable for small scale FTS because of cost concerns and the complexity of the process.

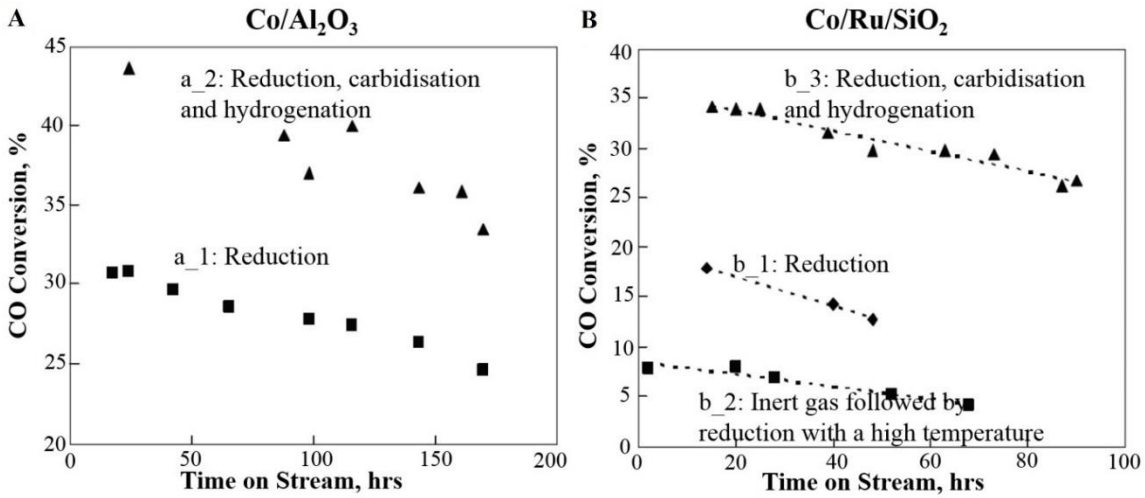

Figure 2. 6: Activity of : (A) 13.3%Co/Al_2O_3 reduced with (a_1) H_2 at 550˚C (a_2) H-C-H at 230-550 ˚C; and (B) 13%Co-0.45%Ru/SiO_2 reduced in (b_1) H_2 at 500˚C (b_2) Ar-H_2 at 500 ˚C (b_3) H-C-H at 230 -500˚C. Reproduced from Ducreux et al. [39] with permission from Institut Français du pétrole.

2.4.2 Activation via the reduction-oxidation-reduction (R-O-R) route

Reduction routes have a critical effect on the performance of cobalt-based catalysts [33, 19, 119-121]. R-O-R cycles are another potential method to improve the catalytic performance of a cobalt catalyst during FTS, where R represents the reduction step and O represents the oxidation step. This may result in: (1) redispersion of the metallic cobalt on the support surface [19]; (2) a higher degree of reduction [121]; (3) modulation of the metal-support interaction [33].

The R-O-R activation method was invented by Kobylinski et al. [117,118] who reported an increase in the catalytic activity of cobalt carbonyl-impregnated catalysts on silica and alumina when they were treated by R-O-R, which was comparable to the activity of Ru-promoted catalysts [119]. Further improvement of the R-O-R activation method was presented by Rytter et al. [122] who denoted a new activation procedure called RXR. X refers to a modifying gas treatment, in which the modifying agent consists of at least one oxidative gas, such as steam, air, CO, CO_2, steam/H_2, CO/H_2, CO followed by air etc. They reported that the treatment in air, steam, steam/H_2, or CO_2 at 300 ˚C improved or stabilized the C_{5+} selectivity; whereas the treatment in H_2/CO = 3 at 300 ˚C or in CO at 300 ˚C followed by in air at 300 ˚C exhibited better catalytic activity than the other oxidative treatments [122].

Hauman et al. [119] demonstrated the effect of R-O-R cycles on the cobalt particle size and dispersion of active species. The authors reported that the average Co_3O_4 particle size decreased from 33 to 9 nm under R-O-R treatment. Further reduction resulted in high metal dispersion of small cobalt crystallites (in the range 3-5 nm) and the reduction was found to be more facile. Oxidation at high oxygen partial pressure (2.3 bar) resulted in smaller cobalt crystallites of about 6 nm. The high-pressure oxidation step led to the rapid break-up of the crystallites and the formation of hollow spheres via the Kirkendall effect.

Cai et al. [123] investigated the use of different oxidizing agents (oxygen and water) during the R-O-R cycle and found that treatment with water vapor at higher evaporator temperatures (100 ˚C) was more efficient in re-dispersing the Co crystallites than treatment in oxygen. It also resulted in smaller crystallites of about 8.1 nm. However, using water as an oxidizer resulted in lower FT activity compared to an R-O-R cycle with oxygen, due to the formation of cobalt silicate that promoted catalyst deactivation. In addition, no re-dispersion was observed for cobalt particles smaller than 11 nm; and it seems that the re-dispersion of cobalt nanoparticles during the oxidation step is strongly dependent on the initial cobalt particle size. Sadasivan et al. [124] reported that the oxidation of Co/MCM-41 nanoparticles (in the size range of 3-29 nm) led to the formation of solid and hollow spheres. Larger particle sizes (29 nm) formed hollow oxide spheres upon oxidation and

were fragmented into small particles during reduction, while smaller particles (<11 nm) did not re-disperse on further reduction.

Mejia et al. [33] investigated the enhancement of activity of FT cobalt-based catalysts by tuning metal-support interactions via R-O-R cycles. Some of these research results are shown in Figure 2.7. The R-O-R cycles increased the activity of Co/TiO_2 and Co/Nb_2O_5 catalysts with the optimum results seen with an oxidation temperature of 200 °C, and a second reduction temperature of 220 °C (Figures 2.7 (A, B, D, E)). The controlled oxidation led hollow cobalt spheres forming via the Kirkendall effect. The second reduction step increased the H_2-uptake for TiO_2 and Nb_2O_5 supported catalysts by two-fold, and slightly decreased the H_2-uptake when using an α-Al_2O_3 support, due to strong metal-support interactions. Tang et al. [120] reported that R-O-R treatment on Co/Al_2O_3 decreased the site density and dispersion of the surface cobalt, which was attributed to sintering of the metal and the formation of irreducible cobalt aluminate. However, the R-O-R treatment increased the CO conversion from 21% to 36% for a $Ru\text{-}Co/Al_2O_3$ catalyst with a marginal increase in methane selectivity. Ruthenium was reported to migrate into the bulk Co which resulted in closer contact between Ru and Co and improved its promotion effect [120]. The R-O-R cycle can be used to regenerate industrial catalysts via re-dispersion of the active phase and could be used as an alternative method to tune the interactions between the metal nanoparticles and the support.

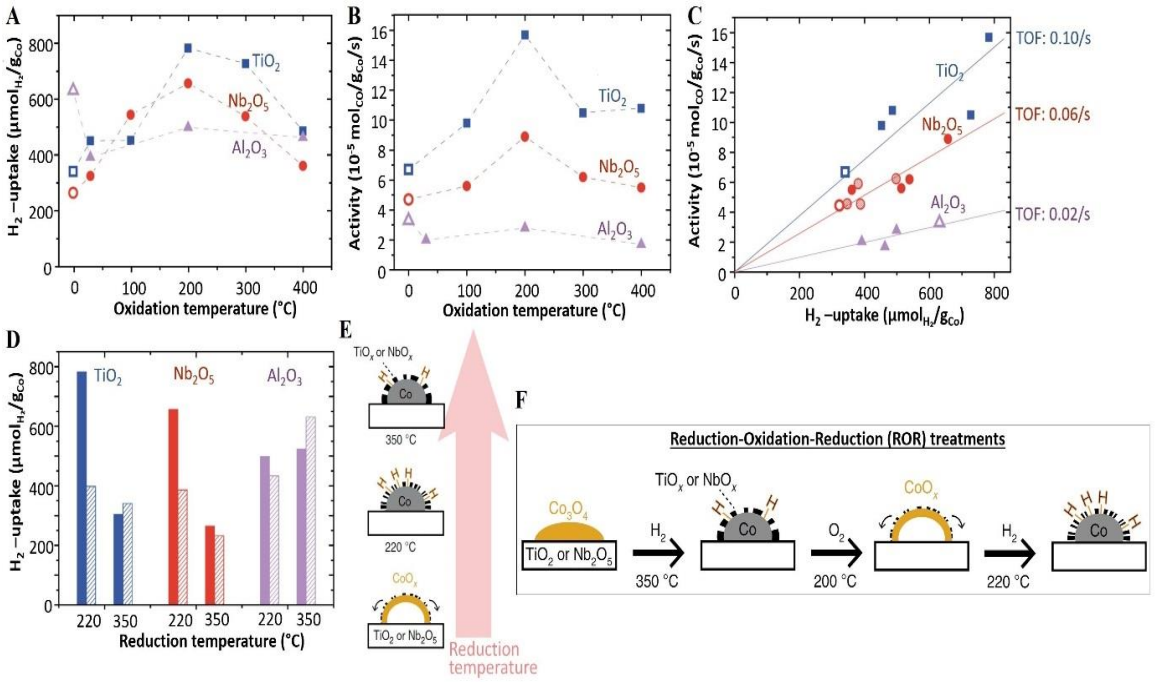

Figure 2. 7: The effect of R-O-R treatments on the exposed cobalt surface area and the catalytic activity: (A) Hydrogen uptake for Co/TiO_2, Co/Nb_2O_5 and $Co/\alpha\text{-}Al_2O_3$ (6%Co loading in each catalyst) after various R-O-R treatments, as determined by H_2-chemisorption; (B) Cobalt-weight-based catalytic activity of Co/TiO_2, Co/Nb_2O_5 and Co/Al_2O_3. (C) Cobalt-weight-based activity as a function of hydrogen uptake for the samples after reduction at 350 °C, followed by oxidation between 30 and 400 °C and reduction at either 220 °C or 250 °C (D) Hydrogen uptake as a function of the second reduction temperature. The dashed bars correspond to the pristine samples after reduction at 220 °C or 350 °C. The solid bars correspond to the samples after reduction at 350 °C followed by oxidation at 200 °C and reduction at 220 or 350 °C (E) Schematic illustration of the effect of the reduction temperature on catalysts supported on reducible oxides (F) Schematic illustration of the effect of R-O-R treatment on cobalt supported on reducible oxides. Reproduced from Mejía et al. [33] with permission from Springer Nature.

2.5 Direct synthesis of metallic Co catalyst without further reduction

H_2 reduction normally operates at a higher temperature, and the reducibility of the catalyst is usually low due to the high cobalt-support interaction [125]. Some researchers [40, 125-128] have tried to eliminate the high temperature reduction step by synthesizing the reduced Co metal catalyst directly which may decrease the complexity and the cost of FTS.

In this regard, Tsubaki and co-workers [40, 128] recently developed a Co/SiO_2 catalyst using the surface impregnation combustion method by using citric acid as both a reductant and a chelating agent. The novel auto combustion method was an interesting attempt to produce uniform and nanostructured metallic cobalt catalysts with a high reduction level [126]. This method was initially developed by the Russian scientists Borovinskaya, Skiniro and Merzhanov [129, 130]. As the metallic Co obtained is highly flammable, catalyst

passivation is conducted at room temperature in diluted oxygen for transfer into the reactor [128]. The Co/SiO_2 catalyst obtained via this method was passivated in 1% O_2 and used directly for FTS (i.e. without further reduction) [40, 128].

The directly synthesized metallic cobalt catalyst exhibits much higher activity than the conventional cobalt catalyst reduced by H_2 at 350 °C for 10 hrs. However, it produced many undesirable products, such as methane and CO_2 (see the results provided in Table 2.4). In a later study, a Ru promoted Co/SiO_2 was prepared by the same research group [128] and used directly for FTS without reduction. The experimental data shows that the addition of a small amount of Ru (1wt%) improved the reducibility and dispersion of the catalyst, which resulted in a significant increase in FTS activity [128]. Thereafter, Zhao et al. [125] created a simple impregnation-carbonation method by introducing glucose as both carbon precursor and reductant to prepare a directly reduced $Co\text{-}C/SiO_2$ catalyst (where C stands for amorphous carbon from the carbonization of glucose). The Co was highly dispersed and used directly in FTS without further reduction (after passivation in diluted oxygen for transfer). It achieved higher catalytic activity, i.e., about two-fold higher, higher CH_4 selectivity and lower C_{5+} selectivity relative to impregnated Co/SiO_2 reduced at 400 ˚C (see Table 2.4). In addition, the smaller Co particle size contributed to the higher selectivity of light hydrocarbons, and the mass of glucose to SiO_2 ratio increased the proportion of Co metal and amorphous carbon that could be placed on the support. Although direct synthesis of reduced Co catalysts favors light hydrocarbon products, the simple impregnation combustion preparation method may have the potential to eliminate the high-temperature reduction step and further simplify the FTS process. It would be interesting to investigate the effect of crystallite size of the metallic Co on catalyst performance.

Table 2. 4: Catalyst characterization and catalytic performance of FTS using directly reduced catalysts.

Catalysts	Preparation and Reduction information	Reducibility (%)	Dispersion (%)	Co Particle size (nm) TEM	FT activity and selectivity				Reaction conditions	Refs.
					CO conv %	Selectivity (%) CH_4	CO_2	C_{5+}		
$15\%C_{N\text{-}reduced}$	Conventional impregnation Co/SiO_2 reduced at 450 ˚C for 10 h in H_2	82	3.1	30	16.7	11.6	1.3	79.2	$H_2/CO=2$, 230 ˚C, 10 bar, 2.38 NL/gcat/h for TOS[a] 15 h.	[40]
$15\%C_{N\text{-}CA\text{-}argon}$	Impregnation combustion method by using citric acid (CA) without reduction	95.2	20.9	3	64.5	40	7.8	43.5		
1%Ru10%Co (CA)	Impregnation combustion method by using citric acid (CA) without reduction, molar ratios of citric acid to nitrates (CA/N) =0.3	___	___	___	41.4	20.5	3.5	59.8	$H_2/CO=2$, 235 ˚C, 10 bar, 2.38 NL/gcat/h	[128]
1%Ru10%Co (FA)	Impregnation combustion method by using formic acid (FA) without reduction, molar ratios of formic acid to nitrates (CA/N) =0.3	___	___	___	38.7	19.4	2.2	65		
10%Co/Q15	Conventional impregnation Co/SiO_2 reduced at 400 ºC for 4 h in H_2	___	2.7	___	28.97	11.22	0.14	82.7	$H_2/CO=2$, 240 ˚C, 10 bar, 4.76 NL/gcat/h, for TOS 10 h	[125]
10%Co-0.5C/Q15	Impregnation-carbonation method by using glucose as both a reductant and carbon precursor without reduction, the mass ratio of glucose to Q15 (SiO_2) is 0.5	___	29.4	___	46.24	32.78	0.29	50.6		

[a] TOS: time on stream

2.6 Effect of other key factors on catalyst activation

The physio-chemical properties of the active phase, specifically shape, size and crystallinity are significant factors that should be optimized during catalyst design. Sections 2.2-2.5 provide a review of the use of different reducing agents and reduction conditions to maximize the dispersion of the most active phase, namely Co(hcp), in order to enhance the

activity of the catalyst. However, dispersion does not only depend on the reduction atmosphere, but also on the overall pretreatments, which includes both the preparation steps and the reduction procedure. The preparation steps include the following: choice of support, preparation method, promoter, and thermal treatment (drying and calcination) conditions. However, these generic issues have been dealt with in many review papers [21,32,37,24,49-54]. This section highlights the effect of the preparation parameters, including pretreatment during catalyst preparation, on the dispersion, reducibility, particle size and active phase of the cobalt catalyst, as well as on catalyst performance during FTS.

Metal-support interactions developed during catalyst preparation are the most significant factor in determining the distribution of the metal nanoparticles across the support surface (dispersion), and the activity of the catalyst [131]. The use of mesoporous or carbon supports have been reported to disperse small cobalt crystallites, due to a defined pore size, which results in high metal dispersion [32,72]. Furthermore, if the preparation conditions are not chosen wisely, they can have a detrimental effect on the catalytic activity as they can induce agglomeration of the metal particles, which results in large Co_3O_4 particles and low metal dispersion [67,132,133]. The performance of cobalt-based FTS seems to be a function of the metal dispersion, crystallite size and the extent of deactivation during FTS [44,45]. Some of these factors are discussed further below.

2.6.1 Cobalt precursors

Numerous studies have demonstrated that the physiochemical properties of cobalt-based catalysts depend on the cobalt precursor and support used [64,73,134-136]. The structure and surface reduction properties of the support are influenced by the nature of the cobalt precursor, which changes the adsorption properties during impregnation by altering the exothermicity of precursor decomposition, which in turn influences the strength of the metal-support interactions [47]. In order to attain highly active cobalt catalysts, the optimal synthesis variables need to be chosen wisely.

Table 2. 5: The catalytic behavior of various cobalt catalysts prepared using different sources of cobalt on CO hydrogenation.

Cobalt source	Catalyst	Reduction conditions		Reduction degree	Dispersion	FT activity and selectivity			Reduction conditions	Reaction Conditions	Refs.
		Reduction agent	T ˚C	%	%	CO conv %	CH_4 sel %	C_{5+} sel %			
Co(N)	10%Co/TiO_2	H_2	250	___	1.4	29.9	15.1	75	H_2 at 250 ˚C, 500 h^{-1}, for 16 h	H_2/CO=2 (10% Ar) at 220˚C, 8 bar, 400 h^{-1}	[134]
Co(A)				___	1.8	24.5	28.5	47.8			
Co(N+A)				___	2.2	36.4	23.4	60.3			
Co(N) + Zn(A)				___	2.3	54.6	14.5	72.1			
Co(N)	10%Co/SiO_2	5%H_2/Ar	400	79	___	29.8	6.6	___	5%H_2/Ar at 400 ˚C	H_2/CO=2 (3% Ar) at 240˚C, 8 bar, 4.8NL/gcat/h	[135]
Co(A)				15	___	6.2	7.6	___			
Co(N+A)				76	___	42.5	6.3	___			
Co(N)	10%Co/0.1%B/TiO_2	H_2	300	42.5	1.7	58	11.5	79.1	H_2, at 300 ˚C, 2000 h^{-1} for 24 h	H_2/CO=2 at 220 ˚C, 8 bar, 350 h^{-1}(of CO)	[70]
Co(Cl)				61	0.8	21	10.1	71.9			
Co(A)				58	2.2	75	12	79			
Co(N)	20%Co/$AlPO_4$	5%H_2/N_2 [b]	400	___	___	57.4	20.6	62.9	5%H_2/N_2 at 400 ˚C for 20 h	H_2/CO=2.02 (9.3% CO_2 and 5% Ar) at 240 ˚C, 20 bar, 2L/gcat/h	[47]
Co(A)				___	___	19.8	22.7	57.4			
Co(Cl)				___	___	17	39.9	36.7			
Co(N)	20%Co/Al_2O_3			___	___	23.3	18.2	65.1			
Co(N)	20%Co/SiO_2	50%H_2/N_2	350	94.77	___	56	27	56	50%H_2/N_2 at 350 or 450 ˚C, 6 L/gcat/h for 12 h	H_2/CO=2 (40% N_2) at 230 ˚C, 10 bar, 7.5L/gcat/h	[138]
Co(A)			450	88.82	___	12	46	52			
Co(Cl)			450	64.24	___	7	52	47			
Co(OH)			350	91.06	___	60	38	59			
Co(N)	10%Co/SBA-15	H2	400	27	20.5	13.2	28.4	46.3	H2, at 400 ˚C, 24L/gcat/h for 10 h	H2/CO=2 (10% Ar) at 220 ˚C, 20 bar, 13.51NL/gcat/h for 20-24 h	[139]
Co(N)	30%Co/SBA-15			88	9.3	33.1	21.3	63.2			
Co(N)	40%Co/SBA-15			89	7.3	30.1	18.5	66.7			
Co(N)	20%Co/SBA-15			62	11.2	23.1	19.5	64.7			
Co(A)	20%Co/SBA-15			28	___	5.5	33.5	35.6			
Co(aa)	20%Co/SBA-15			12	___	5	56.2	1.7			

Co(N): cobalt nitrite; Co(A): cobalt acetate; Co(Cl): cobalt chloride; Co(N+A): cobalt nitrite + cobalt acetate; Zn(A): zinc acetate; Co(OH): cobalt hudroxide; Co(aa): cobalt acetylacetonate

Nitrate precursors are reported to exhibit high catalytic activity and selectivity towards long chain hydrocarbons [47,70,135,137]. Bae et al. [47] reported high CO conversion, high C_{5+} selectivity and low CH_4 selectivity for a catalyst prepared from cobalt nitrate compared to acetate and chloride precursors (see Table 2.5). The nitrate precursor led to facile formation of homogeneous particles and high reducibility, and it seems to be the optimum cobalt precursor. The chloride precursor was reported to form larger Co_3O_4 particles, which led to low metal dispersion and induced chloride impurities during calcination, resulting in pore blockages and poor catalyst activity. In contrast, Li et al. [138] reported a higher CO conversion and C_{5+} selectivity for a catalyst derived from cobalt hydroxide, compared to cobalt nitrate, acetate, and chloride precursors (see Table 2.5).

Panpranot et al. [136] reported that the use of organic precursors (cobalt acetate and cobalt acetylacetonate) results in the formation of extremely small particles that fit into the pores of the support. And mixed compounds may be produced during H_2 reduction, which leads to low CO reactivity [136]. The data in Table 2.5 indicates superior activity for the catalyst prepared using a mixture of nitrate and acetate precursors compared to those prepared using a single precursor. Coville's group reported that the mixing of precursors weakens the metal support interactions, which leads to the formation of large particles that are easily reduced [134]. Iglesia [140] suggested that preparing a catalyst with a high cobalt concentration and site density can be controlled by the reduction of the nitrate precursors introduced via melt and aqueous impregnation methods.

The use of molecular metal precursor complexes, i.e., acetylacetonate, β-diketonate and bismuth (III) salicylate, is currently being investigated to eliminate the traditional solid-state relationships and to reduce the crystallization of the oxides [139,141]. Co/SBA-15 prepared from cobalt acetylacetonate (Co(aa)) displayed the lowest FT activity and C_{5+} selectivity towards high hydrocarbons compared to the nitrate and acetate precursors [139] (see Table 2.5). This was attributed to strong metal-support interactions, which led to the formation of cobalt silicates and low reducibility. The catalyst performance is also a function of cobalt loading (Martínez et al. 2003) (see Table 2.5). Martínez et al. [139] achieved the highest CO conversion with a 30%Co/SBA-15 catalyst due to the high density of the active phase. The density of the active phase seems to be a function of Co loading,

reducibility and metal dispersion [139]. Tavasoli et al. [142] found that an increase in cobalt loading resulted in an increase in the average cobalt cluster size; an improvement in the reducibility of Co_3O_4; a decreased in the cobalt surface interaction with the support and the cobalt dispersion.

2.6.2 Cobalt supports

2.6.2.1 The nature of the support

The macrostructure and microstructure of the support appear to play an important role in how the particles are incorporated and dispersed on the surface, the resulting cobalt crystallite size, and the activity [38, 102, 143,144]. Iglesia [140] found the FTS turnover rates, for the dispersion range of 0.01-0.12, to be independent of the support identity and found a positive correlation between the C_{5+} selectivity and the Co site density. The authors suggest that diffusion constraints decrease chain growth probability and deplete CO within the pellet [140]. Typical industrial supports include high surface area oxides, such as SiO_2, TiO_2 and Al_2O_3 [132, 145,146]. One major drawback associated with metal oxide supports is strong Co-support interaction which results in the formation of irreducible compounds, i.e., Co_2SiO_4, $CoTiO_3$ and $CoAl_2O_4$, that lead to lower Co site densities [147-150]. Elbashir et al. [151] reported that the reduction of Co/Al_2O_3 at 320 ˚C in H_2 did not produce any Co(fcc) or Co(hcp) due to high Co-support interaction, which hindered reduction of the oxides.

The chemical interaction between the support and cobalt nanoparticles may be dependent on the exposed crystal facets of the support. Loedolff et al. [143] reported high metal dispersion of cobalt species when using a hexagonally ordered mesoporous silica support, due to the discrete crystal planes i.e. (100), (110), that allowed specific chemical reactions. Furthermore, the alumina support was found to produce a heterogeneous distribution due to the numerous facets, edges, and corners, and it exhibited lower FT activity compared to the silica supported catalyst [143]. Mesoporous materials favor high cobalt dispersion compared to the conventional oxide supports, due to their narrow pore size distribution [73,152].

Table 2.6 lists the catalytic behavior of various cobalt-based catalysts, which demonstrates the effect of the nature of support material in CO hydrogenation. Jacobs et al. [149] found that the reduction of TiO_2 and Al_2O_3 supported cobalt catalysts is inhibited by greater metal-support interactions, which leads to lower catalytic activity compared to SiO_2 (see Table 2.6). Yaghoobpour et al. [153] found that the synergy between CeO_2 and a binary SiO_2 and TiO_2 mixture resulted in improved FT activity, due to an increase in the bridged-type CO adsorption, which led to lower C_{5+} selectivity relative to ruthenium promoted Co/TiO_2 (see Table 2.6).

The texture and surface acidity of the support have a significant influence on cobalt reducibility, dispersion, and catalytic performance. Bezemer et al. [71] investigated the effect of pH on carbon nanofiber (CN) supported cobalt catalysts. They reported that nucleation occurred exclusively on the support surface when preparing a catalyst with a high pH. This also resulted in highly dispersed cobalt crystallites of about 8 nm after reduction at 350 ˚C, and the catalyst exhibited higher cobalt-specific activity (i.e., about twice as high C_{5+} selectivity and low CH_4 selectivity), than the low-pH sample (see Table 2.6). Furthermore, pH treatment of conventional silica supports (L-SiO_2 and H-SiO_2 in Table 2.6) resulted in similar catalyst selectivity at a similar CO conversion (2%). Pei et al. [154] found an increase in the activity of cobalt supported on activated carbon (AC) doped with SiO_2. The authors [154] reported that doping the AC support with SiO_2 resulted in: (1) inhibited metal agglomeration and significantly improved the catalytic activity (2) promoted the formation of Co_2C, which led to improved selectivity for alcohols (C_6-C_{18}); (3) generated Co(11) species, which facilitated CO insertion.

Carbon-based materials provide an inert surface that weakens the interaction between the support and the metal phase [155, 156]. Tavasoli et al [72] found remarkable FTS activity for cobalt supported on carbon nanotubes (CNT), which surpassed that of a Co/Al_2O_3 catalyst; however, there was a decline in C_{5+} selectivity. Zafari et al. [157] demonstrated the use of reduced graphene oxide (RGO) and graphene nanoparticles (GNs) to support a bimetallic Co-Mn catalyst. The authors found that RGO exhibited higher activity and selectivity towards lower olefins (C_2-C_4) due to the formation of Co_2C and to the high porosity that enhanced the dispersion of Co and Mn when compared to GNs. However, a

typical $CoMn/Al_2O_3$ catalyst exhibits better catalytic activity (higher CO conversion, C_{5+} selectivity and lower CH_4 selectivity) than RGO and GNs supported catalysts (see Table 2.6). Yaghoobpour et al. [153] found that the synergy between CeO_2 and a binary SiO_2 and TiO_2 mixture resulted in improved FT activity due to an increase in the bridged-type CO adsorption which led to lower C_{5+} selectivity relative to ruthenium promoted Co/TiO_2 (see Table 2.6).

Carbon-based supports, together with high pH deposition-precipitation techniques and metal oxide promoters, provide a novel catalyst design to tune the metal-support interactions and increase both the reducibility and the dispersion of the metal species. Commercial catalysts make use of metal oxide supports; therefore, acquiring information on metal-oxide supported catalysts are crucial for the development of effective FT catalysts. Metal oxide supports are associated with relatively strong metal-support interactions and particle growth. The use of promoters and/or low drying and calcination temperatures has been shown to increase the activity and selectivity towards long-chain hydrocarbons, and more detail on this are provided in the following sections. The optimization of catalyst design based on surface science, especially the use of bifunctional catalysts has the potential to lead to another breakthrough in CO or CO_2 hydrogenation in terms of producing special products such as high alcohols and lower olefins.

Table 2. 6: The catalytic behavior of various cobalt catalysts, which demonstrates the effect of the nature of the support material in CO hydrogenation.

Support	Co and promoter loading %	Reduction conditions		Reaction conditions				FT activity and selectivity			Refs.
		Agent & Flow (L/gcat/h)	T °C & Time	H_2/CO	T °C	P bar	GSHV L/gcat/h	CO conv %	CH_4 sel %	C_{5+} sel %	
Al_2O_3	15Co		350, 10h		220	18.9	5	22.7			
SiO_2	15Co	H_2	350, 10h	2	220	24.1	1	64.3	___	___	[149]
TiO_2	10Co		300, 10h		230	24.1	2	58.4			
TiO_2	13Co0.2Ru							23.43	10.32	87.45	
TiO_2	13Co0.2Ru3CeO_2	H_2, 2	400, 20h	2	220	24	2	41.66	15.22	80.69	[153]
SiO_2	13Co0.2Ru3CeO_2							50.46	11.85	83.77	
	15Co							30.2	24	32.8	
	15Co0.2SiO_2							38	13.7	49.3	
AC	15Co2.1SiO_2	10%H_2/Ar	430, 4h	2	220	30	___	52.7	12.3	55.4	[154]
	15Co4.2SiO_2							67.2	12.8	62.8	
	15Co6.3SiO_2							76.6	10.7	65.9	
[a]L-CNF	10.5Co		350, 2h						40	23	
[a]H-CNF	15Co	H_2/He =1/3	350, 2h	2	220	1	___	2	20	53	[71]
[a]L-SiO_2	15Co		600, 2h						40	23	
[a]H-SiO_2	15Co		500, 2h						42	21	
[b]GNS	7.2Co6.9Mn				320			5.4	32	33.2	
[b]RGO	7.8Co7.4Mn	H_2, 1.8	350, 24h	1	320	1	3000 h^{-1}	6.5	29	32	[157]
Al_2O_3	8.3Co4.2Mn				280			37	24	52.6	

[a]L = Low pH; H = high pH; CNF =carbon nanofiber

[b]GNS = graphene nano sheets; RGO = reduced graphene oxide

2.6.2.2 Effect of support pore size

Studies on the effect of the support pore size on FTS activity indicate that support porosity modifies the performance of the catalyst through its effect on the reducibility of the active phase [37,157,158,148]. Arsalanfar et al. [21] reported that the cobalt surface density and dispersion was influenced by the porous structure of the support and that the hydrocarbon selectivity was strongly related to the preparation procedure. Saib et al. [45] reported that the pore size of the silica support significantly influenced the Co_3O_4 crystallite diameter, catalyst dispersion and FT activity. They found that a larger pore size (>10.1 nm) led to the

formation of bigger Co_3O_4 particles, which in turn increased reducibility and decreased the number of active sites on the catalyst surface, which then resulted in a decline in FT activity (see Table 2.7). Xiong et al. [148] investigated the effect of pore size on an alumina supported cobalt catalyst and found that a larger pore size (10-15 nm) resulted in larger Co_3O_4, and decreased the dispersion and reducibility of the Co, which resulted in low FT activity.

Support pore size and surface acidity seem to play a major role in chain growth and product distribution in FT synthesis. Ernst et al. [159] found that a Co/SiO_2 catalyst prepared using the sol-gel technique in acid and base media with a pore diameter less than 4 nm increased both the specific surface area and selectivity to high molecular weight hydrocarbons. In contrast, Kababji et al. [160] reported that small silica pores (<10 nm) promoted the formation of CH_4, while a large pore size increased the probability of long-chain hydrocarbon formation. The modification of silica supports in an acid medium result in microporous catalysts. However, a basic medium promotes more branched polymers; this leads to mesoporous catalytic systems, which are beneficial for CO hydrogenation [159]. Diaz et al. [161] studied the effect of a pore agent and acid treatment on β-silicon carbide in FT synthesis and found that treatment with a pore agent resulted in an increase in the macropore volume, whereas the mesopore volume remained constant. Conversely, treatment with an acid increased the pore volume, due to the removal of metal impurities blocking the SiC pores and promoted reduction of Co. Furthermore, catalysts treated with a pore agent exhibited a higher C_{5+} selectivity, whilst acid treatment promoted cracking of long-chain hydrocarbons and yielded lighter hydrocarbons. However, the CH_4 selectivity of the acid-treated and the untreated catalysts were similar, thus showing that methanation is not a reaction that is acid-site sensitive.

Table 2.7 lists some of the reported data on the effect of pore size and particle size on FTS activity. Support pore sizes between 4-10 nm resulted in Co crystallite sizes of about 3-8 nm. An increase in pore sizes up to 10 nm enhances the FT activity, due to higher metal dispersion. Supports with wide pores (>10 nm) diminish the diffusion resistance and provide a pathway for rapid molecular transfer [46,148]. The interplay between the

crystallite size, pore size and the reduction conditions are discussed further in section 2.6.2.3.

2.6.2.3 Effect of Co crystallite size

CO dissociation reactions are known to be structure-sensitive reactions, with the rates being dependent on the catalyst particle size [162]. A high reduction temperature (> 450 °C) is required to reduce small Co_3O_4 particles [40]. Furthermore, small cobalt crystallites are easily oxidized at elevated pressures; and CO activation becomes more energy intensive, due to the changes in the surface structure [59,163]. Small cobalt crystallites are selective to shorter hydrocarbons, specifically unwanted CH_4 products [59,164]. Den Breejen and co-workers [165] reported a high CH_4 selectivity and lower FT activities for smaller Co crystallites (<6nm) supported on carbon nanofibers reduced in H_2 at 350 ˚C. This was attributed to higher H_2 coverages on the surface of the active sites. Barbier et al. [164] reported that the critical diameter that separates the negative and positive effect on the intrinsic activity for a silica supported cobalt catalyst is 6 nm, with a positive trend for a diameter above 6 nm.

A high reaction temperature or high pressure induces high water partial pressure which increases the formation of Co-support compounds and results in oxidation and sintering of the small cobalt crystallites [149,115,166-168]. Kiss et al. [169] reported the presence of water induced sintering of Co/SiO_2 cobalt crystallites with a size between 5-11 nm, which led to catalyst deactivation. Furthermore, regeneration in H_2 at >400 ˚C and 12 bars decomposed the mixed oxides and recovered small metallic cobalt particles, which suggest that cobalt-silica compounds are formed from small particles. The oxidation of small cobalt crystallites (<4.5 nm) and the formation of irreducible Co-supports compounds during FTS have been identified as the probable cause of the loss in activity during FT [71,170,171].

Table 2. 7: Effect of pore size, and crystallite size on FTS activity.

Catalyst	Pore size	Crystallite size	Reduction degree	Dispersion	FT activity and selectivity			Specification		Ref.
					CO conv	CH_4 sel	C_{5+} sel	Reduction Conditions	Reaction Condition	
	nm	TEM (nm)	%	%	%	%	%			
20%Co/SiO_2	4.6	3	48		44.0	12.0	71.0	H_2, 350 °C for 16 h	H_2/CO=2 15 bar, 220 °C, 0.9 L/gcat/h	[45]
	60	6.7	66		41.0	17.5	69.4			
	10.1	6.9	74		60.0	11.2	74.0			
	14.3	8.3	91		30.0	13.7	72.1			
5%Co/Al_2O_3	15	3.6	33.8	19.8	4.7	14.5	68.7	5% H_2, 350 °C for 10 h	H_2/CO=2 240 °C, 3.6 L/gcat/h	[44]
	18	6.9	46.1	12.7	16.8	13.0	72.0			
	20	9	52.7	10.3	27.7	10.8	74.7			
	23	11.4	56.3	7.4	19.3	10.4	75.8			
	25	12.5	59.3	5.5	13.7	10.2	76.3			
15%Co/SiO_2		6.9			72.6	18.4	64.8	H_2, 400 °C for 5 h	H_2/CO=2, 20 bar, 240 °C, 2.4 L/gcat/h	[172]
		12			56.4	29.2	55.8			
15%Co/MCM-48	2.4	6.8		14.2	25.8	17.79	74.78	H_2, 450°C for 12 h	H_2/CO=2, 230 °C, 10 bars	[46]
15%Co/SBA-15	5.2	8		11.7	59.4	10.97	85.18			
15%Co/SiO_2	10.1	7		23.4	63.2	14.1	80.97			

Cobalt crystallite sizes between 6-10 nm result in high metal dispersion and high FT activity relative to larger ones. However, larger particles result in a high degree of reduction, but lower surface site density, which leads to low FT activity [44,43,162]. Lower production of C_{5+} hydrocarbons has previously been associated with larger crystallite size, due to low metal dispersion [44,45,73,164]. Li et al. [46] and Saib et al. [45] reported a comparable crystallite size for reduced Co/SiO_2 catalysts in H_2 at 450˚C and 350 ˚C, respectively (see Table 2.7). The catalyst reduced at 450 ˚C resulted in higher activity and CH_4 selectivity compared to reduction at 350 ˚C, despite the crystallite size being the same. Park et al. [44] found an alumina supported cobalt catalyst, reduced in 5% H_2 at 350 ˚C, with a crystallite size of about 9 nm, exhibited the highest catalytic activity (see Table 2.7). However, the highest C_{5+} selectivity occurred with a particle size of 12.5 nm, which suggests that the selectivity of long chain hydrocarbons is a function of cobalt particle size and reduction temperature [44].

The use of carbon nanotubes and pH modifiers to control the crystallite size while achieving high metal dispersion, has been demonstrated by Karimi et al. [73]. The authors reported higher FT activity for a functionalized carbon nanotube supported cobalt catalyst with a water surfactant ratio (W/S) of 10, when compared to a catalyst with W/S = 3 or 5. The C_{5+} selectivity was improved by 5%, while the CH_4 selectivity was decreased drastically, i.e., by 44%. This was attributed to the narrow and uniform cobalt distribution with crystallite sizes up to 10 nm. The effect of pH on the crystallite size was further investigated by Klaigaew et al. [173]. They reported that the addition of ethylene glycol to the impregnation solution resulted in a fairly narrow particle size range of 8.3-10.4nm and showed higher activity for FTS.

Reduction conditions and particle size are critical in tuning the product distribution of the Co-based catalyst, while the dispersion of metallic Co is a measure of the activity that could be achieved. Support characteristics, i.e., crystallite size and pore size, have been studied extensively and the optimum pore and crystallite size needed to achieve maximum activity for FTS has been established [45,46,158,174]. Therefore, these parameters can be used as indicators when synthesizing a highly effective FTS catalyst.

2.6.3 Promoters

Promoters have been proven to lower the reduction temperature and improve the reducibility of the catalyst due to hydrogen spillover [14,10,60]. However, promoters must be chosen wisely, as some can poison the surface of the active sites, i.e., Cu [175], and others promote excessive light gas selectivity at high loading, i.e., Pd and Au [60,36,99]. Promoters are used to facilitate the reduction of small cobalt crystals, with the aim of increasing the Co surface site density. However, research indicates that ultra-small crystallites (<2-4.4nm) are more susceptible to oxidation at a higher conversion than larger ones [60]. These oxides can participate in metal sintering, which involves agglomeration of cobalt oxides, and which exacerbates the deactivation rate [99,36,60].

Alkali metal (i.e., Na, K, Li) promotion has been found to be important for use with biomass as a raw material [176] and has been shown to increase the chain growth probability

significantly. Ma et al. [178] studied the performance of promoted Co/AC catalysts and found that K, Ce, and Zr promoters improved the metal dispersion and interaction between the cobalt oxide and AC surface. However, K increased the WGS activity which led to a decline in the FT synthesis activity. Jacobs et al. [149] found that adding metal oxides (B, La, K and Zr) to conventional supports decreased the reducibility of the cobalt and shifted the reduction of Co species to higher temperatures. This is due to increased surface interactions between smaller Co species and the support, which leads to low FT activity.

Eliseev et al. [179] found that alkali metal promotion increased the selectivity of hydrocarbons and increased the concentration of olefins in the gasoline fraction products. Ishida et al. [180] studied the effect of alkali modifiers (Li, Na, K, Cs) on cobalt catalysts for the synthesis of higher alcohols. The authors reported superior catalytic activity and higher alcohol selectivity for the Na-doped catalyst. Sodium (Na) was found to increase surface basicity, decrease the Co nanoparticle size and decrease the reducibility of Co(11) to Co(0), which favored the production of alcohols [180]. Jiao et al. [181] achieved about 94% C_2-C_4 selectivity (at $H_2/CO = 3$) with a bifunctional $ZnCrO_x$/MSAPO composite catalyst, based on the concept of Oxide-Zeolite (OX-ZEO) process. Xie et al. [182] reported higher activity and selectivity towards lower olefins (54%) for a Co/Mn/Na/S catalyst at 250 ˚C and 1 bar. The synergistic effect of metal promoters suppressed CH_4 and CO_2 formation and improved the selectivity towards lower olefins by stimulating the formation of cobalt carbide [182]. In addition, the use of catalysts based on transition metals (Cu, Fe, Co) and noble metals (Rh, Pt, Ru) is widely reported for the synthesis of higher alcohols from CO_2 hydrogenation [102, 183-186].

Although Ni is active for CO hydrogenation, it is not commonly used as an FT catalyst or promoter due to its high selectivity to both methane and short-chain hydrocarbons [17]. Nevertheless, the experimental results proved that Ni can be used as a promoter to reduce the reduction temperature and increase the reducibility of an Al_2O_3 supported Co catalyst [17]. In addition, Rytter et al [187] reported that Ni with a loading of less than 5% could act as a reduction and activation promoter, which resulted in a high catalyst activity and stability. Enger and Holmen [16] summarized the roles of Ni during FTS and concluded

that by increasing the CO/H ratio, the chain growth propagation on Ni can be increased, due to the optimum interaction between the support and Ni.

Diehl and Khodakov [32] reviewed the effect of noble metal (Pd, Pt, Ru and Re) promotion on cobalt-based catalysts and found that noble metals (0.05-0.2 wt%): (1) enhance the reducibility of cobalt; (2) inhibit the formation of Co-support compounds; (3) promote methane formation at high concentrations, (4) crystalize small cobalt particles. Palladium (Pd) exhibited higher hydrogenation activity, but it limited the production of high waxes and hydrocarbons. Pt, Ru and Re enhanced the CO conversion to a greater extent than the hydrocarbon selectivity [32]. Table 2.8 provides a summary of the catalytic effect of a promoter on the reducibility and activity of a cobalt catalyst. Promotion with Re, Ru, Pt, and Ag have a positive effect on the CO conversion and selectivity of cobalt-based catalysts, see Table 2.8. Das et al. [167] achieved maximum C_{5+} selectivity at 0.5% Re promotion, see Table 2.8. Tsubaki et al. [64] found 0.2% Ru to exhibit a higher catalytic effect compared to Pt and Pd (at similar loading). Ma et al. [67] achieved better catalytic performance with 0.84% Re promotion on Co/Al_2O_3 whereas Jacobs et al. [175] found Ag to be a better promoter than Cu, see Table 2.8. Xu et al. [14] reported high catalytic activity for a Co/Al_2O_3 catalyst promoted with 5% Ru compared to promotion with Pt and Pd.

Noble metal promotion seems to have a positive effect on catalytic activity, but should be used at the optimum concentration, in order to improve the hydrocarbon selectivity. In addition, promotion with these metals could result in increased cost of the overall cobalt catalyst design, as they are more expensive than the Co metal (especially Ru and Re). Designing a more active FTS catalyst could improve the overall economics of the process but recycling of these precious metals should be mandatory [32].

Table 2. 8: The effect of promoters on the reducibility and catalytic activity of a cobalt catalyst.

Catalyst	Promoter	Reduction degree	FT activity and selectivity				Reduction conditions	Reaction conditions	Refs.
			CO_2	CO conv	CH_4 sel	C_{5+} sel			
	%	%	%	%	%	%			
10%Co/Al_2O_3		___	___	42.8	8.8	80.8		H_2/CO=2 at 210 ˚C, 8 bar, 6.0 NL/gcat/h	
10%Co/SiO_2	0.5 Re	___	___	40.3	8.7	83.4	H_2, 350 ˚C for 16 h	H_2/CO=2 at 210 ˚C, 8 bar, 4.2 NL/gcat/h	[32]
10%Co/TiO_2		___	___	42.6	8.9	84.8		H_2/CO=2 at 210 ˚C, 8 bar, 3.6 NL/gcat/h	
12%Co/Al_2O_3	___	63.7	0	6.4	27.1	52.2	H_2, 400 ˚C for 8 h	H_2/CO=2 at 240 ˚C, 20 bar and 500 h^{-1}	[14]
	0.5 Ru	86.3	9.3	58.3	15.1	67.4		H_2/CO=2 at 230 ˚C and 20 bar, 500 h^{-1}	
	0.5 Pt	78.9	9.1	61.3	15.6	68			
	0.5 Pd	84.3	7.9	33.1	24.2	57.5			
25%Co/Al_2O_3	___	54.5	0.5	23.7	8.4	85.3	30% H_2/He 350 ˚C, atmospheric P, 4NL/gcat/h for 15 h	H_2/CO=2 at 220 ˚C, 22 bar and 13 NL/gcat/h	[67]
	0.27 Ru	70.7	0.4	33.4	8.1	85.2			
	0.50 Pt	68.4	1.1	25.9	9.2	82.3			
	0.26 Pd	72.1	0.9	22.3	13.8	74.4			
	0.48 Re	67.2	0.4	35.8	7.6	85.5			
15%Co/Al_2O_3	___	___	0.8	28.7	9.6	81.6	30% H_2/He, 350 ˚C, atmospheric P, 4NL/gcat/h for 10 h	H_2/CO=2 at 220 ˚C, 20.3 bar and 4.2NL/gcat/h	[175]
	0.49 Cu	___	0.8	27.9	9.8	77.8			
	1.63 Cu	___	1.5	14.2	15	64.5			
	0.83 Ag	___	1.0	46.7	8.3	82.4			
	2.76 Ag	___	1.1	46.9	7.6	85			
15%Co/Al_2O_3	___	30	1.1	29.8	10.9	85.6	30% H2/He, 350 ˚C, 3.5NL/gcat/h for 10 h	H_2/CO=2 at 220 ˚C, 19.7 bar and 2.1 NL/gcat/h	[167]
	0.2 Re	55	1.3	69.5	10.2	86.2			
	0.5 Re	59	1.4	73.1	10.1	87.5			
	1.0 Re	70	1.5	74.9	11.2	85.9			
10%Co/SiO_2	___	50	1.3	33.5	8.9	___	H_2, 400˚C for 10 h	H_2/CO=2 at 240 ˚C, 10 bar and 4.8 NL/gcat/h	[64]
	0.2 Ru	99.8	4.0	72.3	8.8	___			
	0.2 Pt	5.6	2.8	49.5	13.8	___			
	0.2 Pd	6.3	3.2	57.9	17.8	___			

2.6.4 Thermal treatments: drying and calcination

Drying and calcination are two distinctive steps in the catalyst preparation process that may alter the activity of the catalyst if not done well, particularly with reference to the particle size and the distribution of the metal particles. Calleja et al. [131] reported that the metal distribution of a strongly bonded metal on the support depends on the impregnation conditions, whilst for a weakly bonded metal, the distribution will depend on drying, calcination and reduction conditions. A strong relationship between the support and the metal may result in the formation of unreactive species that inhibit the reduction of cobalt and result in low FTS activity [64,76]. The preparation steps determine the degree of ion exchange, which then defines the obtainable particle size and dispersion [152,188].

2.6.4.1 Drying

Drying is often viewed as a routine step for impregnated catalysts and is mistakenly believed to have minimal (if any) effect on the final catalyst. The variables in the drying phase include atmosphere, temperature, heating rate and time [131]. A few publications have addressed the effect of drying on the distribution of active sites and the Co crystallite size [189-193,131, 119]. Calleja et al. [131] found that: the crystallite size is independent of drying temperature between 100-120 °C; a faster drying rate generates smaller Co crystallite sizes, which results in high metal dispersion and good catalyst performance. Abdouss et al. [192] found the optimum drying conditions for maximum FTS activity to be 120 ℃ and 16 h for a Co-Fe-Mn/MgO catalyst. Van Steen et al. [194] suggested that the use of a low drying temperature and shorter drying time may be a tool for maximizing metal dispersion in Co-based catalysts. In their study, drying at 25 ˚C for 24 h produced a highly active FT catalyst compared to drying at 120 ˚C for 16 h. However, different calcination temperatures were used (300 and 400 ˚C), which could also have had a significant impact on catalytic activity.

The formation of agglomerates upon drying seems to be dependent on the support pore size. Munnik et al [190] prepared cobalt catalysts using three different silica supports, i.e. 3, 8 and 15 nm pore size. The characterization results are shown in Figure 2.8. It indicates that: medium size agglomerates were obtained when drying at 25 °C; homogeneous distributions were obtained at 100 °C, while larger agglomerates were obtained at 150 °C. The structure

of the support plays an important role in the formation of agglomerates: the larger the pore size, the smaller the agglomerates. This can be assigned to the faster drying rate with large pores, especially when drying at 25 °C. Higher activity was observed with catalysts with a homogeneous distribution (achieved by drying at 100 °C), while the agglomerated catalyst exhibited higher C_{5+} selectivity [190]. In addition, Kababji et al. [160] reported a decline in FT activity with an increase in drying and calcination temperature, which was attributed to the aggregation of Co particles, due to sintering and silica migration.

The drying atmosphere has a significant effect on the resulting distribution of the metal particles. Munnik et al. [190] reported that, when using γ-alumina as a support, drying in stagnant air at temperatures above 100 °C resulted in the formation of large agglomerates; while drying in a N_2-atmosphere resulted in a catalyst that is homogeneously distributed, regardless of the temperature. Eggenhuisen et al. [191] obtained a uniform distribution when freeze drying Co/SiO_2 nanoparticles, with an average particle size of 8 nm after calcination in N_2 and 4-6 nm being obtained after decomposition in 1% NO/N_2. Homogeneous distributions of clusters up to 400 nm were obtained with the conventional drying method, but not with freeze drying which restricts precursor mobility during the drying step [191].

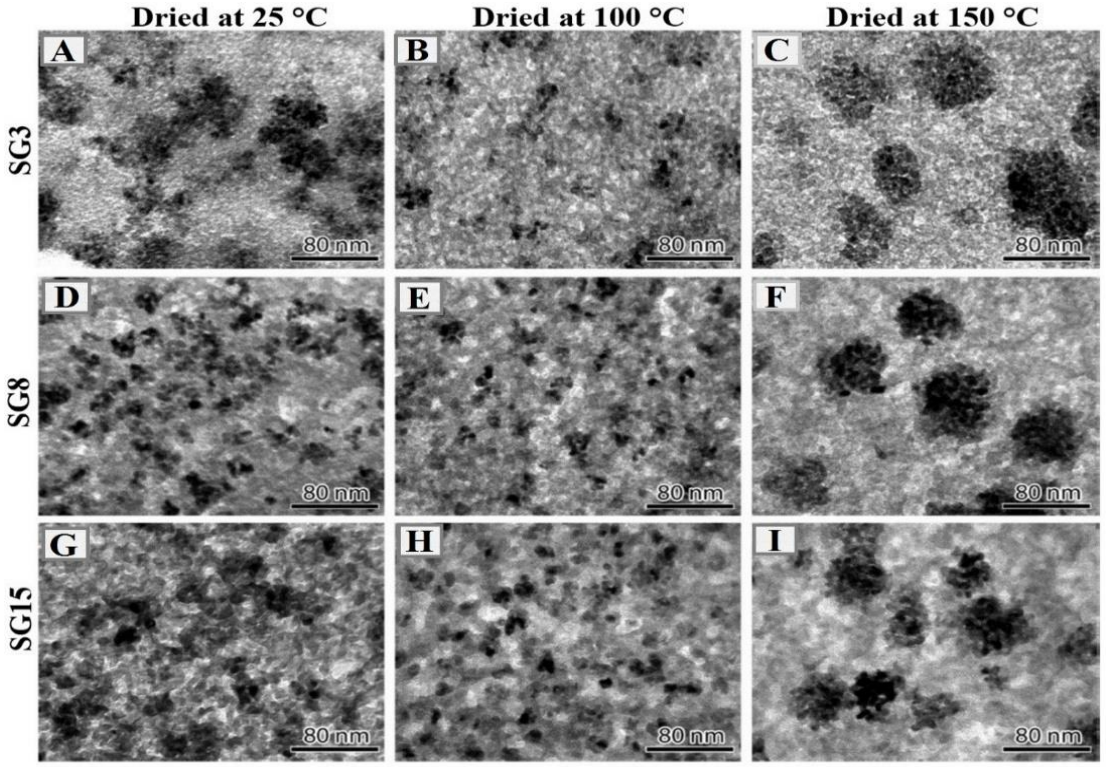

Figure 2. 8: TEM of ex-nitrate cobalt catalysts synthesized using three different silica gels and three different drying temperatures, followed by calcination in N_2. Top row: silica gel with 3 nm pores; Middle row: silica gel with 8 nm pores; Bottom row: silica gel with 15 nm pores. Reproduced from Munnik et al. [190] with permission from the American Chemical Society.

In summary, a mild drying temperature (<120 °C) produces a homogeneous distribution and prevents agglomeration of the crystallite size. Faster drying rates and a small pore size results in high metal dispersion and good catalyst activity. More studies should be done to adequately address the issue of the effect of the drying atmosphere (air, N_2 or vacuum) and the drying rate, in order to provide a basis for a rational design of the drying process. Adsorption occurs during impregnation, therefore, the impact that drying has on the catalyst is dependent on how the metal is bonded with the support.

2.6.4.2 Calcination

Calcination is aimed at decomposing the cobalt precursor to Co_3O_4. Optimization of the calcination process can be achieved by controlling the calcination temperature, the time, and the calcination atmosphere [21,195-198]. Kababji et al. [160] studied the effect of the

calcination and drying temperature on Co/SiO_2 catalysts and found that the catalyst that was calcined at 300 ˚C and dried at room temperature over 24 h exhibited higher FTS activity compared to catalysts that were calcined and dried at a higher temperature. Van Steen et al. [194] reported that calcination at temperatures up to 350 ˚C destroyed the strongly bonded cobalt species, whereas higher calcination temperatures (> 350 ˚C) resulted in the formation of mixed surface compounds that were more difficult to reduce. Furthermore, calcination at a higher temperature has been reported to result in agglomeration of cobalt crystallites, which may lead to low Co site density [126,119,38,199,200]. In addition, Koizumi et al. [200] reported higher FT activity for a Co/SiO_2 catalyst treated with a chelating agent of trans-1,2-diaminocyclohexane-N,N,N',N'-tetraacetic acid ($Co/CyDTA/SiO_2$), calcined at 450 ˚C, with respect to the untreated Co/SiO_2 catalyst. The $Co/CyDTA/SiO_2$ catalyst afforded a 10 C-mol% lower CH_4 selectivity and comparable C_{5+} hydrocarbon selectivity to the untreated Co/SiO_2 catalyst. These results indicate that treatment with the chelating agent during catalyst preparation could suppress the agglomeration of Co_3O_4 species when the catalyst is calcined at higher temperatures and improve the catalyst activity to a greater extent [200].

Jung et al. [201] investigated the influence of calcination atmosphere on the performance of Co/Al_2O_3 catalysts. They reported the following: calcination of catalysts in H_2 yielded both Co(hcp) and Co(fcc), resulting in high activity towards FTS; whilst air calcination led to the formation of Co(fcc) and slightly lower activity (see Table 2.9). Akbari et al. [202] found that the calcination of Fe-Co-MgO in air resulted in smaller particle sizes, which exhibited higher FT activity compared to calcination in Ar. However, the high activity encouraged the formation of CH_4 and CO_2 due to rapid oxidation of the small particles during FTS. Aw et al. [203] found that the decomposition of Co/Ni precursors in the presence of NO gas produced smaller particles, thus enabling better dispersion. Sun et al. [204] reported that calcination of a Co/mesoHZSM-5 catalyst in 1 vol% NO/Ar led to a significant increase in cobalt dispersion and a decrease in catalyst reducibility due to strong metal-support interactions when compared to calcination in air or N_2 flow. The catalyst treated in stagnant air showed the highest activity and selectivity in FTS, due to the increase in the number of small Co_3O_4 particles and cobalt reducibility (see Table 2.9) [204].

Li and Coville [70] reported that larger Co_3O_4 is easily reduced relative to smaller cobalt clusters; however, large cobalt particles exhibit lower FT activity, due to low metal dispersion. A study on the effect of the calcination temperature on the performance of Co-Pt-ZrO_2/Al_2O_3, was done by Sun et al. [198]. It indicated that the support pore size increases with an increase in the calcination temperature from 300-600 ˚C, and this leads to the formation of larger Co_3O_4 particles and low metal dispersion. The data shown in Table 2.9 suggests that: activity depends on Co dispersion rather than reducibility and dispersion depends on the calcination temperature; and the metal-support interactions. An increase in calcination temperature led to a decrease in metal dispersion for all cobalt catalysts supported on SiO_2 and Al_2O_3. Eliminating the calcination step results in even lower metal dispersion and FT activity for boron promoted Co/TiO_2 catalysts, (see Table 2.9).

The calcination temperature can be utilized to tune the product distribution of the FT process. Arsalanfar et al. [205] investigated the effect of calcination conditions on a Co-Ni/Al_2O_3 catalyst by varying the calcination temperature from 500-700 ˚C and the calcination time from 4-10 h. They found that calcinating for 6 h at 550 ˚C delivered better catalytic performance for the production of lower olefins (C_2-C_4) [205]. A further increase in calcination temperature caused the support to crystallize, which led to pore collapse and consequent loss of support area [205]. Tao et al. [195] agreed with this result. They reported that increasing the calcination temperature up to 500 ˚C significantly increased the olefin-paraffin ratio in C_2-C_4, whilst a higher calcinating temperature suppressed the formation of CH_4, which results in increased C_{5+} selectivity [195]. Mirzaei et al. [206] found that the optimum reduction and calcination conditions to maximize the production of lower olefins from Co/Cr were, reduction at 450 ˚C, 1 bar, at an ageing time of 2 h; and calcination at 600 ˚C for 6 h. Cho et al. [207] decreased the acidity of Pd-loaded mesoporous alumina xerogel catalysts by increasing the calcination temperature beyond 700 ˚C, which favored the selectivity of middle distillates during wax hydrocracking. Kamath et al. [208] reported that calcined catalysts had a higher alpha-value (0.87-0.92) compared to uncalcined catalysts (0.79-0.81), due to lower metal-support interactions that were beneficial for FT synthesis.

Briefly, a low calcination temperature (<350 °C) removes the decomposed products of the precursor in metal oxides supports efficiently, while maximizing metal dispersion. Carbon-based supports and bimetallic supports seem to require a higher calcination temperature to achieve high activity enhancement than conversional oxide supports. A high calcination temperature (>500) results in loss of support weight and agglomeration of cobalt particles, which results in catalyst deactivation. The data provided in Table 2.9 and Figure 2.8 indicate the importance of the phenomena occurring during the drying and calcination steps, therefore, they should be given careful consideration when preparing a catalyst.

Table 2. 9: Summary of the catalytic properties of cobalt-based catalysts as a function of the calcination temperature and calcination medium.

Catalyst	Calcination atmosphere				Reduction degree	Dispersion	FT activity and selectivity			Reduction conditions	Reaction conditions	Refs.
	T	Medium	Flow rate	T			CO conv	CH_4 sel	C_{5+} sel			
	°C		h^{-1}	H	%	%	%	%	%			
10%Co/Al_2O_3	20	air		5	54	10	___	___	45	H_2 at 450 °C, 1 bar, 100 h^{-1} for 5 h	H_2/CO = 2, at 210-230 °C, 1 bar, 100 h^{-1} and each test run for 5 h	[209]
	100				51	6.9	___	___	62.2			
	200				49	5.4	___	___	59			
	300				50	5.1	___	___	57.5			
	400				45	3.3	___	___	59.2			
10%Co/SiO_2	20				65	10.3	___	___	66.6			
	100				60	5	___	___	78.3			
	200				59	3.9	___	___	70.7			
	300				56	3	___	___	67.9			
	400				52	1.6	___	___	69.9			
10%Co/0,1%B/TiO_2	without calcination				40.5	0.9	28.5	15.6	70.2	H_2, 300 °C, 1 bar, 2000 h^{-1} for 16 h	H_2/CO = 2, at 250 °C, 8 bar, 350 h-1 for TOS > 400 h	[70]
	200	air	2000	16	51	1.95	49	11.2	76.1			
	300				42.5	1.71	43	11.5	79.1			
	350				40.9	1.69	39	13.2	75.3			
	400				37.6	1.42	35	19	66			
5%Co/SiO_2	450	static air	0	4	85	___	___	7.1	77.3	H_2, 500 °C, 6 h	H_2/CO = 1.88 at 230 °C, 11 bar, 4.78 NL/gcat/h	[210]
5%NTA-Co/SiO_2					85			8.4	72.4			
5%EDTA-Co/SiO_2					12			7.4	75.2			
5%CyDTA-Co/SiO_2					8			10.8	67.9			
15%Co/Al_2O_3	400	H_2	1500	4	___	29.8	58.9	2.3	97.2	5% H_2/N_2, 450 °C for 12 h,	H_2/CO = 2 at 230 °C, 20 bar, 2300 h^{-1}	[201]
15%Co/Ru/Al_2O_3					___	22.8	82.7	3.2	96.2			
15%Co/Al_2O_3		air			___	12.4	50.0	2.6	97.0			
15%Co/Ru/Al_2O_3					___	12.1	79.3	3.6	95.7			
10% Co/meso HZSM-5	350	static air	0	1	28		36	13.5	74	H_2, 400 °C, 1 bar, 6.38 NL/gcat/h for 10 h,	H_2/CO = 1 at 240 °C, 15 bar, 6.38 NL/gcat/h	[204]
		air	4500		34		32.1	14.8	71.7			
		N_2	4500		45		27.8	15.5	70.8			
		1%NO/Ar	4500		___		28.5	18.1	66.8			

2.7 Co phases

The structure of the cobalt catalyst evolves during the reduction and reaction procedures and is very sensitive to these conditions. Co_3O_4 that is present in a freshly calcined catalyst is reduced to CoO, and then to metallic Co, either fcc or hcp, depending on the reduction atmosphere [47,63,69]. (See section 2.2-2.5). It is well established that metallic Co is the active phase that enhances C_{5+} selectivity in Co-based FTS, with Co(hcp) being more active than Co(fcc) [24,48]. Ducreux et al. [39] and Gnanamani et al. [48] both reported that the catalyst containing predominately Co(hcp) stacking increased the FTS catalytic activity significantly. Elbashir et al. [170] reported that amorphous Co or poorly organized Co(hcp) exhibit higher intrinsic activity compared to Co(fcc), as there are more surface defects (corners and edges). Cobalt carbides have been reported to form in the presence of CO during reduction and reaction and can transform back to metallic Co(hcp) in an H_2 atmosphere at temperatures above 150 ˚C or under realistic FT synthesis conditions, which results in enhanced FT activity [75,211,212]. Other Co phases may be formed during the high-pressure FT reaction include the formation of Co-support compounds, which play a major role in the reducibility and activity of Co-based catalysts [155,156].

The oxidation state of cobalt is determined by the reduction conditions and the reduction agent employed. Low temperature reduction predominately results in CoO, which is believed to be inactive for the FT reaction [166,213,214]. However, Melaet et al. [215] reported a two-fold enhancement for CO hydrogenation and a ten-fold enhancement for CO_2 hydrogenation for a Co/TiO_2 catalyst reduced at 250 ˚C in H_2 compared to Co/TiO_2 reduced in H_2 at 450 ˚C. The metal/metal oxide interaction produced a highly active interface with the TiO_2 support, which enhanced the activity of the catalysts, which was more selective to unsaturated hydrocarbons. Wolf et al. [177] investigated the reactivity of mixed metal (Al, Ti) cobalt oxides in FT synthesis and found that cobalt titanate catalyzes the WGS, while an increase in CO_2 selectivity was observed at temperatures above 325 ˚C. The activity of the CoO is still unclear, there is not much literature available as yet.

Cobalt carbides (Co_2C and Co_3C) are known to be inactive for the synthesis of long-chain hydrocarbons for Co-FTS, and to favor methanation. Carbidization (carbide formation) has previously been postulated as being one of the mechanisms that might be responsible for

the deactivation of Co-based catalysts [212,216,132]. Earlier work done by Weller et al. [211] on a cobalt-theoria-kieselguhr catalyst demonstrated that bulk cobalt carbide is catalytically inactive for FTS and that the hydrogenation of carburized catalysts produces metallic cobalt with hcp stacking. Jalama et al. [199] reported that the use of low partial pressure CO, such as 5% CO in He and a high temperature during reduction inhibited the formation of cobalt carbide, which resulted in better catalytic performance. De la Pena O'Shea et al. [31] reported that the presence of H_2 in syngas minimizes the deposition of carbon during the reduction of Co/SiO_2 with syngas, resulting in five times the activity compared to the H_2-reduced catalyst.

A DFT study and the experimental work done by Zhong et al. (106) both demonstrated that Co_2C nanoprisms with exposed (101) and (020) facets exhibit high selectivity towards lower olefins and low methane production. The conventional FT to olefin (FTO) process used for direct production of olefins from syngas derived from coal, biomass and natural gas follows the Anderson-Schulz-Flory distribution, which is characterized by an undesirable 29.2% methane fraction (106). The production of lower olefins from a Co_2C nanostructure, with preference exposure to (101), and (020) facets provide a solution for the unwanted high methane selectivity, while enhancing the formation of unsaturated products [106,46]. Xie et al. [182] found that the synergy between Na and S in a Co/Mn/Na/S catalyst improved the selectivity of lower olefins, and about 54% olefin selectivity was achieved at 240 ˚C and 1 bar. A further increase in pressure (10 bar) was found to shift selectivity towards long-chain hydrocarbons (30% olefins, 59% fuels).

Pei et al. [154] reported that the promotion of activated carbon supports with SiO_2 or Al_2O_3 resulted in direct synthesis of high alcohols, due to the formation of the Co_2C phase. The synergy between the active Co_2C sites and the active Co sites promoted the selectivity of linear alcohols (C_1-C_{18}). Graham et al. [217] reported higher alcohol selectivity on cobalt supported on hydrothermal carbon spheres with partially graphitized surfaces, compared to conventional Al_2O_3. Even though the role of Co_2C in FTS is still a mystery, the use of Co_2C to produce lower olefins and higher alcohols should provide a basis for the design of highly efficient next generation FTS and FTO catalyst.

2.8 Concluding remarks and perspectives

2.8.1 Concluding remarks

Structural changes and surface orientation induced by catalyst pre-treatment processes are key factors to enhanced catalyst activity and stability. This review summarizes the effect of traditional and recently developed pre-treatments with the aim of identifying methods that can optimize the catalyst performance by producing a high cobalt concentration and site density with the right crystallite size.

The production of C_{5+} hydrocarbons via FTS is the crucial design criterion for both catalyst preparation and pre-treatment. The catalyst is usually reduced in H_2 to form metallic cobalt that exhibit good FTS activity and favours the production of long chain hydrocarbons. The structure (i.e., Co(hcp) or Co(fcc)) and the amount (site density) of the metallic cobalt are a function of the activation temperature. The hcp phase is more stable at a low temperature, whilst fcc prefers a high temperature and delivers superior catalytic activity and selectivity for FTS compared to Co(fcc).

Co_2C shows a promising catalytic effect for use in the hydrogenation of CO to high value-added chemicals, such as low olefins and higher oxygenates. Changing the activation atmosphere from H_2 to either CO or syngas, can promote the formation of Co_2C, which inhibits the reaction of CO hydrogenation towards C_{5+} hydrocarbons and is selective to lower olefins and oxygenates. Co_2C can be transformed back to Co(hcp) in H_2 at the normal FT operating temperature, which provides means to produce more active cobalt facets using a combination of pre-treatment methods.

Multiple step pre-treatment cycles (i.e., a combination of different activation methods used in a series) enhances the activity of cobalt catalysts. Structural modifications using three-step (H-C-H) cycles and two-step (C-H) reduction methods increase the formation of Co(hcp) which leads to improved metal dispersion and enhanced catalytic performance. R-O-R cycles promotes the fragmentation of large cobalt particles resulting in cobalt re-dispersion of smaller cobalt nanocrystals; therefore, it could be used to regenerate industrial catalysts and reverse metal sintering.

For a small-scale FT plant, cost concerns push for processes to eliminate the expensive and high temperature pure H_2 reduction step. Two possible solutions are highlighted. One is to activate the catalyst using the same syngas used for the FT reaction; however, contradictory results have been reported, which suggests the need for further research to support this approach. The other solution is to synthesize the metallic Co catalyst and use it directly without any further catalyst activation. Both methods have the potential to decrease the complexity and the cost of FTS.

We also compared and summarized other key factors that govern the reducibility and the activity of the catalyst. A catalyst prepared from cobalt nitrate and mixed precursors (cobalt nitrate + cobalt acetate) exhibits higher catalytic activity when compared to nitrate acetate, chloride and organic precursors. Metal oxide supports are preferred for direct synthesis of long chain hydrocarbons from syngas. However, they are widely associated with strong metal-support interactions and the formation of irreducible compounds, which impacts negatively on catalyst performance. As ideal inert materials, carbon-based supports limit the support-metal interactions and restrict the growth and sintering of metal particles but produce significant amounts of carbon dioxide and methane. Selectivity control remains one of the most difficult, but most important challenges in cobalt FTS. Acid/base treatments could provide a solution to reduce methane production, meanwhile, increase the selectivity of higher molecular weight products. In general, promoters decrease the reduction temperature and improve the reducibility of the catalyst. Metal oxide promoters or bimetallic catalysts provide an alternative method for converting syngas to lower olefins due to the synergy between the metals and the support, which favours the formation of Co_2C. High drying and calcination temperatures result in the agglomeration of the metal particles, while low temperature drying and calcination in air or in H_2 atmosphere limits agglomeration of the cobalt particles, which leads to a homogeneous distribution.

2.8.2 Perspectives

The pre-treatment process affects the dispersion, reducibility, active phases and particle size of the cobalt-based catalyst significantly, and consequently tunes the FTS product spectrums to the production of C_{5+} products, low olefins or higher oxygenates. The standard

H_2 reduction process of FT cobalt catalysts has been under review for decades; however, the optimal activation conditions for both CO and syngas activation (such as the temperature, pressure and CO/H_2 ratio) have not been studied comprehensively. The pre-treatment methods discussed in this work are still under study, therefore, we strongly advise that more research work be done on the use of the new activation agents and reduction procedures, in order to formulate a rational operation design that can be used to successfully activate cobalt catalysts for high activity and targeted product selectivity.

Other suggestions would be the use of syngas and CO activation with the aim of producing value-added chemicals (such as low olefins and high oxygenates) via CO hydrogenation, and the use of bifunctional catalysts to promote the formation of the Co_2C phase to produce high alcohols and hydrocarbons via CO_2 hydrogenation.

More attention should be paid to catalyst preparation such as the use of acid/base treatments (pH deposition-precipitation techniques, polar and non-polar solvents and chelating agents), in order to maximize cobalt dispersion and selectivity to long chain hydrocarbons and to lower the methane production; thermal treatments during drying and calcination procedures to enhance the dispersion of the active phase; functionalized mesoporous or carbon-based supports to control the cobalt crystallite size and to achieve a homogeneous distribution, which is beneficial for cobalt FTS.

2.9 Acknowledgements

The authors are grateful for the support received from the University of South Africa (UNISA), the National Research Foundation (NRF), the South African Research Chairs Initiative (SARChI), the Technology and Human Resources for Industry Programme (THRIP), the South African National Energy Research Institute (SANERI), the Technology Innovation Agency (TIA) and the Department of Science and Technology (DST).

2.10 References

[1] Liu Y, Luo J, Girleanu M, Ersen O, Pham-huu C, Meny C. Efficient hierarchically structured composites containing cobalt catalyst for clean synthetic fuel production from Fischer–Tropsch synthesis. J Catal 2014; 318: 179–192. https://doi.org/10.1016/j.jcat.2014.08.006.

[2] Hu J, Yu F, Lu Y. Application of Fischer–Tropsch Synthesis in biomass to liquid conversion. Catal. 2012; 2: 303–3. https://doi.org/10.3390/catal2020303.

[3] Klavins M, Bisters V, Burlakovs J. Small scale gasification application and perspectives in circular economy. Env. Clim. Tech. 2018; 22: 42–54. DOI: 10.2478/rtuect-2018-0003.

[4] Bocci E, Sisinni M, Moneti M, Vecchione L, Di Carlo A, Villarini M. State of art of small-scale biomass gasification power systems: A review of the different typologies. Energy Proc. 2014; 45: 247–256. https://doi.org/10.1016/j.egypro.2014.01.027.

[5] Ail SS, Dasappa S. Biomass to liquid transportation fuel via Fischer Tropsch synthesis–Technology review and current scenario. Renew. Sust. Energy 2016; 58: 267–286. https://doi.org/10.1016/j.rser.2015.12.143.

[6] Galadima A, Muraza O. Waste to liquid fuels: potency, progress and challenges. Int. J Energy Res. 2015; 39: 1451–1478. https://doi.org/10.1002/er.3360.

[7] Masters C. The Fischer-Tropsch reaction. Adv. Org. Chem. 1979; 17: 61–103. https://doi.org/10.1016/S0065-3055(08)60321-4.

[8] He M, Xiao B, Hu Z, Liu S, Guo X, Luo S. Syngas production from catalytic gasification of waste polyethylene: Influence of temperature on gas yield and composition. Int. J. Hydrogen Energy 2009; 34: 1342–1348. https://doi.org/10.1016/j.ijhydene.2008.12.023.

[9] Shafer WD, Gnanamani MK, Graham UM, Yang J, Masuku CM, Jacobs G, Davis BH. Fischer–Tropsch: Product selectivity–the fingerprint of synthetic fuels. Catal. 2009; 9: 259. https://doi.org/10.3390/catal9030259.

[10] Wang S, Yin Q, Guo J, Ru B, Zhu L. Improved Fischer–Tropsch synthesis for gasoline over Ru, Ni promoted Co/HZSM-5 catalysts. Fuel 2013; 108: 597–603. https://doi.org/10.1016/j.fuel.2013.02.021.

[11] Jahangiri H, Bennett J, Mahjoubi P, Wilson K, Gu S. A review of advanced catalyst development for Fischer-Tropsch synthesis of hydrocarbons from biomass derived syngas. Catal. Sci. Technol. 2014; 4: 2210–29. DOI: 10.1039/C4CY00327F.

[12] Yao Y, Liu X, Hildebrandt D, Glasser D. Fischer−Tropsch synthesis using $H_2/CO/CO_2$ syngas mixtures: A comparison of paraffin to olefin ratios for iron and cobalt based catalysts. Appl. Catal. A Gen. 2012; 433–434: 58–68. https://doi.org/10.1016/j.apcata.2012.04.041.

[13] Martínez-Vargas DX, Sandoval-Rangel L, Campuzano-Calderon O, Romero-Flores M, Lozano FJ, Nigam KDP, Mendoza A, Montesinos-Castellanos A. Recent advances in bifunctional catalysts for the Fischer–Tropsch Process: One-stage production of liquid hydrocarbons from syngas. Ind. Eng. Chem. Res. 2019; 58: 15872-15901. https://doi.org/10.1021/acs.iecr.9b01141.

[14] Xu D, Li W, Duan H, Ge Q, Xu H. Reaction performance and characterization of Co/Al_2O_3 Fischer–Tropsch catalysts promoted with Pt, Pd and Ru. Catal. Lett. 2005; 102: 229–235. https://doi.org/10.1007/s10562-005-5861-7.

[15] Gao J, Liu Q, Gu F, Liu B, Zhong Z, Su F, Recent advances in methanation catalysts for the production of synthetic natural gas. RSC Adv. 2015; 5: 22759–22776. DOI: 10.1039/C4RA16114A.

[16] Enger BC, Holmen A. Nickel and Fischer-Tropsch synthesis. Catal. Rev. 2012; 54: 437-488. https://doi.org/10.1080/01614940.2012.670088.

[17] Voss GJB, RlØystad JB, Voronov A, RØnning M, The state of nickel as promotor in cobalt Fischer–Tropsch synthesis catalysts. Top. Catal. 2015; 58: 896-904. https://doi.org/10.1007/s11244-015-0456-z.

[18] Rytter E, Skagseth TH, Eri S, Sjastad AO, Cobalt Fischer-Tropsch catalysts using nickel promoter as a rhenium substitute to suppress deactivation. Ind. Eng. Chem. Res. 2010; 49: 4140–4148. https://doi.org/10.1021/ie100308f.

[19] Van de Loosdrecht J, Botes FG, Ciobica IM, Ferreira AC, Gibson P, Moodley DJ, Saib AM, Visagie JL, Weststrate CJ, Niemantsverdriet JW. Chapter 7.20. Fischer-Tropsch synthesis: Catalysts and chemistry. In: Reedijk J, Poeppelmeier K, editors. Comp. Inorg. Chem. II. 2013; 7: 525-557. 10.1016/B978-0-08-097774-4.00729-4.

[20] Dry ME. FT catalysts. Studies in Surface Science and Catalysis 152, 2004; 533–600. https://doi.org/10.1016/S0167-2991(04)80464-6.

[21] Arsalanfar M, Mirzaei AA, Bozorgzadeh HR, Samimi A. A review of Fischer-Tropsch synthesis on the cobalt based catalysts. Phys. Chem. Res. 2014; 2: 179–201. 10.22036/PCR.2014.5786.

[22] Xing C, Ai P, Zhang P, Gao X, Yang R, Yamane N. Fischer–Tropsch synthesis on impregnated cobalt-based catalysts: New insights into the effect of impregnation solutions and pH value. J. Energy Chem. 2016; 25: 994–1000. https://doi.org/10.1016/j.jechem.2016.09.008.

[23] Yao Y, Hildebrandt D, Glasser D, Liu X. Fischer−Tropsch synthesis using $H_2/CO/CO_2$ syngas mixtures over a cobalt catalyst. Ind. Eng. Chem. Res. 2010; 49: 11061–11066. https://doi.org/10.1021/ie100414y.

[24] Liu J, Wang P, Xu W, Hensen EJM. Particle size and crystal phase effects in Fischer−Tropsch catalysts. Eng. 2017; 3: 467–476. https://doi.org/10.1016/J.ENG.2017.04.012.

[25] Vosoughi V, Badoga S, Dalai AK, Abatzoglou N. Modification of mesoporous alumina as a support for cobalt-based catalyst in Fischer-Tropsch synthesis. Fuel Proc. Technol. 2017; 162: 55–65. https://doi.org/10.1016/j.fuproc.2017.03.029.

[26] Cui X, Xu J, Zhang C, Yang Y, Gao P, Wu B, Li Y. Effect of pretreatment on precipitated Fe–Mo Fischer–Tropsch catalysts: Morphology, carburization, and catalytic performance. J. Catal. 2011; 282: 35–46. https://doi.org/10.1016/j.jcat.2011.05.020.

[27] Herranz T, Rojas S, Pérez-Alonso FJ, Ojeda M, Terreros P, Fierro JLG. Genesis of iron carbides and their role in the synthesis of hydrocarbons from synthesis gas. J. Catal. 2006; 243: 199–211. https://doi.org/10.1016/j.jcat.2006.07.012.

[28] Jalama K, Kabuba J, Xiong H, Jewell LL. Co/TiO_2 Fischer – Tropsch catalyst activation by synthesis gas. Catal. Comm. 2012; 17: 154–9. https://doi.org/10.1016/j.catcom.2011.10.029.

[29] Bartholomew CH, Stoker MW, Mansker L, Datye A. Effects of pretreatment, reaction, and promoter on microphase structure and Fischer-Tropsch activity of precipitated iron catalysts. Studies Surf. Sci. Catal. 1999; 126: 265–272. https://doi.org/10.1016/S0167-2991(99)80475-3.

[30] Dai X, Yu C. Effects of pretreatment and reduction on the Co/Al_2O_3 catalyst for CO hydrogenation. J. Nat. Gas Chem. 2008; 17: 288–292. https://doi.org/10.1016/S1003-9953(08)60066-3.

[31] De la Peña O'Shea VA, Campos-Martı´n JM, Fierro JLG. Strong enhancement of the Fischer–Tropsch synthesis on a Co/SiO2 catalyst activate in syngas mixture. Catal. Comm. 2004; 5: 635–638. https://doi.org/10.1016/j.catcom.2004.08.005.

[32] Deihl F, Khodakov AY. Promotion of cobalt Fischer-Tropsch catalysts with noble metals: A review. Oil Gas Sci. Technol. 2008; 64: 11–24. https://doi.org/10.2516/ogst:2008040.

[33] Mejía CH, Van Deelen TW, De Jong KP. Activity enhancement of cobalt catalysts by tuning metal-support interactions. Nat. Commun. 2018; 9: 1-8. https://doi.org/10.1038/s41467-018-06903-w.

[34] Petersen AP, Claeys M, Kooyman PJ, Van Steen E. Cobalt-Based Fischer–Tropsch Synthesis: A kinetic evaluation of metal–support interactions using an inverse model system. Catal. 2019; 9: 794. https://doi.org/10.3390/catal9100794.

[35] Garces LJ, Hincapie B, Zerger R, Suib SL. The effect of temperature and support on the reduction of cobalt oxide: An in situ X‑ray diff raction study. J. Phys. Chem. C. 2015; 119: 5484–549. https://doi.org/10.1021/jp5124184.

[36] Sukkathanyawat H, Tungkamani S. Promoter effect on the physico-chemical properties of cobalt based catalyst for CO hydrogenation. Energy Procedia. 2015; 79: 372–377. https://doi.org/10.1016/j.egypro.2015.11.505.

[37] Fu T, Li Z. Review of recent development in Co-based catalysts supported on carbon materials for Fischer–Tropsch synthesis. Chem. Eng. Sci. 2015; 135: 3–20. https://doi.org/10.1016/j.ces.2015.03.007.

[38] Pan Z, Parvari M, Bukur DB. Fischer–Tropsch synthesis on Co/Al2O3 catalyst: Effect of pretreatment procedure. Top Catal. 2014; 57: 470-478. https://doi.org/10.1016/j.apcata.2011.07.012.

[39] Ducreux O, Rebours B, Lynch J, Bazin D. Microstructure of supported cobalt Fischer-Tropsch catalysts. Oil Gas Sci. Technol-Rev lFP 2009; 64: 49–62. https://doi.org/10.2516/ogst:2008039.

[40] Shi L, Zeng C, Lin Q, Lu P, Niu W, Tsubaki N. Citric acid assisted one-step synthesis of highly dispersed metallic Co/SiO_2 without further reduction: As-prepared Co/SiO_2 catalysts for Fischer–Tropsch synthesis. Catal. Today 2014; 228: 206–211. https://doi.org/10.1016/j.cattod.2013.10.013.

[41] Chernavskii PA. Preparation of Fischer-Tropsch catalysts. Kinet. Catal. 2005; 46: 634–640. https://doi.org/10.1007/s10975-005-0119-3.

[42] Gnanamani MK, Jacobs G, Keogh RA, Shafer WD, Sparks DE, Hopps SD, Thomas GA, Davis BH. Fischer-Tropsch synthesis: Effect of pretreatment conditions of cobalt on activity and selectivity for hydrogenation of carbon dioxide. Appl. Catal. A, Gen 2015; 499: 39–46. https://doi.org/10.1016/j.apcata.2015.03.046Get.

[43] Borg Ø, Dietzel PD, Spjelkavik AI, Tveten EZ, Walmsley JC, Diplas S, Eri S, Holmen A, Rytter E. Fischer–Tropsch synthesis: Cobalt particle size and support effects on intrinsic activity and product distribution. J. Catal. 2008; 259: 161-4. https://doi.org/10.1016/j.jcat.2008.08.017.

[44] Park JY, Lee YJ, Karandikar PR, Jun KW, Ha KS, Park HG. Fischer-Tropsch catalysts deposited with size-controlled Co_3O_4 nanocrystals: Effect of Co particle size on catalytic activity and stability. Appl. Catal. A Gen 2012; 411–412: 15–23. https://doi.org/10.1016/j.apcata.2011.10.010.

[45] Saib AM, Claeys M, Van Steen E. Silica supported cobalt Fischer-Tropsch catalysts: Effect of pore diameter of support. Catal. Today 2002; 71: 395–402. https://doi.org/10.1016/S0920-5861(01)00466-7.

[46] Li H, Li J, Ni H, Song D. Studies on cobalt catalyst supported on silica with different pore size for Fischer–Tropsch synthesis. Catal. Lett. 2006; 110: 71–76. https://doi.org/10.1007/s10562-006-0086-y.

[47] Bae JW, Kim SM, Kang SH, Chary KVR, Lee YJ, Kim HJ, Jun KW. Effect of support and cobalt precursors on the activity of Co/$AlPO_4$ catalysts in Fischer-Tropsch synthesis. J. Mol. Catal. A Chem. 2009; 311: 7–16. https://doi.org/10.1016/j.molcata.2009.07.011.

[48] Gnanamani MK, Jacobs G, Shafer WD, Davis BH. Fischer-Tropsch synthesis: Activity of metallic phases of cobalt supported on silica. Catal. Today 2013; 215: 13–17. https://doi.org/10.1016/j.cattod.2013.03.004.

[49] Dalai AK, Davis BH. Fischer–Tropsch synthesis: A review of water effects on the performances of unsupported and supported Co catalysts. Appl. Catal. A Gen. 2008; 348: 1–15. https://doi.org/10.1016/j.apcata.2008.06.021.

[50] Delparish A, Avci AK. Intensified catalytic reactors for Fischer-Tropsch synthesis and for reforming of renewable fuels to hydrogen and synthesis gas. Fuel Process. Technol. 2016; 151: 72–100. https://doi.org/10.1016/j.fuproc.2016.05.021.

[51] Mahmoudi H, Mahmoudi M, Doustdar O, Jahangiri H, Tsolakis A, Gu S, LechWyszynski M. A review of Fischer–Tropsch synthesis process, mechanism, surface chemistry and catalyst formulation. Biofuels Eng. 2017; 2: 11–31. https://doi.org/10.1515/bfuel-2017-0002.

[52] Pei Y, Liu J, Zhao Y, Ding Y, Liu T, Dong W, Zhu H, Su H, Yan L, Li J, Li W. High alcohols synthesis via Fischer−Tropsch reaction at cobalt metal/carbide interface. ACS Catal. 2015; 5: 3620–3624. https://doi.org/10.1021/acscatal.5b00791.

[53] Okoye-Chine CG, Moyo M, Liu X, Hildebrandt D. A critical review of the impact of water on cobalt-based catalysts in Fischer−Tropsch synthesis. Fuel Proc. Technol. 2019; 192: 105–129. https://doi.org/10.1016/j.fuproc.2019.04.006.

[54] Saeidi S, Nikoo MK, Mirvakili A, Bahrani S, Amin NAS, Rahimpour MR. Recent advances in reactors for low-temperature Fischer-Tropsch synthesis: Process intensification perspective. Rev. Chem. Eng. 2015; 31: 209–238. https://doi.org/10.1515/revce-2014-0042.

[55] Rebmann E, Fongarland P, Lecocq V, Diehl F, Schuurman Y. Kinetic modeling of transient Fischer–Tropsch experiments over Co/Al_2O_3 catalysts with different microstructures. Catal. Today 2016; 275: 20–26. https://doi.org/10.1016/j.cattod.2015.11.041.

[56] Paterson J, Peacock M, Ferguson E, Purves R, Ojeda M. In situ diffraction of Fischer–Tropsch catalysts: Cobalt reduction and carbide formation. ChemCatChem. 2017; 9: 3463–3469. https://doi.org/10.1002/cctc.201700754.

[57] Choi J. Reduction of supported cobalt catalysts by hydrogen. Catal Letters 1995; 35: 291–296. https://doi.org/10.1007/BF00807185.

[58] Sage V, Sun Y, Hazewinkel P, Bhatelia T, Braconnier L, Tang L, Chiang K, Batten M, Burke N. Modified product selectivity in Fischer-Tropsch synthesis by catalyst pre-treatment. Fuel Process Technol. 2017; 167: 183–192. https://doi.org/10.1016/j.fuproc.2017.07.002.

[59] Ghampson IT, Newman C, Kong L, Pier E, Hurley KD, Pollock RA, Walsh BR, Goundie B, Wright J, Wheeler MC, Meulenberg RW, DeSisto WJ, Frederick BG, Austin RN. Effects of pore diameter on particle size, phase, and turnover frequency in mesoporous silica supported cobalt Fischer-Tropsch catalysts. Appl. Catal. A Gen. 2010; 388: 57–67. https://doi.org/10.1016/j.apcata.2010.08.028.

[60] Jacobs G, Ma W, Davis B. Influence of reduction promoters on stability of cobalt/g-alumina Fischer-Tropsch Synthesis catalysts. Catalysts; 2014; 4: 49–76. https://doi.org/10.3390/catal4010049.

[61] Chen W, Lin T, Dai Y, An Y, Yu F, Zhong L, Li S, Sun Y. Recent advances in the investigation of nanoeffects of Fischer-Tropsch catalysts. Catal. Today 2018; 311: 8–22. https://doi.org/10.1016/j.cattod.2017.09.019.

[62] Lyu S, Wang L, Zhang J, Liu C, Sun J, Peng B, Wang Y, Rappé KG, Zhang Y, Li J, Nie L. Role of active phase in Fischer−Tropsch synthesis: Experimental evidence of CO activation over single-phase cobalt catalysts. ACS Catal. 2018; 8: 7787–7798. https://doi.org/10.1021/acscatal.8b00834.

[63] Jabłonski JM, Okal J, Potoczna-Petru D, Krajczyk L. High temperature reduction with hydrogen, phase composition, and activity of cobalt/silica catalysts. J. Catal. 2003; 220: 146–160. https://doi.org/10.1016/S0021-9517(03)00287-2.

[64] Tsubaki N, Sun S, Fujimoto K. Different functions of the noble metals added to cobalt catalysts for Fischer–Tropsch synthesis. J. Catal. 2001; 246: 236–246. https://doi.org/10.1006/jcat.2001.3163.

[65] Xiong H, Motchelaho MAM, Moyo M, Jewell LL, Coville NJ. Cobalt catalysts supported on a micro-coil carbon in Fischer–Tropsch synthesis: A comparison with CNTs and CNFs. Catal. Today 2013; 214: 50–60. https://doi.org/10.1016/j.cattod.2012.10.018.

[66] Yang J, Jacobs G, Jermwongratanachai T, Anders DC, Burtron H. Fischer–Tropsch synthesis: Impact of H_2 or CO activation on methane selectivity. Catal. Lett. 2014; 144: 123–132. https://doi.org/10.1007/s10562-013-1099-y.

[67] Ma W, Jacobs G, Keogh RA, Bukur DB, Davis BH. Fischer-Tropsch synthesis: Effect of Pd, Pt, Re, and Ru noble metal promoters on the activity and selectivity of a 25%Co/ Al_2O_3 catalyst. Appl. Catal. A Gen. 2012; 437–438: 1–9. https://doi.org/10.1016/j.apcata.2012.05.037.

[68] Das TK, Jacobs G, Patterson PM, Conner WA, Li J, Davis BH. Fischer–Tropsch synthesis: Characterization and catalytic properties of rhenium promoted cobalt alumina catalysts. Fuel 2003; 82: 805–815. https://doi.org/10.1016/S0016-2361(02)00361-7.

[69] Bian G, Mochizuki T, Fujishita N, Nomoto H, Yamada M. Activation and catalytic behavior of several Co/SiO_2 catalysts for Fischer-Tropsch synthesis. Energ. Fuel 2003; 17: 799–803. https://doi.org/10.1021/ef020236j.

[70] Li J, Coville NJ. Effect of calcination and reduction temperatures on the reduction and activity of Boron-modified Co/TiO_2 Fischer-Tropsch catalyst. S Afr. J. Chem. 2004; 57: 49–52. https://doi.org/10.1021/ef020236j.

[71] Bezemer GL, Radstake PB, Koot V, Van Dillen AJ, Geus JW, De Jong KP. Preparation of Fischer–Tropsch cobalt catalysts supported on carbon nanofibers and silica using homogeneous deposition-precipitation. J. Catal. 2006; 237: 291-302. https://doi.org/10.1016/j.jcat.2005.11.015.

[72] Tavasoli AH, Sadagiani K, Khorashe F, Seifkordi AA, Rohani AA, Nakhaeipour A. Cobalt supported on carbon nanotubes-A promising novel Fischer–Tropsch synthesis catalyst. Fuel Process. Technol. 2008; 89: 491-498. https://doi.org/10.1016/j.fuproc.2007.09.008.

[73] Mehrbod M, Martinelli M, Watson CD, Cronauer DC, Kropf AJ, Jacobs G. Fischer-Tropsch Synthesis: The Characterization and Testing of Pt-Co/SiO_2 Catalysts Prepared with Alternative Cobalt Precursors. Reactions. 2021; 2: 129-60. https://doi.org/10.3390/reactions2020011.

[74] Espinoza RL, Steynberg AP, Jager B, Vosloo AC. Low temperature Fischer–Tropsch synthesis from a Sasol perspective. Appl. Catal. A Gen. 1999; 186: 13–26. https://doi.org/10.1016/S0926-860X(99)00161-1.

[75] Claeys M, Dry ME, Van Steen E, Du Plessis E, Van Berge PJ, Saib AM, Moodley DJ. In situ magnetometer study on the formation and stability of cobalt carbide in Fischer–Tropsch synthesis. J. Catal. 2014; 318: 193–202. https://doi.org/10.1016/j.jcat.2014.08.002.

[76] Patzlaff J, Liu Y, Graffmann C, Gaube J. Interpretation and kinetic modeling of product distributions of cobalt catalyzed Fischer–Tropsch synthesis. Catal. Today 2002; 71: 381–394. https://doi.org/10.1016/S0920-5861(01)00465-5.

[77] Schulz H, Claeys M, Harms S. Effect of water partial pressure on steady state Fischer-Tropsch activity and selectivity of a promoted cobalt catalyst. Stud. Surf. Sci. Catal. 1997; 107: 193–200. https://doi.org/10.1016/S0167-2991(97)80334-5.

[78] Hilmen AM, Schanke D, Hanssen KF, Holmen A. Study of the effect of water on alumina supported cobalt Fischer–Tropsch catalysts. Appl. Catal. A Gen. 1999; 186: 169–188. https://doi.org/10.1016/S0926-860X(99)00171-4.

[79] Storsæter S, Borg Ø, Blekkan EA, Tøtdal B, Holmen A. Fischer–Tropsch synthesis over Re-promoted Co supported on Al_2O_3, SiO_2 and TiO_2: Effect of water. Catal. Today 2005; 100: 343–347. https://doi.org/10.1016/j.cattod.2004.09.068.

[80] Borg Ø, Yu Z, Holmen A. The effect of water on the activity and selectivity for carbon nanofiber supported cobalt Fischer–Tropsch catalysts. Top Catal. 2014; 57: 491–499. https://doi.org/10.1007/s11244-013-0205-0.

[81] Fischer N, Clapham B, Feltes T, Claeys M. Cobalt based Fischer-Tropsch activity and selectivity as a function of crystallite size and water partial pressure. ACS Catal. 2015; 5: 113–121. https://doi.org/10.1021/cs500936t.

[82] Sadeqzadeh M, Chambrey S, Piché S, Fongarland P, Luck F, Curulla-Ferré D, Schweich D, Bousquet J, Khodakov AY. Deactivation of a Co/Al_2O_3 Fischer–Tropsch catalyst by water-induced sintering in slurry reactor: Modeling and experimental investigations. Catal. Today 2013; 215: 52-59. https://doi.org/10.1016/j.cattod.2013.03.022.

[83] Zhang Y, Wei D, Hammache S, Goodwin JG. Effect of water vapor on the reduction of Ru-promoted Co/Al_2O_3. J. Catal. 1999; 188: 281–290. https://doi.org/10.1006/jcat.1999.2666.

[84] Jongsomjit B, Goodwin JG Jr. Co-support compound formation in Co/Al_2O_3 catalysts: Effect of reduction gas containing CO. Catal. Today 2002; 77: 191–204. https://doi.org/10.1016/S0920-5861(02)00245-6.

[85] Kwak G, Kim DE, Kim YT, Park HG, Kang SC, Ha KS, Jun KW, Lee YJ. Enhanced catalytic activity of cobalt catalysts for Fischer–Tropsch synthesis via carburization and hydrogenation and its application to regeneration. Catal. Sci. Technol. 2016 ;6: 4594–4600. DOI: 10.1039/C5CY01399B.

[86] Yao Y, Liu X, Gorimbo J, Xiong H, Fox J, Glasser D, Hildebrand D, Fischer-Tropsch synthesis: A long term comparative study of the product selectivity and paraffin to olefin ratios over an iron-based catalyst activated by syngas or H_2, Appl. Catal. A Gen. 2020; 602:117700. https://doi.org/10.1016/j.apcata.2020.117700.

[87] Kwak G, Woo MH, Kang SC, Park HG, Lee YJ, Jun KW, Ha KS. In situ monitoring during the transition of cobalt carbide to metal state and its application as Fischer–Tropsch catalyst in slurry phase. J. Catal. 2013; 307: 27–36. https://doi.org/10.1016/j.jcat.2013.06.029Get.

[88] Gnanamani MK, Jacobs G, Graham UM, Ribeiro MC, Noronha FB, Shafer WD, Davis BH. Influence of carbide formation on oxygenates selectivity during Fischer-Tropsch synthesis over Ce-containing Co catalysts. Catal. Today 2016; 261: 40–47. https://doi.org/10.1016/j.cattod.2015.08.047.

[89] Peacock M, Purves R, Ojeda M, Ferguson E, Paterson J. In situ diffraction of Fischer-Tropsch catalysts: cobalt reduction and carbide formation. ChemCatChem. 2017; 9: 3463–3469. https://doi.org/10.1002/cctc.201700754.

[90] Xiong J, Ding Y, Wang T, Yan L, Chen W, Zhu H, Lu Y. The formation of Co_2C species in activated carbon supported cobalt-based catalysts and its impact on Fischer–Tropsch reaction. Catal. Lett. 2005b; 102: 265–269. https://doi.org/10.1007/s10562-005-5867-1.

[91] Li J, Xu L, Keogh R, Davis B. Fischer–Tropsch synthesis. Effect of CO pretreatment on a ruthenium promoted Co/TiO_2. Catal Lett 2000; 70: 127–130.

[92] Jalama K. Fischer–Tropsch synthesis over Co/TiO_2 catalyst: Effect of catalyst activation by CO compared to H_2. Catal. Commun. 2016; 74: 71–74. https://doi.org/10.1016/j.catcom.2015.11.004.

[93] Khangale PR, Meijboom R, Jalama K. Fischer-Tropsch synthesis over unpromoted $Co/\gamma\text{-}Al_2O_3$ catalyst: Effect of activation with CO compared to H_2 on catalyst performance. Bull Chem React. Eng. Catal. 2019; 14: 35–41. DOI: https://doi.org/10.9767/bcrec.14.1.2519.35-41.

[94] Pan Z, Bukur DB. Fischer–Tropsch synthesis on Co/ZnO catalyst−Effect of pretreatment procedure. Appl. Catal. A Gen. 2011; 404: 74–80. https://doi.org/10.1016/j.apcata.2011.07.012.

[95] Beuther, H., Kobylinski, T.P., Kibby, C.L. and Pannell RB. Synthesis gas conversion using ruthenium-promoted cobalt catalyst. U.S. Patent: 4,585,798. 1986.

[96] De la Peña O'Shea VA, Homs N, Fierro JLG, De la Piscina PR. Structural changes and activation treatment in a Co/SiO_2 catalyst for Fischer–Tropsch synthesis. Catal. Today 2006; 114: 422–427. https://doi.org/10.1016/j.cattod.2006.02.065.

[97] Fronzo AD. Biomass to liquid process: New kind of cobalt and iron-based catalysts for the Fischer-Tropsch Synthesis. Doctoral Thesis. 2014.

[98] Tsakoumis NE, Dehghan R, Johnsen RE, Voronov A, Van Beek W, Walmsley JC, Borg Ø, Rytter E, Chen D, Rønning M, Holmen A. A combined in situ XAS-XRPD-Raman study of Fischer–Tropsch synthesis over a carbon supported Co catalyst. Catal. Today 2013; 205: 86–93. https://doi.org/10.1016/j.cattod.2012.08.041.

[99] Zhang R, Wen G, Adidharma H, Russell G, Wang B, Radosz M, Fan M. C_2 oxygenates synthesis via Fischer-Tropsch synthesis on Co_2C and Co/Co_2C interface catalysts: How to control the catalyst crystal facet for optimal selectivity. ACS Catal. 2017; 7: 8285–8295. https://doi.org/10.1021/acscatal.7b02800.

[100] Pei Y, Liu J, Zhao Y, Ding Y, Liu T, Dong W, Zhu H, Su H, Yan L, Li J, Li W. High alcohols synthesis via Fischer−Tropsch reaction at cobalt metal/carbide interface. ACS Catal. 2015; 5: 3620–3624. https://doi.org/10.1021/acscatal.5b00791.

[101] Volkova GG, Yurieva TM, Plyasova LM, Naumova MI, Zaikovskii VI. Role of the Cu–Co alloy and cobalt carbide in higher alcohol synthesis. J. Mol. Catal. A Chem. 2010; 158: 389–393. https://doi.org/10.1016/S1381-1169(00)00110-2.

[102] Jiang Y, Long R, Xiong Y. Regulating C–C coupling in thermocatalytic and electrocatalytic CO_x conversion based on surface science. Chem. Sci. 2019; 10: 7310-7326. DOI: 10.1039/C9SC02014D .

[103] Mousavi S, Zamaniyan A, Irani M, Rashidzadeh M. Generalized kinetic model for iron and cobalt based Fischer–Tropsch synthesis catalysts: Review and model evaluation. Appl. Catal. A Gen. 2015; 506: 57–66. https://doi.org/10.1016/j.apcata.2015.08.020.

[104] Lin T, Gong K, Wang C, An Y, Wang X, Qi X, Li S, Lu Y, Zhong L, Sun Y. Fischer −Tropsch Synthesis to olefins: catalytic performance and structure evolution of Co_2C based catalysts under a CO_2 environment. ACS Catal. 2019; 9: 9554–9567. https://doi.org/10.1021/acscatal.9b02513.

[105] Zhao Z, Lu W, Yang R, Zhu H, Dong W, Sun F, Jiang Z, Lyu Y, Liu T, Du H, Ding Y. Insight into the formation of Co@Co_2C catalysts for direct synthesis of higher alcohols and olefins from syngas. ACS Catal. 2018; 8: 228–241. https://doi.org/10.1021/acscatal.7b02403.

[106] Zhong L, Yu F, An Y, Zhao Y, Sun Y, Li Z, Lin T, Lin Y, Qi X, Dai Y, Gu L. Cobalt carbide nanoprisms for direct production of lower olefins from syngas. Nature 2016; 538: 84-87. https://doi.org/10.1038/nature19786.

[107] Sadeqzadeh M, Karaca H, Safonova OV, Fongarland P, Chambrey S, Roussel P, Griboval-Constant A, Lacroix M, Curulla-Ferré D, Luck F, Khodakov AY. Identification of the active species in the working alumina-supported cobalt catalyst under various conditions of Fischer–Tropsch synthesis. Catal. Today 2011; 164: 62-67. https://doi.org/10.1016/j.cattod.2010.12.035.

[108] Tristantini D, Lögdberg S, Gevert B, Borg Ø, Holmen A. The effect of synthesis gas composition on the Fischer–Tropsch synthesis over Co/γ-Al_2O_3 and Co–Re/γ-Al_2O_3 catalysts. Fuel Process Technol. 2007; 88: 643-649. https://doi.org/10.1016/j.fuproc.2007.01.012.

[109] Xu J, Bartholomew CH. Temperature-programmed hydrogenation (TPH) and in situ Mössbauer spectroscopy studies of carbonaceous species on silica-supported iron Fischer-Tropsch catalysts. J. Phys. Chem. B 2005; 109: 2392-2403. https://doi.org/10.1021/jp048808j.

[110] Bukur DB, Lang X, Rossin JA, Zimmerman WH, Rosynek MP, Yeh EB, Li C. Activation studies with a promoted precipitated iron Fischer-Tropsch catalyst. Ind. Eng. Chem. Res. 1989: 1130-40. doi.org/10.1021/ie00092a003.

[111] O'Brien RJ, Xu L, Spicer RL, Davis BH. Activation Study of Precipitated Iron Fischer-Tropsch Catalysts. Energ. Fuel 1996; 10: 921-926. https://doi.org/10.1021/ef9502315.

[112] Pan Z, Parvari M, Bukur DB. Fischer–Tropsch synthesis on Co/ZnO–Two step activation procedure for improved performance. Appl. Catal. A Gen. 2014; 480: 79–85. https://doi.org/10.1016/j.apcata.2014.04.040.

[113] Braconnier L, Landrivon E, Clémençon I, Legens C, Diehl F, Schuurman Y. How does activation affect the cobalt crystallographic structure? An in situ XRD and magnetic study. Catal. Today 2013; 215: 18-23. https://doi.org/10.1016/j.cattod.2013.02.021.

[114] Kobylinski TP, Kibby CL, Pannell RB, Eddy EL. ROR-activated catalyst for synthesis gas conversion. U.S. Patent 4,729,981. 1988.

[115] Saib AM, Moodley DJ. Ciob C IM, Hauman MM, Sigwebela BH, Weststrate CJ, Niemantsverdriet JW, Van de Loosdrechta J. Fundamental understanding of deactivation and regeneration of cobalt Fischer-Tropsch synthesis catalysts. Catal. Today 2010; 154: 271-282. 10.1016/j.cattod.2010.02.008.

[116] Nay B, Smith MR, Telford CD. Catalyst treatment. U.S. Patent 5,728,918. 1998.

[117] Kobylinski TP, Kibby CL, Pannell RB, Eddy EL. Shell Internationale Research Maatschappij BV. Activated cobalt catalyst and synthesis gas conversion using same. U.S. Patent 4,670,414. 1987.

[118] Kobylinski TP, Kibby CL, Pannell RB, Eddy EL. Synthesis gas conversion using ROR-activated catalyst. U.S. Patent: 4,605,676. 1986.

[119] Hauman MM, Saib AM, Moodley DJ, Du Plessis E, Claeys M, Van Steen E. Re-dispersion of cobalt on a model Fischer–Tropsch catalyst during Reduction–Oxidation–Reduction cycles. ChemCatChem. 2012; 1947: 1411–1419. https://doi.org/10.1002/cctc.201200034.

[120] Tang L, Yamaguchi D, Leita B, Sage V, Burke N, Chiang K. The effects of oxidation–reduction treatment on the structure and activity of cobalt-based catalysts. Catal. Commun. 2015; 59: 166–169. https://doi.org/10.1016/j.catcom.2014.10.021.

[121] Jermwongratanachai T, Jacobs G, Ma W, Shafer WD, Gnanamani MK, Gao P, Kitiyanan B, Davis BH, Klettlinger JL, Yen CH, Cronauer DC. Fischer–Tropsch synthesis: Comparisons between Pt and Ag promoted Co/Al_2O_3 catalysts for reducibility, local atomic structure, catalytic activity, and oxidation–reduction (OR) cycles. Appl. Catal. A Gen. 2013; 464: 165-80. https://doi.org/10.1016/j.apcata.2013.05.040.

[122] Rytter E, Sigrid E, Rune M, Odd AL. Fischer-Tropsch catalysts. UK Patent: GB2473071. 2011.

[123] Cai J, Jiang F, Liu X. Exploring pretreatment effects in Co/SiO2 Fischer-Tropsch catalysts: Different oxidizing gases applied to oxidation-reduction process. Appl. Catal. B Env. 2017; 210: 1-3. https://doi.org/10.1016/j.apcatb.2017.03.036.

[124] Sadasivan S, Bellabarba RM, Tooze RP. Size dependent reduction–oxidation–reduction behaviour of cobalt oxide nanocrystals. Nanoscale. 2013; 5: 11139-11146. DOI: 10.1039/C3NR02877A .

[125] Zhao Y, Liu C, Song Y, Zhang Q, Zhu M, Liu Z, Liu Z. Direct synthesis of the reduced Co-C/SiO2 as an efficient catalyst for Fischer-Tropsch synthesis direct. Ind. Eng. Chem. Res. 2018; 57: 1137–1145. https://doi.org/10.1021/acs.iecr.7b04149.

[126] Shi L, Tao K, Kawabata T, Shimamura T, Zhang XJ, Tsubaki N. Surface impregnation combustion method to prepare nanostructured metallic catalysts without further reduction: As-burnt Co/SiO_2 catalysts for Fischer-Tropsch synthesis. ACS Catal. 2011; 1: 7197–7203. https://doi.org/10.1021/cs200294d.

[127] Shi L, Shen W, Yang G, Fan X, Jin Y, Zeng C, Matsuda K, Tsubaki N. Formic acid directly assisted solid-state synthesis of metallic catalysts without further reduction: As-prepared Cu/ZnO catalysts for low-temperature methanol synthesis. J. Catal. 2013; 302: 83–90. https://doi.org/10.1016/j.jcat.2013.02.025.

[128] Phienluphon R, Shi L, Sun J, Niu W, Lu P, Zhu P, Vitidsant T, Yoneyama, Y, Chen Q, Tsubaki N. Ruthenium promoted cobalt catalysts prepared by an auto combustion method directly used for Fischer–Tropsch synthesis without further reduction. Catal. Sci. Technol. 2014; 4: 3099–3107. DOI: 10.1039/C4CY00402G.

[129] Moore JJ, Feng HJ. Combustion synthesis of advanced materials: Part 1. Reaction parameters, Prog Mater Sci. 1995; 39: 243-273. https://doi.org/10.1016/0079-6425(94)00011-5.

[130] Merzhanov AG. Self-propagating high-temperature synthesis: Twenty years of search and findings. In: Munir ZA, Holt JB editors. Combustion and plasma synthesis of high-temperature materials. Wiley-VCH, Weinheim, 1990: 1-53.

[131] Calleja G, De Lucas A, Van Grieken R. Cobalt/HZSM-5 zeolite catalyst for the conversion of syngas to hydrocarbons. Appl. Catal. A Gen. 1991; 68: 11–29. https://doi.org/10.1016/S0166-9834(00)84090-7.

[132] Cheng J, Hu P, Ellis P, French S, Kelly G, Lok CM. Density functional theory study of iron and cobalt carbides for Fischer-Tropsch synthesis. J. Phys. Chem. C 2010; 114: 1085-1093. https://doi.org/10.1021/jp908482q.

[133] Jahangiri H, Bennett J, Mahjoubi P, Wilson K, Gu S. A review of advanced catalyst development for Fischer-Tropsch synthesis of hydrocarbons from biomass derived syn-gas. Catal. Sci. Technol. 2014; 4: 2210–29. DOI: 10.1039/C4CY00327F.

[134] Madikizela-Mnqanqeni NN, Coville NJ. The effect of cobalt and zinc precursors on Co(10%)/Zn(x%)/TiO_2 (x=0,5) Fischer-Tropsch catalysts. J. Mol. Catal. A Chem. 2005; 225: 137–142. https://doi.org/10.1016/j.molcata.2004.09.004.

[135] Sun S, Tsubaki N, Fujimoto K. The reaction performances and characterization of Fischer–Tropsch synthesis Co/SiO_2 catalysts prepared from mixed cobalt salts. Appl. Catal. A Gen. 2000; 202: 121–131. https://doi.org/10.1016/S0926-860X(00)00455-5.

[136] Panpranot J, Kaewkun S, Praserthdam P, Goodwin JG. Effect of cobalt precursors on the dispersion of cobalt on MCM-41. Catal. Lett. 2003; 91: 95–102. https://doi.org/10.1023/B:CATL.0000006323.17873.78.

[137] Sietsma JR, Meeldijk JD, Den Breejen JP, Versluijs‐Helder M, Van Dillen AJ, De Jongh PE, De Jong KP. The preparation of supported NiO and Co_3O_4 nanoparticles by the nitric oxide controlled thermal decomposition of nitrates. Angew. Chem. Int. Ed. 2007; 46: 4547-4549. https://doi.org/10.1002/anie.200700608.

[138] Li X, Almkhelfe H, Bedford NM, Back TC, Hohn KL, Amama PB. Characterization and catalytic behavior of Fischer–Tropsch catalysts derived from different cobalt precursors. Catal. Today 2019; 338: 40-51. https://doi.org/10.1016/j.cattod.2019.05.023.

[139] Martínez A, López C. Márquez F, Díaz I. Fischer–Tropsch synthesis of hydrocarbons over mesoporous Co/SBA-15, J. Catal. 2003; 220: 486–499. https://doi.org/10.1016/S0021-9517(03)00289-6.

[140] Iglesia E. Design, synthesis, and use of cobalt-based Fischer-Tropsch synthesis catalysts. Appl. Catal. A Gen. 1997; 161: 59-78. https://doi.org/10.1016/S0926-860X(97)00186-5.

[141] Thurston JH, Trahan D, Ould-Ely T, Whitmire KH. Toward a general strategy for the synthesis of heterobimetallic coordination complexes for use as precursors to metal oxide materials: synthesis, characterization, and thermal decomposition of $Bi_2(Hsal)_6{\cdot}M(Acac)_3$ (M = Al, Co, V, Fe, Cr). Inorg. Chem. 2004; 43: 3299-3305. https://doi.org/10.1021/ic035284d.

[142] Tavasoli AH, Sadaghiani K, Nakhaeipour A, Ahangari M. Cobalt loading effects on the structure and activity for Fischer-Tropsch and water-gas shift reactions of Co/Al_2O_3 catalysts. Iran J Chem. Chem. Eng. 2007; 26: 9-16. 10.30492/IJCCE.2007.7664.

[143] Loedolff MJ, Goh BM, Koutsantonis GA, Fuller RO. Supported heterogeneous catalysts: What controls cobalt nanoparticle dispersion on alumina. New J. Chem. 2018; 42: 14894-14900. DOI: 10.1039/C8NJ03076F.

[144] Bartholomew CH. History of cobalt catalyst design for FTS. In Proceedings of the National Spring Meeting of the American Institute of Chemical Engineers (AIChE'03) 2003.

[145] Mehl S, Ferstl P, Schuler M, Toghan A, Brummel O, Hammer L, Schneider MA, Libuda J. Thermal evolution of cobalt deposits on Co_3O_4(111): Atomically dispersed cobalt, two-dimensional CoO islands, and metallic Co nanoparticles. Phys. Chem. Chem. Phys. 2015; 17: 23538-23546. DOI: 10.1039/C5CP03922C.

[146] Ali S, Zabidi NAM, Subbarao D. Correlation between Fischer-Tropsch catalytic activity and composition of catalysts. Chem. Cent. J. 2011; 5: 68. https://doi.org/10.1186/1752-153X-5-68.

[147] Kim CU, Kim YS, Chae HJ, Jeong KE, Jeong SY, Jun KW, Lee KY. Effect of cobalt catalyst type and reaction medium on Fischer-Tropsch synthesis. Korean J. Chem. Eng. 2010; 27: 777–784. https://doi.org/10.1007/s11814-010-0135-5.

[148] Xiong H, Zhang Y, Wang S, Li J. Fischer–Tropsch synthesis: The effect of Al_2O_3 porosity on the performance of Co/Al_2O_3 catalyst, Catal. Comm. 2005a; 6: 512-516. https://doi.org/10.1016/j.catcom.2005.04.018.

[149] Jacobs G, Das TK, Zhang Y, Li J, Racoillet G, Davis BH. Fischer–Tropsch synthesis: support, loading, and promoter effects on the reducibility of cobalt catalysts. Appl. Catal. A Gen. 2002; 233: 263–281. https://doi.org/10.1016/S0926-860X(02)00195-3.

[150] Bessell S. Support effects in cobalt-based Fischer-Tropsch catalysis. Appl. Catal. A Gen. 1993; 96: 253-268. https://doi.org/10.1016/0926-860X(90)80014-6.

[151] Elbashir NO, Dutta P, Manivannan A, Seehra MS, Roberts CB. Impact of cobalt-based catalyst characteristics on the performance of conventional gas-phase and supercritical-phase Fischer–Tropsch synthesis. Appl. Catal. A Gen. 2005; 285: 169-180. https://doi.org/10.1016/j.apcata.2005.02.023.

[152] Flores C, Batalha N, Marcilio NR, Ordomsky VV, Khodakov AY. Influence of impregnation and ion exchange sequence on metal localization, acidity and catalytic performance of cobalt BEA zeolite catalysts in Fischer‐Tropsch Synthesis. ChemCatChem. 2019; 11: 568–574. https://doi.org/10.1002/cctc.201800728.

[153] Yaghoobpour E, Zamani Y, Zarrinpashne S, Zamaniyan A. Profound synergetic effect of metal oxide promoters and TiO_2–SiO_2 binary support in cobalt Fischer‐Tropsch catalyst. J. Chin. Chem. Soc. 2020; 67: 751-765. https://doi.org/10.1002/jccs.201900326.

[154] Pei Y, Ding Y, Zhu H, Du H. One-step production of C1–C18 alcohols via Fischer-Tropsch reaction over activated carbon-supported cobalt catalysts: Promotional effect of modification by SiO2. Chinese J. Catal. 2015; 36: 355-361. https://doi.org/10.1016/S1872-2067(14)60252-7.

[155] Khodakov AY, Bechara R, Griboval-Constant A. Fischer–Tropsch synthesis over silica supported cobalt catalysts: mesoporous structure versus cobalt surface density. Appl. Catal. A: Gen. 2003; 254: 273-288. https://doi.org/10.1016/S0926-860X(03)00489-7.

[156] Yang Y, Jia L, Meng Y, Hou B, Li D, Sun Y. Fischer–Tropsch synthesis over ordered mesoporous carbon supported cobalt catalysts: the role of amount of carbon precursor in catalytic performance. Catal. Lett. 2012; 142: 195-204. https://doi.org/10.1007/s10562-011-0747-3.

[157] Zafari R, Abdouss M, Zamani Y. Effect of Mn and reduced graphene oxide for the Fischer–Tropsch reaction: An efficient catalyst for the production of light olefins from syngas. React. Kinet. Mech. Catal. 2020; 129: 707-724. https://doi.org/10.1007/s11144-020-01742-7.

[158] Song D, Li J. Effect of catalyst pore size on the catalytic performance of silica supported cobalt Fischer–Tropsch catalysts. J. Mol. Catal. A Chem. 2006; 247: 206-212. https://doi.org/10.1016/j.molcata.2005.11.021.

[159] Ernst B, Hilaire L, Kiennemann A. Effects of highly dispersed ceria addition on reducibility, activity and hydrocarbon chain growth of a Co/SiO_2 Fischer–Tropsch catalyst. Catal. Today 1999; 50: 413-427. https://doi.org/10.1016/S0920-5861(98)00519-7.

[160] Kababji AH, Joseph B, Wolan JT. Silica-supported cobalt catalysts for Fischer–Tropsch synthesis: Effects of calcination temperature and support surface area on cobalt silicate formation. Catal. Lett. 2009; 130: 72-78. https://doi.org/10.1007/s10562-009-9903-4.

[161] Díaz JA, Calvo-Serrano M, De la Osa AR, García-Minguillán AM, Romero A, Giroir-Fendler A, Valverde JL. β-silicon carbide as a catalyst support in the Fischer–Tropsch synthesis: Influence of the modification of the support by a pore agent and acidic treatment. Appl. Catal. A Gen. 2014; 475: 82-89. https://doi.org/10.1016/j.apcata.2014.01.021.

[162] Carballo JMG, Yang J, Holmen A, García-Rodríguez S, Rojas S, Ojeda M, Fierro JLG. Catalytic effects of ruthenium particle size on the Fischer–Tropsch Synthesis. J. Catal. 2011; 284: 102–108. https://doi.org/10.1016/j.jcat.2011.09.008.

[163] Rytter E, Holmen A. On the support in cobalt Fischer–Tropsch synthesis−Emphasis on alumina and aluminates. Catal. Today 2016; 275: 11–19. https://doi.org/10.1016/j.cattod.2015.11.042.

[164] Barbier A, Tuel A, Arcon I, Kodre A, Martin GA. Characterization and catalytic behavior of Co/SiO_2 catalysts: Influence of dispersion in the Fischer–Tropsch reaction. J. Catal. 2001; 116: 106–116. https://doi.org/10.1006/jcat.2001.3204.

[165] Den Breejen JP, Radstake PB, Bezemer GL, Bitter JH, Frøseth V, Holmen A, de Jong KD. On the origin of the cobalt particle size effects in Fischer− Tropsch catalysis. J. American Chem. Soc. 2009; 131: 7197-7203. https://doi.org/10.1021/ja901006x.

[166] Van Berge PJ, Van de Loosdrecht J, Barradas S, Van der Kraan AM. Oxidation of cobalt based Fischer–Tropsch catalysts as a deactivation mechanism. Catal. Today 2000; 58: 321-334. https://doi.org/10.1016/S0920-5861(00)00265-0.

[167] Das TK, Jacobs G, Patterson PM, Conner WA, Li J, Davis BH. Fischer–Tropsch synthesis: Characterization and catalytic properties of rhenium promoted cobalt alumina catalysts. Fuel 2003; 82: 805–815. https://doi.org/10.1016/S0016-2361(02)00361-7.

[168] Moodley DJ, Van de Loosdrecht J, Saib AM, Niemantsverdriet HJW. The formation and influence of carbon on cobalt-based Fischer-Tropsch synthesis catalysts: An integrated review. In: Davis BH, Occelli ML, Speight JG editors. Advances in Fisher-Tropsch Synthesis, Catalysts and Catalysis. CRC Press, 2008: 49-81. 10.1201/9781420062571.ch4.

[169] Kiss G, Kliewer CE, DeMartin GJ, Culross CC, Baumgartner JE. Hydrothermal deactivation of silica-supported cobalt catalysts in Fischer–Tropsch synthesis. J. Catal. 2003; 217: 127-140. https://doi.org/10.1016/S0021-9517(03)00054-X.

[170] Elbashir NO, Dutta P, Manivannan A, Seehra MS, Roberts CB. Impact of cobalt-based catalyst characteristics on the performance of conventional gas-phase and supercritical-phase Fischer–Tropsch synthesis. Appl. Catal. A Gen. 2005; 285: 169-180. https://doi.org/10.1016/j.apcata.2005.02.023.

[171] Van de Loosdrecht J, Balzhinimaev B, Dalmon JA, Niemantsverdriet JW, Tsybulya SV, Saib AM, Van Berge PJ, Visagie JL. Cobalt Fischer-Tropsch synthesis: deactivation by oxidation. Catal. Today 2007; 123: 293-302. https://doi.org/10.1016/j.cattod.2007.02.032.

[172] Li H, Wang J, Chen C, Jia L, Li D. Effects of macropores on reducing internal diffusion limitations in Fischer–Tropsch synthesis. RSC Adv. 2017; 7:9436–9445. DOI: 10.1039/C6RA27166A.

[173] Klaigaew K, Samart C, Chaiya C, Yoneyama Y, Tsubaki N, Reubroycharoen P. Effect of preparation methods on activation of cobalt catalyst supported on silica fiber for Fischer–Tropsch synthesis. Chem. Eng. J. 2015; 278: 166–173. https://doi.org/10.1016/j.cej.2014.11.025.

[174] Rane S, Borg Ø, Yang J, Rytter E, Holmen A. Effect of alumina phases on hydrocarbon selectivity in Fischer–Tropsch synthesis. Appl. Catal. A Gen. 2010; 388: 160-167. https://doi.org/10.1016/j.apcata.2010.08.038.

[175] Jacobs G, Ribeiro MC, Ma W, Ji Y, Khalid S, Sumodjo PTA, Davis BH. Group 11 (Cu, Ag, Au) promotion of 15%Co/Al_2O_3 Fischer–Tropsch synthesis catalysts. Appl. Catal. A Gen. 2009; 361: 137–151. https://doi.org/10.1016/j.apcata.2009.04.007.

[176] Tsakoumis NE, Rønning M, Borg Ø, Rytter E, Holmen A. Deactivation of cobalt based Fischer–Tropsch catalysts: A review. Catal. Today 2010; 154: 162–182. https://doi.org/10.1016/j.cattod.2010.02.077.

[177] Wolf M, Roberts SJ, Marquart W, Olivier EJ, Luchters NT, Gibson EK, Catlow CR, Neethling JH, Fischer N, Claeys M. Synthesis, characterization and water–gas shift activity of nano-particulate mixed-metal (Al, Ti) cobalt oxides. Dalton Trans. 2019; 48: 13858-13868. DOI: 10.1039/C9DT01634A.

[178] Ma WP, Ding YJ, Lin LW. Fischer-Tropsch Synthesis over activated-carbon-supported cobalt catalysts: Effect of Co loading and promoters on catalyst performance. Ind. Eng. Chem. Res. 2004; 43: 2391-2398. https://doi.org/10.1021/ie034116q.

[179] Eliseev OL, Tsapkina MV, Dement'eva OS, Davydov PE, Kazakov AV, Lapidus AL. Promotion of cobalt catalysts for the Fischer-Tropsch synthesis with alkali metals. Kinet. Catal. 2013; 54: 207-212. https://doi.org/10.1134/S0023158413020055.

[180] Ishida T, Yanagihara T, Liu X, Ohashi H, Hamasaki A, Honma T, Oji H, Yokoyama T, Tokunaga M. Synthesis of higher alcohols by Fischer–Tropsch synthesis over alkali metal-modified cobalt catalysts. Appl. Catal. A Gen. 2013; 458: 145-154. https://doi.org/10.1016/j.apcata.2013.03.042.

[181] Jiao F, Li J, Pan X, Xiao J, Li H, Ma H, Wei M, Pan Y, Zhou Z, Li M, Miao S. Selective conversion of syngas to light olefins. Science 2016; 351: 1065-1068. DOI: 10.1126/science.aaf1835.

[182] Xie J, Paalanen PP, Van Deelen TW, Weckhuysen BM, Louwerse MJ, De Jong KP. Promoted cobalt metal catalysts suitable for the production of lower olefins from natural gas. Nat. Comm. 2019; 10: 1-10. https://doi.org/10.1038/s41467-018-08019-7.

[183] Morales-Guio CG, Cave ER, Nitopi SA, Feaster JT, Wang L, Kuhl KP, Jackson A, Johnson NC, Abram DN, Hatsukade T, Hahn C. Improved CO_2 reduction activity towards C_{2+} alcohols on a tandem gold on copper electrocatalyst. Nat. Catal. 2018; 1: 764-771. https://doi.org/10.1038/s41929-018-0139-9.

[184] Baker JE, Burch R, Hibble SJ, Loader PK. Properties of silica-supported Cu/Co bimetallic catalysts in the synthesis of higher alcohols. Appl. Catal. 1990; 65: 281-292. https://doi.org/10.1016/S0166-9834(00)81603-6.

[185] Bordoloi A, Anton J, Ruland H, Muhler M, Kaluza S. Metal–support interactions in surface-modified Cu–Co catalysts applied in higher alcohol synthesis. Catal. Sci. & Tech. 2015; 5: 3603-3612. DOI: 10.1039/C5CY00421G.

[186] Tackett BM, Gomez E, Chen JG. Net reduction of CO_2 via its thermocatalytic and electrocatalytic transformation reactions in standard and hybrid processes. Nat. Catal. 2019; 2: 381-386. https://doi.org/10.1038/s41929-019-0266-y.

[187] Rytter E, Sigrid E, Rune M, Odd AL. Fischer-Tropsch catalysts. UK Patent: GB2473071. 2011.

[188] Chen YW, Wang HT, Goodwin Jr JG. Effect of preparation methods on the catalytic properties of synthesis. J. Catal. 1983; 83: 415–427. https://doi.org/10.1016/0021-9517(83)90066-0.

[189] Lekhal A, Glasser BJ, Khinast JG. Impact of drying on the catalyst profile in supported impregnation catalysts. Chem. Eng. Sci. 2001; 56: 4473–4487. https://doi.org/10.1016/S0009-2509(01)00120-8.

[190] Munnik P, Krans NA, De Jongh PE, De Jong KP. Effects of drying conditions on the synthesis of Co/SiO_2 and Co/Al_2O_3 Fischer-Tropsch catalysts. ACS Catal. 2014; 4: 3219–3126. https://doi.org/10.1021/cs5006772.

[191] Eggenhuisen TM, Munnik P, Talsma H, De Jongh PE, De Jong KP. Freeze-drying for controlled nanoparticle distribution in Co/SiO_2 Fischer–Tropsch catalysts. J. Catal. 2012; 297: 306–313. https://doi.org/10.1016/j.jcat.2012.10.024.

[192] Abdouss M, Arsalanfar M, Mirzaei N, Zamani Y. Effect of drying conditions on the catalytic performance, structure, and reaction rates over the Fe-Co-Mn/MgO catalyst for production of light olefins. Bull Chem. React. Eng. Catal. 2018; 13: 97. https://doi.org/10.9767/bcrec.13.1.1222.97-112.

[193] Chernavskii PA. Preparation of Fischer-Tropsch catalysts. Kinet. Catal. 2005; 46: 634–640. https://doi.org/10.1007/s10975-005-0119-3.

[194] Van Steen E, Sewell GS, Makhothe RA, Micklethwaite C, Manstein H, De Lange M, O'Connor CT. TPR study on the preparation of impregnated Co/SiO_2 catalysts. J. Catal. 1996; 162: 220-229. https://doi.org/10.1006/jcat.1996.0279.

[195] Tao Z, Yang Y, Ding M, Li T, Xiang H, Li Y. Effect of calcination behaviors on precipitated iron–manganese Fischer–Tropsch synthesis catalyst. Catal. Lett. 2007; 117: 130-135. https://doi.org/10.1007/s10562-007-9118-5.

[196] Mirzaei AA, Shahriari S, Arsalanfar M. Effect of preparation conditions on the catalytic performance of Co/Ni catalysts for CO hydrogenation. J. Nat. Gas Sci. and Eng. 2011; 3: 537-546. https://doi.org/10.1016/j.jngse.2011.06.003.

[197] Hemmati MR, Kazemeini M, Khorasheh F, Zarkesh J. Investigating the effect of calcination repetitions on the lifetime of $Co/\gamma\text{-}Al_2O_3$ catalysts in Fischer–Tropsch synthesis utilising the precursor's solution affinities. J. Taiwan Inst. Chem. E 2013; 44: 205-213. https://doi.org/10.1016/j.jtice.2012.11.003.

[198] Sun Y, Sun QW, Jiang FK, Liu JS, Zhang ZS. Effects of calcination and reduction temperatures on the performance of $Co\text{-}Pt\text{-}ZrO_2/Y\text{-}Al_2O_3$ catalysts for Fischer-Tropsch synthesis. J. Fuel Chem. and Tech. 2012; 40: 54-58. https://doi.org/10.1016/S1872-5813(12)60007-3.

[199] Jalama K. Fischer–Tropsch synthesis over Co/TiO_2 catalyst: Effect of catalyst activation by CO compared to H_2. Catal. Commun. 2016; 74: 71–74. https://doi.org/10.1016/j.catcom.2015.11.004.

[200] Koizumi N, Ibi Y, Hongo D, Hamabe Y, Suzuki S, Hayasaka Y, Shindo T, Yamada M. Mechanistic aspects of the role of chelating agents in enhancing Fischer–Tropsch synthesis activity of Co/SiO_2 catalyst: Importance of specific interaction of Co with chelate complex during calcination. J. Catal. 2012; 289:151-163. https://doi.org/10.1016/j.jcat.2012.02.003.

[201] Jung J, Lee J, Choi G, Ramesh S, Ju D. The characterization of micro-structure of cobalt on γ-Al_2O_3 for FTS: Effects of pretreatment on Ru-Co/γ-Al_2O_3. Fuel 2014; 149: 1–12. https://doi.org/10.1016/j.fuel.2014.09.001.

[202] Akbari M, Mirzaei AA, Arsalanfar M. Microemulsion based synthesis of promoted Fe–Co/MgO nano catalyst: Influence of calcination atmosphere on the physicochemical properties, activity and light olefins selectivity for hydrogenation of carbon monoxide. Mat. Chem. and Phys. 2020: 123003. https://doi.org/10.1016/j.matchemphys.2020.123003.

[203] Aw MS, Črnivec IG, Djinović P, Pintar A. Strategies to enhance dry reforming of methane: Synthesis of ceria-zirconia/nickel–cobalt catalysts by freeze-drying and NO calcination. Int. J. Hydrogen Energy 2014; 39: 12636-12647. https://doi.org/10.1016/j.ijhydene.2014.06.083.

[204] Sun X, Sartipi S, Kapteijn F, Gascon J. Effect of pretreatment atmosphere on the activity and selectivity of Co/meso HZSM-5 for Fischer–Tropsch synthesis. New J. Chem. 2016; 40: 4167-4177. DOI: 10.1039/C5NJ02462E.

[205] Arsalanfar M, Akbari M, Mirzaei N, Abdouss M. Light olefin production on the Co–Ni catalyst: calcination conditions, and modeling and optimization of the process conditions by a statistical method. New J. Chem. 2020; 44: 7467-7483. DOI: 10.1039/C9NJ04404C.

[206] Mirzaei AA, Galavy M, Beigbabaei A, Eslamimanesh V. Preparation and operating conditions for cobalt cerium oxide catalysts used in the conversion of synthesis gas into light olefins. J Iranian Chem. Soc. 2007; 4: 347-363. https://doi.org/10.1007/BF03245986.

[207] Cho KM, Park S, Seo JG, Youn MH, Nam I, Baeck SH, Chung JS, Jun KW, Song IK. Effect of calcination temperature of alumina supports on the wax hydrocracking performance of Pd-loaded mesoporous alumina xerogel catalysts for the production of middle distillate. Chem. Eng. J. 2009; 146: 307-314. https://doi.org/10.1016/j.cej.2008.10.008.

[208] Kamath G, Badoga S, Shakouri M, Hu Y, Dalai AK. Influence of calcination on physico-chemical properties and Fischer–Tropsch activity of titanosilicate supported cobalt catalysts with different pore sizes. Appl. Catal. A Gen. 2020: 117563. https://doi.org/10.1016/j.apcata.2020.117563.

[209] Lapidus A, Krylova A, Rathouskp J, Zukal A. Hydrocarbon synthesis from carbon monoxide and hydrogen on impregnated cobalt catalysts II. Activity of 10%Co/Al_2O_3 and 10%Co/SiO_2, catalysts in Fischer–Tropsch synthesis. Appl. Catal. A Gen. 1992; 80: 1–11. https://doi.org/10.1016/0166-9834(91)85113-A.

[210] Mochizuki T, Hara T, Koizumi N, Yamada M. Surface structure and Fischer–Tropsch synthesis activity of highly active Co/SiO_2 catalysts prepared from the impregnating solution modified with some chelating agents. Appl. Catal. A Gen. 2007; 317: 97-104. https://doi.org/10.1016/j.apcata.2006.10.005.

[211] Weller S, Hofer LJE, Anderson RB. The role of bulk cobalt carbide in the Fischer—Tropsch synthesis. J. Am. Chem. Soc. 1948; 70: 799-801. https://doi.org/10.1021/ja01182a108.

[212] Karaca H, Safonova OV, Chambrey S, Fongarland P, Roussel P, Griboval-Constant A, Lacroix M, Khodakov AY. Structure and catalytic performance of Pt-promoted alumina-supported cobalt catalysts under realistic conditions of Fischer–Tropsch synthesis. J. Catal. 2011; 277: 14-26. https://doi.org/10.1016/j.jcat.2010.10.007.

[213] Van Steen E, Claeys M, Dry ME, van de Loosdrecht J, Viljoen EL, Visagie JL. Stability of nanocrystals: Thermodynamic analysis of oxidation and re-reduction of cobalt in water/hydrogen mixtures. J. Phys. Chem. B 2005; 109: 3575-3577. https://doi.org/10.1021/jp045136o.

[214] Fischer N., Claeys M. In situ characterization of Fischer–Tropsch catalysts: a review, J. Phys. D Apply Phys. 2020, 53: 293001. doi.org/10.1088/1361-6463/ab761c/meta.

[215] Melaet G, Ralston WT, Li CS, Alayoglu S, An K, Musselwhite N, Kalkan B, Somorjai GA. Evidence of highly active cobalt oxide catalyst for the Fischer–Tropsch synthesis and CO_2 hydrogenation. J. Am. Chem. Soc. 2014; 136: 2260-2263. https://doi.org/10.1021/ja412447q.

[216] Mohandas JC, Gnanamani MK, Jacobs G, Ma W, Ji Y, Khalid S, Davis BH. Fischer–Tropsch synthesis: characterization and reaction testing of cobalt carbide. ACS Catal. 2011; 1: 1581-1588. https://doi.org/10.1021/cs200236q.

[217] Graham UM, Jacobs G, Gnanamani MK, Lipka SM, Shafer WD, Swartz CR, Jermwongratanachai T, Chen R, Rogers F, Davis BH. Fischer–Tropsch Synthesis: Higher oxygenate selectivity of cobalt catalysts supported on hydrothermal carbons. ACS Catal. 2014; 4: 1662-72. https://doi.org/10.1021/cs400965t.

3.1 Introduction

With the aim of investigating the active phase in cobalt Fischer-Tropsch synthesis, different reducing agents, supports and operating conditions were used. Traditional supports such as SiO_2, TiO_2 and Al_2O_3, which have been widely studied, were used to get a better understanding of the FTS reaction without any support complications. The FT experiments were carried out in a solid-gas regime in a fixed bed reactor (FBR) to study the product spectrum of each catalyst at similar reaction conditions. Some novel experiments such as the addition of CO during standard H_2 reduction or reducing with syngas at different activation temperatures were investigated. The experiments are aimed at collecting valuable and sufficient data to understand the role of cobalt species in FTS and to contribute to the in-depth understanding of FT by providing generic conclusions that can be applied in the design of Co-based catalysts. The data was collected throughout the experiments, with time on stream (TOS), until a steady state was reached.

The Fischer-Tropsch reaction is very complex and a slight change in the pre-treatment procedure can result in a very different product spectrum. A brief discussion of the experimental procedures that were used to prepare and pre-treat the catalysts as well as the experimental equipment used are all included in this chapter. We also describe the methods and principles that were used to characterise the catalyst and process the original data. The chapters that will follow include detailed accounts of the work performed to evaluate the use of different reducing gases (H_2/syngas), different reduction temperatures, different supports and promoters. All the experiments were conducted at NECSA (South African Nuclear Energy corporation) laboratory situated in Pretoria.

3.2 Materials and chemicals used

3.2.1 Gases

The gases that were used in the NECSA laboratory were supplied by AFROX (African Oxygen) Ltd. The gas components present in the particular mixture was indicated by the composition certificate hanging on the gas cylinder. Ultra-high purity (>99.9997%) were used for the reduction of the catalysts, the FTS reaction and for the gas chromatographs (GC) as carrier gases.

Three kinds of reducing gases were used to reduce the catalysts prior to FTS experiments. Some of the catalysts were reduced with pure H_2, some a mixture of syngas with $H_2/CO/N_2$ with 10 vol.% of N_2 and the last group of catalysts was activated in a series of reducing agents, starting with the reduction in pure H_2 followed by CO then back to H_2, namely H-C-H.

3.2.2 Catalyst support

The cobalt metal was loaded onto silica, titania and alumina support. The cobalt [$Co(NO_3)_2.6H_2O$], silica gel, and alumina support were supplied by Sigma-Aldrich and titania [(TiO_2) P25] supplied by Degussa. The effect of promotion was studied using ruthenium which was also supplied by Sigma-Aldrich.

3.3 Experimental set up

Several experiments were carried out in a gas-solid regime with different reduction mixtures using the different supported catalysts. The P and ID diagram for the experimental set-up is shown below in Figure 3.1, together with a general explanation of the product analysis.

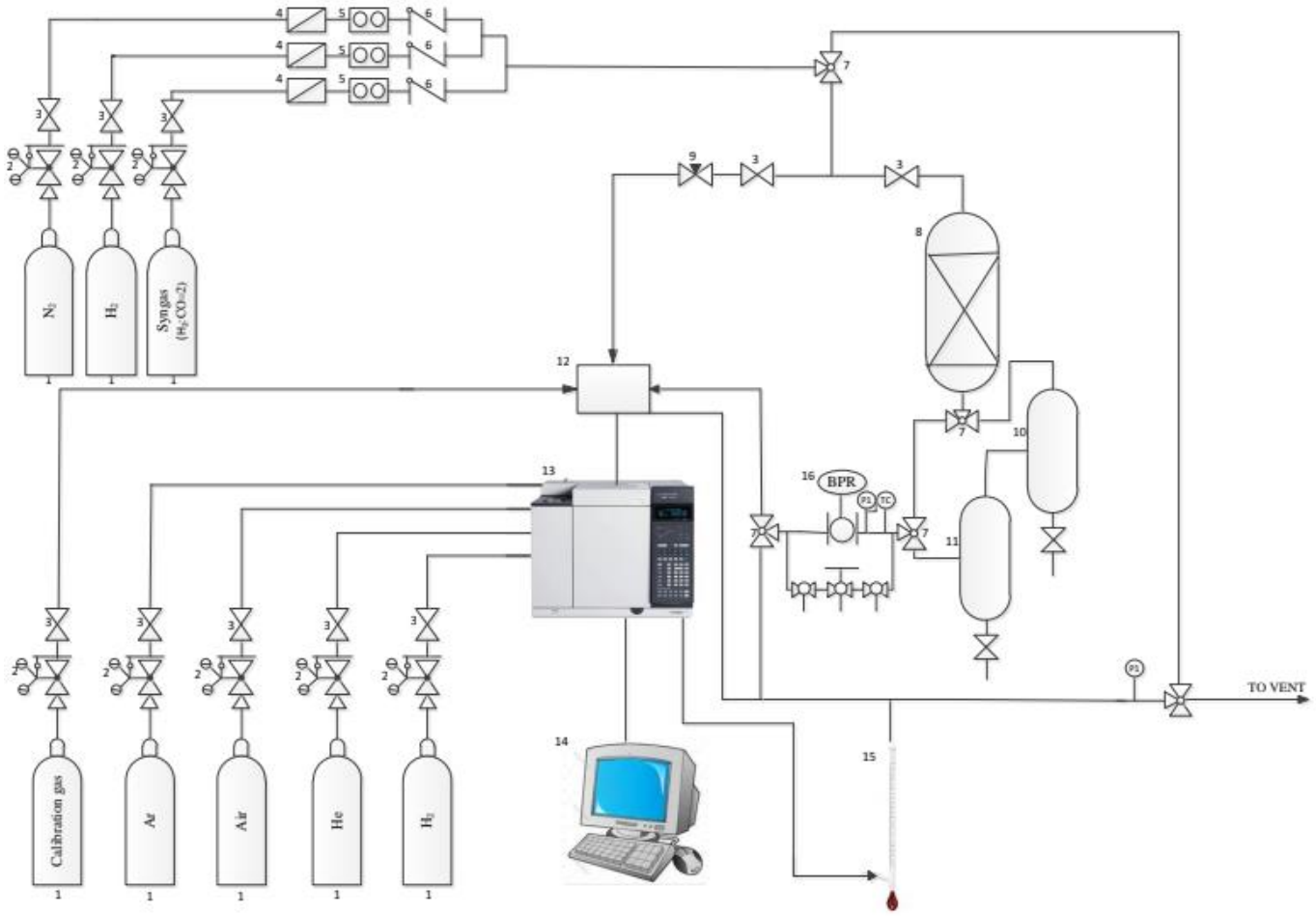

Figure 3. 1: Experimental set up 1. gas cylinders; 2. pressure regulators; 3. shut-off valves; 4. filters; 5. mass flow controllers; 6. one-way valves 7. three-way valves; 8. fixed bed reactor; 9. Back pressure regulator; 10. hot condensable product trap; 11. cold condensable product trap; 12. switching valve box; 13. online GC (Agilent 7890A); 14. computer (for data collection); 15. bubble meter; 16. back pressure regulator.

The desired gas compositions were controlled by setting the flow rates of the gases using the mass flow controllers (Brooks instrument) shown in Figure 3.2 as number 5. The model catalysts under study, Co/TiO_2, Co/SiO_2 and/or Co/Al_2O_3, were prepared at the Chemical Engineering laboratory at UNISA and were packed into the column of the reactor. Catalyst packing was done carefully, the catalyst was placed at the centre of the reactor supported by packed ceramic balls on both sides to fill up the reactor volume. These ceramic stainless-steel balls also assist in pre-heating the syngas mixture before it comes into contact with the catalyst, further details are given in section 3.4. The reactor has two products traps

(number 10 and 11 in Figure 3.2) that are controlled by a back-pressure regulator (Swagelok). Wax was collected using the heated hot trap (at 150 ˚C), number 10 Figure 3.2, and removed periodically. The product tubes from the reactor were kept at 200 ˚C to prevent condensation. Oil and water were collected in the high-pressure cold trap, number 11 Figure 3.2, and also removed periodically as the reaction proceeds.

The product stream leaving the reactor was then sent into the on-line Gas Chromatography (Agilent GC, number 13 Figure 3.2) and fed into the sampling loop to analyse the gaseous hydrocarbons. The stream leaving the GC after a sample has been taken was then sent to a bubble meter and used to indicate the tailgas flow rate and thereafter to the vent.

3.3.1 The reactor system

The tubular fixed bed reactor (FBR) was supplied by the Autoclave Engineers. The dimensions and specifications are given in Figure 3.2 below. FBR reactors are designed for low temperature Fischer-Tropsch (180-250 ˚C) with the aim of producing linear waxes which can be hydrocracked to produce a high-quality diesel.

The FBR reactor is made out of stainless steel (length 204 mm and diameter 8mm), the heating element and the thermocouple wall co-act to control and maintain the temperature at the desired operating temperature. The middle stainless-steel tube provides free movement to the middle thermocouple, to move up and down, which is used to indicate the temperature at different axial positions in the bed. Ceramic balls are loaded on top or bottom sides of the catalyst to support the catalyst bed and to preheat the inlet gas. The quartz wool placed at either the top or bottom of the catalyst bed, which is used to rest the catalyst. The independent heating jackets were placed outside the reactor along the axial direction to heat up the reactor and to make sure that the temperature profile of the catalyst bed was flat. The reactor was also covered by a thermal blanket to prevent any thermal runaway.

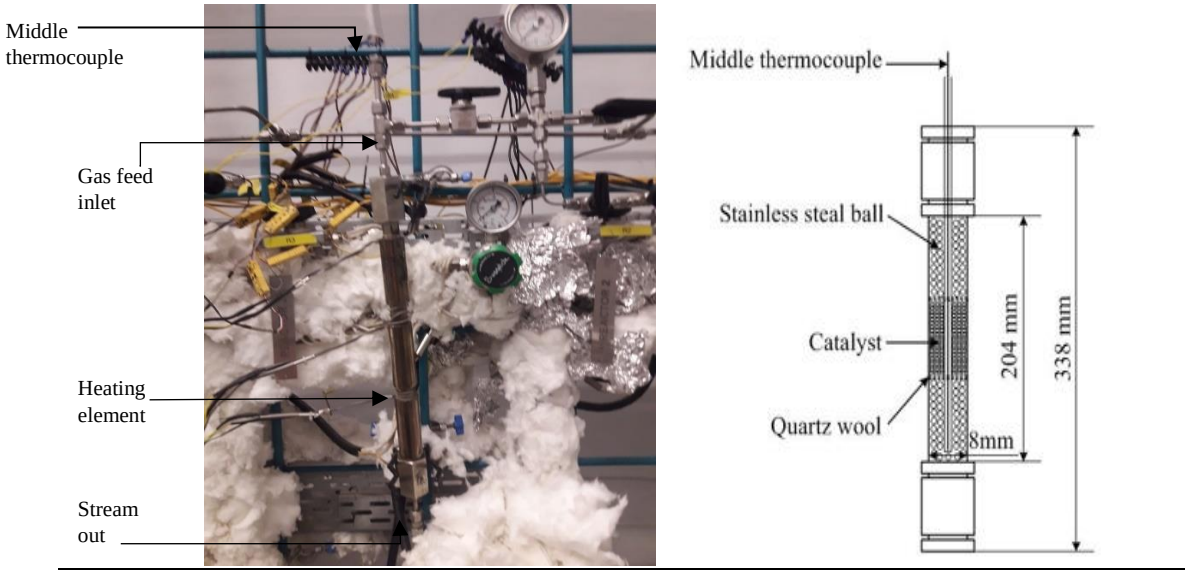

Figure 3. 2: The layout of a micro-scale FBR

3.3.2 Catalyst

This work will not particularly focus on developing and testing new catalyst materials but rather investigate the reaction behaviour of Fischer-Tropsch synthesis using traditional cobalt-based catalysts. Typical supported cobalt catalysts were prepared and used in the study. The supports used were SiO_2, TiO_2 and Al_2O_3, and two silica catalysts were prepared, one promoted with 0.25% Ru-Co/SiO_2 and one without Ru (Co/SiO_2) to perform a comprehensive study. The preparation of the catalyst followed a classic impregnation procedure and basic characterisation were performed, which include TPR, BET, XRF, TEM and XRD and we also performed the novel in-situ catalyst characterisation using *in-situ*-XRD (PXRD).

3.3.2.1 Catalyst Preparation

The model catalysts used for this study consisted of 15 wt% cobalt and the balance being the support weight. Chapters 4-7 gives detailed preparation and experimental procedures used to study these catalysts. Furthermore, these chapters have been prepared as form of papers for future publication in a journal article, therefore, in order to avoid any repetition, please refer to these chapters for further details.

A. Catalyst Characterisation

Different types of characterisation techniques were employed to study the physicochemical characteristics of the model catalysts. These include: (i) the temperature programmed reduction (TPR), which analyses the reduction kinetics of an oxidised catalyst precursor; (ii) Brunauer-Emmett-Teller (BET), which determines the surface area and the porosity of the catalyst; (iii) X-ray fluorescence (XRF), which determines the metallic content in the fresh catalysts; (iv) Transmission Electron Microscopy (TEM), which studies the morphology and particle size of the active phase and how it is dispersed on the surface of the support; (v) *in situ* powder X-ray diffraction (PXRD) and X-ray diffraction (XRD), which is used to identify crystalline phases in the catalyst by means of lattice structural parameters, and for particle size measurements. The XRD and PXRD characterisation techniques are somewhat similar, the only difference being that PXRD identify the phase abundance and particle size of the active metal during reduction whilst with XRD, identification of the phases takes place at room temperature. Lastly, X-ray photoelectron spectroscopy (XPS) experiments were performed to determine the chemical and electronic state composition as well as the elemental composition. Please refer to Chapters 4-7 for further details on the characterisation procedures.

B. Catalyst Reduction

Catalyst activation was done in-situ in a FBR, prior to FTS reaction, at different reduction temperatures using different reducing agents. About a gram of catalyst was loaded into the reactor for each run. The reduction of supported cobalt catalysts was studied for a temperatures range of 220-350 ˚C. Pure gasses (H_2, CO) and premixed syngas were used to reduce the catalysts at a constant flow rate of 60 ml(NTP)/min. The temperature was gradually increased at a steadily rate of 1-5 ˚C/min to the desired reduction temperature and once the temperature has been reached, it was kept constant for 16 hrs, see Figure 3.3 for an example of the temperature programme.

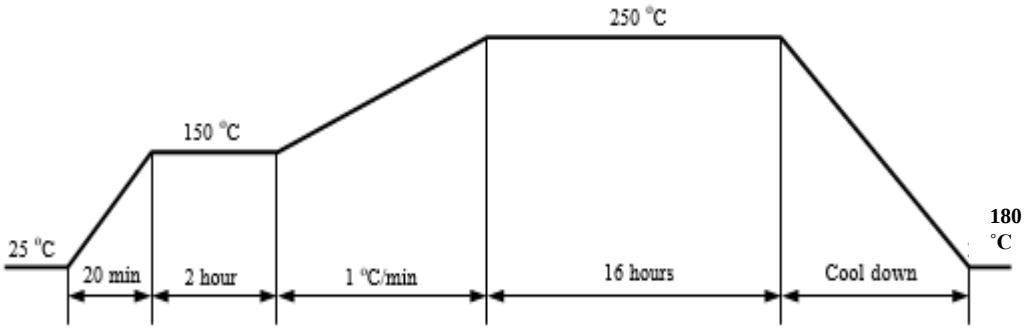

Figure 3. 3: A depiction of the reduction temperature profile for catalyst reduction at 250˚C

C. Catalyst testing

For the FTS experiments the fixed bed microreactor was kept at 210 °C and 20 bars until steady state was reached. An FTS gas stream (H_2:CO:N_2 ratio = 6:3:1) was introduced into the reactor at a flow of 60 Nml/min. The product analysis was conducted online using the Agilent gas chromatograph. Gases were all supplied by African oxygen (AFROX Ltd).

3.4 Product Analysis

The product stream consists of three phases: gaseous phase, an oil phase and a wax phase. The gaseous phase stream was analysed with a gas chromatograph (Agilent GC) for the gaseous components, which were CO, H_2, N_2, CO_2, α-olefins C_2-C_5 and linear paraffins C_1-C_{10}. The Agilent GC is equipped with three detectors namely flame ionising detector (FID), thermal conductor detector (TCD)-A and TCD-B, the hydrocarbon products detected were analysed using the FID, and the CO, CO_2 and N_2 components were all analysed by the TCD-A, while H_2 was detected by the TCD-B. All detectors used Argon (AFROX Ltd. 99.99%) as carrier gas.

The oven is first maintained at an initial temperature of 35 ˚C for 5 minutes, thereafter it is slowly increased to 200 ˚C at a rate of 3 ˚C/min. Once the temperature has reached 200 ˚C, it is then maintained at this temperature for 60 minutes. The analysis time per sample takes roughly about 120 minutes in total. A monitor is connected to the GC, where all the information from the detectors regarding the sample is captured and stored using a software

called ChemStation. The GC related parameters are listed in Table 3.1 and an online GC chromatogram is shown in Figure 3.4.

The GC was calibrated with a premixed calibration gas, in which all the gases were known with their corresponding molar fractions. The calibration gas cylinder contained H_2, CO, CO_2, N_2,CH_4, C_2H_4 and C_2H_6. Table 3.2 gives the composition of the calibration gas. The C_1 and C_2 hydrocarbons were calibrated directly since they are present in the calibration mixture. For the remaining hydrocarbons in the gas phase which cannot be calculated directly, the calibration for C_2 and the corresponding response factors was used to extrapolate these hydrocarbons. An example of the mass balance calculations will be described in the section that follows.

The analysis of the oil and wax products can be carried out using an off-line GC with an FID on a DB-5 capillary column. These condensed phases can be analysed directly from the GC peak area percentages. The peak identification can be performed using an injection of pure components.

Table 3. 1: The online GC parameters

Detector	Front TCD T = 250 ˚C	AUX TCD T = 250 ˚C	Front FID T = 250 ˚C
Column	1-RESTEK, Molesieve 13X, 80/100 mush, 1.0mm * 2.00m * 1/16", max temp: 350 ˚C 2-RESTEK, Hayesep Q, 100/120 mush, 0.75mm * 1m * 0.95mm, max temp: 275 ˚C	3-RESTEK, Molesieve 13X, 80/100 mush, 1.0mm * 2.00m * 1/16", max temp: 350 ˚C 4-RESTEK, Hayesep Q, 100/120 mush, 0.75mm * 1m * 0.95mm, max temp: 275 ˚C	5-CP-Sil 5 CB, 25m * 150μm * 2 μm, max temp: 350 ˚C
Carrier gas	UHP He, flow rate 30 ml(NTP)/min	UHP N_2, flow rate 30 ml(NTP)/min	UHP N_2, flow rate 30 ml(NTP)/min
Six-way valve	/	200 ˚C	200 ˚C
Ten-way valve	200 ˚C	200 ˚C	/
Oven temperature program	Hold at 50 ˚C for 5 min, heat to 80 ˚C at 10 ˚C/min, hold at 80 ˚C for 17 min	Hold at 50 ˚C for 5 min, heat to 80 ˚C at 10 ˚C/min, hold at 80 ˚C for 17 min	Hold at 50 ˚C for 5 min, heat to 200 ˚C at 25 ˚C/min, hold at 200 ˚C for 12.2 min
Product analysis	N_2, CO, CO_2, H_2O and CH_4	H_2	C_1-C_{13}

Table 3. 2: Calibration gas components and composition

Component	Mole percentage (%mol)
H_2	49.99
CO_2	4.9
N_2	10.4
CO	31.4
CH_4	2.62
C_2H_4	0.21
C_2H_6	0.48

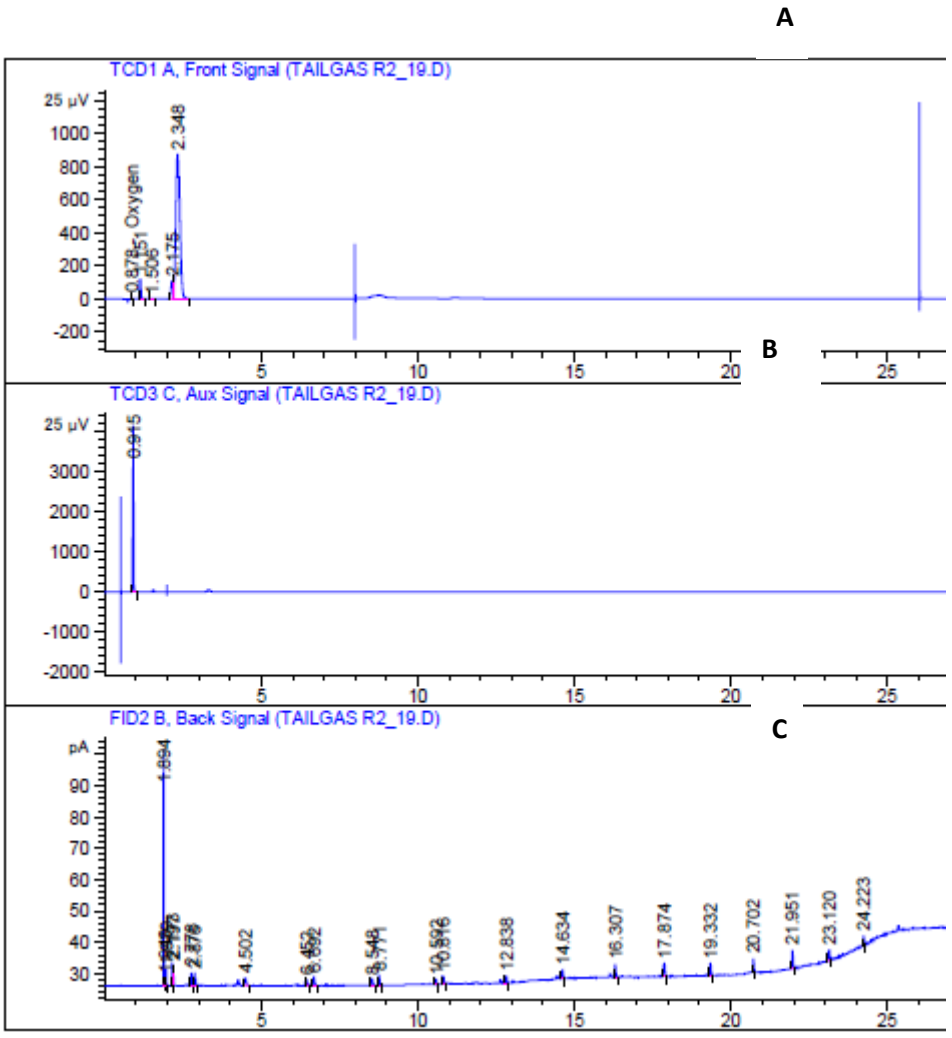

Figure 3. 4: Typical on-line analysis and typical off-line analysis: (a) on-line TCD gas phase data; (b) on-line TCD gas phase data for H_2; (c) on-line FID gas phase products data. The reaction conditions were at 20 bar gauge, 210 ˚C, 60 ml(NTP)/(min·gcat) and syngas mixture of $H_2/CO/N_2$=60%/30%/10% over a cobalt based catalyst.

3.4.1 Data calculation and analysis

To convert the peak areas obtained from the GC to molar compositions for each component, we used the mass balanced calculations as demonstrated by Lu [1] and Yali [2]. A calibration mixture of $CO/H_2/CO_2/N_2/CH_4/C_2H_4/C_2H_6$ was used as an external standard. The analysis of the GC peak areas for the calibration was used to obtain the relationship between the known molar compositions of the calibration gas and the peak areas. Therefore, for any compound either in the reactant or product stream can be presented using the equation below:

$$\%X_{GAS} = AX_{GAS}/AX_{CAL} * \%X_{CAL}$$

Where: $\%X_{GAS}$ is the molar percentage of the compound. AX_{GAS} is the GC integrated area peak corresponding to the compound X, AX_{CAL} is the GC integrated area peak corresponding to the compound X in the calibration gas and $\%X_{CAL}$ is the molar percentage of compound X in the calibration gas.

The olefin and paraffin products with a carbon number higher that 2, which cannot be calibrated directly from the calibration gas, the calibration data for the reference compound (C) and the relative response factor (R) was used to calculate the mole percentage using the following expression:

$$\%X_{GAS} = AX_{GAS}/AC_{CAL} * \%C_{CAL} * RF_{XC}$$

Where: $\%C_{CAL}$ is the molar percentage of the reference compound X in the calibration gas. AC_{CAL} is the GC integrated area peak corresponding to the compound C in the calibration gas, and RF_{XC} is the relative response factor of the compound X with respect to the reference compound C.

The molar response factors of the olefins and paraffins for the hydrocarbon products are presented in Table 3.4. In the calculations we used C_2H_4 as a reference for olefins and C_2H_6 for the paraffins.

Table 3. 3: Hydrocarbons response factors (using C2 as a reference)

Carbon Number	Olefin	Paraffin
2	1	1
3	0.7	0.74
4	0.55	0.55
5	0.47	0.47
6	0.4	0.4
7	0.35	0.35
8	0.32	0.32
9	0.28	0.28
10	0.24	0.24
11	0.21	0.21
12	0.19	0.19
13	0.18	0.18
14	0.17	0.17
15	0.15	0.15

During the FTS reaction, N_2 was added to the feed gas, which serves as an internal standard as it does not react under FTS conditions. Therefore, the relationship between the molar flow rate of N_2 in the feed gas and the effluent gasses can be represented as shown below:

$$F_{in}X_{N2,in} = F_{out}X_{N2,out}$$

Where: F_{in} represents the total molar flowrate of the feed, F_{out} is the molar flowrate of the outlet, $X_{N2,in}$ is the molar fraction of N_2 in the feed and $X_{N2,out}$ represents the outlet molar fraction for N_2.

Therefore, the rate of CO conversion can then be calculated as follows:

$$-rCO = F_{CO,in} - F_{CO,out} / m$$

Where: $F_{CO,in}$ represents the molar flowrate of CO in the feed and $F_{CO,out}$ represent the flowrate of CO going out, rCO is the rate of CO conversion in mol/min/gCat and m (gCat) is the mass of the catalyst in grams.

The molar flowrates of CO in the feed gas and in the outlet stream can also be represented using the expressions below:

$$F_{CO,in} = F_{in}X_{CO,in}$$
$$F_{CO,out} = F_{out}X_{CO,out}$$

Where: $X_{CO,in}$ and $X_{CO,\ out}$ the feed and outlet gas molar fractions of CO, respectively.

Using the expressions given above the rate of CO consumption can be expressed as:

$$-rCO = F_{CO,in}X(\frac{N_{2\,out}}{N_{2\,in}}) - F_{CO,out} / mCat$$

We calculated the rate of conversion for each catalyst directly from the expression given below as $X_{CO,in}$ and X_{N2},in are known from the calibration gas cylinder and $X_{CO,out}$ and

X_{N2},out are obtained from the GC analysis of the effluent gas stream. F_{out} was calculated from the gas volumetric flow rate at the reactor exit with an assumption of the ideal gas law. Therefore, the expression of the %CO conversion is as follows:

$$\%CO = X_{CO,in} - X_{CO,out} * [\frac{N_{2_{in}}}{N_{2_{out}}} * 100] / X_{CO,in}$$

The rate of formation of a gas product θ_i then becomes:

$$r\theta_i = F_{out} X\theta_i / mCat$$

where $r\theta_i$ is the rate in mol/min/gCat and $X\theta_i$ the molar fraction of product θ_i in the reactor outlet .

3.4 References

[1] Lu X. Fischer-Tropsch Synthesis:Towards understanding (Doctoral dissertation), 2012.

[2] Yao Y. Fischer–Tropsch synthesis using CO_2 containing syngas mixtures over cobalt and iron-based catalysts. University of Witwatersrand, Johannesburg, 2011.

CHAPTER 4: ROLE OF CoO-Co NANOPARTICLES SUPPORTED ON SIO_2 IN FISCHER-TROPSCH SYNTHESIS: EVIDENCE FOR ENHANCED CO DISSOCIATION AND OLEFIN HYDROGENATION

The material in this chapter has been published in the Fuel Processing Technology journal. Reference: Shiba NC, Yao Y, Forbes RP, Okoye-Chine CG, Liu X, Hildebrandt, D. Role of CoO-Co nanoparticles supported on SiO_2 in Fischer-Tropsch synthesis: Evidence for enhanced CO dissociation and olefin hydrogenation. Fuel Proc. Tech., 2021; 216: 106781. https://doi.org/10.1016/j.fuproc.2021.106781

Abstract

The role of mixed CoO-Co nanoparticles dispersed on a SiO_2 support for the Fischer-Tropsch synthesis (FTS) has been evaluated. The multiphase CoO-Co/SiO_2 demonstrated high activity for the Fischer-Tropsch (FT) reaction, water-gas shift (WGS) and hydrogenation reactions. The results were the experimental evidence that the CoO-Co interface assisted both the activation of CO and the hydrogenation of R-CHx intermediates. A new mechanism, "CoO-Co H-assisted CO dissociation", was hypothesized to explain the high CO reactivity and selectivity to linear paraffinic products. The synergistic effect between CoO and Co˚ promotes the FT activity, which provides the valuable information for the design of the commercial FT cobalt-based catalysts.

4.1 Introduction

Metallic Co (Co^0) is known to be the active phase for the Fischer-Tropsch (FT) reaction, which converts syngas to long-chain paraffin and olefins, shown by Reactions A and B below [1-6]. Cobalt catalysts need to be activated to reduce the Co oxides to Co^0. A typical reduction procedure uses H_2 at temperatures between 350-400 ˚C, causing the catalyst to undergo a two-stage reduction process ($Co_3O_4 \rightarrow CoO \rightarrow Co$) [1-2]. It has been reported that CoO is active for the water-gas shift (WGS) reaction (Reaction C) [6-7] and methanation reaction (Reaction D) [8]. The partial reduction of Co-based FT catalysts has been reported to suppress the FT reaction, as the CoO species promote the formation of CH_4 and CO_2 via the methanation and WGS reactions, respectively [7-8]. However, a few studies have reported the positive effects of CoO on the FT reaction.

(A) FT chain growth reaction (syngas to olefin):

$$nCO + 2nH_2 \rightarrow C_nH_{2n} + nH_2O$$

(B) FT chain growth reaction (syngas to paraffin):

$$nCO + (2n+1)H_2 \rightarrow C_nH_{2n+2} + nH_2O$$

(C) WGS reaction:

$$CO + H_2O \rightarrow CO_2 + H_2$$

(D) Methanation reaction:

$$CO + 3H_2 \rightarrow CH_4 + 2H_2O$$

(E) Olefin hydrogenation reaction:

$$C_nH_{2n} + H_2 \rightarrow C_nH_{2n+2}$$

This work reports the role of mixed CoO-Co nanoparticles dispersed on a SiO_2 support, which exhibits high catalytic activity for FT synthesis (FTS). Several Co catalysts supported on SiO_2, Al_2O_3, and TiO_2 with a Co 15 wt% metal loading were prepared. Each catalyst was reduced at temperatures ranging from 250 ˚C to 350 ˚C with H_2. Complementary characterization detailing the evolution of the Co containing crystalline phases and their average crystallite sizes during reduction was obtained using *in-situ* powder x-ray diffraction (*in-situ* PXRD). The activity and selectivity of the three catalysts were determined by flowing syngas over the reduced catalysts and comparing the resulting data. The measurement uncertainty estimation of the %CO conversion and product selectivity and formation rate is set at a relative error of 10%, which follows from repetition experiments recovery. Product determination was carried out via the Agilent GC which was calibrated weekly. Identical catalyst preparation, characterization and FT testing procedures were used and are included in the Supplementary information. The Co/Al_2O_3 and Co/TiO_2 catalysts were studied and included in this paper for reference only.

4.2 Experimental Procedure

4.2.1 Catalyst preparation

All the supports (TiO_2, SiO_2 and Al_2O_3) were obtained from Sigma Aldrich and pre-treated prior to use. Catalysts with a 15 wt% metal loading were prepared using the incipient wetness impregnation technique. The procedure used was as follows

The support materials were first calcined under airflow at 500 °C for 6 h. Calcination of the support was done to convert the loose ceramic powders to granules, in order to control the particle size of the support used for the final catalyst. The support was then crushed and sieved into particle sizes ranging between 300 and 600 µm. An aqueous solution of Co (II) nitrate hexahydrate [$Co(NO_3)_2.6H_2O$] was prepared and used to impregnate on the support material. The pre-catalysts were dried at room temperature overnight followed by drying at 40 ˚C for 3h. This was done using the method detailed by Kababji et al. [9] who showed that drying catalyst samples at low temperatures allowed for better control of the crystalline size and avoiding agglomeration of the metal precursor on the support surface. Subsequently, the pre-catalysts were dried at 110 ˚C for 6 h, so as to ensure the removal of any absorbed water. The pre-catalysts were each calcined under flowing air at 350 °C for 8 h, in order to decompose the cobalt nitrate to cobalt oxide, so as to produce catalysts with the general formula Co_3O_4/TiO_2, Co_3O_4/SiO_2 and Co_3O_4/Al_2O_3.

4.2.2 Catalyst characterisation

The catalyst surface area and porosity were measured by nitrogen physisorption at -196 °C using a Micromeritics Tristar 3000 surface area and porosity analyser. Prior to measurement, the sample was degassed at 200 °C for 6 h. The surface area was obtained using the Brunauer-Emmett-Teller (BET) method. The total pore volume was determined at a relative pressure of 0.99. The pore size distributions were evaluated from the desorption branches on the isotherms using the Barrett-Joyner-Halenda (BJH) method.

Temperature-programmed reduction (TPR) experiments were performed using a 500 mg sample of catalyst under a mixture of 5 vol% H_2 in Ar flowing at 30 cm^3/min. The temperature was ramped at a rate of 10 ˚C/min until it reached 900 ˚C. A thermal conductivity detector (TCD) was used to determine the hydrogen consumption. Additional TPR analysis was conducted on the SiO_2-supported catalyst, with the temperature being ramped to either 250 or 350 ˚C at a rate of 5 ˚C/min; thereafter the temperature was kept constant for 6 h.

Ex situ powder X-ray diffraction (XRD) patterns were obtained using a Phillips X'Pert Pro X-ray Diffractometer equipped with a monochromated Cu Kα X-ray source, flat plate geometry sample stage and pixel detector. To identify the crystalline phases present, the samples were scanned in the 2θ range of 20˚ to 80˚at a scan speed of 0.2 s/step.

X-ray fluorescence (XRF) was used to measure the amount of cobalt in the catalyst. The sample was loaded into the palletiser and pressurised to 10 KPa for a few minutes. The sample pellet was then placed in the XRF machine sample holder for analysis.

Transmission Electron Microscopy (TEM) was used to observe the distribution of cobalt in each of the three catalysts. TEM was performed using a JEOL 2010F instrument operating at 200 KV. Samples were prepared by embedding non-reduced catalyst particles in a resin and preparing slices of nominal 50 nm thickness using a Richert Jung Ultracut E ultramicrotome.

The in-situ powder X-ray diffraction (PXRD) measurements were obtained using an Anton-Paar XRK900 furnace under a flowing H_2 atmosphere (HP, 1 atm), in the temperature range from 30 °C to 430 °C at a rate of 0.17 °C/min. The XRK900 was attached to a Bruker D8 Advance diffractometer equipped with a Cu Kα X-ray source and a VÅNTEC detector. For all PXRD data presented here, the crystalline phase identification was done using DIFFRAC.EVA (Version 2. Release 2014) using the ICDD PDF2 database (Release 2016). Phase quantification was done using the Rietveld method as implemented in Bruker AXS TOPAS software (Version 5, 2014).

4.2.3 Catalyst testing

FT reactions were conducted in a fixed bed microreactor at 210 °C and 20 bars. The samples (1 g of catalyst) were reduced in-situ in pure H_2 at atmospheric pressure and 60 Nml/min. Three different reduction temperatures, 250 °C, 300 °C, and 350 °C were used for the reduction of each of the catalysts. The reactor was maintained at the reduction temperature for 16 h. The reactor was then cooled down to 180 °C. Thereafter, a typical FTS feed gas stream was introduced into the reactor, comprising 60 mol% H_2 and 30 mol% CO (H_2:CO ratio = 2:1) balanced in N_2, and flowing at 60 Nml/min. The reactor's pressure was initially gradually increased to 20 bar, and thereafter the temperature of the reactor was gradually

increased to the reaction temperature. Similar FTS conditions were used for all catalysts. The product analysis was conducted using an online Agilent gas chromatograph (GC-Agilent 7890A) with one TCD and two FID detectors. The gases were all supplied by African Oxygen (AFROX Ltd).

The online GC was calibrated weekly with a premixed gas which contained H_2, CO, CO_2, N_2, CH_4, C_2H_4 and C_2H_6. The composition of the calibration gas is given in table 4.1 and an example of the GC analysis for the calibration gas is shown in table 4.2. The C_1 and C_2 hydrocarbons were calibrated directly and the remaining hydrocarbons in the gas phase were calculated using the calibration for C_2 and the corresponding response factors [10]. The average calibration results are then used to fix the feed gas composition and to calculate the %CO conversion as well as the products compositions. The peak areas as shown in Table 4.2 are very close to each other, which indicate a good repeatability of the online GC.

Table 4. 1: Mole fraction of each component in the calibration gas.

Component calibration gas mixture	**H_2**	**CO_2**	**N_2**	**CO**	**CH_4**	**C_2H_4**	**C_2H_6**
Composition (% by mole)	49.90	4.90	10.40	31.40	2.62	0.21	0.48

Table 4. 2: Calibrated GC peak areas for calibration gas mixture.

H_2	**CO_2**	**N_2**	**CO**	**CH_4**	**C_2H_4**	**C_2H_6**
6477.11	517.96	1321.33	3693.73	803.65	133.94	323.40
6468.82	512.35	1318.49	3644.97	818.17	135.92	326.36
6465.86	509.16	1314.47	3647.75	817.45	136.34	329.75

All the experimental runs were held for more than 100 hours to reach a steady state. The last five data points were then used to calculate the average percentages for the CO conversion and products' selectivity and formation rate as reported in Figures 4.4 & 4.6 in the manuscript as well as the graphical abstract. The equations used to calculate the reactant reaction rate, conversion, the product formation rate and selectivity are as follows:

(1) CO reaction rate (R_{CO}, mol/min/gcat)

$$R_{CO} = F_{in}y_{CO,in} - F_{out}y_{CO,out} \quad (a)$$

where F_{in} and F_{out} are the gas flow rate in (feed gas) and out (tailgas), respectively, mol/min/gcat; $y_{CO,in}$ and $y_{CO,out}$ are the CO compositions in the feed gas and tailgas, respectively, %.

(2) CO conversion ($\%CO_{conv}$)

$$\%CO_{conv} = \frac{R_{CO}}{F_{in}y_{CO,in}} * 100 \quad (b)$$

(3) Hydrocarbon product Cn formation rate (carbon based) (R_{C_n}, mol/min/gcat)

$$R_{C_n} = F_{out}y_{C_n} * n \quad (c)$$

where y_{C_n} is the percentage of the product Cn in the tailgas, %; n is the carbon number.

(4) Hydrocarbon product Cn selectivity (carbon based) (S_{C_n}, %)

$$S_{C_n} = \frac{R_{C_n}}{R_{CO}} \quad (d)$$

(5) CO_2 formation rate (R_{CO_2}, mol/min/gcat)

$$R_{CO_2} = F_{out}y_{CO_2} \quad (e)$$

where y_{CO_2} is the percentage of the product CO_2 in the tailgas, %.

(6) CO_2 selectivity (S_{CO_2}, %)

$$S_{CO_2} = \frac{R_{CO_2}}{R_{CO}} \quad (f)$$

The gas compositions in the feed gas and tailgas ($y_{CO,in}$, $y_{CO,out}$, are y_{CO_2}) were obtained by the online GC which was calibrated with a calibration mixture as shown in Tables 4.1-4.2. For further details about the calculations please refer to reference [10]. Based on the calculations, the error of all the data is set to less than 10%. The experimental error is added in all the Figures in the form of error bars.

4.3 Results and Discussion

4.3.1 Catalyst Characterisation

The BET surface area and the average pore sizes for all the catalysts are listed in Table 4.3. The mesoporous structure of the SiO_2 support was retained upon Co impregnation and it displayed a large specific surface area compared to the Al_2O_3 and TiO_2 supports, due to smaller pore sizes of about 6.78 nm, see Table 4.3. Table 4.3 indicates a large pore size distribution for both Al_2O_3 and TiO_2 supports; 43.11 and 38.13 nm, respectively. A drastic decrease in pore size was observed after impregnation on the TiO_2 support accompanied by a noticeable increase in the surface area. This could mean that the Co was successfully deposited into both the pores of the supports and onto the surface. The alumina support showed a slight increase in the surface area and a drastic decrease in the pore size which suggests that most of the Co was deposited into the pores of the alumina support.

Table 4. 3: BET surface area and pore size for the three supports and cobalt based catalysts.

Catalyst/Support	Surface area m^2/g	Pore volume cm^3/g	Pore size (nm)
TiO_2	24.15	0.22	38.13
Co/TiO_2	88.44	0.20	3.25
SiO_2	456.50	0.84	6.78
Co/SiO_2	406.99	0.74	6.23
Al_2O_3	107.51	1.06	43.11
Co/Al_2O_3	115.83	0.57	4.40

The TEM study of the catalysts showed good contrast between the support and the Co_3O_4 particles. The dark regions in Figure 4.1 represent the metal oxide. The Co_3O_4 particles exhibited a nearly spherical shape and appear to be better and more uniformly dispersed on the SiO_2 supported catalyst, see Figure 4.1a. The TiO_2 support grains are cubic in shape and resulted in the Co_3O_4 agglomerates being dispersed on the sides and edges of the cubes, thus forming an uneven distribution as can be seen from the particle size distribution, see Figure 4.1b. The Al_2O_3 supported catalyst shown in Figure 4.1c exhibits substantial structural differences with a decrease in TEM magnification. SiO_2 provides the ideal surface for better distribution of Co, due to the exposed discrete crystal facets. These observations suggest that the nature of the support particles determines the particle size and the distribution of the metal.

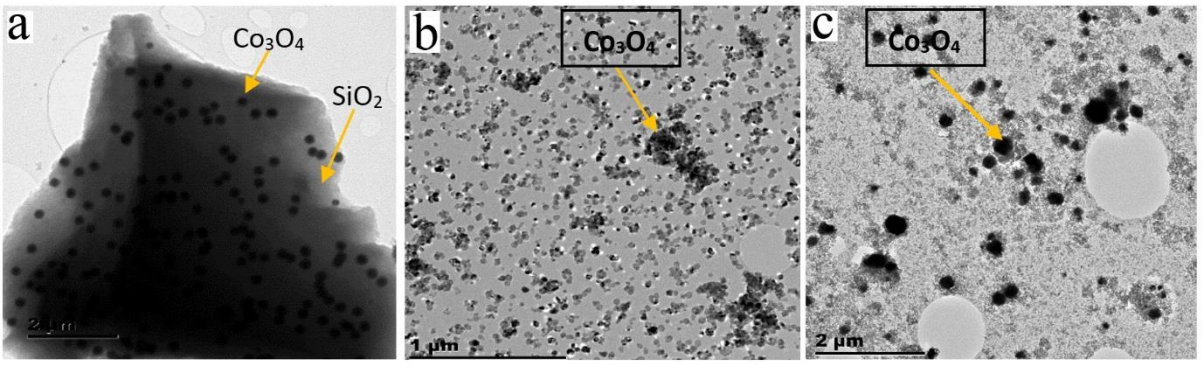

Figure 4. 1: TEM micrograph images of a freshly calcined catalyst: a: Co/SiO_2; b: Co/TiO_2; c: Co/Al_2O_3.

The TPR results as shown in Figure 4.2 demonstrate that the support type has a profound influence on the reducibility of the cobalt species. The difference between the TPR profiles of the catalysts might be caused by the extent of interaction between the support and the metal particles. It has been reported in literature that the strength of the metal support interactions is in the order of Al_2O_3> TiO_2> SiO_2 [11-12]. In agreement, we found the Co/SiO_2 catalyst to reduce at a much lower temperature compared to Co/TiO_2 and Co/Al_2O_3 catalysts, which suggests that Co metal is weakly attached on the silica support compared to the other supports.

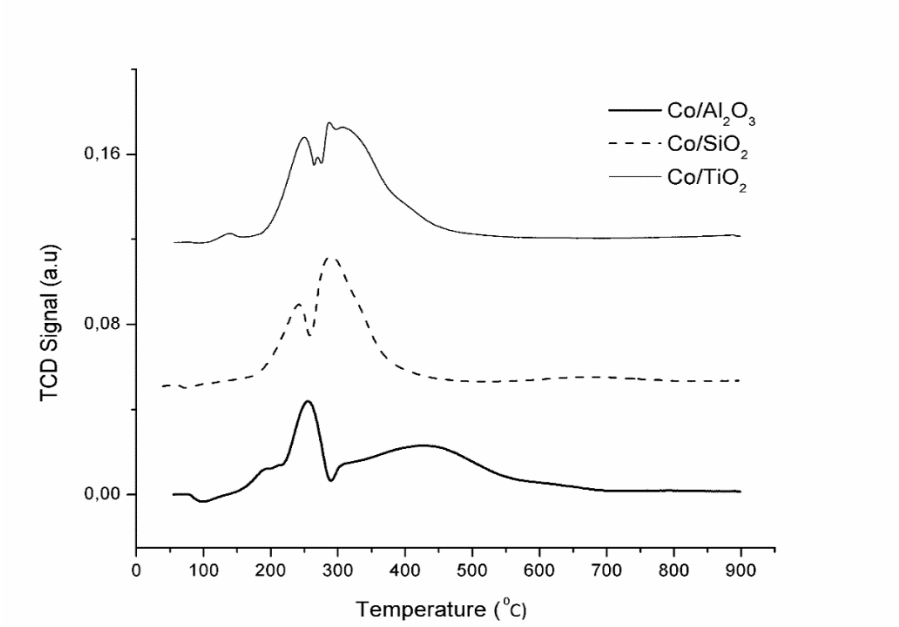

Figure 4. 2: TPR profiles for Co/Al_2O_3, Co/SiO_2 and Co/TiO_2 after calcination.

The average Co_3O_4 particle size, as determined by XRD, was smallest for the SiO_2-supported catalyst (see Table 4.4). The largest Co_3O_4 particles were observed with the Al_2O_3 sample (about 33 nm) followed by TiO_2 (21.5 nm) and lastly SiO_2 (17 nm). Table 4.4 lists the metal content in each catalyst, which was determined by XRF. The XRF Co loading was found to be about 14-15wt%, which corresponds with the theoretical loading calculated during catalyst preparation.

Table 4. 4: XRD results for the particle sizes of the calcined catalysts and XRF results for the actual cobalt loadings of the cobalt-based catalysts.

Catalyst	**XRD (nm)**	**XRF Co content**
	Co_3O_4	wt %±0.03
Co/TiO_2	21.5	14.0
Co/SiO_2	17.0	14.5
Co/Al_2O_3	33.0	15.2

In-situ PXRD was used to monitor the change in the relative phase abundance and average crystallite sizes during reduction with H_2 of the Co/SiO_2 catalyst. The quantitative phase analysis (QPA) results were obtained via Rietveld refinement of the *in-situ* PXRD data, the results are shown in Figure 4.3. The QPA showed that the Co/SiO_2 catalyst contained Co_3O_4 in the calcined state, at the start of the reduction. No crystalline phases owing to the SiO_2 support were observed in the *in-situ* PXRD data as these phases are amorphous. The data shows that the reduction of the Co/SiO_2 catalyst proceeded via a two-step process, where Co_3O_4 was first reduced to CoO, followed by the subsequent reduction of CoO to Co^0. The CoO phase was first observed at temperatures above 190 ^oC, while the Co^0 (fcc/hcp) phases were obtained at temperatures above 310 ^oC. However, at the end of the experiment, the reduction of CoO to Co^0 was incomplete with approximately 29 % of the CoO still present at temperatures of about 380 ^oC. No further changes in the relative phase abundances of these phases were observed up to 430 ^oC (Figure 4.3a). The Co(fcc) phase was found to be the dominant Co containing phase, with less than 15% of the Co being present as the Co(hcp) phase. The Co(hcp) crystallite size was about 5 nm, while the Co(fcc) crystallite size was nearly twice as large as that of Co(hcp). In addition, the crystallite sizes of both Co(fcc) and Co(hcp) remained stable with increasing reduction temperature, which indicates that there is little/no agglomeration or sintering during H_2 reduction, even at 430 $^\circ C$.

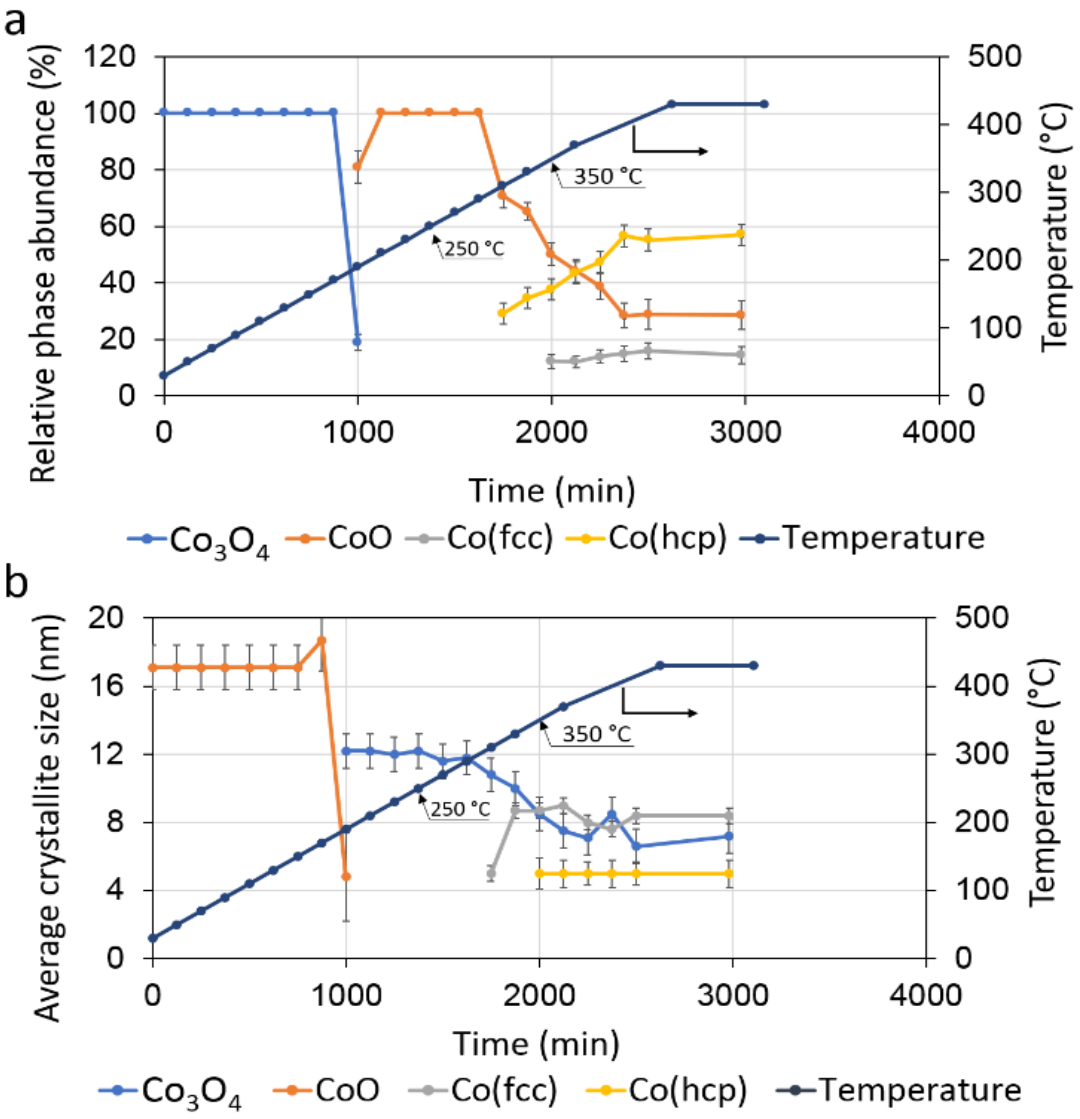

Figure 4. 3: In-situ PXRD analysis results during H_2 reduction of the Co/SiO_2 catalyst with increasing the reduction temperature: (a) Relative phase abundance for the crystallite phase; (b) average crystallite size.

4.3.2 Catalyst Testing

Figure 4.3 shows the effect of reduction temperature on %CO conversion. The Co/SiO_2 catalyst showed the highest FT activity when it was reduced at a temperature of 250 ˚C. However, the activity was observed to decrease with increasing reduction temperature (Figure 4.4). Conversely, the data showed that the %CO conversion increased with increasing reduction temperature for the Co/TiO_2, and Co/Al_2O_3 catalysts (Figure 4.4). The

activity trends obtained for both TiO_2 and Al_2O_3 supported catalysts are in line with the literature, which reports that increasing reduction temperatures up to 400 ˚C, generally improves the %CO conversion [3-4]. Bian et al. also reported the similar trends for SiO_2 supported catalysts [13]. In general, this occurs because the amount of Co oxides reduced to Co^0 increases with the reduction temperature and as Co^0 is active for FTS, this results in an observed increase in the %CO conversion. However, in the present study, the Co/SiO_2 catalyst behaved differently than the Co/Al_2O_3 and Co/TiO_2 catalysts under study, as well as that has been reported in literature [3-4,13].

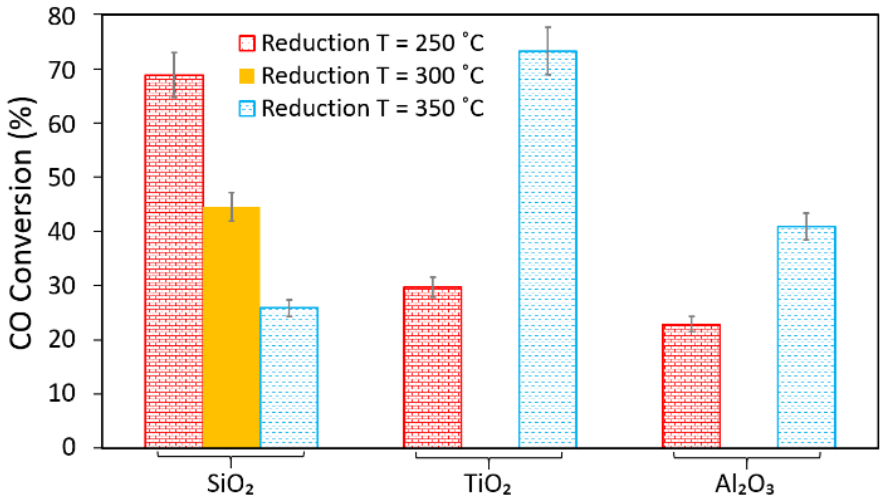

Figure 4. 4: The effect of reduction temperature on %CO conversion for the Co/SiO_2, Co/TiO_2, and Co/Al_2O_3 catalysts. The legend indicates the reduction temperature (˚C). Reaction conditions: $H_2/CO = 2$, 20 bar, 210 ˚C and 60 Nml/min.

Based on the BET, XRF, TEM, PXRD and TPR characterization data for the freshly prepared catalysts, it was observed that: (i) SiO_2 has a smaller pore size and a larger surface area than Al_2O_3 and TiO_2 (Table 4.3); (ii) The Co loading of the three catalysts was found to be similar with 14.0 wt%, 14.5 wt% and 15.2 wt% Co calculated for the Co/TiO_2, Co/SiO_2 and Co/Al_2O_3 catalysts respectively (Table 4.4); (iii) The Co was found to exist as Co_3O_4 particles after impregnation; (iv) The Co_3O_4 particles exhibited a nearly spherical shape and appeared to be better and more uniformly dispersed on the SiO_2 support than those supported on either Al_2O_3 and TiO_2 (Figure 4.1); (v) The Co/SiO_2 catalyst had the

smallest average crystallite size, about 17 nm after calcination compared to Co/TiO_2 with 22 nm and Co/Al_2O_3 with 33 nm (Table 4.4); and (vi) The TPR analysis results indicated that the reduction temperature for the Co/SiO_2 catalyst was lower than that of either Co/TiO_2 or Co/Al_2O_3, which may be due to weaker metal-support interactions (Figure 4.2). Silica supports have been reported to exhibit lower metal-support interactions compared to Al_2O_3 and TiO_2 supports [14-15]. Support characteristics are an important consideration when developing an active heterogeneous catalyst [16-17]. We believe that the behavior shown in Figure 4.4 may be due to the combination of support morphology and the strength of metal support interactions.

The *in-situ* PXRD results indicate that at 250 ˚C Co primarily exists as CoO and not Co^0, see Figure 4.3. Therefore, three different TPR experiments were conducted to support this observation. They include reduction experiments where: (i) the catalyst was reduced in H_2 by gradually increasing the reduction temperature up to 900 ˚C; (ii) the catalyst was reduced in H_2 at 350 ˚C for 6 h, and (iii) the catalyst was reduced at 250 ˚C for 6 h. The results of these experiments are shown in Figure 4.5. Two reduction peaks were observed which corresponds to the two-step reduction procedure observed with the *in-situ* PXRD. The area under the second peak in Figure 4.5C (corresponding to a reduction temperature of 250 ˚C) is smaller relative to that in Figure 4.5b (reduction temperature 350 ˚C). This suggests that the two phases, namely Co^0 and CoO, coexisted after reduction with CoO being more abundant than Co˚ for the catalyst reduced at 250 ˚C than 350 ˚C. These results are consistent with the *in-situ* PXRD data. In summary, Figures 4.3 and 4.5 indicate that the density of Co^0 increased with reduction temperature from 250 to 350 ˚C, conversely, the amount of CoO decreased. Therefore, the %CO conversion on the Co/SiO_2 catalyst (Figure 4.4) appears to be related to the amount of CoO present in the reduced catalyst. A higher %CO conversion was obtained (Figure 4.4) when the higher abundance of CoO was observed, corresponding to a low reduction temperature. The conversion decreased as the amount of CoO on the catalyst decreased and this corresponds to an increase in the reduction temperature.

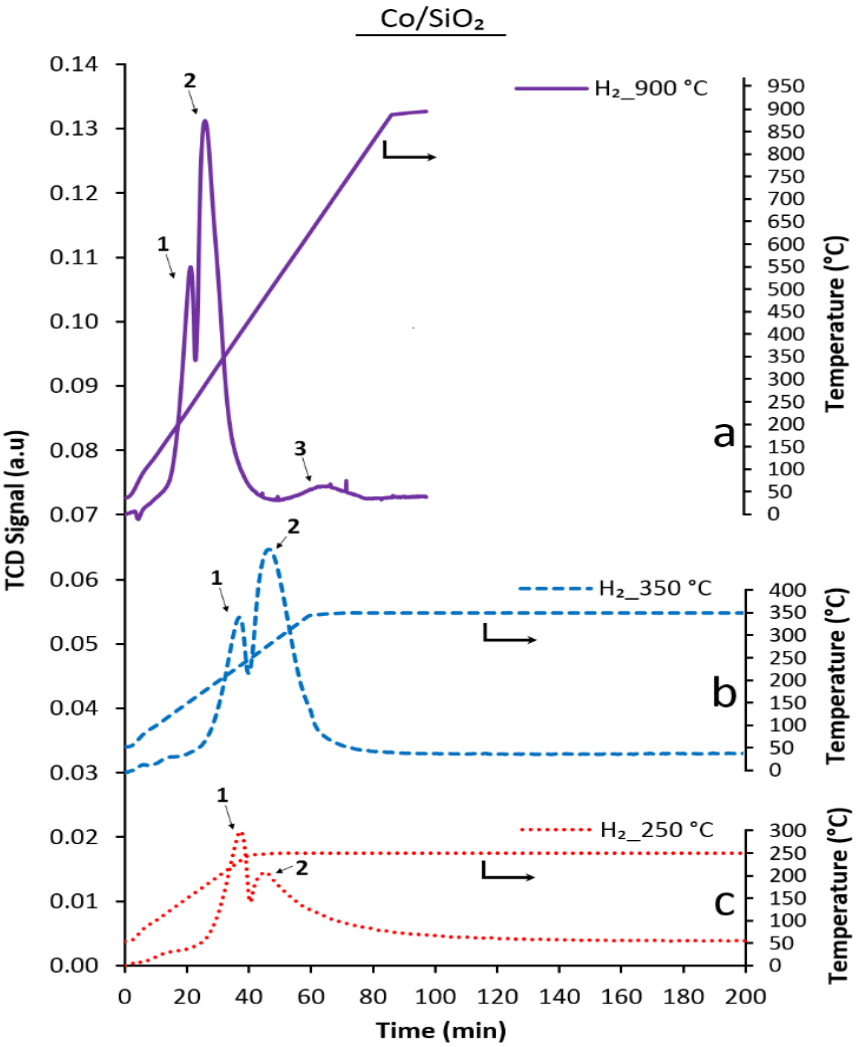

Figure 4. 5: TPR profiles for Co/SiO_2. Reduction condition: 5 vol% H_2 in Ar at 30 ml/min and atmosphere: (a) reduction temperature increased from room temperature to 900 ˚C with a ramping rate of 10 ˚C/min ; (b) reduction temperature increased from room temperature to 350 ˚C with a ramping rate of 5 ˚C/min and kept at 350 ˚C for 6 h; (c) reduction temperature increased from room temperature up to 250 ˚C with a ramping rate of 5 ˚C/min and kept at 250 ˚C for 6 h.

The higher FT activity observed over the SiO_2 catalyst can also be related to the particle size. Table 4.5 compares the cobalt particle size and reducibility of the catalysts when reduced at 250 and 350 ˚C, obtained via in-situ XRD. From the results in Table 4.5, it can be deduced that reducing at a low temperature leads to a low reducibility and smaller Co particles for the catalysts supported on TiO_2 and Al_2O_3. Even though the average Co particle size decreased with an increase in the reduction temperature for the SiO_2 catalyst, this catalyst exhibited the smallest particle size when reduced at 250 ˚C compared to Co/TiO_2

and Co/Al_2O_3 catalysts. However, only CoO was present at 250 ˚C for the SiO_2 and Al_2O_3 catalyst whilst the TiO_2 catalyst was reduced to a mixture of 17% Co and CoO, see Table 4.5. But, according to the TPR results in Figure 4.5, the SiO_2 catalyst also reduced to a mixture of Co and CoO, the Co might be too small to be picked up by the XRD, which may be due to a shorter reduction time for the in-situ XRD. A new reduction program for the in-situ XRD was highly suggested, and more information has been reported in our Chapter 7. Therefore, this means that the SiO_2 catalyst had the highest CoO site density at 250 ˚C which led to a higher FT activity observed over this catalyst. Even though the Co/TiO_2 catalyst might have more Co metal reduced that Co/SiO_2, the smaller particle size, which correlated to a higher metal site density, boots the FT activity to a greater extent.

Table 4. 5: The %reduction and Co particle size for the Co catalysts reduced at different temperatures, obtained via in-situ XRD. Reaction conditions: 20 bar, 210 ºC and 60 Nml/min of syngas ($H_2/CO/N_2$=60%/30%/10%).

Catalyst	Red. Temp. ˚C	%Red. Co	%CoO	Particle size (nm)
Co/SiO_2	250	0	100	12.2
	350	50	50	8.7
Co/TiO_2	250	17	83	12.7
	350	100	0	13.2
Co/Al_2O_3	250	0	100	14.6
	350	23	67	21.7

Figure 4.6 shows the FT reaction rate, WGS reaction rate and C_{5+} selectivity with TOS. The data in Figure 4.6 indicates that: (1) The order of the FT reaction rates is Co/SiO_2> Co/TiO_2 > Co/Al_2O_3 for all the runs. The FT reaction rate for the three catalysts decreased with time on steam (TOS) from 10 h to around 70 h. This indicates that the fresh catalysts need around 70 h to stabilize before the reaction achieves steady state; (2) For the first 130 hours, only Co/SiO_2 had a WGS reaction activity, while there was no WGS activity for

either TiO_2 or Al_2O_3 supported catalysts. When the operating temperature of the Al_2O_3 supported catalyst was changed from 200 ˚C to 210 ˚C, a certain amount of CO_2 was detected; (3) The C_{5+} selectivity stabilized at a value between 60-80%, for all the catalysts. The lower C_{5+} selectivity for Co/SiO_2 may be attributed to the higher CO_2 selectivity (corresponding to higher WGS reaction rate). It is worth noting that the trends for the FT and WGS reaction rates for the Co/SiO_2 catalyst are quite similar, which indicate that there is a direct relationship between the FT and WGS reaction rates with TOS. From the stoichiometry of the FT reaction, the higher the FT reaction rate, the more water is produced. The amount of the water produced by the FT reaction is a crucial factor and it controls the rate of the WGS reaction.

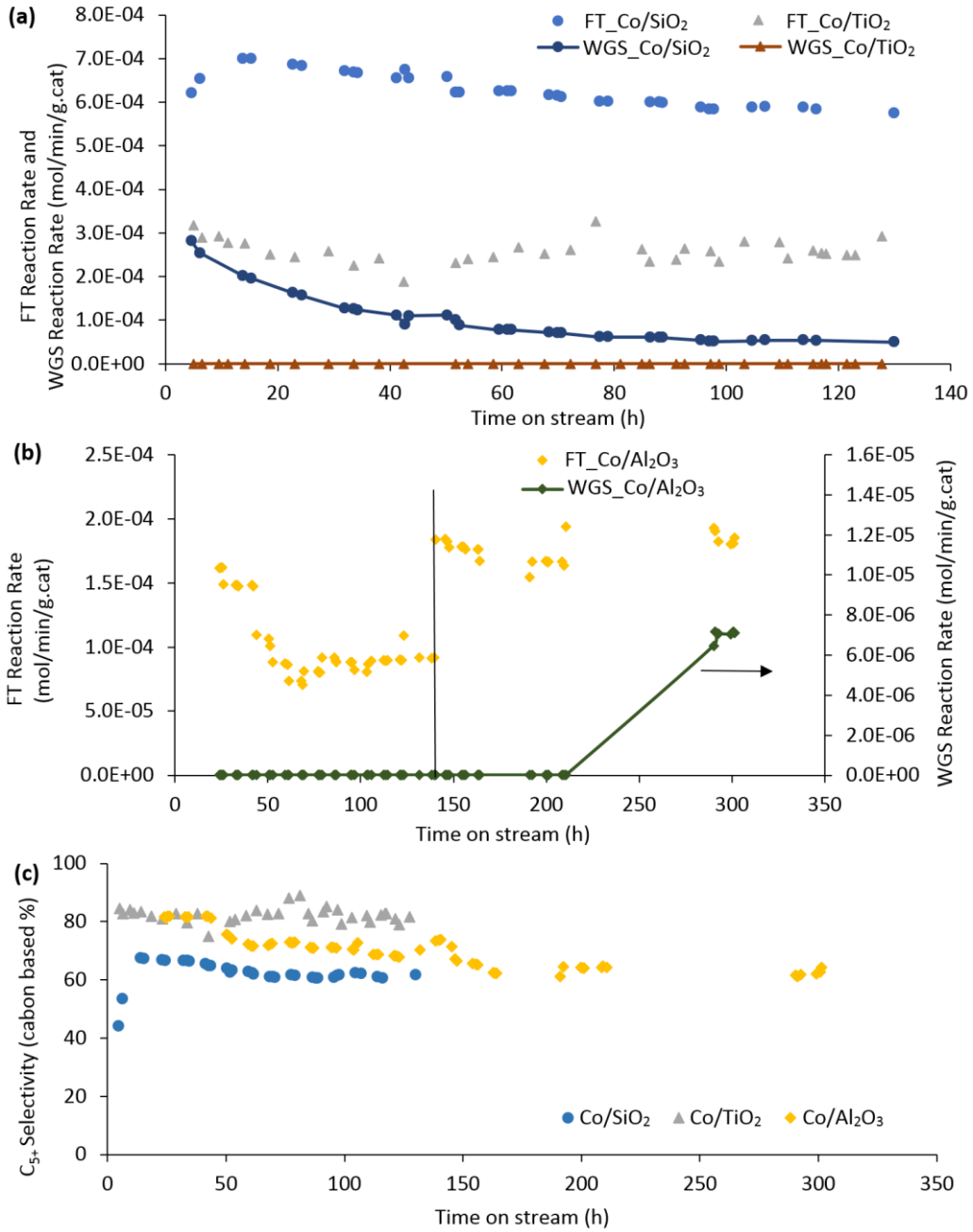

Figure 4. 6: The Fischer-Tropsch (FT) reaction rate, water gas shift (WGS) reaction rate and C_{5+} selectivity (carbon based) with time on stream (TOS) for three different Co-based catalysts reduced at 250 ˚C, respectively: (a) FT reaction rate and WGS reaction rate for Co/SiO_2 and Co/TiO_2; (b) FT reaction rate and WGS reaction rate for Co/Al_2O_3; (c) C_{5+} selectivity for Co/SiO_2, Co/TiO_2 and Co/Al_2O_3, respectively. Reaction conditions: 210 ˚C, 60 Nml/min, 20 bar for SiO_2 and TiO_2 supported catalysts; 200 ˚C with TOS from 0 to145 h and 210 ˚C with TOS from 146 to 210 h, 60 Nml/min, 20 bar for Al_2O_3 supported catalyst.

To understand the role of CoO during FTS, the effect of reduction temperature on the formation rates for CO_2, hydrocarbon products, and the paraffin to olefin ratio (P/O) were plotted and compared. The results are shown in Figure 4.7. When the Co/SiO_2 catalyst was reduced at 250 °C, significant amounts of CO_2 and CH_4 were obtained, which showed that CoO is active for both the WGS and methanation reactions. This is in agreement with prior studies reported in the literature [6-8]. Furthermore, the formation rates decreased with increasing reduction temperature, indicating that the proportion of CoO in the catalyst decreased with the reaction rates commensurately. The P/O ratio also decreased with increasing reduction temperature. This suggests that the presence of CoO enhances the production of paraffinic products. A possible explanation is that olefin products might reabsorb on the active sites and be hydrogenated by hydrogen dissociated on the CoO site to form paraffins (see reaction E). The high CH_4 selectivity and P/O ratio indicate that CoO is active for hydrogenation reactions.

Table 4.6 shows that the partially reduced catalysts (Co/SiO_2 and Co/Al_2O_3) were found to have a higher P/O ratio at a lower reduction temperature (250 ˚C) compared to that at 350 ˚C. The production of paraffinic products on the partially reduced catalysts supported on both SiO_2 and Al_2O_3 made it possible to explain all the data based on hypothesis of the secondary hydrogenation of olefins caused by the presence of abundant CoO that assisted the dissociation of H_2 to produce more H* intermediates. In contrast, the Co/TiO_2 catalyst had a higher P/O ratio at a higher reduction temperature, which indicates the interaction of $Co/CoO\text{-}TiO_2$ is different to the interactions of $Co/CoO\text{-}SiO_2$ and $Co/CoO\text{-}Al_2O_3$. It is worth noting that the trends in the P/O ratio are similar for both Co/SiO_2 and Co/Al_2O_3: the more CoO, the higher the P/O ratio.

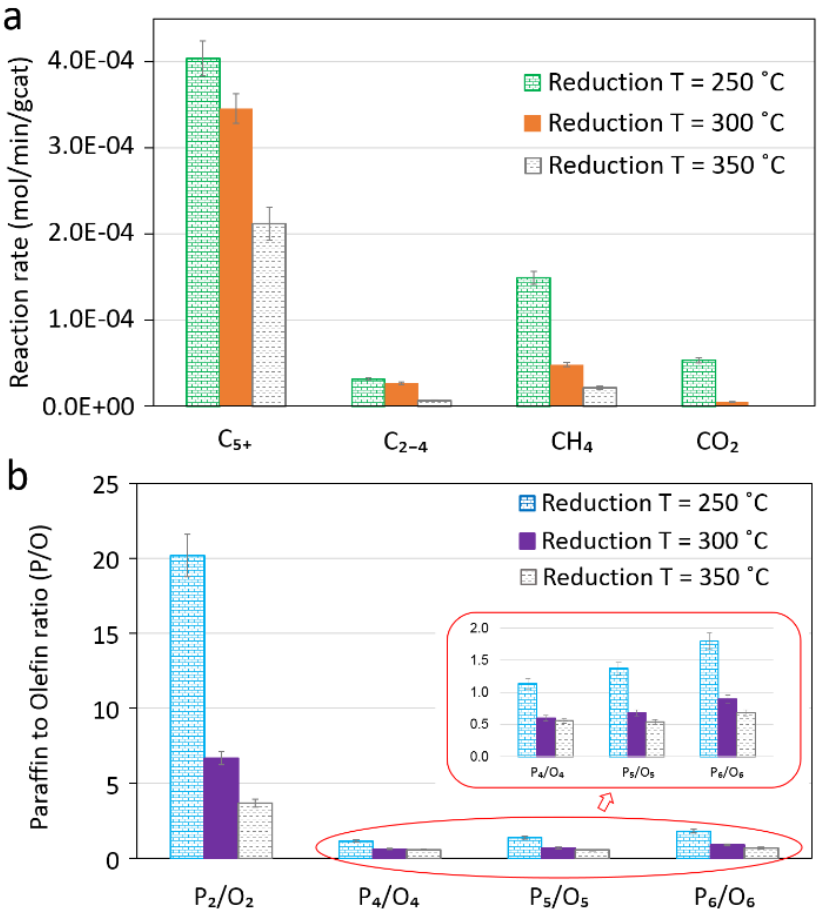

Figure 4. 7: The effect of reduction temperature on the product formation rates (a) and paraffin to olefin ratio (P/O) (b) for a Co/SiO_2 catalyst. The data reported is the average of the steady-state data. The legend indicates the catalyst reduction temperature (˚C). Reaction conditions: $H_2/CO = 2$, 20 bar, 210 ˚C and 60 Nml/min.

Table 4. 6: The paraffin to olefin (P/O) ratio for the Co catalysts reduced at different temperatures. Reaction conditions: 20 bar, 210 ºC and 60 Nml/min of syngas ($H_2/CO/N_2$=60%/30%/10%).

	Reduction Temperature	**Selectivity %**			
Catalyst	**[˚C]**	**P_2/O_2**	**P_3/O_3**	**P_4/O_4**	**P_5/O_5**
	250	20.18	0.99	1.13	1.40
Co/SiO_2	350	3.68	/	0.56	0.54
	250	12.42	2.12	1.95	2.87
Co/Al_2O_3	350	5.20	0.67	0.50	0.62
	250	7.72	1.31	1.56	1.51
Co/TiO_2	350	16.56	/	3.19	3.74

Figure 4.8 shows that for both Co/SiO_2 and Co/Al_2O_3 catalysts, higher P_4/O_4 ratios were obtained when the catalysts were partially reduced at 250 ˚C compared to those reduced at 350 ˚C. On the contrary, for the Co/TiO_2 catalyst, the P/O ratio was much higher for the catalyst reduced at 350 ˚C compared to the catalyst reduced at 250 ˚C. The Co/SiO_2 catalyst had a very high P_4/O_4 ratio initially, followed by a rapid decrease in the P_4/O_4 ratio with TOS, which later stabilized at a higher ratio than that observed a 350 ˚C (Figure 4.8 (a)). Comparing Figure 4.6 (a) and Figure 4.8(a), the FT reaction rate, WGS reaction rate and P/O ratios all decreased with TOS for the first 80 hours of the reaction, which may be attributed to further reduction of CoO to metallic Co under syngas atmosphere. The change in the P_4/O_4 ratio for the Co/TiO_2 catalyst reduced at 350 ˚C was very different to the other trends; firstly, it increased to achieve a maximum value and then decreased. Although it is hard to explain this observed behavior, we would like to highlight that a higher P_4/O_4 ratio was obtained for the Co/TiO_2 catalyst reduced at higher temperature.

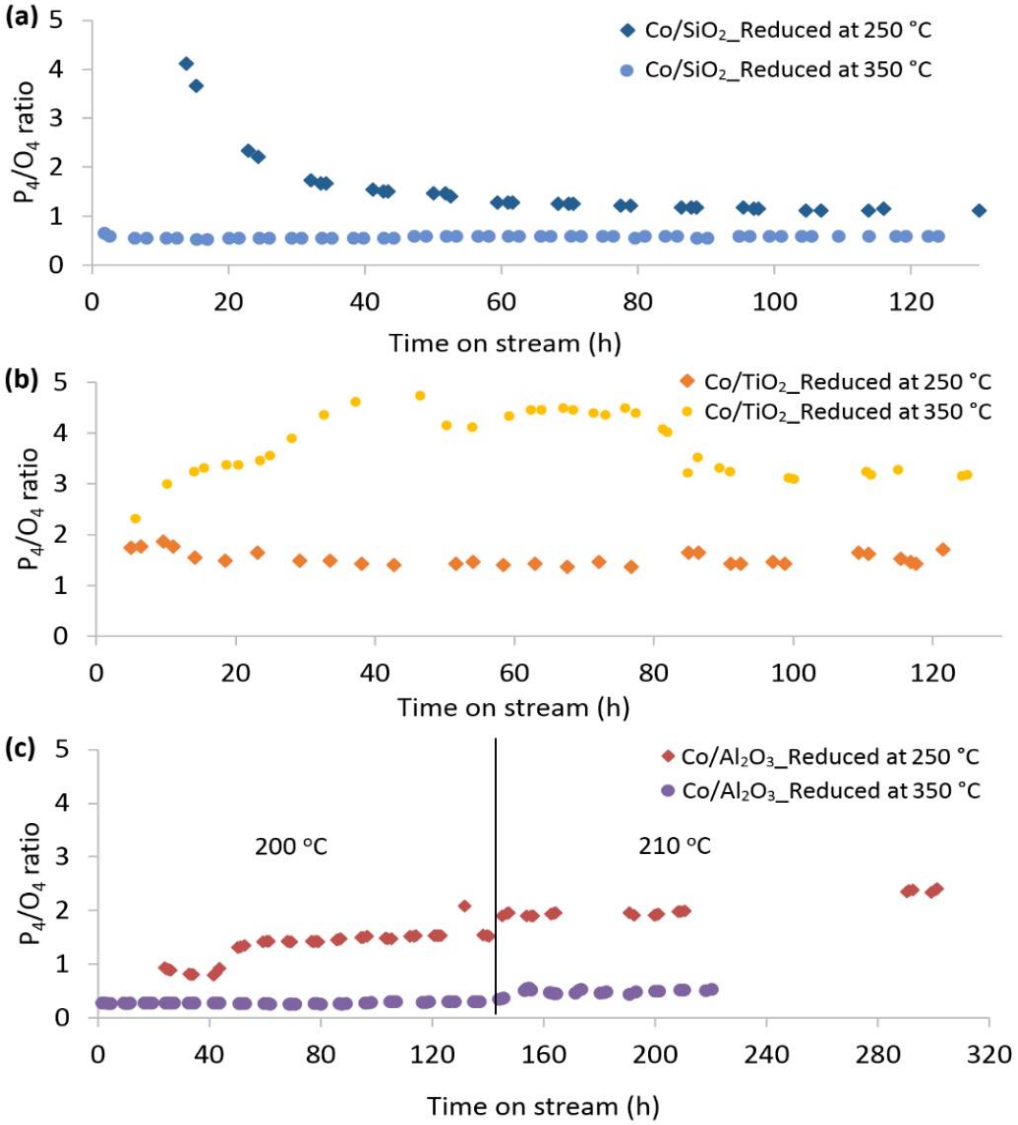

Figure 4. 8. The paraffin to olefin (P/O) ratio with TOS for three different Co catalysts reduced at 250 ˚C and 350 ˚C, respectively: (a) Co/SiO_2, (b) Co/TiO_2, (c) Co/Al_2O_3. Reaction conditions: 210 ˚C, 60 Nml/min, 20 bar for SiO_2 and TiO_2 supported catalysts; 200 ˚C with TOS from 0 to145 h and 210 ˚C with TOS from 146 to 210 h, 60 Nml/min, 20 bar for Al_2O_3 supported catalyst.

The most important finding of these experiments is that the long-chain hydrocarbon (C_{5+}) reaction rate decreased with increasing reduction temperature, which indicates that CoO does not only catalyze the WGS and CH_4 formation reactions but may either react or assist in the FT chain growth reaction occurring on Co^0 sites. The FT reaction is a stepwise chain growth reaction, and CO and H_2 react to form monomers. These monomers then in turn

react in a stepwise fashion to form the FT products. According to the literature, the rate-limiting step is the dissociation of CO, which occurs at Co^0 active sites. Any factors that could increase the dissociation rate of CO, and therefore the formation of the monomers, will increase the rate of the FT reaction [18-19].

The promotion of the FT catalysts by metal oxides, and in particular, MnO and ZrO_2, has been studied by Johnson et al [20-21]. They report that the interactions between adsorbed CO and the metal oxide could assist in CO dissociation, contributing to the observed positive promotion effects. In addition, Breejen et al [22]. reported that the MnO loading contributed to an increase in $*CH_x$ coverage, which resulted in an increased C-C coupling probability. A few researchers have reported on the role of CoO on the chain growth reaction. To the best of our knowledge, only one paper has reported that CoO was more active than Co^0; however, this catalyst was supported on TiO_2 rather than on SiO_2 [23]. In this work it was also reported that the activity of CoO/SiO_2 was much lower than that of Co^0. These results indicated that the CoO phase can catalyze the FT reaction. However, this depends on various factors, including the characteristics of the support. Furthermore, Johnson et al. [20-21], Breejen et al. [22], and Melaet et al. [23] all reported that metal oxide promoters result in lower P/O ratios. However, our experimental data showed that the P/O ratio (Figure 4.4) increased with increasing CoO, which indicated that CoO/SiO_2 may activate CO via different mechanisms compared to other catalysts that had previously been reported [20-23].

There are two commonly reported CO activation mechanisms in literature [24-25] namely: (1) the direct CO dissociation mechanism ($*CO \rightarrow *C$, $*C+H* \rightarrow CH*$); and (2) the H-assisted CO dissociation mechanism ($*CO + H* \rightarrow HCOH* \rightarrow CH*+OH*$) where CH* has also been reported to be the monomer for chain growth. The results reported by Iglesia's group [25] indicate that the H-assisted CO activation route was the preferred route for Co-based catalysts. The high CH_4 formation rate and P/O ratio (Figure 4.7) observed in these experiments, indicated that H_2 might be easily absorbed and activated by CoO. This activated H* might either (i) assist the *C-O bond dissociation, thereby increasing the rate of CO conversion to the chain-growth monomer and thus the observed FT reaction rate: or (ii) react with a hydrocarbon precursor ($*C_n$) to form paraffins, thereby increasing the P/O ratio.

Comparing the results from the present work with results from the literature [20-25], we deduce that there is a synergy between the CoO and Co^0 assisted activation of CO to monomers, which leads to improved FT activity for the Co/SiO_2 catalyst. H_2 absorbs and dissociates on CoO; the dissociated H* could then bridge between the CoO and Co^0 sites to interact with the adsorbed CO on the Co^0 sites or could react with absorbed olefins to hydrogenate them to paraffins. This proposed bridge-type H_2 assisted CO dissociation would result in an increased rate of CO dissociation, leading to an increase in FT reaction rate as well as the increased P/O ratio observed experimentally. This proposed new mechanism, which we call the "CoO-Co H assisted CO dissociation," is illustrated in Scheme 4.1, wherein step (1) H-assisted CO dissociation occurs or in step (2) paraffin formation pathways on the interface of CoO-Co occurs.

The results reflect that the abundance of CoO significantly affects the performance of an FT Co-based catalyst. We recommend more research to determine the function of the CoO-Co interface and optimize the proportion of CoO to Co^0 for maximum activity, as well as to determine the effect of the support characteristics on the relations between the Co metal and the surface phases. Some important points that we would like to highlight are:

1. The CoO phase in the Co/SiO_2 catalyst promotes both the FTS and hydrogenation reactions.
2. The Co/SiO_2 catalyst is active for both the WGS and FT reactions, making it suitable for converting syngas with a low H_2/CO ratio, such as that derived from coal or biomass to higher hydrocarbons. The WGS reaction plays a significant role in converting $CO + H_2O$ to H_2 and balancing the H_2/CO ratio.
3. The Co/SiO_2 catalyst can be activated at 250 ˚C, which corresponds to the reaction temperature for low-temperature FTS. The expensive high-temperature reduction step could thus be avoided, which could substantially decrease both the capital and operating costs of FT processes. This could be important for the development and profitability of a small-scale biomass to liquid process plant.
4. The linear paraffinic product produced is good for the production of a high cetane number diesel fuel and soft/hard waxes.

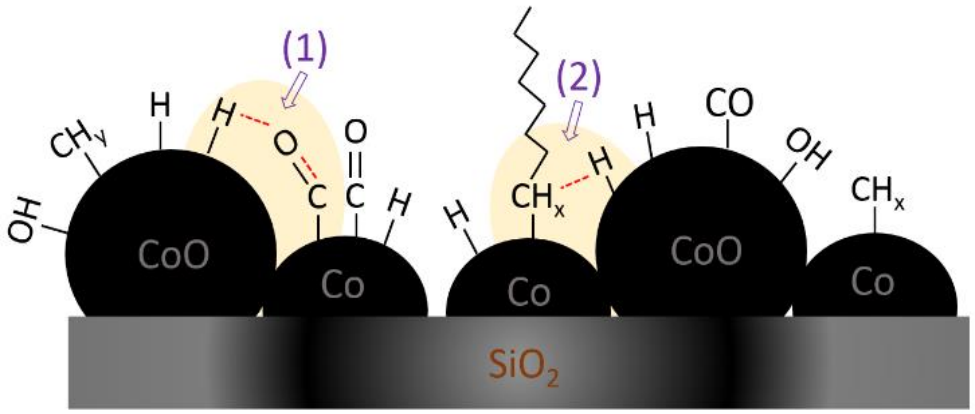

Scheme 4.1: A schematic diagram of the proposed H assisted CO dissociation and paraffin formation pathways at the CoO-Co interface.

4.4 Conclusions

A catalyst consisting of multi-phase CoO-Co supported on SiO_2 was successfully synthesized by activating the catalyst at a low reduction temperature of 250 ^oC. The CoO-Co/SiO_2 catalyst demonstrated high activity for both the water gas shift (WGS) and Fischer Tropsch (FT) reactions. The experimental results indicate that the multi-phase CoO-Co phase assisted the activation of CO and hydrogenation of R-CH_x intermediates. A new mechanism called the "CoO-Co H-assisted CO dissociation mechanism" was hypothesized to explain the high CO activity and selectivity to linear paraffinic products. This catalyst is suitable for converting H_2-lean syngas to liquid fuels. Furthermore, it eliminates the need for a high-temperature reduction step, which could be beneficial and cost-effective for commercial FT processes.

4.5 Acknowledgments

The authors are grateful for the support received from the University of South Africa and the South Africa National Research Foundation (NRF UID 95445 and 117793).

4.6 References

[1] Ma W, Jacobs G, Qian D, Ji Y, Klettlinger JL, Hopps SD, Davis BH. Fischer-Tropsch synthesis: Synergistic effect of hybrid Pt-Cd additives on a 15% Co/Al_2O_3 catalyst. Appl. Catal. A Gen. 2020; 600: 117610. https://doi.org/10.1016/j.apcata.2020.117610.

[2] Mahmoudi H, Jahangiri H, Doustdar O, Akbari N, Wood J, Tsolakis A, Wyszynski ML. Maximizing paraffin to olefin ratio employing simulated nitrogen-rich syngas via Fischer-Tropsch process over Co_3O_4/SiO_2 catalysts. Fuel Proc. Tech. 2020; 208: 106477. https://doi.org/10.1016/j.fuproc.2020.106477.

[3] Jalama K, Kabuba J, Xiong H, Jewell LL. Co/TiO_2 Fischer–Tropsch catalyst activation by synthesis gas. Catal. Comm. 2012; 17: 154-9. https://doi.org/10.1016/j.catcom.2011.10.029.

[4] Johnson BG, Bartholomew CH, Goodman DW. The role of surface structure and dispersion in CO hydrogenation on cobalt. J. Catal. 1991; 128: 231-47. https://doi.org/10.1016/0021-9517(91)90080-N.

[5] Lyu S, Wang L, Zhang J, Liu C, Sun J, Peng B, Wang Y, Rappé KG, Zhang Y, Li J, Nie L. Role of active phase in Fischer–Tropsch synthesis: Experimental evidence of CO activation over single-phase cobalt catalysts. ACS Catal. 2018; 8: 7787-98. https://doi.org/10.1021/acscatal.8b00834.

[6] L. Gavrilović, E.A. Jørgensen, U. Pandey, K.R. Putta, K.R. Rout, E. Rytter, M. Hillestad, E.A. Blekkan, Fischer-Tropsch synthesis over an alumina-supported cobalt catalyst in a fixed bed reactor– Effect of process parameters, Catal. Today 2020. https://doi.org/10.1016/j.cattod.2020.07.055.

[7] Lancelot C, Ordomsky VV, Stéphan O, Sadeqzadeh M, Karaca H, Lacroix M, Curulla-Ferré D, Luck F, Fongarland P, Griboval-Constant A, Khodakov AY. Direct evidence of surface oxidation of cobalt nanoparticles in alumina-supported catalysts for Fischer–Tropsch synthesis. ACS Catal. 2014; 4: 4510-5. https://doi.org/10.1021/cs500981p.

[8] Wang B, Liu S, Hu Z, Li Z, Ma X. Active phase of highly active Co_3O_4 catalyst for synthetic natural gas production. RSC Adv. 2014; 4: 57185-91. DOI: 10.1039/C4RA12214C.

[9] Y. Yao, Fischer–Tropsch synthesis using CO_2 containing syngas mixtures over cobalt and iron-based catalysts, PhD Thesis, University of Witwatersrand, Johannesburg. 2011.

[10] Slemr J, Slemr F, D'Souza H, Partridge R. Study of the relative response factors of various gas chromatograph–flame ionisation detector systems for measurement of C_2–C_9 hydrocarbons in air. Journal of Chromatography A. 2004; 1061: 75-84. DOI: 10.1016/j.chroma.2004.10.037.

[11] Jacobs G, Das TK, Zhang Y, Li J, Racoillet G, Davis BH. Fischer–Tropsch synthesis: support, loading, and promoter effects on the reducibility of cobalt catalysts. Appl. Catal. A Gen. 2002; 233: 263-81. https://doi.org/10.1016/S0926-860X(02)00195-3.

[12] Borg Ø, Dietzel PD, Spjelkavik AI, Tveten EZ, Walmsley JC, Diplas S, Eri S, Holmen A, Rytter E. Fischer–Tropsch synthesis: Cobalt particle size and support effects on intrinsic activity and product distribution. J. Catal. 2008; 259: 161-4. https://doi.org/10.1016/j.jcat.2008.08.017.

[13] Bian G, Mochizuki T, Fujishita N, Nomoto H, Yamada M. Activation and catalytic behavior of several Co/SiO_2 catalysts for Fischer-Tropsch synthesis. Energy & Fuels. 2003; 17: 799-803. https://doi.org/10.1021/ef020236j.

[14] Martínez A, López C, Márquez F, Díaz I. Fischer–Tropsch synthesis of hydrocarbons over mesoporous Co/SBA-15 catalysts: the influence of metal loading, cobalt precursor, and promoters. J. Catal. 2003; 220: 486-99. https://doi.org/10.1016/S0021-9517(03)00289-6.

[15] Mehrbod M, Martinelli M, Martino AG, Cronauer DC, Kropf AJ, Marshall CL, Jacobs G. Fischer-Tropsch synthesis: Direct cobalt nitrate reduction of promoted Co/TiO_2 catalysts. Fuel. 2019; 245: 488-504. https://doi.org/10.1016/j.fuel.2019.02.083.

[16] Abrokwah RY, Rahman MM, Deshmane VG, Kuila D. Effect of titania support on Fischer-Tropsch synthesis using cobalt, iron, and ruthenium catalysts in silicon-microchannel microreactor. Molec. Catal. 2019; 478: 110566. https://doi.org/10.1016/j.mcat.2019.110566.

[17] Kababji AH, Joseph B, Wolan JT. Silica-supported cobalt catalysts for Fischer–Tropsch synthesis: effects of calcination temperature and support surface area on cobalt silicate formation. Catal. Lett. 2009; 130: 72-8. https://doi.org/10.1007/s10562-009-9903-4.

[18] Filot IA, Zijlstra B, Broos RJ, Chen W, Pestman R, Hensen EJ. Kinetic aspects of chain growth in Fischer–Tropsch synthesis. Faraday discussions. 2017; 197: 153-64. https://doi.org/10.1039/C6FD00205F.

[19] van Santen RA, Markvoort AJ, Ghouri MM, Hilbers PA, Hensen EJ. Monomer formation model versus chain growth model of the Fischer–Tropsch reaction. J. Phys. Chem. C. 2013; 117: 4488-504. https://doi.org/10.1021/jp310245m.

[20] Johnson GR, Bell AT. Role of ZrO_2 in promoting the activity and selectivity of co-based Fischer–Tropsch synthesis catalysts. ACS Catal. 2016; 6: 100-14. https://doi.org/10.1021/acscatal.5b02205.

[21] Johnson GR, Werner S, Bell AT. An investigation into the effects of Mn promotion on the activity and selectivity of Co/SiO_2 for Fischer–Tropsch synthesis: evidence for enhanced CO adsorption and dissociation. ACS Catal. 2015; 5: 5888-903. https://doi.org/10.1021/acscatal.5b01578.

[22] den Breejen JP, Frey AM, Yang J, Holmen A, van Schooneveld MM, de Groot FM, Stephan O, Bitter JH, de Jong KP. A highly active and selective manganese oxide promoted cobalt-on-silica Fischer–Tropsch catalyst. Top. Catal. 2011; 54: 768. DOI 10.1007/s11244-011-9703-0.

[23] Melaet G, Ralston WT, Li CS, Alayoglu S, An K, Musselwhite N, Kalkan B, Somorjai GA. Evidence of highly active cobalt oxide catalyst for the Fischer–Tropsch synthesis and CO_2 hydrogenation. J. American Chem. Soc. 2014; 136: 2260-3. https://doi.org/10.1021/ja412447q.

[24] Qi Y, Yang J, Chen D, Holmen A. Recent progresses in understanding of Co-based Fischer–Tropsch catalysis by means of transient kinetic studies and theoretical analysis. Catal. Lett. 2015; 145: 145-61. https://doi.org/10.1007/s10562-014-1419-x.

[25] Ojeda M, Nabar R, Nilekar AU, Ishikawa A, Mavrikakis M, Iglesia E. CO activation pathways and the mechanism of Fischer–Tropsch synthesis. J. Catal. 2010; 272: 287-97. https://doi.org/10.1016/j.jcat.2010.04.012.

CHAPTER 5: THE EFFECT OF PRE-TREATMENT CONDITIONS ON THE ACTIVITY AND SELECTIVITY OF Co-BASED CATALYSTS FOR CO HYDROGENATION

The material in this chapter has been publishes in the Reactions journal. Reference: Shiba NC, Yao Y, Liu X, Hildebrandt D. The Effect of pre-treatment conditions on the activity and selectivity of cobalt-based catalysts for CO hydrogenation. Reactions. 2021: 3; 258-74.

Abstract

We investigated the effect of pre-treatment conditions on the activity and selectivity of cobalt catalysts for Fischer-Tropsch synthesis (FTS) by varying both the reduction atmosphere and the reduction temperature. Catalysts supported on SiO_2, Al_2O_3 and TiO_2, prepared via incipient wetness impregnation, were evaluated and activation temperatures in the range 250-350 ˚C were considered. Activation with syngas led to a better product selectivity (low CH_4, high selectivity to liquid hydrocarbons, and low paraffin to olefin ratio) than the catalysts reduced in H_2 at lower activation temperatures. The Co_xC species suppressed the hydrogenation reaction, and it is hypothesized that this resulted in the high selectivity of olefins observed for the syngas pre-treated catalysts. Based on the experimental results, it is postulated that a synergistic effect between Co^0 and Co_xC promotes the production of the long chain hydrocarbons and suppresses the formation of CH_4. Furthermore, it is hypothesized that the Co_xC species promoted the high selectivity of olefins, observed over the syngas pre-treated catalysts. In addition, for systems aimed at producing lower olefins, syngas activation is recommended; and for the FTS plants that focus on maximizing the production of higher molecular weight products, they might need to consider H_2-activation. These results provide insights for the future FTS catalyst design and for target-products driven operations.

5.1 Introduction

Fischer-Tropsch synthesis (FTS) is a structure-sensitive reaction that converts syngas derived from natural gas, coal and biomass to valuable chemicals and synthetic fuels over a metal-based catalyst [1]. Cobalt (Co) catalysts have attracted more attention in the recent years due to their high intrinsic hydrogenation activity, selectivity towards liquid

hydrocarbons, lower water gas shift (WGS) activity than iron and lower costs compared to noble metals [2-3]. Many supports have been reported in literature, and currently silica (SiO_2), alumina (Al_2O_3), and titania (TiO_2), are used for commercial FTS operations [4]. The hydrogenation activity of the cobalt metal, which is recognized as the active phase, is highly dependent on its structure. Co particles that are hexagonally packed (hcp) are found to be more reactive than the face-centred cubic (fcc) structure [5-6]. Evidence from previous studies suggests that the Co particle size is influenced by the support pore size [7-9]. Borg [10] studied the dependency of the Co particle size on the Al_2O_3-support pore diameter and found that: (i) large Co particles were formed in the large pores and smaller ones formed in the narrow pores; (ii) the degree of reduction increased with the pore size; and (iii) the C_{5+} (C_{5+} refers to the long chain hydrocarbons with carbon numbers equal or higher than 5) selectivity also increased with the pore size.

In some cases, the interaction between these supports and the metal can be too strong, which may leave a fraction of the cobalt chemically inactive after reduction. For example, Jacobs et al. [11] reported a lower degree of reduction for Al_2O_3- and TiO_2-supported catalysts due to high metal-support interactions compared to the SiO_2 support. Strong metal-metal oxides interactions have been demonstrated to play an important role in the reactivity of alumina-supported catalysts. A specific feature in these catalysts is incomplete reduction and possibly the insertion of Co ions into the alumina lattice to form spinel structures and as a result, the catalysts exhibit low reducibility and FT activity [12]. To overcome this issue, several strategies such as the modification of the support to minimise deleterious support metal interactions have been put forward. Soled et al. [13] demonstrated that the use of silicon substitutions in the TiO_2 lattice and the treatment of the TiO_2 support using an irreducible oxide ZrO_2 can inhibit the formation of Co-support interactions and thereby enhance the reducibility of the catalysts. Other strategies to limit the solid-state chemistry interactions between Co and the support include the use of neutral supports such as carbon nanofibers [14] and small amounts of noble metals [15].

Significant efforts have been devoted to enhancing the catalytic activity of FTS catalysts and to reducing the costs of the FTS process. Hydrogen (H_2) is used to activate the Co_3O_4

species in freshly prepared catalysts to active metallic Co. A few studies documented the use of syngas as an alternative reducing agent to H_2 [16-18]. The general consensus is that syngas reduction promotes the formation of cobalt carbides (Co_xC, x =2, 3), which transform back to metallic Co(hcp) under normal FT operating conditions thus improving the FT activity [18] or that the inactive Co_xC blocks the Co metal active sites leading to catalyst deactivation [19]. De la Pena O'Shea et al. [16] achieved a significantly higher activity (90% CO conversion) with a Co/SiO_2 catalyst pre-treated in syngas compared to either H_2 or CO-reduction. The improvement in activity was attributed to the increase in the number of Co active sites (high metal dispersion). The formation of Co_2C during FTS has been confirmed by Claeys et al. [20] and reported to act as a methanation site [21-22]. While the role of Co_2C is widely debated in FTS, Co_2C nanoprisms increase the selectivity towards alcohols and olefins [19,23].

Syngas reduction is conducted at relatively low temperatures (<280 ˚C) to avoid catalyst coking resulting from the degradation of liquid products, and to limit the deposition of inactive surface carbon via the Boudouard reaction [18,24]. Graphitic carbon has been reported to strongly suppress CH_4 formation, however, it cannot be removed from the surface, thus blocking the Co active sites and resulting in catalyst deactivation [24]. On the contrary, De la Pena O'Shea [16] reported that no graphitic carbon was observed after the syngas treatment at 500 ˚C due to the simultaneous presence of H_2 and CO, which minimises the formation of carbon. Reducing the catalyst at a low temperature with syngas still produces a fraction of CoO, which is believed to be inactive in FTS [25], and to catalyse the WSG reaction [26]. In our earlier work, we reported that the intimate contact between CoO and Co metal as well as formation of Co-CoO interfaces under FT reaction conditions catalyses the FT reaction for a SiO_2-supported catalyst pre-treated in H_2 at 250 ˚C [27].

Although there is a large body of work on the effect of the reduction temperature including the support characteristics on various Co-based catalysts reduced under H_2, not as much attention has been paid to determine how temperature and support identity influences the reduction of Co species under syngas reduction. As H_2 is an expensive gas, the use of syngas as both reaction and reducing agents, at lower reduction temperatures, can potentially cut-

down the start-up and running costs of an FT process. Here, we report on the activity and selectivity of Co catalysts supported on TiO_2, SiO_2, and Al_2O_3, reduced at two temperatures (250, 350 ˚C) under two reductive agents (H_2, syngas), per catalyst, to compare their influence on CO hydrogenation.

5.2 Experimental Set Up

5.2.1 Catalyst preparation

In this work, three kinds of supports, TiO_2, SiO_2 and Al_2O_3 were used for the preparation of the 15% Co/support catalysts. The catalysts were prepared via incipient wetness impregnation of cobalt nitrate solution ($Co(NO_3)_2 \bullet 6H_2O$) onto these three kinds of supports, respectively. The chemicals used were outsourced from Sigma Aldrich. Catalysts were dried at room temperature overnight followed by mild drying at 40 ˚C for 3 hours and calcination at 350 ˚C for 8 hours. Drying and calcination were carried out in an air atmosphere.

5.2.2 Catalyst characterization

Brunauer-Emmet-Teller (BET) experiments were conducted on the fresh catalysts prior to reduction or reaction to determine the sample surface area and pore size. BET experiments followed the usual procedure. The sample was firstly subjected to a degassing chamber at 200 ˚C for 6 h and treatment was done at a relative pressure of 0.99 ($P_a/P_0 = 0.99$, where P_a is the actual gas pressure and P_0 is the vapor pressure of the adsorbing gas) to obtain the pore volume and -196 ˚C to obtain the surface area and porosity by nitrogen physisorption. Furthermore, the Barrett-Joyner-Halenda (BJH) method was used to obtain the pore sizes from the desorption branches on the isotherms.

The morphology of the catalysts was characterized by transmission electron microscopy (TEM). The samples for TEM studies were prepared by ultrasonic dispersion of the catalysts in ethanol and the suspensions were added dropwise onto a copper grid. The TEM investigations were carried out using a JEOL-JEM-100CX II (100 kV) transmission electron microscope equipped with a NARON energy-dispersive spectrometer and a

germanium detector. X-ray diffraction (XRD) studies were performed using a Philips PW 1710 spectrometer with monochromatic Cu-Kα radiation to determine the catalyst particle size and crystalline structures. The measurements were made on calcined catalysts and the average Co_3O_4 particle size was calculated from the most intense peak, with the use of Scherrer formula [6], for each catalyst.

The reduction behaviour and the interaction between the active phase and the support of each catalyst were examined using the temperature programmed reduction (TPR) technique. The TPR experiments were carried out with a thermal conductivity detector (TCD) to determine the hydrogen consumption. The catalyst (500 mg) was placed in a quartz tubular reactor fitted with a thermocouple for continuous temperature measurements. The reactor was heated with a furnaced designed for the TPR machine, at a ramping rate of 10 ˚C/min, under a mixture of 5 vol% H_2 in an air flow of 30 cm^3/min.

5.2.3 Reduction and reaction procedures

Three fixed bed reactors with the same size (ID=8mm) were used in this study. One gram of Co/SiO_2, Co/Al_2O_3 and Co/TiO_2 catalysts was loaded into the three reactors, respectively. The three catalysts followed the same activation procedure: to reduce the Co_3O_4 in a flow of either H_2 or syngas (H_2/CO ratio of 2) at two different temperatures, namely 250 ˚C and 350 ˚C, and atmosphere pressure. After catalyst reduction, the catalysts were cooled down to 180 ˚C. Thereafter, the same syngas used for catalyst reduction was introduced into the reactor for FTS. The catalyst reactivity and product distribution were evaluated at 20 bar, 210 ˚C and 60 ml/min with syngas.

The tail-gases from the three reactors were monitored and analyzed by an online GC (Agilent 7890B): the hydrocarbon products were analyzed by a flame ionization detector (FID); whist the other gases (H_2, CO, N_2 and CO_2) were analyzed by two TCDs.

5.3 Results

5.3.1 Catalyst characterization

Table 5.1 lists the physical properties of the catalysts. It shows that the Al_2O_3 supported catalyst has a larger pore size and a larger particle size than the catalysts supported on TiO_2 and SiO_2. Both the TEM and XRD results demonstrate that the crystalline size is mainly dependent on the support pore size. Smaller-pored supports such as the SiO_2 distribute smaller Co_3O_4 nanocrystallites.

Table 5. 1: Physical properties of the catalysts and reactor used in this work**.**

Catalyst	15% Co/SiO_2	15% Co/Al_2O_3	15% Co/TiO_2
Catalyst BET pore size (nm)	6.8	43.1	38.7
Catalyst BET surface area (nm)	407.0	115.8	88.4
TEM average particle size (nm)	26	38	28
XRD crystalize size (nm)	17	33.0	21.5
Reactor	Fixed bed reactor		
Reactor diameter (mm)	0.8	0.8	0.8
Catalyst weight loaded into the reactor (g)	1	1	1

The crystal morphology of the catalysts is illustrated in Figure 5.1, determined via TEM. In the cross sections, the visible darker dense areas represent Co_3O_4 particles, and the lighter areas corresponds to the support. The Co_3O_4 particles seemed to be more highly dispersed on the TiO_2 support followed by SiO_2 support then the Al_2O_3 support. This might be due to the smaller TiO_2 support particles that are observed in Figure 5.1. The large Co_3O_4 particles observed on the alumina support suggest that the support had a wider pore, which is in line with the BET results (Table 5.1), thus distributing bigger particles than TiO_2 and SiO_2. The Co_3O_4 particles on the Al_2O_3 and SiO_2 supports seem to be spherical shape, whilst on the TiO_2, the cobalt particles assumed the shape of the TiO_2 support particles, in this case cubic/rhombus shaped.

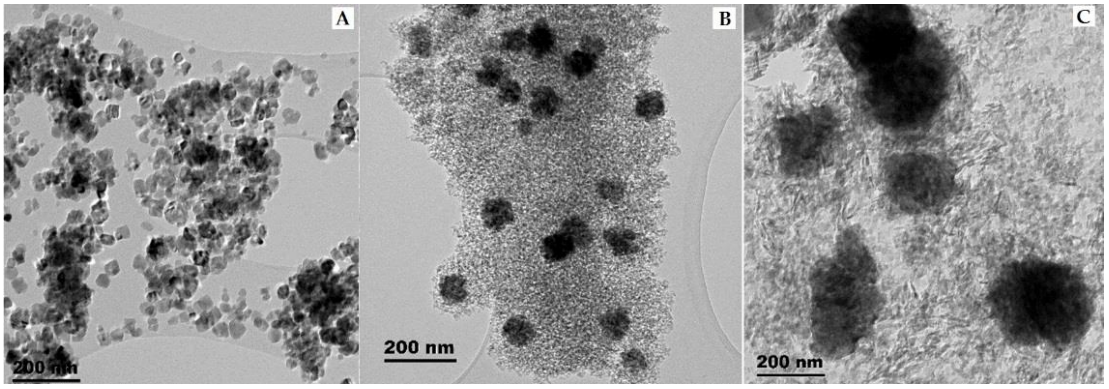

Figure 5. 1: TEM micrograph images of a freshly calcined catalyst: (A) Co/TiO_2, (B) Co/SiO_2 and (C) Co/Al_2O_3.

The XRD patterns for the model catalysts (Co/TiO_2, Co/SiO_2, Co/Al_2O_3) are presented in Figure 5.2. XRD characteristics of Co_3O_4 were detected for all the calcined catalysts with Co/TiO_2 and Co/Al_2O_3 showing distinctive Co_3O_4 crystalline features, marked with a black circle, see Figure 5.2A & B. The Co/SiO_2 diffractogram show considerably broad features, which suggests that the silica support is likely amorphous, and contains smaller Co_3O_4 nanoparticles. The average Co_3O_4 crystallite size (Table 5.1) was calculated from the Scherrer equation [6]. The Co_3O_4 crystallite size varied slightly as a function of the pore size, with Co/Al_2O_3 showing the biggest size (33.0 nm) owing to its large pore size followed by Co/TiO_2 (21.5 nm) and then lastly Co/SiO_2 (17 nm).

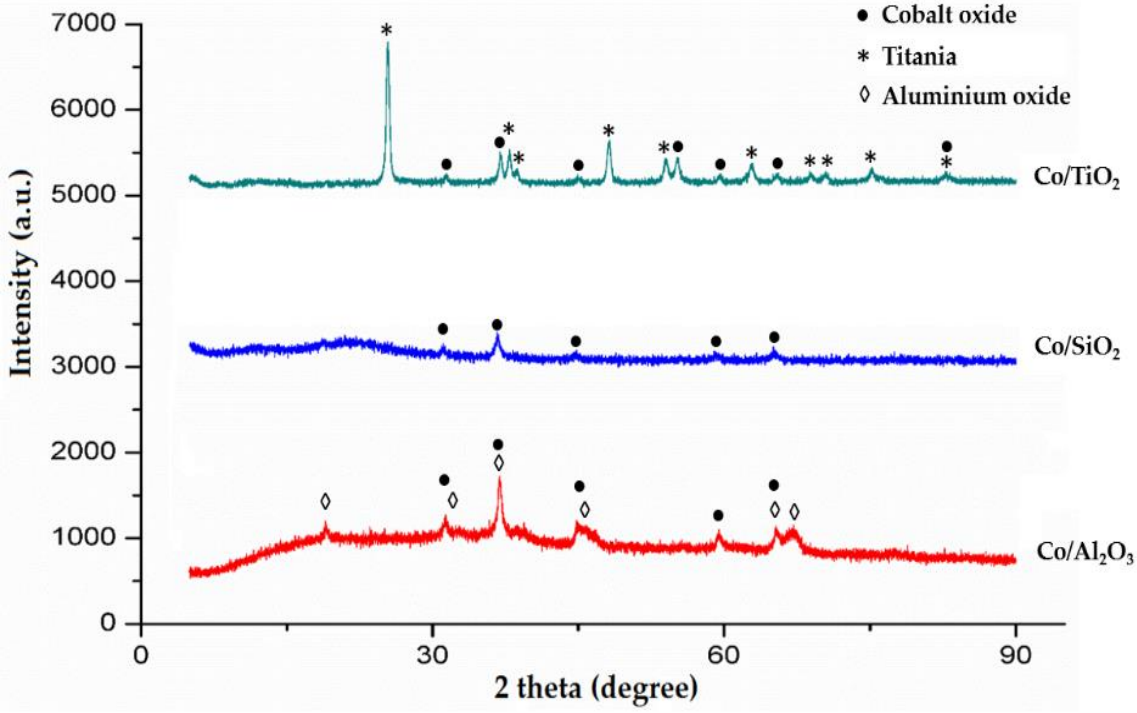

Figure 5. 2: XRD diffractions of a freshly calcined catalyst: (A) Co/TiO_2, (B) Co/SiO_2 and (C) Co/Al_2O_3.

The TPR reduction profiles presented in Figure 5.3 for the three kinds of catalysts, showed two reduction peaks which are similar to those observed for bulk Co_3O_4 oxide. These profiles point to a two-step reduction process: the first one of low intensity starts at approximately 260 ˚C and overlaps with the more intense second peak whose maximum occurs at about 300 ˚C for Co/TiO_2 and Co/SiO_2 catalysts and for Co/Al_2O_3 the peak started around 300 ˚C and the second peak emerged at around 450 ˚C. Other than the fact that the second reduction peak for the Al_2O_3-supported catalyst emerged at a higher temperature than the second peak on the TiO_2- or SiO_2-supported catalysts, it also extended its shoulder to a higher magnitude, in this case 700 ˚C. Therefore, the reduction process of Co_3O_4 can be described by the reduction of Co^{3+} ions present in the spinel structure of a fresh catalyst into Co^{2+} with subsequent structural change to CoO, followed by the reduction of Co^{2+} ions to Co^0 metal. The results observed on the Al_2O_3-supported sample suggests that the catalyst supported on Al_2O_3 is harder to reduce than the one supported by TiO_2 or SiO_2, which may be due to strong metal-support interactions, which is in line with literature [2,11].

Furthermore, a higher reduction temperature was required for the reduction of the Al_2O_3-supported catalyst compared to TiO_2- and SiO_2-supported catalysts as observed from of the reduction profiles (Figure 5.3), which might be due to that the cobalt particles diffused into the Al_2O_3 lattice and formed the irreducible compounds, such as cobalt aluminates.

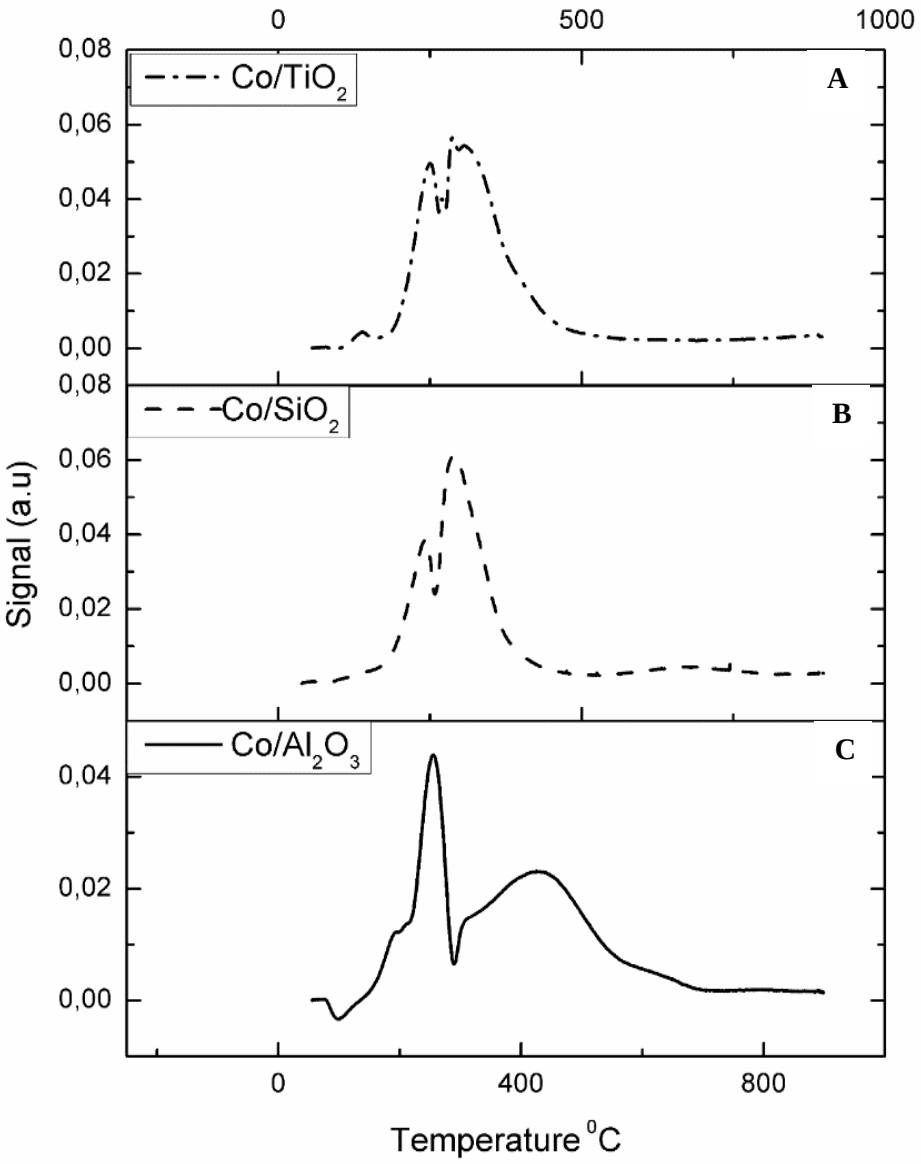

Figure 5. 3: TPR reduction profiles for (A) Co/TiO_2 (dashed and dotted line); (B) Co/SiO_2 (dashed line) and (C) Co/Al_2O_3 (solid line). Reproduced from Shiba et al. [27] with permission from Elsevier, License number 5053041467597.

5.3.2 Catalyst activity and selectivity

5.3.2.1 Reaction rate

The Fischer-Tropsch (FT) activity and selectivity of the supported cobalt catalysts is illustrated in Figures 5.4-5.10. The catalysts pre-treated in H_2 exhibited higher CO reaction rates compared to the samples reduced in syngas, at all reduction temperatures, see Figure 5.4. For the syngas pre-treatment, the CO reaction rates were found to be higher at a higher reduction temperature (350 ˚C) for all the samples. Similar results to the syngas pretreatment were observed, higher CO reaction rates were achieved at a higher reduction temperature for all the three catalysts reduced in H_2 (except for the SiO_2 catalyst reduced in H_2 at 250 ˚C).

The Co/SiO_2 catalyst with the highest surface area and lowest particle size (Table 5.1) was the most active catalyst when it reduced in H_2 at 250 ˚C, see Figure 5.4(B). The high surface area of SiO_2 support and the lower metal-support interaction enhanced the reducibility and the dispersion of the metal. Our previous research [27] report that the oxidesed Co/SiO_2 catalyst, in H_2 at 250 ˚C, formed a multiphase of $CoO\text{-}Co/SiO_2$, and this CoO-Co interface promoted the CO dissociation and secondary olefin hydrogenation reaction, thus leading to a higher FT reaction rate [27].

Compared with SiO_2- and Al_2O_3-supported catalyts, the TiO_2-supported catalyst presented the highest CO reaction rates, when reduced either in H_2 or syngas at all temperatures except for the H_2-reduction at 250 ˚C. The lower surface area, observed via BET (Table 5.1) for the TiO_2-supported catalyst, promoted the agglomeration of the Co_3O_4 as larger Co_3O_4 particles which might have increased their reducibility and enhanced their catalytic activity. The low activity over the Al_2O_3-supported catalyst with biggest Co_3O_4 particles (XRD: 33.0 nm in Table 5.1) must be related to the strong metal-support interaction (see Figure 5.3) and low metal dispersion due to the large cobalt particles. For further discussion, please refers to Section 5.4.

The CO reaction rates were found to be higher at a higher reduction temperature (350 ˚C) for all the samples, except for the syngas pre-treated TiO_2 supported sample and H_2-pre-treated SiO_2 supported sample. The SiO_2 supported catalyst showed higher reaction rates

at 250 ˚C compared to 350 ˚C, see Figure 5.4(B). Our previous work over the SiO_2 sample demonstrated the effect of Co-CoO bonding promoting the FT reaction thus leading to a higher FT reaction rate at a lower reduction temperature (250 ˚C) when the CoO density is higher than the density observed at 350 ˚C [27].

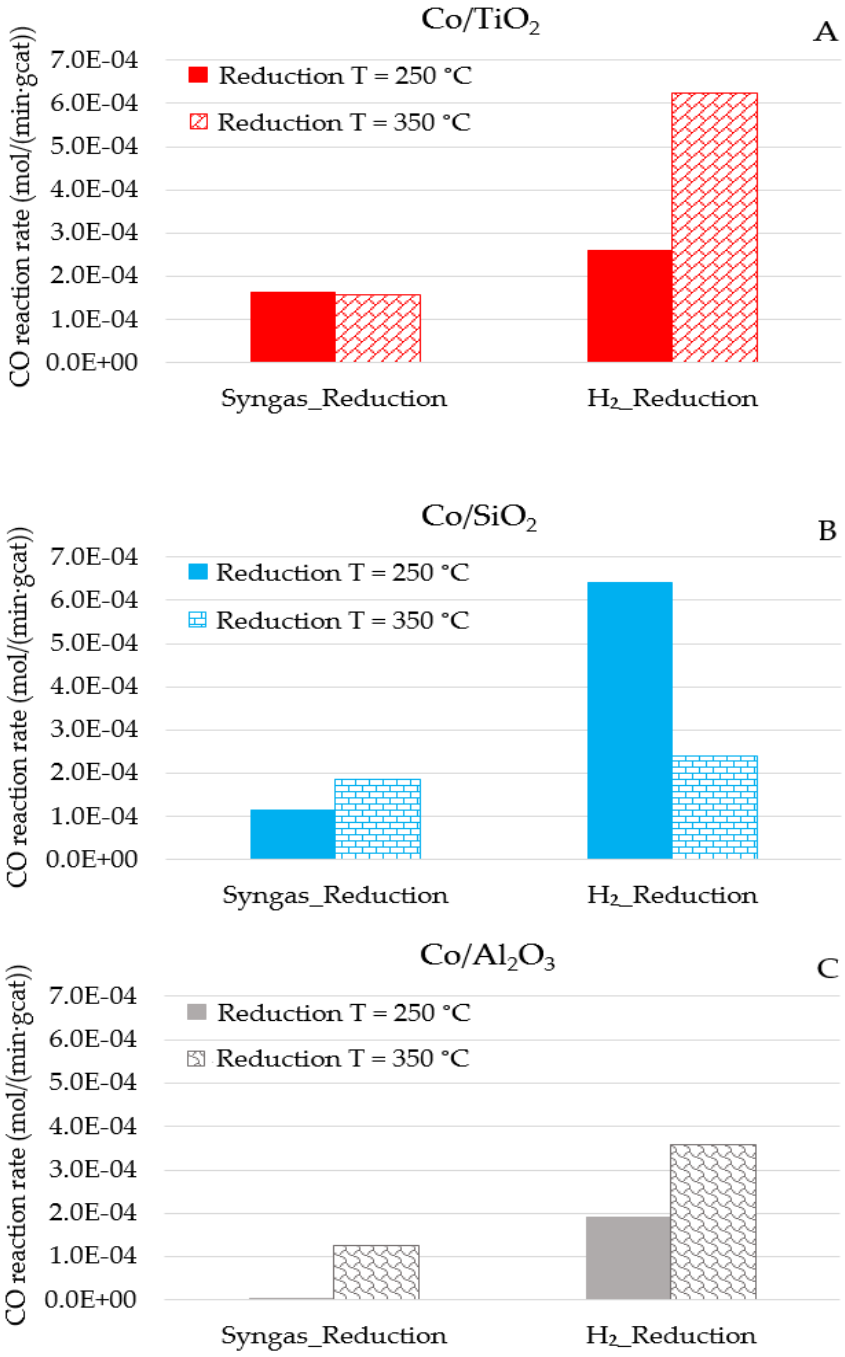

Figure 5. 4: CO reaction rate as a function of reducing agent and temperature: (A) for Co/TiO_2; (B) for Co/SiO_2 and (C) for Co/Al_2O_3. Reaction conditions: 20 bar, 60 ml/min and 210 °C.

5.3.3 Product formation rate

The overall product formation rate as a function of temperature is illustrated in Figures 5.5 & 5.6. Changing the reduction medium from H_2 to syngas led to a complete change in the formation of products. A noticeable effect is the lower CH_4 formation rate observed for all the samples treated with syngas compared to H_2, excluding the Co/SiO_2-supported catalyst treated with syngas at 350 ˚C. Co/TiO_2 showed the lowest CH_4 formation rate followed by Co/SiO_2 and then Co/Al_2O_3, at all reduction temperatures, see Figure 5.5. Another observation is that the CH_4 formation rate is higher for the syngas-treated samples at 350 ˚C, whereas for the H_2-treated samples, higher CH_4 formation rates were observed at 250 ˚C, except for the catalyst supported on SiO_2.

For long chain hydrocarbons (C_{5+}), higher formation rates were observed over the H_2-treated samples compared to the catalysts reduced in syngas, see Figure 5.5, due to higher CO reaction rates. Figure 5.6 shows that: (1) for H_2 reduction, higher C_{5+} formation rates were achieved at a higher reduction temperature for both TiO_2 and Al_2O_3 supported catalysts; while for the SiO_2-supported catalysts, higher C_{5+} formation rate were obtained at a lower reduction temperature; (2) for syngas reduction, higher C_{5+} formation rate were observed at a higher reduction temperature for both Al_2O_3- and SiO_2-supported catalysts, while there is only a slight difference between the C_{5+} formation rates at T = 250 °C and T = 350 °C for the catalyst supported by TiO_2.

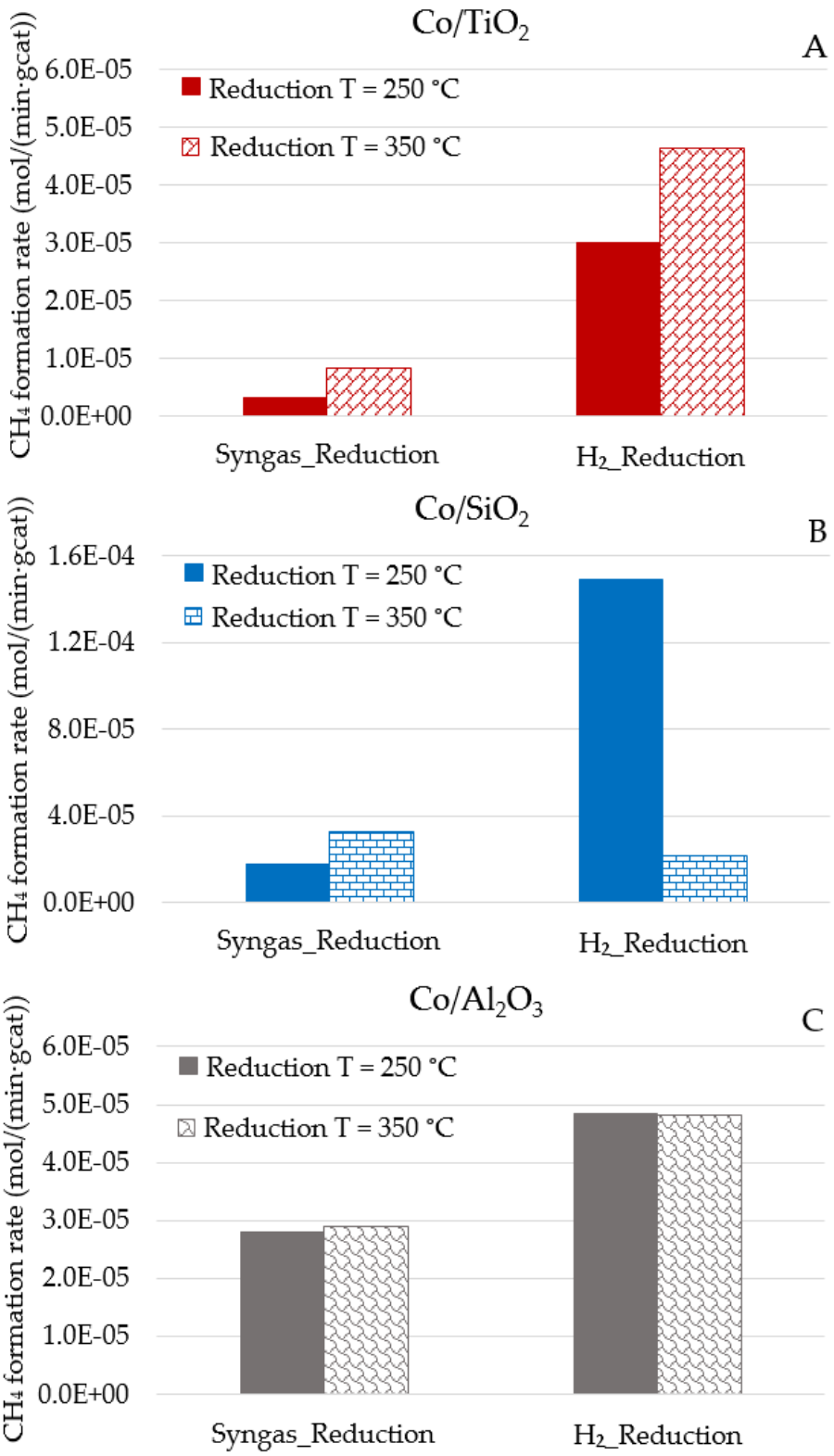

Figure 5. 5: CH_4 formation rate as a function of reducing agent and temperature: (A) for Co/TiO_2; (B) for Co/SiO_2 and (C) for Co/Al_2O_3. Reaction conditions: 20 bar, 60 ml/min and 210 °C.

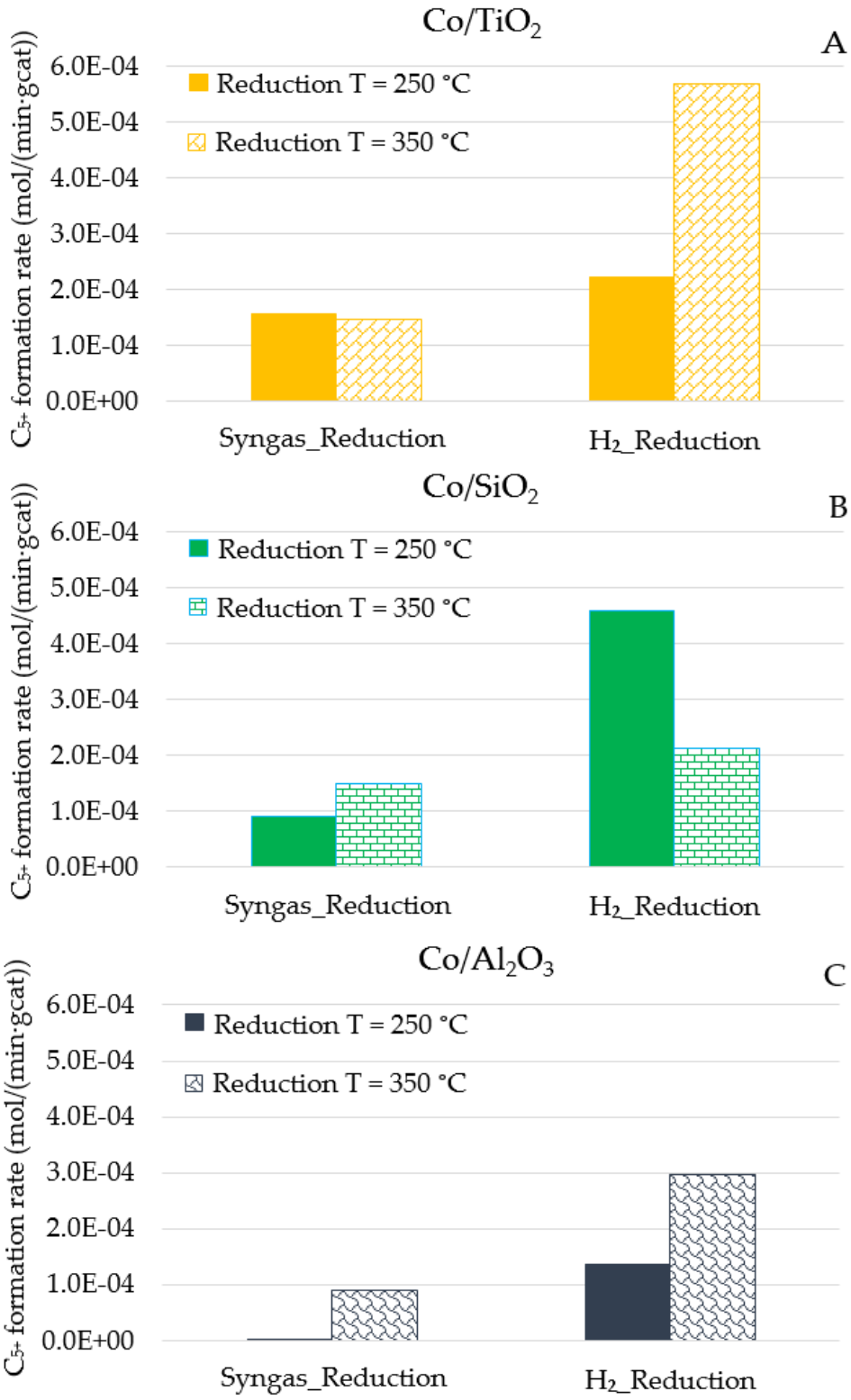

Figure 5. 6: C_{5+} formation rate as a function of reducing agent and temperature: (A) for Co/TiO_2; (B) for Co/SiO_2 and (C) for Co/Al_2O_3. reaction conditions: 20 bar, 60 ml/min and 210 °C.

5.3.4 Product selectivity

The effect of syngas- or H_2-pre-treatment on the selectivity of the model cobalt catalysts as a function of temperatures is shown in Figures 5.7 & 5.8. All syngas-treated samples showed better CH_4 selectivity (Co/TiO_2: H_2 = 12%, syngas = 2%; Co/SiO_2: H_2 = 23% syngas =16%; Co/Al_2O_3: H_2 = 25% syngas = 6%) and a higher C_{5+} selectivity (Co/TiO_2: H_2 = 81%, syngas = 96%; Co/SiO_2: H_2 = 62% syngas = 70%; Co/Al_2O_3: H_2 = 62%, syngas = 93%) compared to H_2-reduced samples, at T = 250˚C. Increasing the syngas reduction temperature, increased the CH_4 selectivity and decreased C_{5+} selectivity, whereas for the H_2 treated samples, an increase in the reduction temperature decreased the CH_4 selectivity and increased C_{5+} selectivity for all the three catalysts (Figure 5.8 (B)).

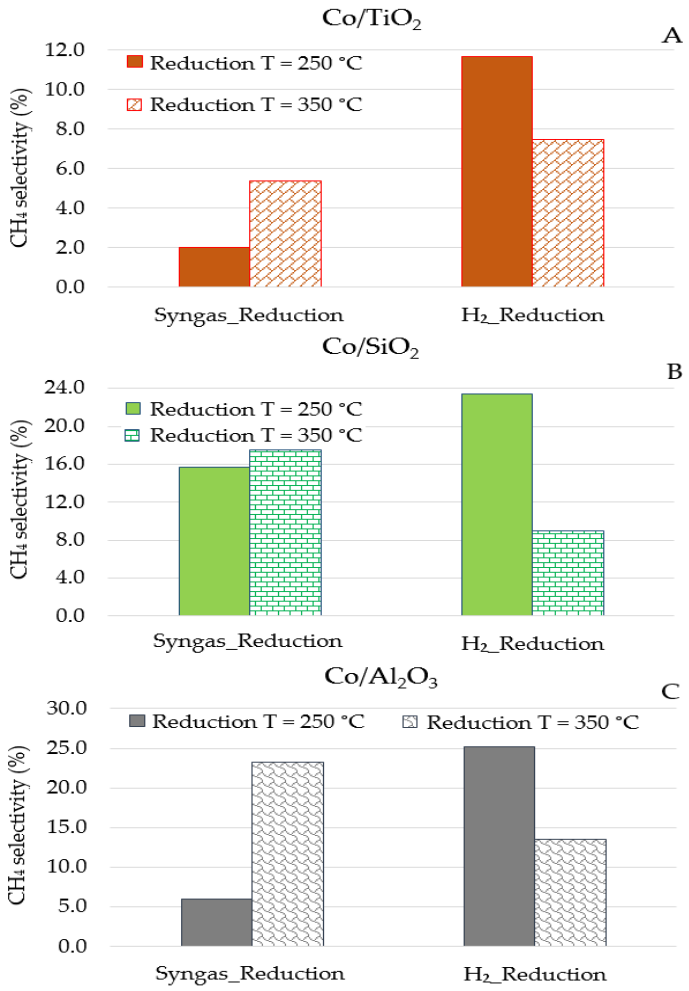

Figure 5. 7: The selectivity of CH_4 as a function of reducing agent and temperature: (A) for Co/TiO_2; (B) for Co/SiO_2 and (C) for Co/Al_2O_3. Reaction conditions: 20 bar, 60 ml/min and 210 °C.

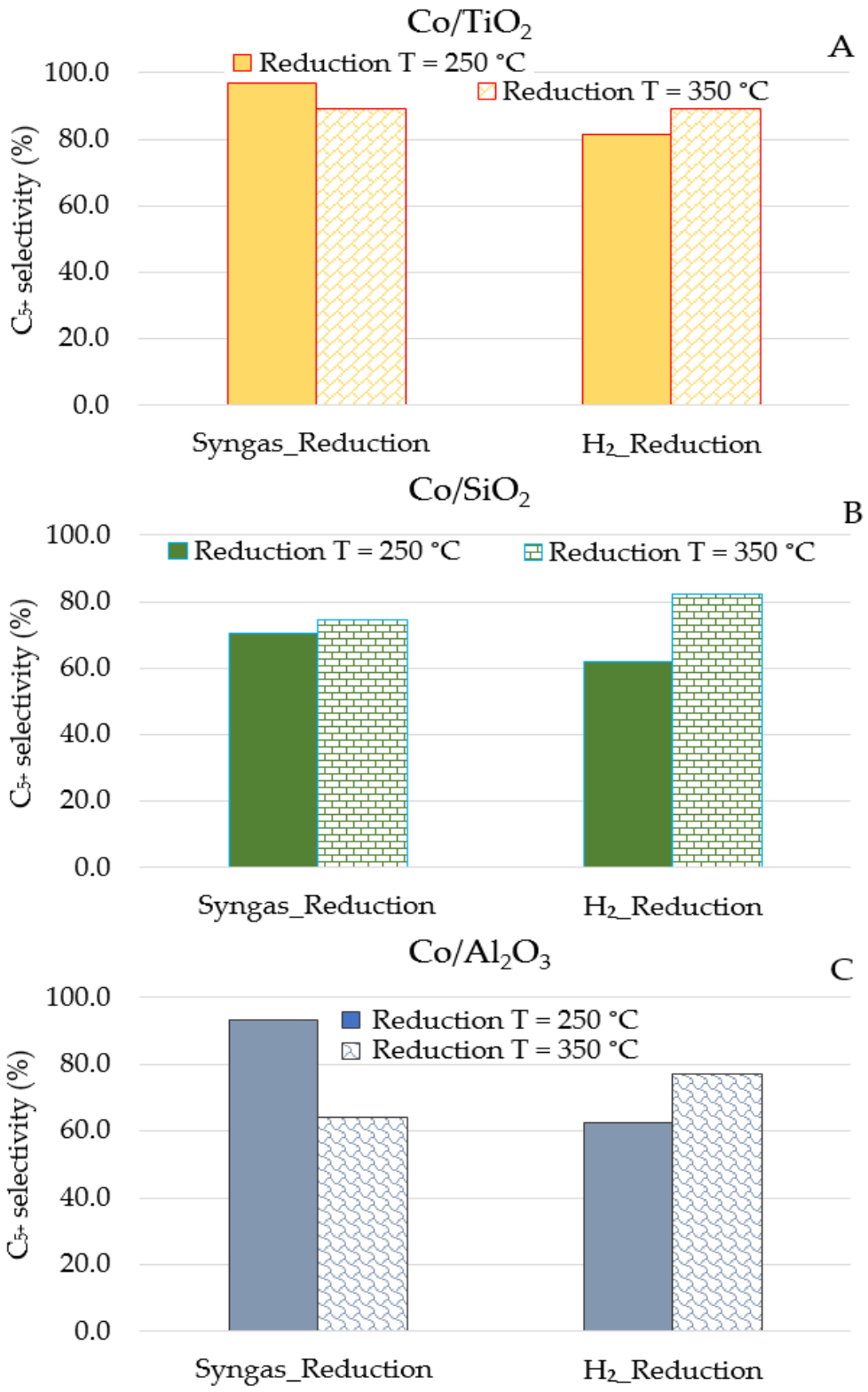

Figure 5. 8: The selectivity of C_{5+} as a function of reducing agent and temperature: (A) for Co/TiO_2; (B) for Co/SiO_2 and (C) for Co/Al_2O_3. Reaction conditions: 20 bar, 60 ml/min and 210 °C.

5.3.5 Paraffin to olefin (P/O) ratio

P/O ratio is a very important factor which reflects the selectivity of the paraffin (P) and olefin (O) products, a higher P/O ratio represents the products that are more paraffinic; and a lower value indicate a higher selectivity to olefinic products. P_n/O_n represents the parafin to olefin ratio with carbon number n. In the current work, the P_2/O_2 (ethan/ethylene) and P_4/O_4 (butane/butene) ratios were reported in Figure 5.9 for the catalysts either reduced by syngas or H_2 at different reduction temperatures. For the Co/TiO_2 catalyst, pre-treatment with syngas (at both 250 °C and 350 °C) produced more olefins than paraffins compared to the H_2-pre-treatment. For Co/SiO_2 and Co/Al_2O_3, similar results as for the Co/TiO_2 catalysts was obtained with the syngas-treated Co/TiO_2 catalysts, T= 250 °C. However, syngas pre-treatment at 350 °C, produced more paraffin products over the Co/Al_2O_3 catalyst compared to H_2-pre-treatment at a similar reduction temperature.

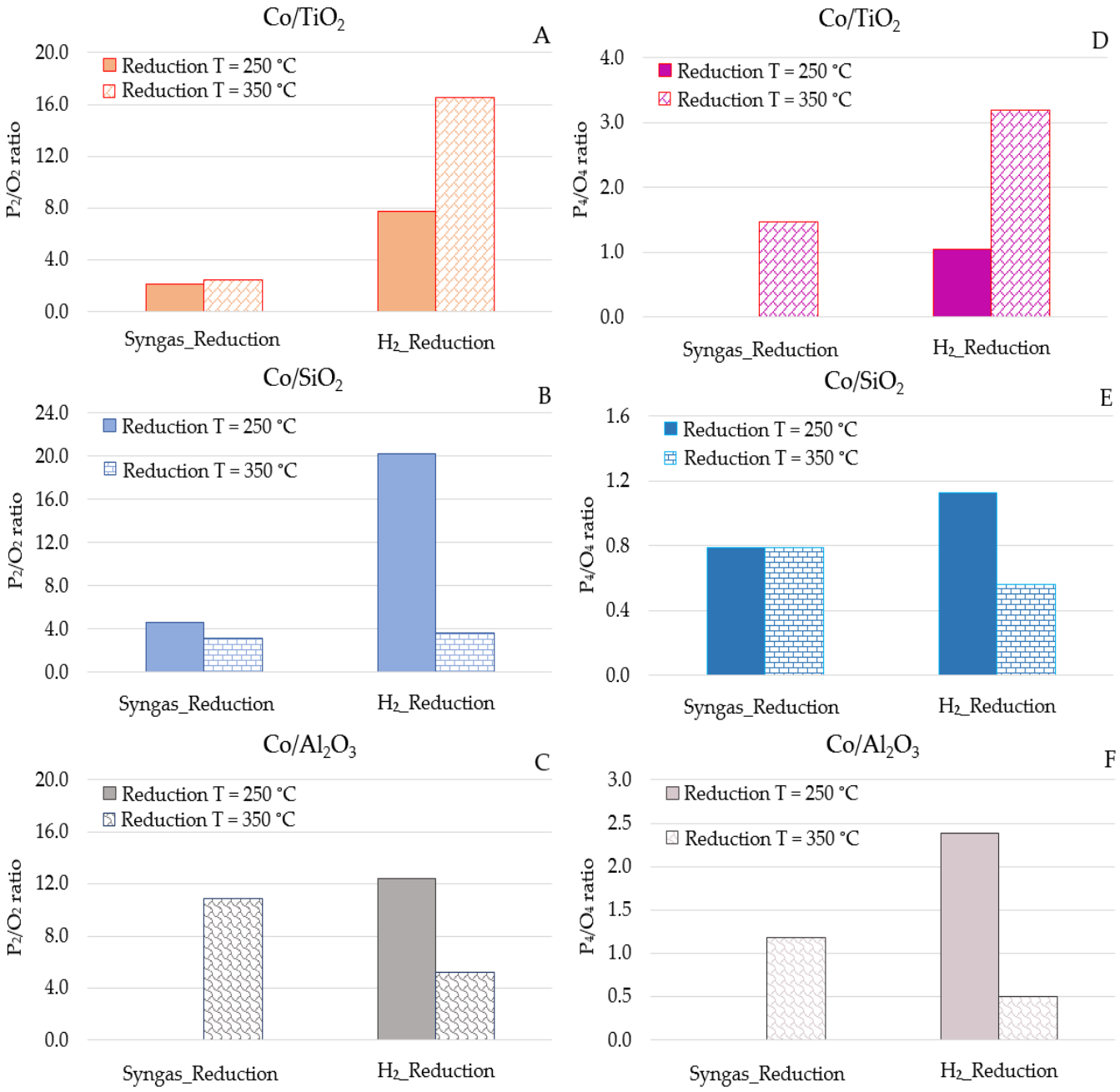

Figure 5. 9: Paraffin to olefin ratio as a function of reducing agent and temperature: (A) P_2/O_2 for Co/TiO_2; (B) P_2/O_2 for Co/SiO_2 and (C) P_2/O_2 for Co/Al_2O_3; (D) P_4/O_4 for Co/TiO_2; (E) P_4/O_4 for Co/SiO_2 and (F) P_4/O_4 for Co/Al_2O_3. Reaction conditions: 20 bar, 60 ml/min and 210 °C.

5.4 Discussion and Implications

With the aim to understand the reaction pathways observed with different pre-treatment agents at different reduction temperatures, the author replotted some of the data reported in Figures 5.4-5.9, to highlight the important findings of this work, the results are shown in Figure 5.10. The syngas treated catalysts afforded a lower CO reaction rate compared to H_2-treated samples (Figure 5.4 and Figure 5.10 (A)). This could be attributed to the lower Co site density caused by incomplete reduction of Co_3O_4 to metallic Co^0. Metallic Co^0 is known to be the active phase for the conversion of syngas to hydrocarbon products [20], therefore, the lower the Co^0 density the lower the CO hydrogenation activity. Our findings are in line with Gnanamani et al. [28] who reported that cobalt catalysts do not reduce completely under syngas treatment.

Catalyst pretreatment is a way to transform cobalt oxides to active sites. For H_2 reduction, cobalt oxides are reduced in H_2 to form Co^0, in the meantime, there is still some cobalt oxides (Co_3O_4 and/or CoO) left due to partial reduction depending on the reduction temperature or the extent of metal-support interactions. For syngas (a mixture of H_2/CO) reduction, the presence of CO in the mixture can also react with the cobalt oxides to form cobalt carbides (Co_xC), which has been confirmed by Peacock et al. [29] and Claeys et al. [30] using the in-situ magnetometer. In addition, the Boudouard reaction ($2CO = CO_2 + C$) may happen when the operating temperature is high. Figure 5.11 lists the possible cobalt phases after cobalt catalyst reduction under different atmospheres.

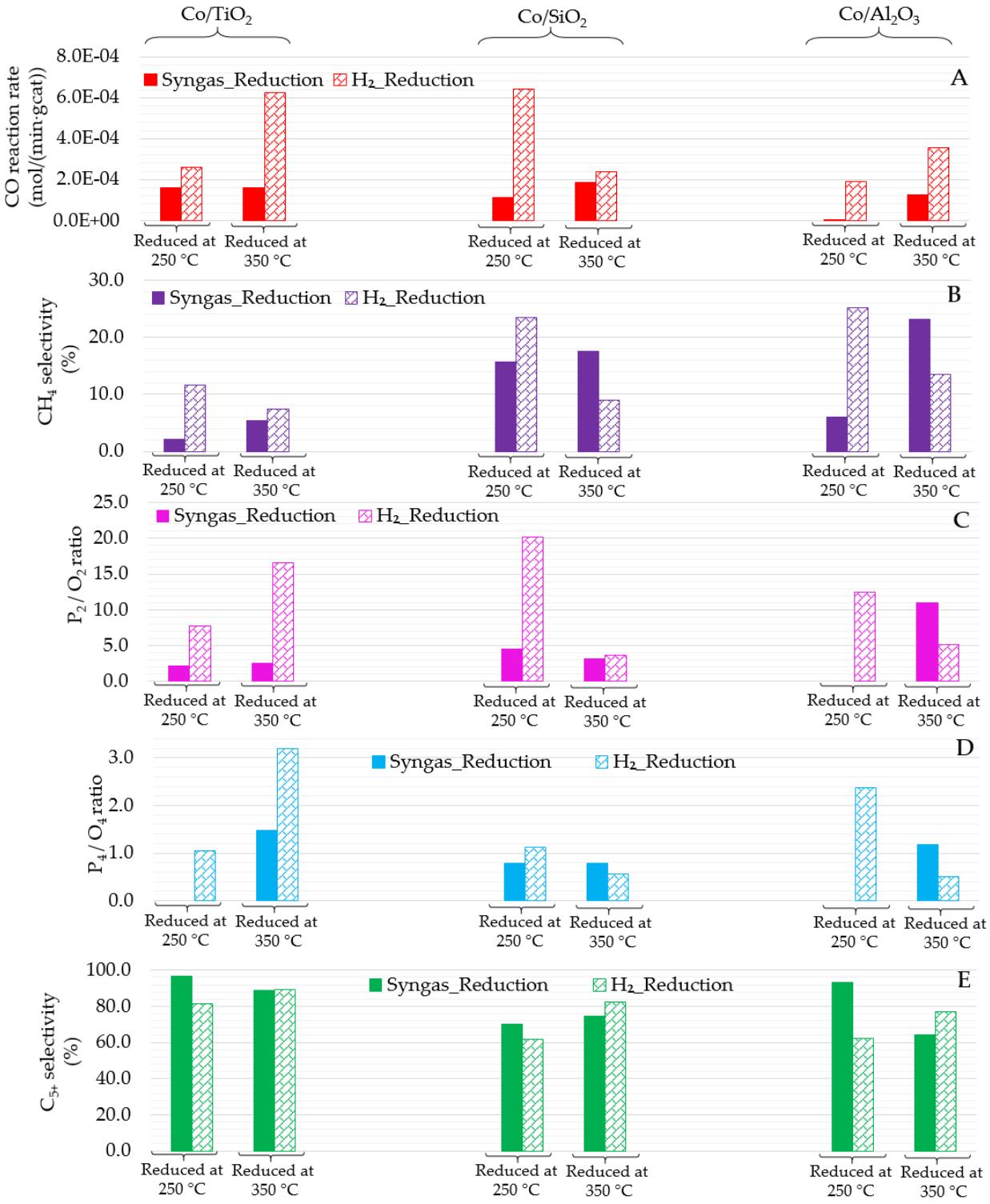

Figure 5. 10: CO reaction rate and product selectivity as a function of reducing agent and temperature: (A) CO reaction rate; (B) CH_4 selectivity and (C) P_2/O_2 ratio; (D) P_4/O_4 ratio; (E) C_{5+} selectivity. Reaction conditions: 20 bar, 60 ml/min and 210 °C. P_2/O_2 refers to ethane/ethylene; P_4/O_4 refers to butane/butene.

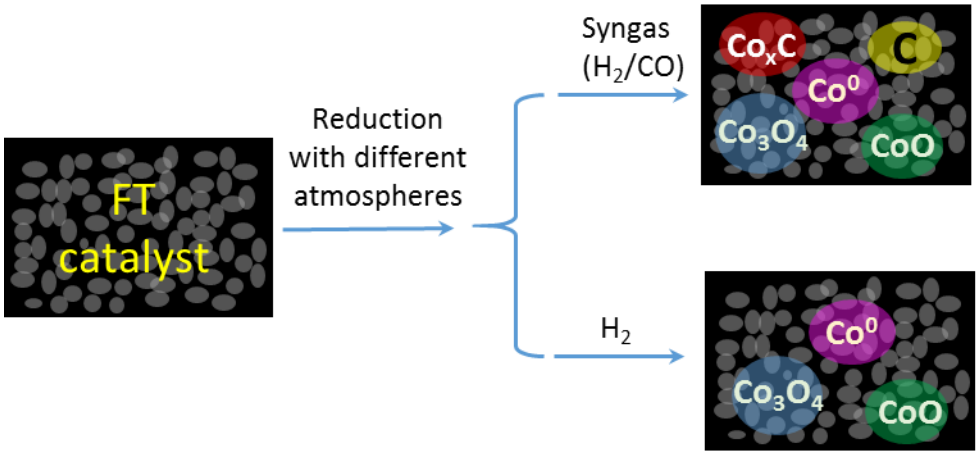

Figure 5. 11: Cobalt phases during pre-treatment of the cobalt-based FT catalyst.

From our experimental data (see Figures 5.10 (B-D)), with syngas reduction at 250 °C, all the three catalysts had a much lower CH_4 selectivity and lower P/O ratio compared to the catalysts treated with H_2 at 250 °C, which indicates that the CO hydrogenation reaction to paraffins was suppressed during the low temperature syngas reduction. These experimental results may be evidence of the Co_2C phase promoting the formation of olefins by suppressing the olefin hydrogenation reaction. Furthermore, the existence of the metallic Co-hcp phase, obtained from further reduction of cobalt via the Co_xC intermediate, could catalyze the FT chain growth reaction by converting syngas to light olefins which in turn react to form longer chain hydrocarbons for syngas treated catalysts reduced at 250 °C; this reaction path is not the dominant mechanism for H_2 reduced catalysts at these reduction temperatures.

To support this argument, we performed an XRD analysis on the spent Co/SiO_2 catalysts reduced at 250 ˚C, the results are shown in Figure 5.12. Figure 5.12 indicate that Co_2C (indicated by green hollow stars) was formed during the reduction in syngas, for all the catalysts. The Co/SiO_2 showed more intense Co_2C peaks which could be related to a higher Co_2C content. This rational experimental design demonstrated that the SiO_2 catalyst had a higher carbon diffusion rate due to weaker Co-silica interactions compared to the TiO_2- and Al_2O_3-supported catalysts. Furthermore, the SiO_2 catalyst showed a broader and higher intense peak around 20˚ which corresponds to the wax products $(CH_2)_X$. This could be

attributed to the high activity that was achieved at 250 ˚C which might have deposited wax products on the surface of the catalyst, whilst for TiO_2 and Al_2O_3, a low conversion was achieved.

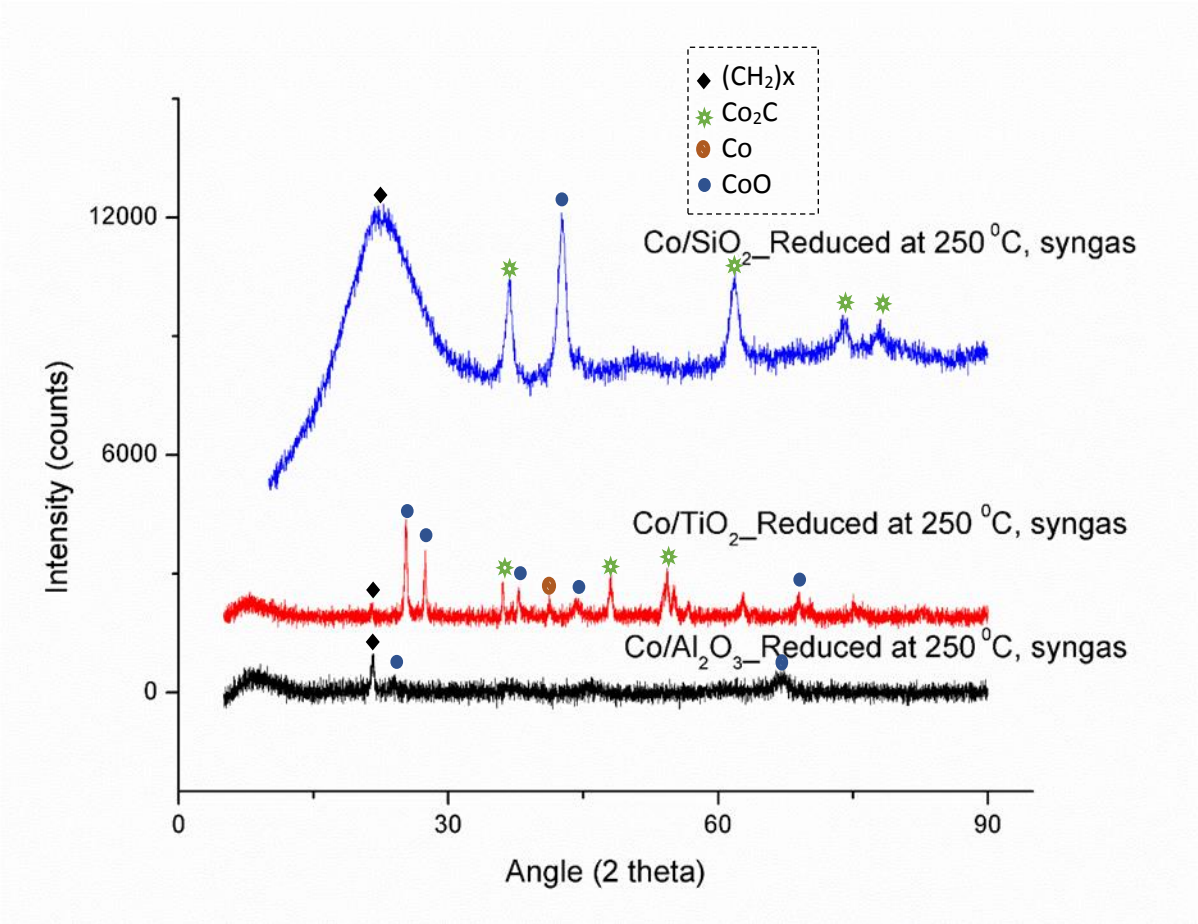

Figure 5. 12*:* XRD patterns for the spent Co/SiO_2, Co/TiO_2 and Co/Al_2O_3 catalysts reduced in syngas at 250 ˚C.

Based on our results, it is hypothesized that cobalt in association with the cobalt carbides enhances the production of higher hydrocarbons. Jiao et al. [31] and Gnanamani e al. [28] both support this hypothesis, in that they both suggest that Co_2C contributes to the selectivity of light olefin products and alcohol formation via a CO insertion mechanism. In addition, Jalama et al. [18] reported a higher olefin to paraffin ratio for the samples pre-treated in syngas than in H_2 which was attributed to the presence of the Co_2C phase. The large shift in product selectivity by changing the activation conditions (as shown in Figures

5.5-5.9) has led us to believe that the method of activation of cobalt as well as the corresponding temperature play vital roles in the subsequent hydrogenation of CO.

A higher reduction temperature was found to increase the selectivity of C_1 in detriment to all other hydrocarbons (Figure 5.10), when syngas was used as a reducing agent. At 350 °C, the Boudouard reaction may happen, and the carbonaceous deposits on the surface could act as methanation sites and decrease the number Co of active sites available for FTS. Findings over these catalysts suggest that carburization and surface carbon deposits are feasible under syngas reduction and that this may cause an increase in both the C_{5+} selectivity or CH_4 selectivity depending on the amount of carbon available. Our finding is in line with Lee et al. [32] who reported that surface carbonaceous deposits can exist in two forms, namely active carbon or graphitic carbon, and that the active carbon can hydrogenate to methane under normal FT conditions. In the case of H_2-pre-treated samples, an increase in the reduction temperature from 250 °C to 350 °C led to the production of higher hydrocarbons. These results demonstrate that C_{5+} hydrocarbon formation is a function of temperature and that a high reduction temperature is associated with a higher reducibility of Co_3O_4 to Co^0; therefore, it can be deduced that Co^0 is selective to the production of C_{5+} hydrocarbons.

This study also reflects on the effect of support properties on the performance of cobalt catalysts under different pre-treatment conditions. The catalyst supported on TiO_2 exhibited the highest selectivity towards liquid products with the lowest CH_4 selectivity, when treated in both H_2 and syngas. This can be attributed to the higher Co site density observed via TEM (Figure 5.1A) and a higher reducibility, as established by the TPR profile in Figure 5.3, due to weaker metal interactions. On the other hand, Al_2O_3 showed the least selectivity, when both syngas and H_2 were used as a pre-treatment feed, due to the lower metal dispersion caused by large Co_3O_4 particles, observed via TEM and XRD, that were formed due to the large alumina support pores, observed via BET, see Table 5.1. In the case of the SiO_2 support, the TPR reduction profile resembled that of the TiO_2 support suggesting that the SiO_2 support is also weakly bonded to the Co metal. However, the Co/SiO_2 catalyst showed a different reactivity to that of TiO_2 due to different active sites, a large surface

area and a lower metal dispersion than the catalyst supported on TiO_2, see Figure 5.1C. The large surface area for SiO_2 enhanced its catalytic activity due to easily reducible and accessible active sites leading to active special interactions, which is in line with findings by Solsona et al. [33]. The support identity therefore plays a major role in the performance of the catalyst. Two parameters seem to determine the catalytic activity of the Co_3O_4 nanoparticles; (1) the Co particle size which is influenced by the support pore size; (2) the extent of metal-metal oxide interactions which determines the specific nature of the active sites.

5.5 Conclusions

The purpose of this study is to show the advantages of using syngas as a reducing agent for Co-FTS catalysts. To this end, we demonstrated the effect of the pre-treatment conditions by comparing the activity and product selectivity of the catalysts treated with syngas or H_2 at different temperatures. A lower CH_4 selectivity, higher C_{5+} selectivity and lower P/O ratio were observed for the catalysts treated with syngas at 250 ˚C compared to the catalysts reduced either with H_2- at 250 ˚C or syngas at 350 ˚C. The formation of the Co_xC phase formed during the reduction in syngas may either: (1) act as an active site for the production of lower olefins or (2) suppress the hydrogenation reaction. Based on the experimental results, it is hypothesized that there may be synergy between Co^0 and Co_xC to convert CO and H_2 to long chain hydrocarbons.

Author Contributions: Conceptualization, Y.Y. and X.L.; methodology, N.S., Y.Y. and X.L.; software, N.S.; validation, Y.Y., X.L. and D.H.; formal analysis, N.S.; investigation, N.S.; resources, Y.Y., D.H. and X.L.; writing—original draft preparation, N.S.; writing—review and editing, Y.Y. and D.H.; supervision, Y.Y; project administration, Y.Y and X.L.; funding acquisition, D.H.; All authors have read and agreed to the published version of the manuscript.

Acknowledgments: The authors are grateful for the support received from the University of South Africa (UNISA) and the South Africa National Research Foundation (NRF UID 95445 and 117793).

Conflicts of Interest: The authors declare no conflict of interest. The funders had no role in the design of the study; in the collection, analyses, or interpretation of data; in the writing of the manuscript, or in the decision to publish the results.

5.6 References

[1] Kliewer CE, Soled SL, Kiss G. Morphological transformations during Fischer-Tropsch synthesis on a titania-supported cobalt catalyst. Catal. Today. 2019; 323: 233-256. https://doi.org/10.1016/j.cattod.2018.05.021.

[2] Chen PP, Liu JX, Li WX. Carbon Monoxide Activation on Cobalt Carbide for Fischer–Tropsch Synthesis from First-Principles Theory. ACS Catal. 2019; 9: 8093-8103. https://doi.org/10.1021/acscatal.9b00649.

[3] Dalai AK, Davis BH. Fischer–Tropsch synthesis: a review of water effects on the performances of unsupported and supported Co catalysts. Appl. Catal. A-Gen. 2008; 348: 1-15. https://doi.org/10.1016/j.apcata.2008.06.021.

[4] Voß M, Borgmann D, Wedler G. Characterization of alumina, silica, and titania supported cobalt catalysts. J. Catal. 2002; 212: 10-21. https://doi.org/10.1006/jcat.2002.3739.

[5] Lyu S, Wang L, Zhang J, Liu C, Sun J, Peng B, Wang Y, Rappé KG, Zhang Y, Li J, Nie L. Role of active phase in Fischer–Tropsch synthesis: Experimental evidence of CO activation over single-phase cobalt catalysts. ACS Catal. 2018; 8: 7787-7798. https://doi.org/10.1021/acscatal.8b00834.

[6] Borg Ø, Dietzel PDC, Spjelkavik AI, Tveten EZ, Walmsley JC, Diplas S, Eri S, Holmen A, Rytter E. Fischer–Tropsch synthesis: Cobalt particle size and support effects on intrinsic activity and product distribution. J. Catal. 2008; 259: 161-164. https://doi.org/10.1016/j.jcat.2008.08.017.

[7] Rytter E, Holmen A. On the support in cobalt Fischer–Tropsch synthesis—Emphasis on alumina and aluminates. Catal. Today. 2016; 275: 11-19. https://doi.org/10.1016/j.cattod.2015.11.042.

[8] Khodakov AY, Griboval-Constant A, Bechara R, Zholobenko VL. Pore size effects in Fischer Tropsch synthesis over cobalt-supported mesoporous silicas. J. Catal. 2002; 206: 230-241. https://doi.org/10.1006/jcat.2001.3496.

[9] Song D, Li J. Effect of catalyst pore size on the catalytic performance of silica supported cobalt Fischer–Tropsch catalysts. J. Mol. Catal. A-Chem. 2006; 247: 206-212. https://doi.org/10.1016/j.molcata.2005.11.021

[10] Borg Ø, Eri S, Blekkan EA, Storsæter S, Wigum H, Rytter E, Holmen A. Fischer–Tropsch synthesis over γ -alumina-supported cobalt catalysts: Effect of support variables. J. Catal. 2007; 248: 89-100. https://doi.org/10.1016/j.jcat.2007.03.008.

[11] Jacobs G, Das TK, Zhang Y, Li J, Racoillet G, Davis BH. Fischer–Tropsch synthesis: support, loading, and promoter effects on the reducibility of cobalt catalysts. Appl. Catal. A: Gen. 2002; 233: 263-281. https://doi.org/10.1016/S0926-860X(02)00195-3.

[12] Zhang J, Chen J, Ren J, Li Y, Sun Y. Support effect of Co/Al_2O_3 catalysts for Fischer–Tropsch synthesis. Fuel. 2003; 82: 581-586. https://doi.org/10.1016/S0016-2361(02)00331-9.

[13] Soled SL, Iglesia E, Fiato RA, Baumgartner JE, Vroman H, Miseo S. Control of metal dispersion and structure by changes in the solid-state chemistry of supported cobalt Fischer–Tropsch catalysts. Topics Catal. 2003; 26: 101-109. https://doi.org/10.1023/B:TOCA.0000012990.83630.f9.

[14] Vosoughi V, Badoga S, Dalai AK, Abatzoglou N. Effect of pretreatment on physicochemical properties and performance of multiwalled carbon nanotube supported cobalt catalyst for Fischer–Tropsch Synthesis. Ind. Eng. Chem. Res. 2016; 55: 6049-6059. https://doi.org/10.1021/acs.iecr.5b04381.

[15] Mehrbod M, Martinelli M, Martino AG, Cronauer DC, Kropf AJ, Marshall CL, Jacobs G. Fischer-Tropsch synthesis: Direct cobalt nitrate reduction of promoted Co/TiO_2 catalysts. Fuel. 2019; 245: 488-504. https://doi.org/10.1016/j.fuel.2019.02.083.

[16] De la Peña O'Shea VA, Campos-Martin JM, Fierro JLG. Strong enhancement of the Fischer–Tropsch synthesis on a Co/SiO_2 catalyst activate in syngas mixture. Catal. Commun. 2004; 5: 635-638. https://doi.org/10.1016/j.catcom.2004.08.005.

[17] Tsubaki N, Sun S, Fujimoto K. Different functions of the noble metals added to cobalt catalysts for Fischer–Tropsch synthesis. J. Catal. 2001; 199: 236-246. https://doi.org/10.1006/jcat.2001.3163

[18] Jalama K, Kabuba J, Xiong H, Jewell LL. Co/TiO_2 Fischer–Tropsch catalyst activation by synthesis gas. Catal. Commun. 2012; 17: 154-159. https://doi.org/10.1016/j.catcom.2011.10.029

[19] Dai Y, Zhao Y, Lin T, Li S, Yu F, An Y, Wang X, Xiao K, Sun F, Jiang Z, Lu Y. Particle size effects of cobalt carbide for Fischer–Tropsch to olefins. ACS Catal. 2018; 9: 798-809. https://doi.org/10.1021/acscatal.8b03631.

[20] Claeys M, Dry ME, van Steen E, van Berge PJ, Booyens S, Crous R, van Helden P, Labuschagne J, Moodley DJ, Saib AM. Impact of process conditions on the sintering behavior of an alumina-supported cobalt Fischer–Tropsch catalyst studied with an in-situ magnetometer. ACS Catal. 2015; 5: 841-852. https://doi.org/10.1021/cs501810y.

[21] Yang J, Jacobs G, Jermwongratanachai T, Anders DC, Burtron H. Fischer–Tropsch synthesis: Impact of H_2 or CO activation on methane selectivity. Catal. Lett. 2014; 144: 123–132. https://doi.org/10.1007/s15062-013-1099-y.

[22] Li J, Xu L, Keogh R. Davis B. Fischer–Tropsch synthesis: Effect of CO pretreatment on a ruthenium promoted Co/TiO_2. Catal. Lett. 2000; 70: 127–130. https://doi.org/10.1023/A:1018833217001.

[23] Pei YP, Liu JX, Zhao YH, Ding YJ, Liu T, Dong WD, Zhu HJ, Su HY, Yan L, Li JL, Li WX. High alcohols synthesis via Fischer–Tropsch reaction at cobalt metal/carbide interface. ACS Catal. 2015; 5: 3620-3624. https://doi.org/10.1021/acscatal.5b00791.

[24] Chen W, Kimpel TF, Song Y, Chiang FK, Zijlstra B, Pestman R, Wang P, Hensen EJ. Influence of carbon deposits on the cobalt-catalyzed Fischer–Tropsch reaction: Evidence of a two-site reaction model. ACS Catal. 2018; 8: 1580-1590. https://doi.org/10.1021/acscatal.7b03639.

[25] Fischer N, Clapham B, Feltes T, Claeys M. Cobalt-based Fischer–Tropsch activity and selectivity as a function of crystallite size and water partial pressure. Acs Catal. 2015; 5: 113-121. https://doi.org/10.1021/cs500936t.

[26] Tucker CL, van Steen E. Activity and selectivity of a cobalt-based Fischer-Tropsch catalyst operating at high conversion for once-through biomass-to-liquid operation. Catal. Today.2020; 342: 115-123. https://doi.org/10.1016/j.cattod.2018.12.049.

[27] Shiba NC, Yao Y, Forbes RP, Okoye-Chine CG, Liu X, Hildebrandt D. Role of CoO-Co nanoparticles supported on SiO_2 in Fischer-Tropsch synthesis: Evidence for enhanced CO dissociation and olefin hydrogenation. Fuel Proc. Tech. 2021; 216: 106781. https://doi.org/10.1016/j.fuproc.2021.106781.

[28] Gnanamani MK, Jacobs G, Keogh RA, Shafer WD, Sparks DE, Hopps SD, Thomas GA, Davis BH. Fischer-Tropsch synthesis: Effect of pretreatment conditions of cobalt on activity and selectivity for hydrogenation of carbon dioxide. Appl Catal A, Gen. 2015; 499: 39–46. https://doi.org/10.1016/j.apcata.2015.03.046.

[29] Peacock M, Purves R, Ojeda M, Ferguson E, Paterson J. In situ diffraction of Fischer-Tropsch catalysts: cobalt reduction and carbide formation. ChemCatChem. 2017; 9: 3463–3469. https://doi.org/10.1002/cctc.201700754.

[30] Claeys M, Dry ME, van Steen E, Du Plessis E, Van Berge PJ, Saib AM, Moodley DJ. In situ magnetometer study on the formation and stability of cobalt carbide in Fischer–Tropsch synthesis. J. Catal. 2014; 318: 193–202. https://doi.org/10.1016/j.jcat.2014.08.002.

[31] Jiao F, Li J, Pan X, Xiao J, Li H, Ma H, Wei M, Pan Y, Zhou Z, Li M, Miao S. Selective conversion of syngas to light olefins. Science. 2016; 351: 1065-1068. DOI: 10.1126/science.aaf1835.

[32] Lee DK, Lee JH, Ihm SK. Effect of carbon deposits on carbon monoxide hydrogenation over alumina-supported cobalt catalyst. Appl. Catal. 1988; 36: 199-207. https://doi.org/10.1016/S0166-9834(00)80115-3.

[33] Solsona B, Davies TE, Garcia T, Vázquez I, Dejoz A, Taylor SH. Total oxidation of propane using nanocrystalline cobalt oxide and supported cobalt oxide catalysts. Appl. Catal. B Env. 2008, 84, 176-84. https://doi.org/10.1016/j.apcatb.2008.03.021.

CHAPTER 6: THE EFFECT OF SUPPORT PROPERTIES AND ACTIVATION TEMPERATURE ON Co-BASED CATALYSTS FOR FISCHER-TROPSCH SYNTHESIS

This work has been prepared in a form of a paper for future publication in a journal.

Abstract

The effect of support properties and activation temperature was investigated in Fischer-Tropsch synthesis at industrially relevant conditions (210 ˚C, 20 bar, 60 Nml/min/gCat) over cobalt-based catalysts. The support material was found to have a profound influence on the FT activity and product distribution. The Co/TiO_2 catalyst afforded a high C_{5+} selectivity, low CH_4 selectivity and more paraffinic products compared to the SiO_2 and Al_2O_3 supported catalysts. The better performance shown by the Co/TiO_2 catalyst was attributed to a high Co reducibility and favourable intrinsic Co particle size. Oxidised Co components supported TiO_2, reduced at temperatures 220-250 ˚C, showed no WGS activity. However, the catalyst showed some WGS activity when the reduction temperature was increased to 350 ˚C. This suggests that at higher temperatures and water partial pressures, small Co particles were oxidised to CoO, an active phase for WGS. On the contrary, both SiO_2 and Al_2O_3 supported catalysts showed some WGS activity when reduced at 250 ˚C, when the amount of CoO was higher. Based on the experimental results, it is postulated that: (1) the product selectivity is dependent on the partial pressure of water, a high-water partial pressure favors the formation of paraffins or C_{5+} hydrocarbon products due to enhanced secondary hydrogenation reactions; (2) the WGS activity depends both on the water partial pressure and the interaction between the metal and the support. In this case, the $Co\text{-}CoO\text{-}TiO_2$ interface is not as active as $Co\text{-}CoO\text{-}SiO_2$ or $Co\text{-}CoO\text{-}Al_2O_3$. The interaction between Co and $CoO\text{-}Al_2O_3$ promoted the WGS even at relatively lower CO conversions; (3) the C_{5+} and CH_4 selectivity was found to be independent of the bulk CoO, and it increased with an increase in the reduction temperature for all the catalysts.

6.1 Introduction

The production of liquid hydrocarbons via hydrogenation of CO serves as an alternative fuel generating process. This process is called the Fischer-Tropsch synthesis (FTS) and it utilises syngas (H_2/CO) derived from abundant sources such as biomass and natural gas [1]. Recently, the FTS process stimulated renewed interests due to the depletion of fossil fuels as well as environmental concerns raised by an increase in atmospheric anthropogenic emissions of greenhouse gases. Among the reported transition metal-based catalysts used to catalyse this process, supported cobalt (Co) catalysts are the most potent catalysts known. Owing to its high activity, favourable C_{5+} selectivity, low efficiency of water gas shift (WGS) compared to iron and lower price than noble metals such as platinum [2-3]. Some of the observed deviations in the selectivity of long-chain hydrocarbons (C_{5+}) over Co-catalysts have been attributed to different: (i) Co particle size [4]; (ii) extents of α-readsorption which is governed by the degree of mass transfer (i.e., pore size, active site density, porosity, and particle size) [5-6]; (iii) water partial pressures [6]. These factors governing the product selectivity are reflecting on the influence of nature of the support material and the role it plays in facilitating the secondary reactions as well as the FT reaction.

Supported cobalt catalysts consist of the Co metal dispersed as small crystallites on a high surface area material support. Typical industrially used supports include silica (SiO_2), alumina (Al_2O_3) and titania (TiO_2) [7-8]. Several studies have addressed the effect of support materials on the FTS process and the presented evidence show that the support properties, preparation, and pre-treatment methods are fundamental parameters governing the Co size, Co site density, the nature of the Co species and consequently, the catalytic activity [9-11]. Strong metal-support interactions and particle agglomeration induced by the preparation method are widely reported to be responsible for low reducibility and low FT activity, in particular, for alumina-supported catalysts [1,10]. Jacobs et al. [10] studied the effect of support characteristics on the reducibility of Co-based catalysts and found that the reduction of Al_2O_3- and TiO_2-supported catalysts was hindered by strong metal support interactions and the formation of mixed irreducible oxides from strongly bonded small Co particles. Loedolff et al. [12] achieved a high Co density, uniformly dispersed on a mesoporous SiO_2 support, which was attributed to a high surface concentration of discrete crystal planes, i.e. (100), (101), that makes it ideal for specific chemical interactions, compared to the Al_2O_3 support. Abrokwah et al. [13] investigated the effect of TiO_2 support on FTS using Co, Fe and Ru catalysts and reported strong metal-support interactions for Co and Fe catalysts, which led to a decline in FTS performance,

with Co showing the least activity. This shows that the FTS process has limitations. Considerable efforts are being made to address these limitations, which include the use of promoters to weaken the metal-support interactions [14] or mild calcination and drying temperatures to limit the chances of agglomeration [15]. However, there is still uncertainties regarding the fundamental aspects governing the product selectivity of the catalysts.

Cobalt-based catalysts are first treated under a reducing atmosphere, H_2 being the commonly used agent, to reduce the Co_3O_4 species, present in a freshly calcined catalyst, to a zero valent state Co metal, which is believed to be the active phase for FTS [16]. Studies on the effect of pre-treatment conditions on the FTS activity and selectivity are well documented [17-18]. A general consent is addressed in the literature that reducing at a low temperature result in incomplete reduction of Co_3O_4 to CoO or a mixture of CoO and Co˚, whereas, at higher temperatures (>450˚C) the reduction leads to support weight loss, agglomeration of Co particles, and as a result, a decline in activity [15]. While CoO is believed to be inactive for FTS [19], others find it active for methanation [20], WGS [21]and to be the probable cause of deactivation [22]. Saib et al. [23] and Iglesia [24] reported that small Co crystallites (<6 nm diameter) re-oxidise and deactivate rapidly in the presence of water. However, considering surface energies, the recent thermodynamic analysis shows that only particles smaller than 4.4 nm will oxidise under FTS conditions and oxide shells may form around the metallic core, which speeds up deactivation [25,26].

To our best knowledge, FTS studies focused on the support characteristics and the reduction temperature are aimed at finding the optimal reduction/reaction conditions to improve the CO conversion activity. Little attention has been given to the effect of support and reduction temperature on the surface Co-species and their reactivity in FTS. Our previous study on the role of Co species supported on SiO_2 in FTS demonstrated that different reduction temperatures may significantly influence both FT and WGS reaction rates [27]. Here, we reported mixed CoO-Co nanoparticles, achieved by reducing the catalyst at a low temperature (250 ˚C), which afforded a high activity for both FTS and WGS reactions that surpassed the activity found for the same catalyst when treated at 350 ˚C [27]. The improvement in FTS activity was attributed to the synergistic effect formed between the CoO and Co metal particles, which promoted the FT reaction and at the same time the CoO was still active for WGS, as observed in literature [28]. In addition, Malaet et al. [29] observed a samilar trend for Co nanoparticles dispersed on TiO_2, which showed a higher FT activity when

treated at 250 ˚C compared to 350 ˚C. In this study, it was believed that the CoO promoted the FTS reaction by forming a catalytically active phase with TiO_2 that improved FTS activity [29]. However, they did not discuss the effect of CoO on the WGS activity. These studies suggest that Co-CoO may work together to improve the FT reaction and WGS reaction and that the reaction rates are further affected by the nature of the support. However, this raises questions as to, does this mechanism route work only for catalysts reduced at a low temperature (at high residual CoO) or can it occur even at high temperatures where the rate of oxidation of small cobalt particles to cobalt oxide is high.

The emergence of new studies on the role of the CoO phase has triggered our interests to study the effect support properties on metallic and oxidised Co components at different reduction temperatures and their reactivity in FTS. The-state-of-art situation of FTS to value added chemicals is far from being optimal. Modification of the traditional FTS process either by controlling the support effects or reduction temperature effect to improve the catalytic performance is vital. In the present work, the properties of various cobalt catalysts supported on TiO_2, SiO_2 and Al_2O_3, were characterised using *in-situ* XRD to monitor the surface relationships between the support and the metal and studied for FTS. The reduction temperature was varied at a range 220-350 ˚C to evaluate the impact of the Co oxidation state and their catalytic performance in FTS. We present evidence of no WGS activity for the partially reduced CoO/TiO_2 catalysts, whereas the latter was observed when Al_2O_3 and SiO_2 were used as supports. Furthermore, all catalysts showed more paraffinic products when the rate of CO hydrogenation was high, 350 ˚C for TiO_2 and 250 for both SiO_2 and Al_2O_3 catalysts.

6.2 Experimental

6.2.1 Catalyst preparation

In order to investigate the support and temperature effect, three commercial supports (TiO_2, SiO_2 and Al_2O_3), purchased from Sigma Aldrich, were used to anchor the FTS catalysts. The catalysts, with 15 wt% metallic cobalt contents, were prepared by the incipient wetness impregnation method using cobalt nitrate as a precursor and dried at room temperature overnight followed by subsequent drying at 40 ˚C for 3 h and then calcination in an air atmosphere at 350 ˚C for 8h, thereafter named Co/TiO_2, Co/SiO_2 and Co/Al_2O_3.

6.2.2 Catalyst characterisation

Temperature-programmed reduction (TPR) studies were performed in a U-shaped tubular quartz reactor heated by an electrical furnace, for calcined catalysts. The calcined catalysts were loaded into the reactor (0.2 g of catalyst) and heated at a rate of 10 ˚C/min to 930 ˚C in a gas consisting of 7% H_2 in Ar, at a gas flow rate of 30 ml/min. H_2 consumption was measured by analysing the effluent gas using a thermal conductivity detector. Additional TPR analysis was conducted on the TiO_2-supported catalyst for a temperature range of 220-350 ˚C at a rate of 5˚C/min, the sample was kept at the desired temperature for 6 h.

Transmission Electron Microscopy (TEM) was used to investigate the shape, size, and orientation of the cobalt particles on different supports. The TEM samples were prepared by embedding the catalysts particles in a resin to prepare slices of nominal 50 nm thickness using Richrt Jung Ultracut E ultramicrotome. A JEOL 2010F instrument operating at 200 KV was used for the TEM measurements.

Powder X-ray diffraction (XRD) studies were performed in a Phillips X'Pert Pro X-ray Diffractometer equipped with a monochromated CuKα X-ray source at ambient temperature. The measurements were done on crushed calcined catalysts and average Co_3O_4 particle sizes were calculated from the most intense Co_3O_4 line ($2\theta = 36.9^\circ$), using the Scherrer formula [30].

The cobalt content was measured by X-ray fluorescence (XRF). The point of zero charge was measured by using a 0.1 M NaCl solution. 1.25 g of support was introduced to the volume corresponding to 23.75 g of NaCl solution. The sample was palletised and pressurised at 10 Kpa for a few minutes and then transferred into the XRF sample holder for analysis.

The in-situ powder X-ray diffraction (PXRD) measurements were carried out using an Anton-Paar XRK900 furnace under a flowing H_2 atmosphere (HP, 1 atm). The temperature was increased from room temperature to 450 °C at a rate of 18 °C/min. The crystalline phase identification was done using DIFFRAC.EVA (Version 2. Release 2014) and the ICDD PDF2 database (Release 2016). Phase quantification was done using the Rietveld method as implemented in Bruker AXS TOPAS software (Version 5, 2014). Data collection was measured every 20° and then every 2 hours for the isotherm at 450 °C.

6.2.3 Catalyst testing

Catalysts were evaluated at 20 bar, 210˚C and 60 ml/min/gcat with the H_2/CO ratio of 2 in a fixed-bed reactor. Three fixed -bed reactors with the size were used in this study. The catalysts, 1 gram of each Co/TiO_2, Co/SiO_2 and Co/Al_2O_3, were reduced in a flowing H_2 at a temperature range of 220-350 ˚C for 16h at atmospheric pressure prior to reaction. The catalyst was then cooled to a temperature lower that 180 ˚C before switching to syngas and adjusting the temperature and pressure to reaction conditions. The liquid products were collected in a cold trap and wax was collected in a hot trap. The gas effluents were analysed by use of Agilent Gas Chromatography (GC-7890A) with two thermal conductivity detectors (TCDs) and one flame ionisation detector (FID). The gas hydrocarbons were analysed through FID. The inorganic products were analysed by two TCDs. Pre-treatment and reaction gases were all supplied by African Oxygen (AFROX Ltd). For further information on the pre-treatment and reaction conditions, please refer to Table 6.1.

Table 6. 1:Catalyst reduction and reaction conditions for Co based FT catalysts.

Catalyst	Reduction conditions					Reaction conditions				
	Agent	T °C	P bar	FR Nml/min	Time h	Syngas Composition	T °C	P bar	FR Nml/min	TOS h
15%Co/TiO_2	H_2	220 250 350	1	60	16	60%H_2/30%CO/10%N_2	210	20	60	0-130 0-128 0-124
15%Co/SiO_2	H_2	250 300 350	1	60	16	60%H_2/30%CO/10%N_2	210	20	60	0-130 0-132 0-122
15%Co/Al_2O_3	H_2	250 350	1	60	16	60%H_2/30%CO/10%N_2	200 210 200 210	20	60	0-115 116-208 0-115 116-210

TOS: time on stream

6.3 Results and Discussions

6.3.1 Catalyst characterisation

Figure 6.1 shows representative medium-resolution TEM micrographs for A. Co/TiO_2, B Co/SiO_2 and C. Co/Al_2O_3 fresh model catalysts. The TEM images show cobalt nanoparticles (higher contrast) dispersed on the support nanoparticles (less contrasted against the carbon coating of the TEM grid), for all the catalysts. Co_3O_4 clusters are seen on the Co/TiO_2 micrograph, Figure 6.1A, which can be attributed to the natural cubic shape of the TiO_2 particles, which led to distribution of Co-nanocrystals on the sides of the cubes, thus forming a collection of particles on one side and an uneven distribution. On the other hand, the Co_3O_4 particles appear to be spatially dispersed on the SiO_2 supported catalyst with one distinctive particle size and a spherical shape, see Figure 6.1B. The %Co on the surface substantially dropped on the alumina due to large Co particles, as observed via ex-situ XRD (see Figure 6.1C at 200 nm). A mixture of spherical (at 200 nm scale) and rod-shaped needle-like cobalt oxide particles is seen at 100 nm scale (yellow squares and orange circles, respectively), for the Al_2O_3-supported catalyst. The presence of needle-like Co_3O_4 structures on the Al_2O_3-supported catalyst could represent the formation of Boehmite (AlO(OH)) due to thermal treatments during catalyst preparation, i.e., drying and calcination.

In contrast, other studies on alumina supported catalysts reported the emergence of needle-like configurations from a spent catalyst rather than on a freshly prepared catalyst [19,26]. These structures were assigned to the formation of Boehmite due to high water partial pressures and the effect of this phase on the catalytic activity and selectivity could not be determined [19,26]. In addition, Co_3O_4 aggregates were also observed on the Al_2O_3 support. The morphology of alumina is rather complex and the transition between the different phases is not as clear-cut as depicted in the Figure 6.1C. A large number of polymorphs exist that are formed upon dehydration, i.e Boehmite, Bayerite and Diaspore, which can be obtained [1].

The particle size distributions from the TEM images were determined using an Image J software which showed a nearly monomodal distribution, rather than narrow Gaussian-like behaviour with d(Co_3O_4) of 28, 26, and 38 nm for Co/TiO_2, Co/SiO_2, and Co/Al_2O_3 , respectively. The standard deviations for the surface-averaged particle size distributions lay in the range of 0.4%, corresponding to all cases. In addition, Fast Fourier transform patterns were analysed at selected areas of each catalyst to confirm the location and heterogeneous

distribution of the Co_3O_4 nanoparticles across the supports (see Figure 6.2). Figures 6.2A and 6.2B show a spatial distribution of small Co_3O_4 crystallites and regions of agglomeration are observed on the TiO_2 support. Regions of good Co_3O_4 dispersion are observed on the Al_2O_3 support, which seem to be uniformly distributed across the surface, which can be attributed to the bigger-sized Co_3O_4 particles that are easily picked up by the TEM machine, see Figure 6.2C.

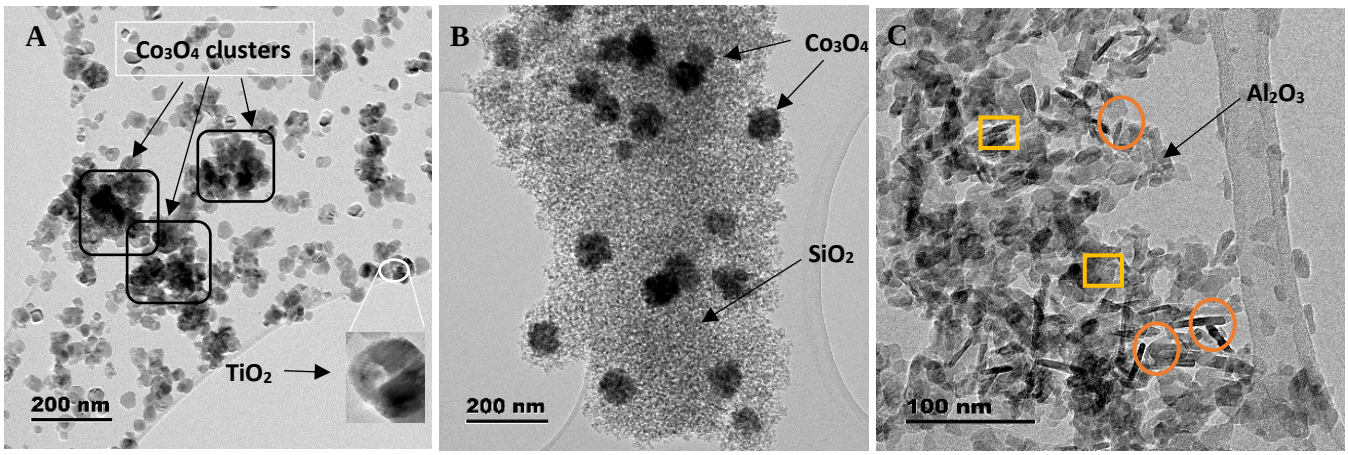

Figure 6. 1: TEM micrograph images of a freshly calcined **A.** Co/TiO_2 **B.** Co/SiO_2 **C.** Co/Al_2O_3

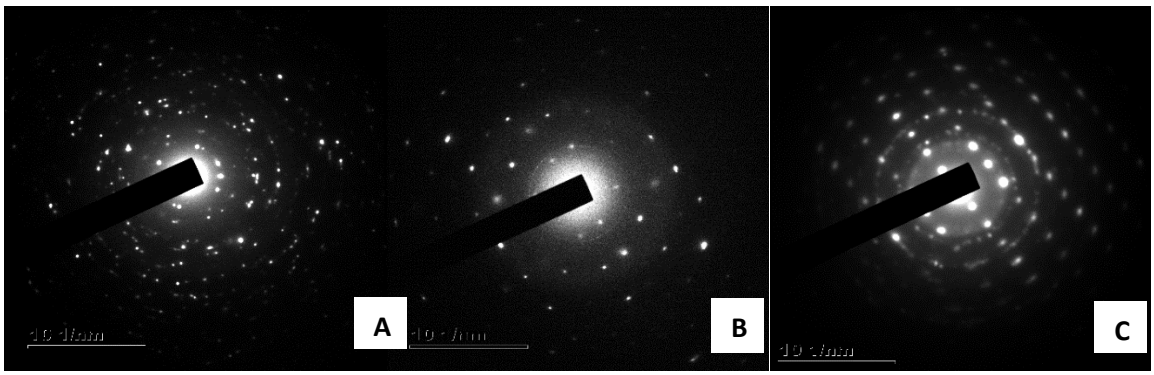

Figure 6. 2: Fast Fourier transformation patterns at selected areas of the cobalt nanoparticles **A.** Co/TiO_2 **B.** Co/SiO_2 **C.** Co/Al_2O_3

The TPR-H_2 curves of the catalysts presented in Figures 6.3A and Figure 6.4, show two reduction peaks, for all samples treated up to 900 ˚C. The two reduction peaks with a maximum around 200-290 ˚C (marked 1) and 300-400 ˚C (marked 2) can be related to the two-stage reduction of Co_3O_4 to CoO followed by a subsequent reduction of CoO to metallic cobalt Co^0, respectively. The reduction profile of Co/Al_2O_3 catalyst present the second reduction peak at 400 ˚C with a shoulder extending to higher temperature of about 700 ˚C, which is probably related to the reduction of Co(II) species present in ion exchange position or to the reduction of cobalt aluminate, see Figure 6.4A. Comparison of the reduction profiles in Figure 6.3A and 6.4 allow us to suggest that Co/Al_2O_3 is hardly reduced as compared to Co/SiO_2 or Co/TiO_2 catalysts, which can be attributed to stronger metal-support interactions, in agreement with literature [17]. The formation of irreducible cobalt aluminates (with the general formula $Co_xAl_yO_4$) by diffusion of Co into the Al_2O_3 lattice during calcination, inhibits the reduction of cobalt [30-31]. On the other hand, the Co/TiO_2 and Co/SiO_2 catalyst present a shorter and narrow first reduction peak than the second peak while Al_2O_3 show longer narrow first reductions peaks and shorter broader second peaks. This suggest that for TiO_2 and SiO_2, the reduction of Co_3O_4 to CoO is much quicker compared to Al_2O_3. In addition, the broadest of the second reduction peak might reflect on the degree of reducibility, in this case, Al_2O_3 has the shortest and broadest second peaks which is related to lower reducibility. Therefore, it can be postulated that TiO_2 and SiO_2 undergoes a more facile reduction, at temperatures lower than the temperatures required to Co/Al_2O_3, which could be due to weaker TiO_2/SiO_2-Co bondages.

Additional TPR profiles were acquired for the TiO_2 support at temperatures between 220 and 350 ˚C, the results are showed in Figure 6.3B-D. The reduction profile for the sample treated up to 350 ˚C showed two reduction peaks related to Co_3O_4 to CoO and CoO to Co, see Figure 6.3B. A decrease in the reduction temperature led to only one reduction peak which corresponds to the partial reduction of Co_3O_4 to CoO, see Figure 6.3C and Figure 6.4D. The broadness of the reduction peak decreases with a decrease in the reduction temperature, which suggest that the amount of Co_3O_4 converted to CoO declines with the reduction temperature. The data in Figure 6.3B suggests that 350 ˚C is an ideal reduction temperature for Co_3O_4/TiO_2.

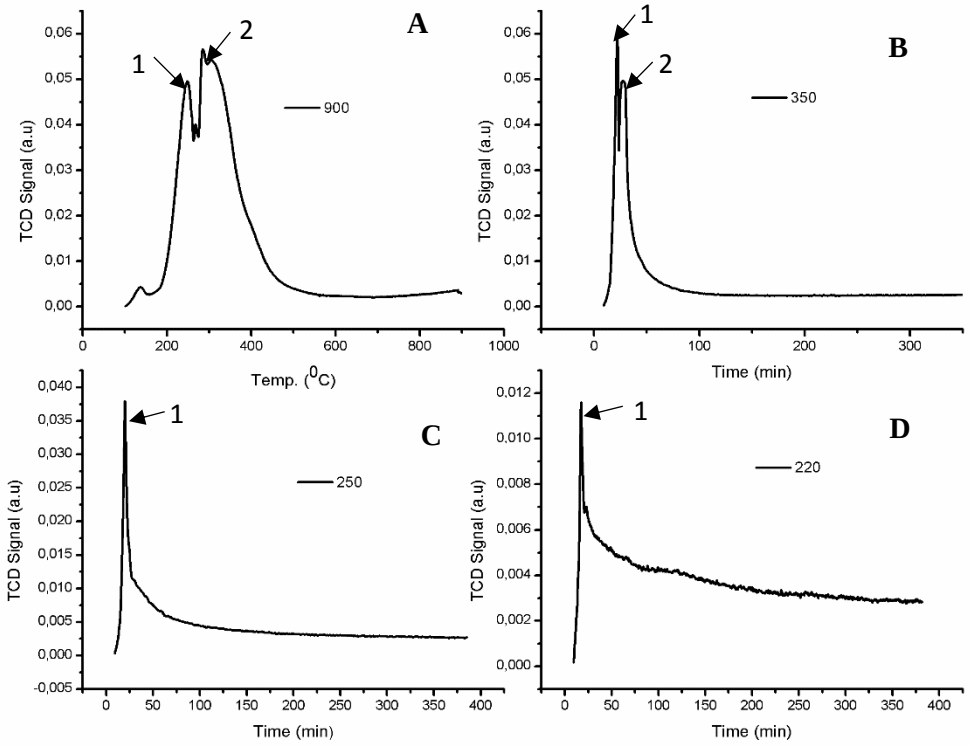

Figure 6. 3: TPR reduction profiles for Co/TiO_2, reduced up to A. 900 ˚C; B. 350 ˚C; C. 250 ˚C and D. 220 ˚C

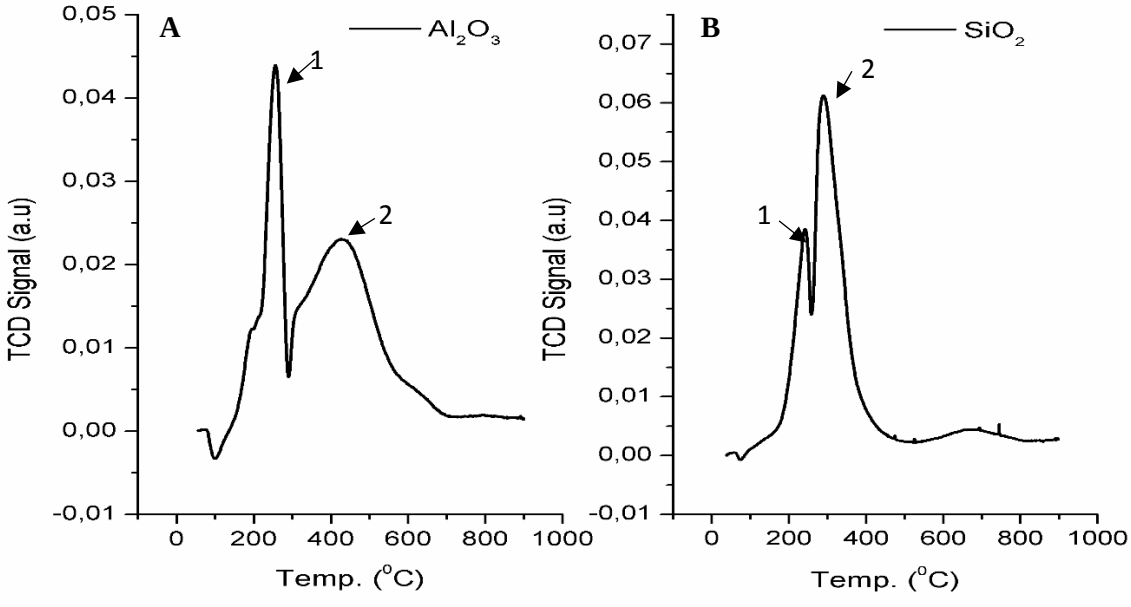

Figure 6. 4: TPR reduction profiles for the cobalt-based catalysts under study A.$CoAl_2O_3$ and B. Co/SiO_2

Table 6.2 collects the textual properties of the model catalysts obtained via XRD, TEM and *in-situ* powder XRD (PXRD) and XRF. The cobalt metallic content was confirmed using XRF technique to range between 14-15 wt%, which is closer to the theoretical content that was calculated during catalyst preparation, see Table 6.2. The particle sizes determined by TEM were slightly larger than those determined from the XRD results, see Table 6.2. This is attributed to the different techniques; the TEM technique accounts for the multi-sized single crystallites, while XRD analysis estimates the size from the broadest diffraction peak and assumes that all particles are spherical in shape.

The clusters observed on the TiO_2 support comprised individual nanoparticles, rather than a single large agglomerate of Co_3O_4. The *in-situ* PXRD results for the Co_3O_4 particles at room temperature are comparable to the *ex-situ* XRD results reported in Table 6.4. The Co_3O_4 particle size decreased during the H_2 treatment (monitored via *in-situ* PXRD), and the results are presented in Table 6.4. The Co particle sizes reduced from 23.4 to 12.7 nm with H_2-treatment at 250 ˚C, for TiO_2-supported sample. Further increase in temperature (up to 350 ˚C) led to a slight increase in the Co(fcc) particle size (13.2 nm), which is the dominate phase after reduction in H_2 (see Figure 6.5) with traces of Co(hcp) with a particle size of 5.0 nm. A similar trend was observed on the Al_2O_3-supported catalyst, where the Co(fcc) particle size is substantially higher than that estimated at 250 ˚C with residual CoO (about 15.4 nm), owing to a strong interaction between Co_3O_4 powder and the alumina particles. However, no sintering was observed on the catalyst supported on SiO_2 see Table 6.2, suggestive of an incomplete reduction. No CoO remained after reduction for the TiO_2 sample and about 12% residual CoO was found on the Al_2O_3 sample. The in-situ XRD data is in line with the TPR data which showed that the reduction of the TiO_2 and SiO_2 samples is much simpler compared to Al_2O_3.

In order to determine the dispersion of Co nanoparticles distributed on the freshly prepare catalysts, we first calculated the mean Co particle size from the XRD Co_3O_4 particle size, using the equation $d(Co^{\circ}) = 3/4\ d(Co_3O_4)$, followed by $D = 96/d(Co^{\circ})$ as demonstrated by Sun et al. [18] and Prieto et al. [32]. The corresponding metal dispersions (D)and mean Co particle sizes d(Co) are collected in Table 6.2. As observed, the Al_2O_3 support displays the lowest metal dispersion (3.87%) corresponding to the large $d(Co_3O_4)$ = 33 nm in line with the *in-situ* PXRD

and TEM results. The metal distribution increased with a decrease in particle size and reducibility as observed with TPR.

Table 6. 2: XRD, TEM and XRF results for the particle size and actual loading of the cobalt-based catalysts.

Catalyst	XRD (nm)			In-situ XRD (nm)					TEM	XRF Co content
				25˚C	250 ˚C	350 ˚C				
	Co_3O_4 [15]	d(Co˚)[a]	D[b] %	Co_3O_4	CoO	CoO	Co(fcc)	Co(hcp)	nm	wt %±0.03 [15]
Co/TiO_2	21.5	16.1	5.96	23.4	12.7	0.0	13.2	5.0	28.0	14.0
Co/SiO_2	17.0	12.8	7.50	17.1	12.2	8.3	8.7	5.0	26.0	14.5
Co/Al_2O_3	33.0	24.8	3.87	34.2	14.6	15.4	21.7	5.0	38.0	15.2

[a]Mean cobalt particle size calculated from XRD data, using d(Co˚) = 3/4 d(Co_3O_4)

[b]Cobalt metal dispersion calculated from XRD data, using the relation D = 96/d(Co˚)

In-situ PXRD diffractions were obtained during reduction of the catalysts, by increasing the temperature stepwise up to 430 °C. The XRD diffraction patterns were then used for the Retvield Refinement, in order to obtain the relative phase abundance and average crystallite sizes (see Figures 6.5 and 6.6). The two-step change from Co_3O_4 to CoO, and CoO to metallic Co was observed during the H_2-treatment, for all the catalysts, which is in line with the TPR data shown in Figure 6.4. The Co_3O_4 to CoO step transformation was observed at approximately 190 °C for all the supported catalysts, which is lower than the initial temperature of the first TPR peak. The slight difference could be caused by the difference in the ramping rates: 10 °C/min for TPR and 0.16 °C/min for *in-situ* PXRD. The CoO completely disappears at around 290 °C for the TiO_2-supported catalyst, as can be seen in Figure 6.5A. Traces of CoO were observed for both the SiO_2 and Al_2O_3 supported catalysts throughout the reduction, with about 29% and 12.3% phase abundance, respectively, remaining at 430 ˚C, see Figure 6.5B and 6.5C.

Metallic Co(fcc) started appearing at temperatures of about 270, 310, 330 °C for the Co/TiO_2, Co/SiO_2 and Co/Al_2O_3 catalysts, respectively. This is consistent with the TPR data reported in

Figure 6.4. The Co(hcp) was observed from 350 °C for both the Al_2O_3 and SiO_2 catalysts, whilst for the TiO_2 support, the latter emerged quite early (at about 250 °C). These results suggest that the reduction of TiO_2 is much simpler compared to the other supports and that complete reduction can be achieved at temperatures of about 430 ˚C. The results are slightly different from the TPR data as shown in Figure 6.4, which shows that the SiO_2 supported catalyst was easier reduced than the TiO_2 supported, which might be due to the difference in the ramping rates between TPR analysis and in situ XRD analysis. It is worth noting that almost similar amounts of Co(fcc) and Co(hcp) were found in the TiO_2 sample after H_2 reduction, whereas Co(fcc) was more in abundant than Co(hcp) in the SiO_2 and Al_2O_3 supported catalysts, see Figure 6.5.

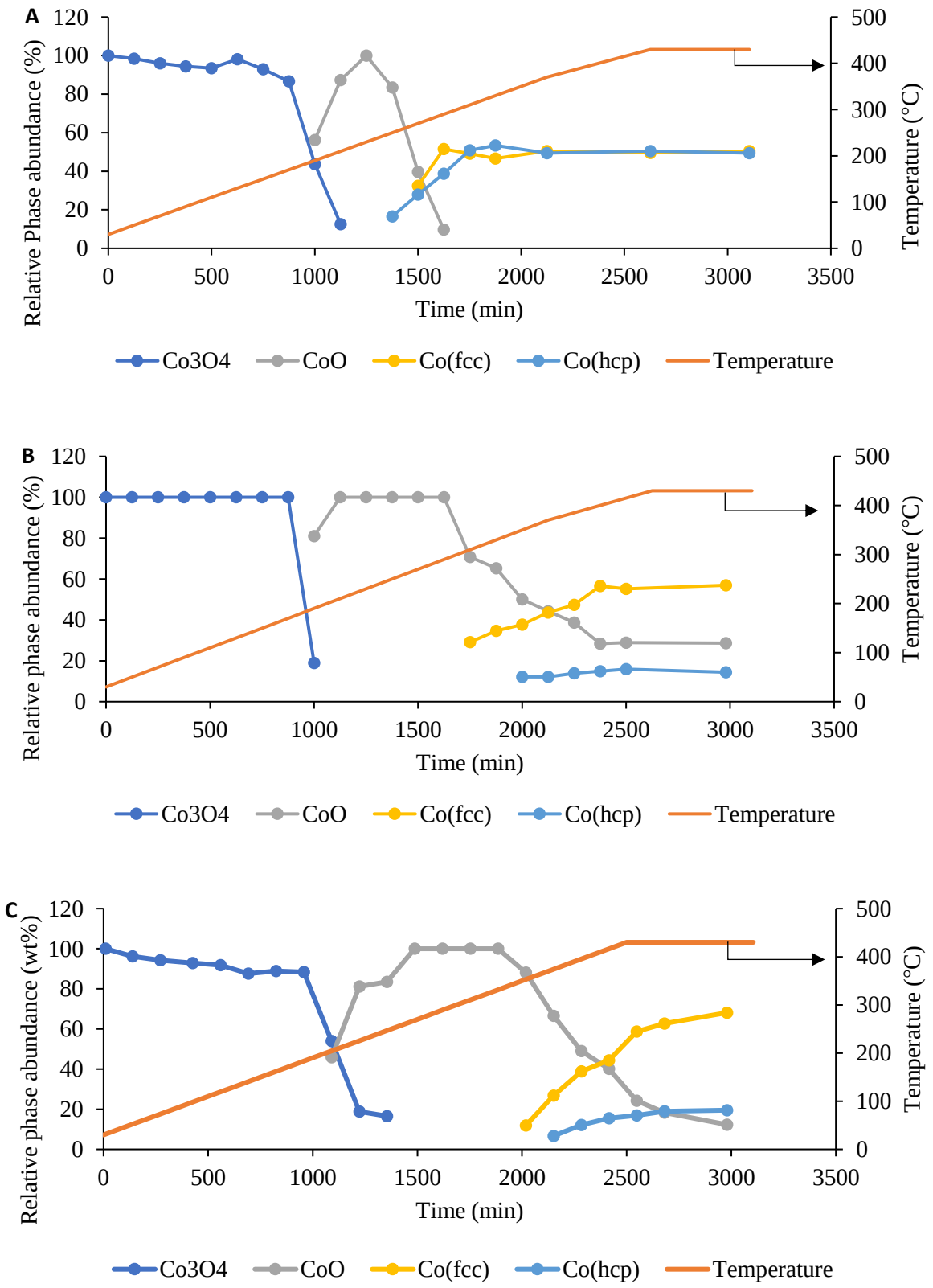

Figure 6. 5: Relative phase abundance for the crystallite phase observed during H_2 reduction of the model catalysts: A. Co/TiO_2; B. Co/SiO_2; and C. Co/Al_2O_3.

The average cobalt crystallite sizes during reduction were determined from the Rietveld refinements and are reported in Figure 6.6. The initial Co_3O_4 particle size was found to be 23.4 nm, 17.1 nm and 34.2 nm for TiO_2, SiO_2 and Al_2O_3 at 30 °C, respectively. These sizes are consistent with the *ex-situ* XRD and TEM data of the freshly calcined catalysts, see Table 6.2. The CoO particle size decreased from 20.3 to 14.2 nm between room temperature and 190 °C for the TiO_2-supported catalyst, see Figure 6.6A. The reduction of CoO was quite slow for the other supports and resulted in an initial and final crystallite size of about 12.2 and 10.6 nm to 8.5 and 5 nm for SiO_2 and Al_2O_3 supports, respectively(see Figure 6.6B and 6.6C).

During the second reduction step (CoO→Co), the Co(fcc) particle size increased for the TiO_2 and Al_2O_3 supported catalyst, while it remained the same for the SiO_2 supported catalyst. The average particle size of Co(fcc) for the three catalysts with the reduction temperature in a range of (330-430 °C) were in an order of: $SiO_2<TiO_2<Al_2O_3$, which corresponds to the pore sizes of the supports with Al_2O_3 having the biggest pore size [27]. The apparent increase in Co(fcc) crystallite size can be explained by the restructuring of surface species or the effect of the chemical reaction on the surface, such as, agglomeration of the particles on both the TiO_2 and Al_2O_3 supported catalyst, see Figure 6.6C. It is worth noting that the crystallite size of Co(hcp) for all the supports was fairly constant, about 5 nm, at the end of the reduction. In addition, the results in Figure 6.6 clearly show that the crystallite size of Co(fcc) is much bigger than that for Co(hcp) for all the three catalysts, which is consistent with the results obtained by Ghampson et al. [33].

The crystallite size is a critical factor in FTS catalyst development, as it is related to metal dispersion and consequently, the activity for the catalyst. Park et al. [34] obtained a positive trend for both the CO conversion and C_{5+} selectivity with particle size in the size range of 4 to 10.7 nm for an alumina-supported cobalt catalyst. A further increase in particle size beyond this range resulted in a decline in CO conversion, but an increased in C_{5+} selectivity and a decreased methane productivity. The effect of the Co species (CoO, Co(hcp) and Co(fcc)) on the activity and selectivity for FTS will be discussed in detail in the next section.

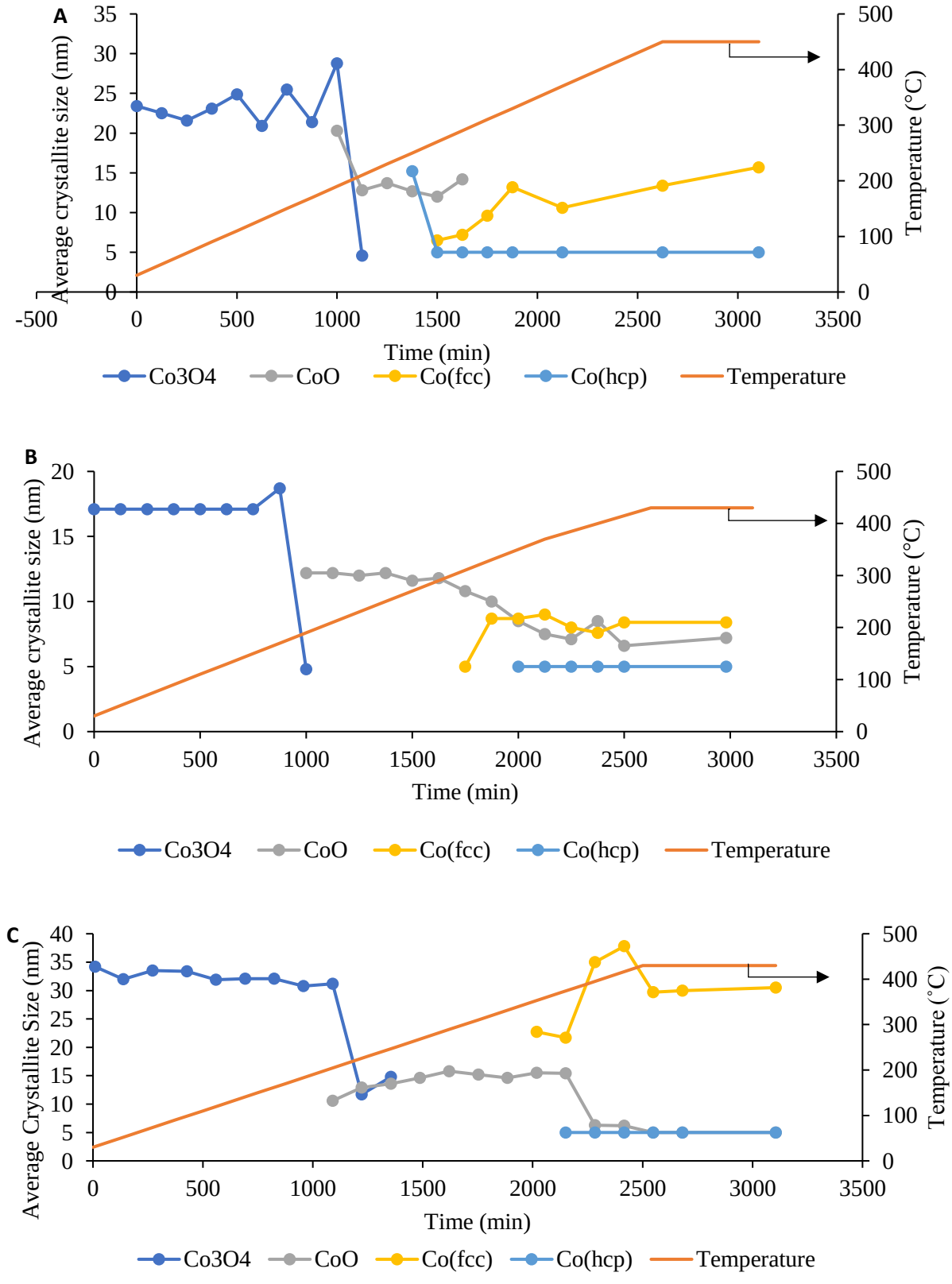

Figure 6. 6: The change in average crystallite size with the increase in H_2-reduction temperature up to 450 ºC**:** A. Co/TiO_2 B. Co/SiO_2 and C. Co/Al_2O_3

6.3.2 Catalyst Testing

6.3.2.1 FT Reactivity

Fischer-Tropsch experiments were performed on Co/TiO_2, Co/SiO_2 and Co/Al_2O_3 catalysts in a fixed bed reactor at 210 ˚C, 20 bar and 60 Nml/min/gCat. Each of the catalysts was reduced in a pure stream of H_2 (purity = 99.99%) for 16 h prior to the FT reaction. The detailed reduction and reaction conditions are listed in Table 6.1. The influence of the reduction temperature and support properties on the activity of these catalyst is presented in Figures 6.7, 6.8 and Table 6.3. The conversion of CO, selectivity to liquid products, CH_4 and CO_2 were analysed and plotted against time on stream (TOS). The Co/TiO_2 catalyst appears to be the most active and most selective to liquid products (C_{5+} hydrocarbons), when treated at 350 ˚C, see Figure 6.7A and Figure 6.8A. The activity of the TiO_2-supported catalyst increases with reduction temperature, which is in line with findings by Luo et al. [35] and Bian et al. [36]. The partially reduced Co/TiO_2 catalyst (at 250 ˚C) still achieved a high C_{5+} selectivity compared to the other catalysts but exhibited a lower CO conversion compared to the Co/SiO_2 catalyst. Furthermore, the Co/TiO_2 catalyst exhibited the lowest CH_4 selectivity (Figure 6.8B) at all reduction temperatures compared to the SiO_2- and Al_2O_3-supported catalysts. Owing to its surface chemistry, the catalyst achieved a high reduction of Co^{3+} or Co^{2+} to Co^0 even at lower temperature as 250 ˚C, as it was observed via i*n-situ* PXRD in Figure 6.5A. The Co/TiO_2 had the highest Co metal content at all reduction temperatures, which favour the production of long chain hydrocarbons, see Figure 6.5A and Figure 6.1A. Presented evidence in literature suggests that metallic Co is selective for C_{5+} hydrocarbons [37] and our findings over the TiO_2-supported catalysts are in line with this observation. The TPR data for the reduction of Co/TiO_2 at 220 ˚C shows that only a little amount of Co_3O_4 was converted to CoO, see Figure 6.3C, however the catalyst showed an increase in activity with TOS which suggests that the catalyst could have undergone further reduction upon the introduction of H_2-rich syngas into the reactor. The FT reaction rate increased steadily with TOS, even for the catalyst reduced at 350 ˚C, which indicates that the FTS system is a very reducing environment and there could be further reduction of CoO particles to Co^0.

The reaction activity of the catalyst supported on SiO_2 was quite the opposite to that of TiO_2. The activity decreased with an increase in the reduction temperature. This behaviour has been addressed in our previous work [27] and it was attributed to the decrease in CoO phase, which

forms catalytically active phase with the silica support and promoted the FT reaction to some extent. The SiO_2-supported catalyst has the second highest C_{5+} selectivity and lowest CH_4 production compared to the other model catalysts under study, Figure 6.8. Even at a lower CO conversion, for the catalyst reduced at 350 ˚C, similar activity trends were observed. This is the experimental evidence that metallic Co is responsible for the production of long-chain hydrocarbons compared to other Co-phases. On the other hand, the alumina supported catalyst had the least FT activity and selectivity, yet it followed the same trends as the Co/TiO_2 catalyst, in terms of activity (see Figure 6.7C). The TPR, *in-situ* PXRD and TEM results showed that the Al_2O_3 catalyst exhibit a low reducibility and low metal dispersion, which is inhibited by strong metal interactions and the diffusion of small Co particles into the Al_2O_3-support lattice, forming irreducible aluminates compounds with the cobalt species.

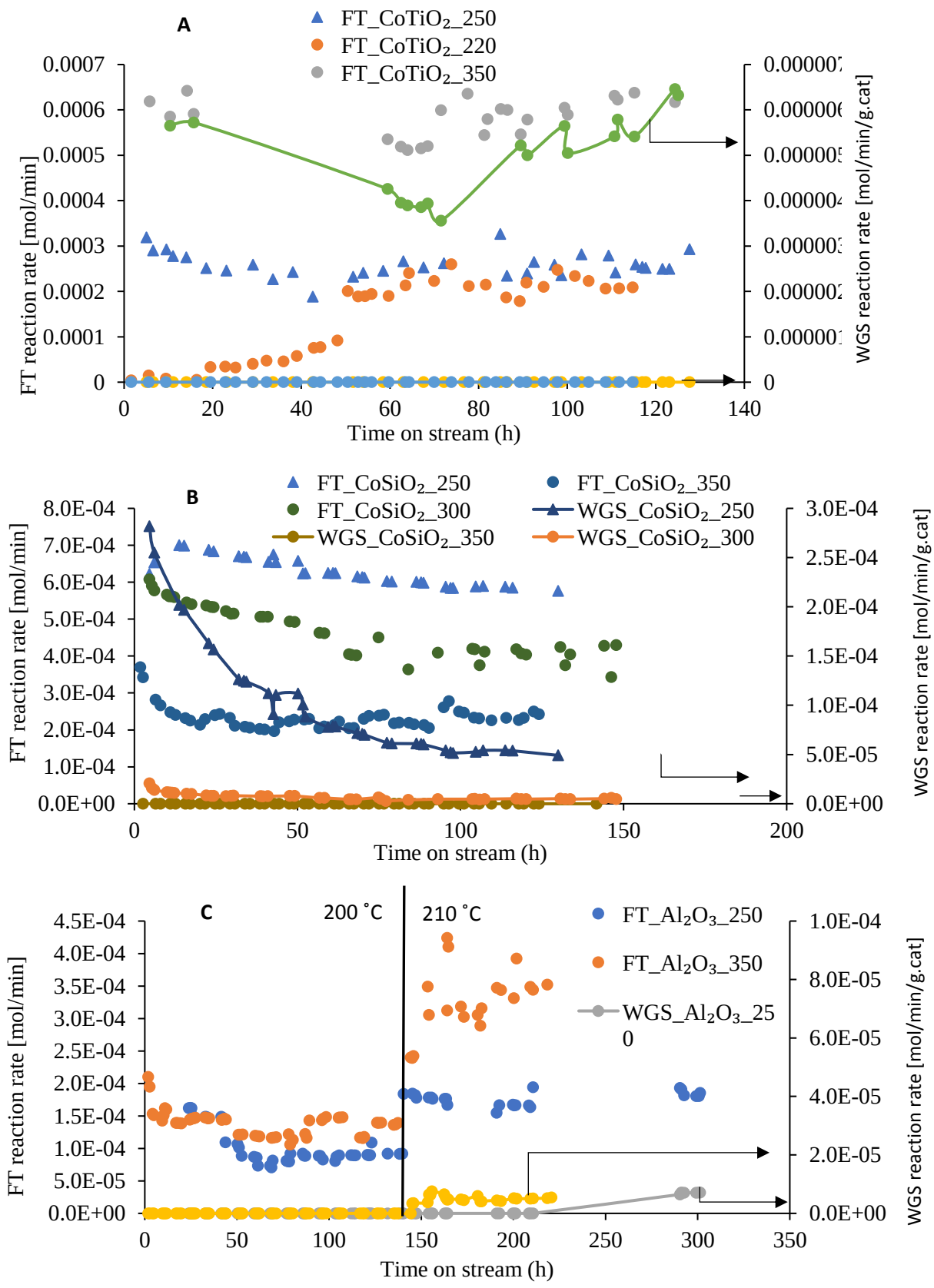

Figure 6. 7: The effect of reduction temperature on FT and WGS activity with time on stream (TOS) for **A.** Co/TiO_2; **B.** Co/SiO_2 and **C.** Co/Al_2O_3. Reaction conditions: P_{Tot} = 20 bar; T= 200-210 ˚C; H_2/CO = 2; FR = 60 Nml/min.

The experimental result from this work also points out to the influence of Co particle size on the C_{5+} selectivity. Sintering of Co metal particles dispersed on Al_2O_3 is demonstrated by the *in-situ* PXRD characterisation results presented in Table 6.2, from 14.6 nm CoO to 21.7 nm Co(fcc). The thermal treatment in H_2 led to the formation of large cobalt clusters, which decreased the Co-support interaction and improved the reducibility of the catalyst as well as the selectivity towards longer hydrocarbons (C_{5+}). Larger cobalt particles are reported to behave more like bulk Co_3O_4 with respect to their reducibility than smaller particles [8] and are more selective to high molecular weight hydrocarbon and CO_2 [4,6]. Our findings are in line with Xiong et al. [38] and Park et al. [34], who reported that an increase in the particle size showed a remarkable increase in the C_{5+} selectivity and reducibility of the catalyst. No metallic Co was found on the Al_2O_3 supported catalyst at a lower reduction temperature, which suggests greater Co-support interactions, see Figures 6.4A and 6.5C. This led to lower Co reducibility and FT activity compared to catalysts reduced at 350 ˚C. The CH_4 selectivity was highest at a low reduction temperature, see Table 6.4 and Figure 6.8, for all the catalysts. This may be attributed to the partial reduction of Co_3O_4 to CoO, which catalyses the methane reaction. Wang et al. [20] reported that CoO is active for CO methanation while metallic Co showed no activity.

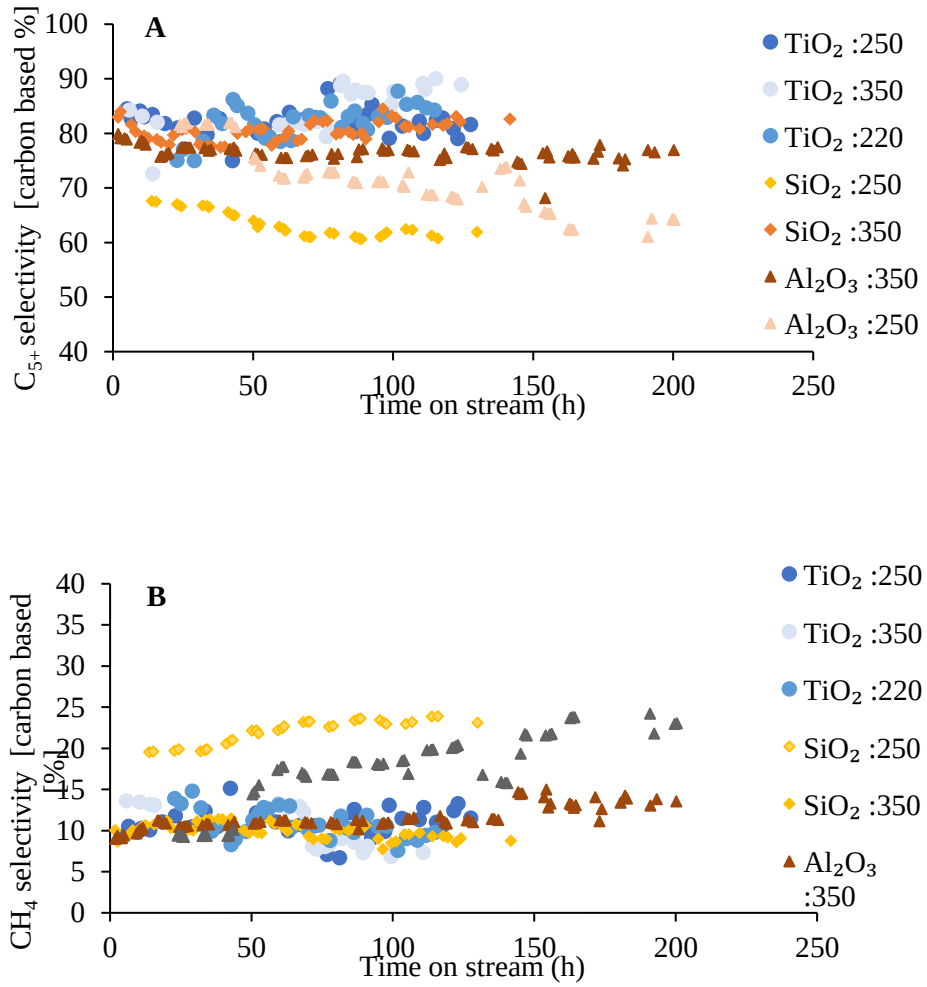

Figure 6. 8: The effect of reduction temperature on the selectivity A. C_{5+} and B. CH_4 with time on stream (TOS) for Co/TiO_2; Co/SiO_2 and Co/Al_2O_3. The legend indicates the reduction temperature (˚C). Reaction conditions: P_{Tot} = 20 bar; T= 200-210 ˚C; H_2/CO = 2; FR = 60 Nml/min.

Figure 6.9 shows the relationship between the CH_4 selectivity and the C_{5+} selectivity at different reduction temperatures. The C_{5+} selectivity is inversely proportional to the CH_4 selectivity. In addition, the C_{5+} selectivity increased with an increase in the Co site density, which is obtainable at a higher reduction temperature. The results obtained in this study are in agreement with previous studies. Iglesia [24] found a positive correlation between the Co site density and the C_{5+} hydrocarbon selectivity, which was consistent with the current research results. Li et al. [37] reported that hydrocarbon products are produced on metallic sites, whereas methane is produced on surface carbides.

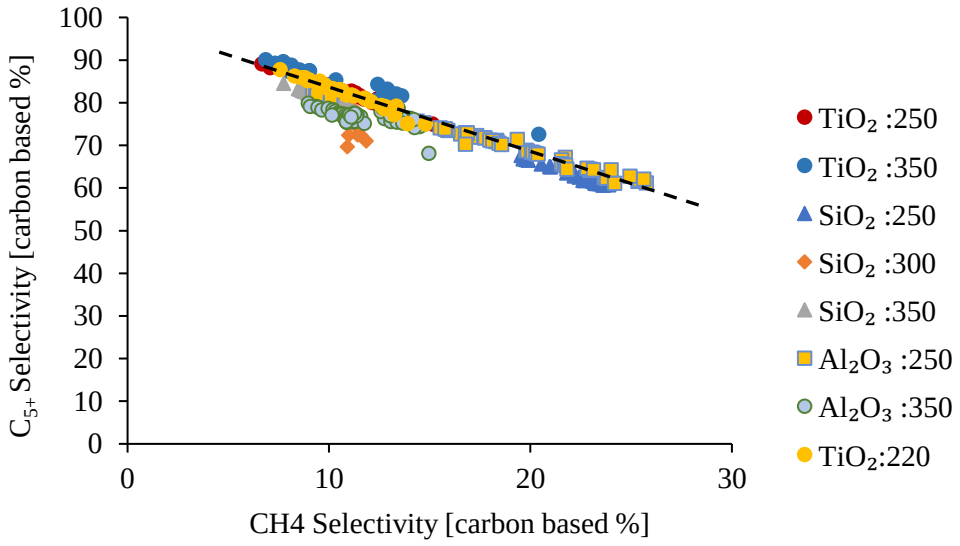

Figure 6. 9: The relationship between C_{5+} and CH_4 selectivity for cobalt-based catalysts with SiO_2, Al_2O_3 and TiO_2 as supports, pre-treated at different reduction temperatures. The legend indicates the catalyst (on different supports), and the reduction temperature (˚C). Reaction conditions: P_{Tot} = 20 bar; T= 200-210 ˚C; H_2/CO = 2; FR = 60 Nml/min.

Table 6. 3: Steady state conversion and selectivity for cobalt-based catalysts. P_{Tot} = 20 bar; T= 210 ˚C; H_2/CO = 2; FR = 60 Nml/min.

Catalyst	Red. T(˚C)	FT activity and product selectivity (C%)				WGS rate	FT rate	H_2O rate	Alpha	Av.	Formation rate (*10^{-5})	
		CO	CO_2	CH_4	C_{5+}	$10^{\wedge-5}$	$10^{\wedge-4}$		(α_{C3-6})	P_5/O_5	O_5	P_5
Co/SiO_2	250	69	8	23	62	5.280	5.85	5.32	0.63	1.397	2.47	3.47
	300	43	1.3	11	75	0.509	4.00	3.95	0.79	0.699	0.37	0.26
	350	26	0	9	82	0.000	2.45	2.45	0.83	0.539	0.14	0.07
Co/TiO_2	220	25	0	9.5	85	0.000	2.21	2.21	0.81	0.743	0.06	0.04
	250	31	0	12	81	0.000	2.61	2.61	0.75	1.507	0.07	0.07
	350	72	0.9	8	89	0.588	6.19	6.13	0.84	3.738	0.03	0.12
Co/Al_2O_3	250	23	3.7	25	62	0.711	1.84	1.77	0.71	2.865	0.04	0.13
	350	42	1.5	14	77	0.522	3.54	3.48	0.75	0.623	0.17	0.11

6.3.2.2 WGS Reactivity

We studied the effect of indigenous water on the activity and selectivity of cobalt Fischer-Tropsch catalysts by varying the reduction temperature and monitoring the CO_2 selectivity. The partially reduced catalysts (at 220/250 ˚C) supported on TiO_2 were found to be inactive for the WGS reaction. This observation was made from the amount of CO_2 detected from the FT product stream, in which no CO_2 was detected for this case, see Table 6.3. The *in-situ* PXRD results indicate that the reduction of Co/TiO_2 at a low temperature (220/250 ˚C) led to a mixture of CoO and Co˚ (see Figure 6.5A) while the TPR data (Figure 6.3B & 6.3C) showed that at 220 or 250 ˚C the catalyst only consisted of CoO and residual Co_3O_4. The Co˚ might be too little to be detected via the TPR method. We performed an additional *in-situ* PXRD, where the temperature was increased gradually to 220 or 250 or 350 ˚C and kept for 6 h to determine the phase change during the reduction, the results are reported in Figure 6.10. Figure 6.10 indicate that at 220 ˚C cobalt was present as a mixture of CoO and Co_3O_4 whereas at 250 ˚C, only CoO was observed. CoO is believed to be active for WGS reaction [21,17], yet $CoO\text{-}TiO_2$ and $Co_3O_4\text{-}CoO\text{-}TiO_2$ were found to be inactive for WGS, showing a 0% selectivity of CO_2.

The following possible explanations were postulated to account for the 0% CO_2 selectivity observed over the Co/TiO_2 catalysts reduced at a low temperature: (1) the CoO might have reduced further under the syngas atmosphere to metallic Co, which is not active for the WGS reaction; (2) at low FT reaction rates or low water partial pressures, there is no WGS reaction; (3) the interaction between CoO and TiO_2 particles might be inactive for WGS and (4) CoO is active for FTS. However, comparable amounts of CO_2 were produced from the metallic Co catalyst reduced at 350 ˚C. This may be attributed to the high FT rate at high CO conversions, see Figure 6.7A, which results in a high H_2O partial pressure that may oxidise the metallic Co to CoO ($Co˚ + H_2O \rightarrow CoO$), an active phase for WGS and results in CO_2 production. Figure 6.11C indicate that an increase in the reduction temperature increases the selectivity of H_2O for TiO_2 supported catalysts, thus increasing the WGS activity as shown in Figure 6.11A. In accordance with previous studies, Wolf et al. [21] suggested that oxidised surface Co could catalyse the WGS reaction and increase the selectivity of CO_2. Others have demonstrated that high reaction rates and CO conversions increase the partial pressure of water, which results in the oxidation of Co species and an increase in the WGS activity [17,26,39,40].

While many have declared CoO inactive for FTS [19,40], the Co/SiO_2 catalyst, reduced at 250˚C, showed the highest FT activity and CO_2 selectivity compared to its metallic Co counterpart reduced at 350 ˚C, see Table 6.3. Furthermore, the CO_2 activity was also higher when the FT and H_2O reaction rate were both high (see Figure 6.7B), than at 350 ˚C. According to the previously reported data for the Co/SiO_2 catalyst, the synergistic effect of $CoO\text{-}Co\text{-}SiO_2$ catalysed the FT reaction. No WGS activity was detected for the Co/SiO_2 catalyst reduced at 350 ˚C, see Figure 6.11 A, which is attributed to higher reduction of cobalt oxides to metallic Co and to lower water partial pressures, see Figure 6.11. Similar reaction pathways were observed over the partially reduced Co/Al_2O_3 catalyst , cobalt was present as CoO after reduction and no metallic Co was detected or formed, see Figure 6.5C, yet the catalyst still produced small amounts of CO_2, at a low CO conversion (23%). These results indicate that the WGS activity is affected by the water partial pressure stipulated at higher CO conversions as well as the interaction between the cobalt oxide species and the support. In this case, it is postulated that the interaction between $Co\text{-}CoO\text{-}Al_2O_3$ promoted the WGS activity. A further increase in the reduction temperature up to 350 ˚C led to even smaller amount of CO_2 produced due to a higher conversion of CoO to metallic Co. These results provide the experimental evidence that CoO is active for both FT and WGS reaction. Taking into consideration both literature and the experimental results from this study, we can safely suggest that the WGS reaction is a function of water partial pressure at high CO conversions and the interaction between the Co and the support.

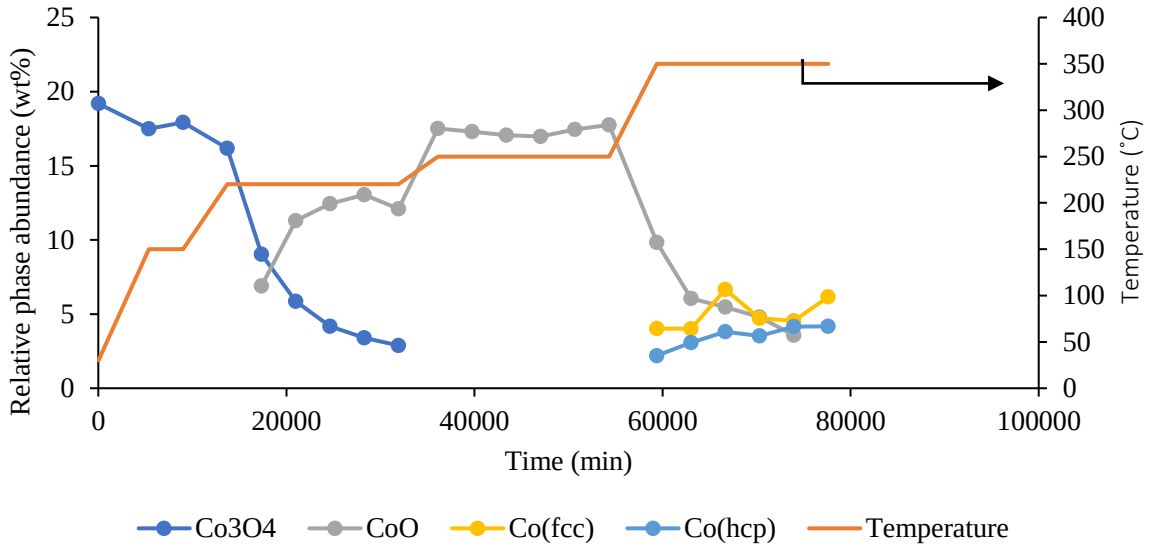

Figure 6. 10: Relative phase abundance for the crystallite phase observed during H_2 reduction of the model Co/TiO_2 catalyst with a stepwise reduction and a 6h dwelling at 220, 250 and 350 ˚C.

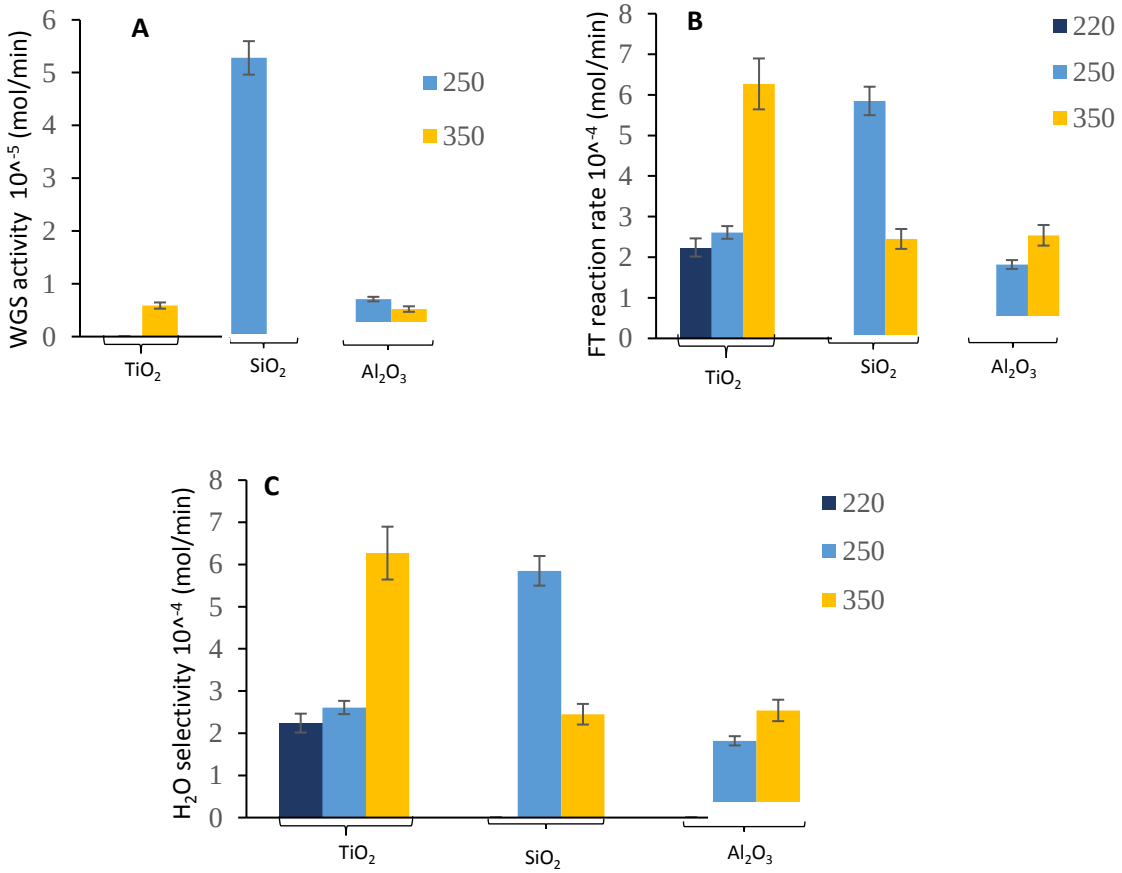

Figure 6. 11: The effect of reduction temperature on **A.** WGS activity; **B.** FT reaction rates; **C.** H_2O selectivity for Co/TiO_2, Co/SiO_2 and Co/Al_2O_3. Reaction conditions: P_{Tot} = 20 bar; T= 200-210 ˚C; H_2/CO = 2; FR = 60 Nml/min.

6.3.2.3 P/O ratio

P/O ratio is used to represent the selectivity of the paraffin (P) and olefin (O) products. A higher P/O ratio indicates a higher selectivity to paraffin products. Figure 6.12 indicate the P/O ratio for the model cobalt catalysts treated at different reduction temperatures and similar reaction conditions. For the catalyst supported on TiO_2, the P_2/O_2 ratio was significantly increased with increasing reduction temperature (Figure 6.12A1). A somewhat similar behaviour was observed for the P_5/O_5 ratio of the Co/TiO_2 catalysts, Figure 6.12A (2-3). The P_5/O_5 ratio increased with the pre-treatment temperature from 220 ˚C to 350 ˚C and the P_5/O_5 ratio was found to be more stable than the P_2/O_2 ratio, for the catalyst reduced at 350 ˚C. The decline in the P_2/O_2 ratio may be attributed to further increase in the amount of water produced in the reactor, Figure 6.7A show a gradual increase in WGS activity with TOS, which might have detrimental effect on the rate of secondary hydrogenation. Nevertheless, TiO_2 had more paraffinic products produced at a higher pre-treatment temperature than a lower activation temperature. While many studies report a positive influence of high-water partial pressures at high CO conversions on paraffinic products [11,41-42], we observed the same effect for the TiO_2-supported catalyst pre-treated at 350 ˚C. This may be due to the increase in water partial pressure (see Figure 6.12A) which enhanced the degree of secondary hydrogenation of olefins and as a result a high ratio of paraffin/olefin is observed.

The P/O ratios decreased with an increase in the reduction temperature for both SiO_2 and Al_2O_3 supported catalysts, see Figures 6.12B(1-2), and 6.12C(1-2). This suggests that the partially reduced catalyst promoted the production of the saturated hydrocarbons. Our previous finding over the partially reduced SiO_2-supported catalyst [27] suggest that the CoO-Co-support interface improved the hydrogenation of olefins to produce a higher P/O ratio. In this case, this explanation may work for the SiO_2 and Al_2O_3 supported catalysts but not for the TiO_2-supported catalyst. The TiO_2-Co-CoO interface is not active for the WGS reaction and for the secondary hydrogenation of olefins to paraffins. Another possible reason could be the low rate of secondary hydrogenation at low water partial pressures as observed in Figure 6.11A and Figure 6.11C thus resulting in low paraffin production. Storseater et al. [11] found that the degree of secondary reactions and chain termination depends on the partial pressure of water and resident time for different supports. At high CO conversions and high-water partial pressures, there is more secondary reactions of olefins [8].

The second explanation may only work for the SiO_2-supported catalyst. We assumed that the water partial pressure is lower at 350 ˚C than 250 ˚C since we observed a decrease in the WGS activity as we increase the reduction temperature for the SiO_2 catalyst, see Figure 6.11A. Therefore, we postulate that the low partial pressures of water reduced the rate of secondary reactions for the SiO_2-supported catalyst that was reduced at 350 ˚C. For the Al_2O_3-supported catalyst, Figure 6.11C shows a high-water partial pressure at 350 ˚C than at 250 ˚C, yet the sample reduced at 250 ˚C still afforded a higher P/O ratio. This can be attributed to the CoO-Co interaction with Al_2O_3 which might have promoted the hydrogenation of olefins to a certain point. Several researchers reported that P/O ratio decreases with an increase in the particle size of the Co species and increases with the CO conversion [34,41-42].

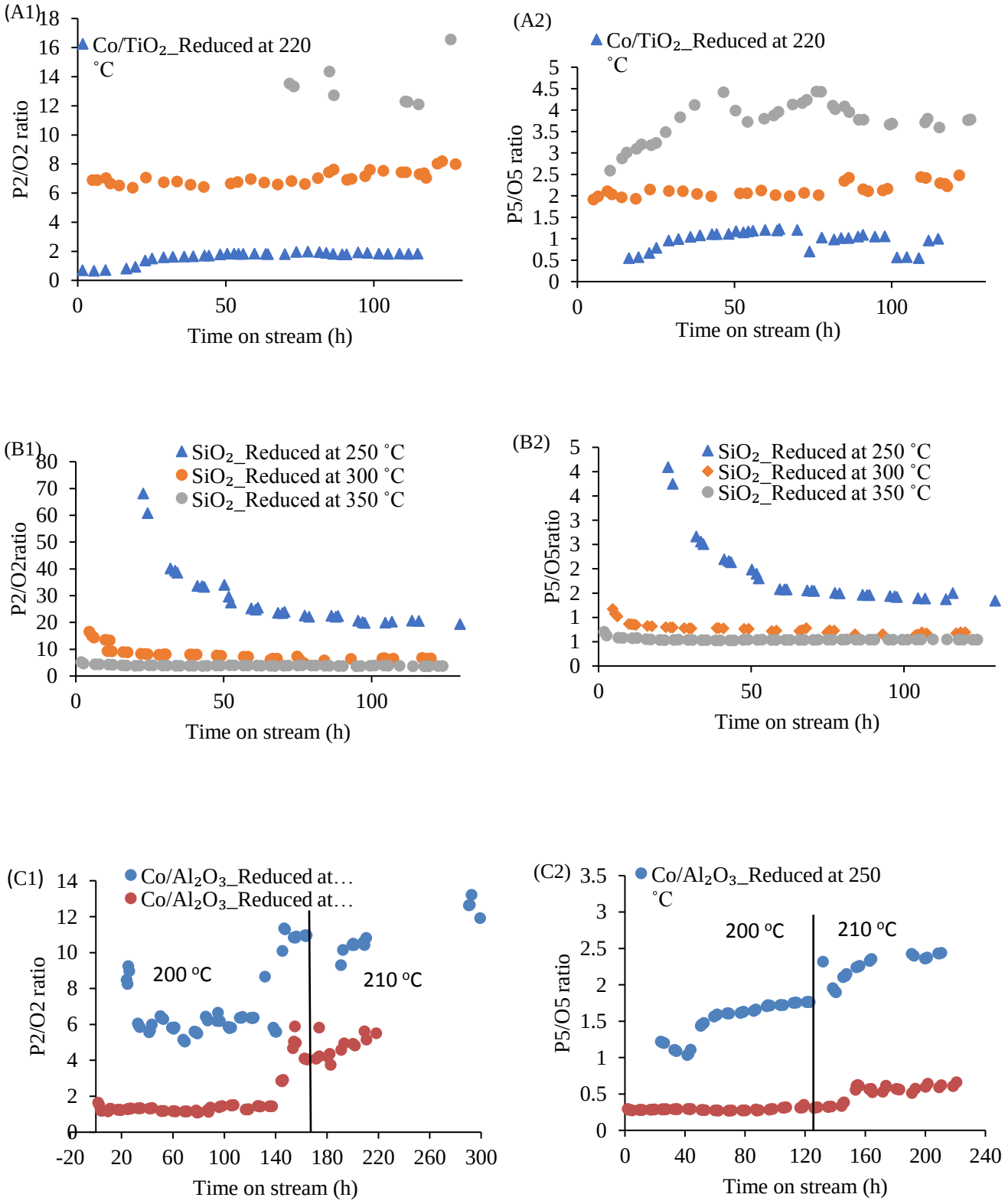

Figure 6. 12: The P/O ratio for cobalt-based catalysts A. Co/TiO_2 B. Co/SiO_2 and C. Co/ Al_2O_3, pretreated at different reduction temperatures. The legend indicates the catalyst (on different supports), and the reduction temperature (˚C). Reaction conditions: P_{Tot} = 20 bar; T= 200-210 ˚C; H_2/CO = 2; FR = 60 Nml/min.

6.4 Discussion

This section focused on the discussion of the work reported in Section 6.3.2

The Co/TiO_2 catalyst, with an average crystallite size of about 13.2 nm Co-fcc, exhibited the highest %CO conversion, C_{5+} selectivity and low CH_4 production, when reduced at 350 ˚C, compared to the SiO_2 and Al_2O_3 supported catalysts with particle sizes of about 8.7 and 21.7 nm, respectively. This may be attributed to the complete reduction of cobalt oxides to metallic Co as observed via in-situ XRD (Figure 6.5), and the higher abundance of Co(hcp), about 50%, compared to reduced SiO_2 and Al_2O_3 catalysts with only 12.2% and 7% Co(hcp), respectively see Figure 6.5. The substantial structural differences resulted in different metal distribution and FT reactivity. The Al_2O_3 and TiO_2 supports are known to exhibit numerous crystal faces, edges and corners, which might not facilitate a preferred chemical interaction with the nanoparticles, in comparison to the SiO_2 support material [12,43]. The TiO_2-support particles exhibited resembled a cubic shape, which led to a heterogeneous distribution and the formation Co_3O_4 clusters due to the numerous facets, Figure 6.3A. Therefore, at low reduction temperatures, the TiO_2 support could not form active species with the CoO and as a result, it achieved a low CO conversion, yet it afforded a high C_{5+} selectivity with minimal CH_4 production compared to the SiO_2- and Al_2O_3-supported catalysts. The Al_2O_3 supported catalyst had the least activity at all reduction temperatures, owing to the greater metal-support interactions observed via TPR and *in-situ* PXRD and irregular particle shapes, which led to an uneven distribution and low metal distribution. Furthermore, the low FT activity can be attributed to the large Co_3O_4 particle sizes that were formed due to larger pore sizes which are easy to reduce yet result in a lower active sites density.

An increase in the C_{5+} selectivity and P/O ratio at high CO conversions has been attributed to enhanced secondary reactions to olefins, for the TiO_2 catalyst. For the Co/SiO_2 catalyst reduced at 250˚C, the C_{5+} selectivity firstly increased to a maximum value then decreased gradually to reach a steady state value, Figure 6.8 A[27]. This observation was accompanied by a rapid catalyst deactivation within the first 100 h of the reaction and the C_{5+} selectivity at 250 ˚C settled at a lower value than the amount produced at 350 ˚C, when the partial pressure of water was lower. This can be attributed to the increase in the water partial pressure at high CO conversions which enhanced the secondary hydrogenation reaction, thus favoring the production of long chain hydrocarbons.

However, a further increase in the amount of water present had a detrimental effect on the C_{5+} selectivity. Previous studies have shown the extent of C_{5+} dependency on the amount of present water, that is simulated at high CO conversions [27,11,41,44]. Rytter et al. [45] reported that selectivity drops at higher CO conversions (above 80%) due to the significant increase in the hydrogen concentration from the WGS reaction. At high CO and H_2O partial pressures, Co species can easily be re-oxidised by water, and this affects the density sites available for olefin readsorption and consequently the C_{5+} selectivity [11,19].

Metallic Co is known to be the active phase for FT reaction, which converts syngas to long chain paraffin and olefins. The partial reduction of Co based FT catalysts has been reported to supress CO hydrogenation, due to the formation of intermediate CoO species, which promotes the formation of CH_4 and CO_2 via methanation and WGS reaction, respectively [20,28]. Fischer et al. [19] reported that the partial pressure of water is negligible at low CO conversions. In agreement, no WGS was observed on the TiO_2 catalyst reduced at a temperature range of 220-250 ˚C. A further increase in the reduction temperature led to the formation of significant amounts of CO_2, which suggests the presence of the CoO phase and WGS activity. The WGS activity was accompanied by an increase in the rate of secondary hydrogenation reactions and as a result, a higher P/O ratio was observed. A few publications reported the positive effect of CoO on the FT reaction with a significant WGS activity for catalyst reduced at a lower temperature [27,29]. In our previous study, it was postulated that CoO may assist to dissociate of CO and increase the rate of CO conversion to chain growth monomer thus facilitating the FT activity and hydrogenation of olefins to paraffins [27]. However, for Co/TiO_2 there was no WGS activity observed at a low temperature, which suggests that this statement may be true for the SiO_2 and Al_2O_3 supports which can form unique and active bonds with CoO. However, the Al_2O_3 supported catalyst afforded a low FT activity at a lower reduction temperature despite being able to form the active $CoO\text{-}Co\text{-}Al_2O_3$ interface. The low FT activity may be due to the low reducibility that produced very little Co which decreased the FT rate. Therefore, the extent of CoO-Co promotion may be dependent on the metal-support interactions obtained during catalyst preparation.

This study reflects on the effect of the nature of the support particles which determines the distribution of the Co metal, the interaction between the Co and support and consequently, the

catalytic activity during FTS. Furthermore, the long chain hydrocarbon reaction rate was much higher for the catalyst reduced at 350 ˚C than the one reduced at 250 ˚C, for all the catalysts. This suggests that metallic Co assist the chain growth reaction (FT reaction) to convert ($CO+H_2$) to liquid products. The FTS reaction is a stepwise chain growth reaction, firstly, on the catalyst surface, both CO and H_2 react together to convert to initiators and monomers and any factors that could assist the conversion of the initiators and the monomers will promote the chain growth reaction.

6.5 Conclusions

The effect of titania, silica and alumina support properties were investigated for FTS at different reduction temperatures (220-350 ˚C). *ex-situ* XRD diffraction patterns confirmed that cobalt is present as Co_3O_4 on the catalysts in their calcined state. The reducibility of the catalysts increased with a decreased in particle size, observed by TPR. The Co_3O_4 particles appeared in clusters on the TiO_2 support whereas Co_3O_4 existed as single crystals, spatially dispersed on the SiO_2 and Al_2O_3 supports. Larger Co_3O_4 particles were observed on the Al_2O_3 support with different substantial structural pointing out to the presence of other alumina-Co compounds such as boehmite that can be formed during calcination. The activity and selectivity data obtained showed that an increase in the reduction temperature led to a marked increase in the C_{5+} selectivity, chain growth probability and a decrease in the CH_4 selectivity, for all Co catalysts. The Co/TiO_2 catalyst exhibited the highest activity when treated at 350 ˚C due to higher reducibility, the intrinsic particle size (Co(fcc) = 8.7 nm) and high Co(hcp) abundance. No WGS activity was observed for the TiO_2 supported catalysts at a low reduction temperature. However, an increase in the reduction temperature increased the water partial pressure thus leading to the oxidation of small cobalt particles and as a result, WGS activity.

In addition, more paraffinic products were attained due to enhanced secondary hydrogenation of olefins at high water partial pressures. For alumina supported catalysts, a similar trend to the TiO_2-supported catalyst, in terms of activity and selectivity of the targeted products, was observed. However, WGS activity decreased with an increase in the reduction temperature. It is worth noting that the Al_2O_3 supported catalyst exhibited WGS activity at a low CO conversion (23%) and low reaction rates, which suggest that the WGS reaction might be a

function of water partial pressure as well as the amount of CoO present or the intimacy between the support and CoO. For the SiO_2 supported catalyst, an increase in the reduction temperature; decreased the activity of the catalyst but did not affect the selectivity. This might be attributed to the decrease in the CoO phase which formed a unique bond with the SiO_2 support and catalysed the FT reaction resulting in a higher activity of the partially reduced catalysts. Rapid catalyst deactivation was observed on the partially reduced silica supported catalysts due to extremely high-water partial pressures at high CO conversion.

6.6 Acknowledgments

The authors are grateful for the support received from the University of South Africa and the South Africa National Research Foundation (NRF UID 95445 and 117793).

6.7 References

[1] Zhang J, Chen J, Ren J, Li Y, Sun Y. Support effect of Co/Al_2O_3 catalysts for Fischer–Tropsch synthesis. Fuel. 2003; 82: 581-6. https://doi.org/10.1016/S0016-2361(02)00331-9.

[2] Jiang Y, Wang H, Li S, Yang C, Zhong L, Gao P, Sun Y. Toward a Full One-Pass Conversion for the Fischer–Tropsch Synthesis over a Highly Selective Cobalt Catalyst. Ind. & Eng. Chem. Res. 2020; 59: 8195-201. https://doi.org/10.1021/acs.iecr.0c00764.

[3] Niu C, Xia M, Chen C, Ma Z, Jia L, Hou B, Li D. Effect of process conditions on the product distribution of Fischer-Tropsch synthesis over an industrial cobalt-based catalyst using a fixed-bed reactor. Appl. Catal. A Gen. 2020; 601:117630. https://doi.org/10.1016/j.apcata.2020.117630.

[4] Savost'yanov AP, Yakovenko RE, Sulima SI, Bakun VG, Narochnyi GB, Chernyshev VM, Mitchenko SA. The impact of Al_2O_3 promoter on an efficiency of C_{5+} hydrocarbons formation over Co/SiO_2 catalysts via Fischer-Tropsch synthesis. Catal. Today. 2017; 279: 107-14. https://doi.org/10.1016/j.cattod.2016.02.037.

[5] Bartolini M, Molina J, Alvarez J, Goldwasser M, Almao PP, Zurita MJ. Effect of the porous structure of the support on hydrocarbon distribution in the Fischer–Tropsch reaction. J. Power Sourc. 2015; 285: 1-1. https://doi.org/10.1016/j.jpowsour.2015.03.081.

[6] Hodala JL, Moon DJ, Reddy KR, Reddy CV, Kumar TN, Ahamed MI, Raghu AV. Catalyst design for maximizing C_{5+} yields during Fischer-Tropsch synthesis. Int. J. Hydrogen Energy. 2021; 46(4): 3289-301. https://doi.org/10.1016/j.ijhydene.2019.12.021.

[7] Borg Ø, Blekkan EA, Eri S, Akporiaye D, Vigerust B, Rytter E, Holmen A. Effect of calcination atmosphere and temperature on γ-Al_2O_3 supported cobalt Fischer-Tropsch catalysts. Top. Catal. 2007 (1); 45: 39-43. https://doi.org/10.1007/s11244-007-0237-4.

[8] Borg Ø, Eri S, Blekkan EA, Storsæter S, Wigum H, Rytter E, Holmen A. Fischer–Tropsch synthesis over γ-alumina-supported cobalt catalysts: effect of support variables. J. Catal. 2007(2); 248: 89-100. https://doi.org/10.1016/j.jcat.2007.03.008.

[9] Trépanier M, Dalai AK, Abatzoglou N. Synthesis of CNT-supported cobalt nanoparticle catalysts using a microemulsion technique: role of nanoparticle size on reducibility, activity and selectivity in Fischer–Tropsch reactions. Appl. Catal. A Gen. 2010; 374: 79-86. https://doi.org/10.1016/j.apcata.2009.11.029

[10] Jacobs G, Das TK, Zhang Y, Li J, Racoillet G, Davis BH. Fischer–Tropsch synthesis: support, loading, and promoter effects on the reducibility of cobalt catalysts. Appl. Catal. A Gen. 2002; 233: 263-81. https://doi.org/10.1016/S0926-860X(02)00195-3.

[11] Storsæter S, Borg Ø, Blekkan EA, Holmen A. Study of the effect of water on Fischer–Tropsch synthesis over supported cobalt catalysts. J. Catal. 2005(1); 231: 405-19. https://doi.org/10.1016/j.jcat.2005.01.036.

[12] Loedolff MJ, Goh BM, Koutsantonis GA, Fuller RO. Supported heterogeneous catalysts: what controls cobalt nanoparticle dispersion on alumina. New J. Chem. 2018; 42: 14894-900. DOI: 10.1039/C8NJ03076F.

[13] Abrokwah RY, Rahman MM, Deshmane VG, Kuila D. Effect of titania support on Fischer-Tropsch synthesis using cobalt, iron, and ruthenium catalysts in silicon-microchannel microreactor. Molec. Catal. 2019; 478: 110566. https://doi.org/10.1016/j.mcat.2019.110566.

[14] Gholami Z, Tišler Z, Rubáš V. Recent advances in Fischer-Tropsch synthesis using cobalt-based catalysts: a review on supports, promoters, and reactors. Catal. Reviews. 2020: 1-84. https://doi.org/10.1080/01614940.2020.1762367.

[15] Shiba NC, Yao Y, Liu X, Hildebrandt D. Recent developments in catalyst pretreatment technologies for cobalt based Fisher–Tropsch synthesis. Rev. Chem. Eng. 2021(1); 1. https://doi.org/10.1515/revce-2020-0023.

[16] Botes FG, Niemantsverdriet JW, Van De Loosdrecht J. A comparison of cobalt and iron-based slurry phase Fischer–Tropsch synthesis. Catal. Today. 2013; 215: 112-20. https://doi.org/10.1016/j.cattod.2013.01.013.

[17] Borg Ø, Dietzel PD, Spjelkavik AI, Tveten EZ, Walmsley JC, Diplas S, Eri S, Holmen A, Rytter E. Fischer–Tropsch synthesis: Cobalt particle size and support effects on intrinsic activity and product distribution. J. Catal. 2008; 259: 161-4. https://doi.org/10.1016/j.jcat.2008.08.017.

[18] Sun X, Sartipi S, Kapteijn F, Gascon J. Effect of pretreatment atmosphere on the activity and selectivity of Co/meso HZSM-5 for Fischer–Tropsch synthesis. New J. Chem. 2016; 40: 4167-77. DOI: 10.1039/C5NJ02462E.

[19] Fischer N, Clapham B, Feltes T, Claeys M. Cobalt-based Fischer–Tropsch activity and selectivity as a function of crystallite size and water partial pressure. ACS Catal. 2015; 5: 113-21. https://doi.org/10.1021/cs500936t.

[20] Wang B, Liu S, Hu Z, Li Z, Ma X. Active phase of highly active Co_3O_4 catalyst for synthetic natural gas production. RSC adv. 2014; 4: 57185-91. DOI: 10.1039/C4RA12214C.

[21] Wolf M, Roberts SJ, Marquart W, Olivier EJ, Luchters NT, Gibson EK, Catlow CR, Neethling JH, Fischer N, Claeys M. Synthesis, characterisation and water–gas shift activity of nano-particulate mixed-metal (Al, Ti) cobalt oxides. Dalton Trans. 2019; 48: 13858-68. DOI: 10.1039/C9DT01634A.

[22] Moodley DJ. On the deactivation of cobalt-based Fischer-Tropsch synthesis catalysts. American Chemical Society, Division of Petrochemical Chemistry. 2008; 53: 122-5.

[23] Saib AM, Moodley DJ, Ciobîcă IM, Hauman MM, Sigwebela BH, Weststrate CJ, Niemantsverdriet JW, Van de Loosdrecht J. Fundamental understanding of deactivation and regeneration of cobalt Fischer–Tropsch synthesis catalysts. Catal. Today. 2010; 154: 271-82. https://doi.org/10.1016/j.cattod.2010.02.008.

[24] Iglesia E. Design, synthesis, and use of cobalt-based Fischer-Tropsch synthesis catalysts. Appl. Catal. A Gen. 1997; 161: 59-78. https://doi.org/10.1016/S0926-860X(97)00186-5.

[25] van Steen E, Claeys M, Dry ME, van de Loosdrecht J, Viljoen EL, Visagie JL. Stability of nanocrystals: thermodynamic analysis of oxidation and re-reduction of cobalt in water/hydrogen mixtures. J. Phys. Chem. B. 2005; 109: 3575-7. https://doi.org/10.1021/jp045136o.

[26] Claeys M, Dry ME, van Steen E, van Berge PJ, Booyens S, Crous R, van Helden P, Labuschagne J, Moodley DJ, Saib AM. Impact of process conditions on the sintering behavior of an alumina-supported cobalt Fischer–Tropsch catalyst studied with an in situ magnetometer. ACS Catal. 2015; 5: 841-52. https://doi.org/10.1021/cs501810y.

[27] Shiba NC, Yao Y, Forbes RP, Okoye-Chine CG, Liu X, Hildebrandt D. Role of CoO-Co nanoparticles supported on SiO_2 in Fischer-Tropsch synthesis: Evidence for enhanced CO dissociation and olefin hydrogenation. Fuel Proc. Tech. 2021(2); 216: 106781. https://doi.org/10.1016/j.fuproc.2021.106781.

[28] Tucker CL, van Steen E. Activity and selectivity of a cobalt-based Fischer-Tropsch catalyst operating at high conversion for once-through biomass-to-liquid operation. Catal. Today. 2020; 342: 115-23. https://doi.org/10.1016/j.cattod.2018.12.049.

[29] Melaet G, Ralston WT, Li CS, Alayoglu S, An K, Musselwhite N, Kalkan B, Somorjai GA. Evidence of highly active cobalt oxide catalyst for the Fischer–Tropsch synthesis and CO_2 hydrogenation. J. American Chem. Soc. 2014; 136: 2260-3. https://doi.org/10.1021/ja412447q.

[30] Storsæter S, Tøtdal B, Walmsley JC, Tanem BS, Holmen A. Characterization of alumina-, silica-, and titania-supported cobalt Fischer–Tropsch catalysts. Journal of catalysis. 2005(2); 236: 139-52. https://doi.org/10.1016/j.jcat.2005.09.021.

[31] Jacobs G, Ji Y, Davis BH, Cronauer D, Kropf AJ, Marshall CL. Fischer–Tropsch synthesis: Temperature programmed EXAFS/XANES investigation of the influence of support type, cobalt loading, and noble metal promoter addition to the reduction behavior of cobalt oxide particles. Appl. Catal. A Gen. 2007; 333: 177-91. https://doi.org/10.1016/j.apcata.2007.07.027.

[32] Prieto G, Martínez A, Concepción P, Moreno-Tost R. Cobalt particle size effects in Fischer–Tropsch synthesis: structural and in situ spectroscopic characterisation on reverse micelle-synthesised Co/ITQ-2 model catalysts. J. Catal. 2009; 266: 129-44. https://doi.org/10.1016/j.jcat.2009.06.001.

[33] Ghampson IT, Newman C, Kong L, Pier E, Hurley KD, Pollock RA, Walsh BR, Goundie B, Wright J, Wheeler MC, Meulenberg RW. Effects of pore diameter on particle size, phase, and turnover frequency in mesoporous silica supported cobalt Fischer–Tropsch catalysts. Appl. Catal. A Gen. 2010; 388: 57-67. https://doi.org/10.1016/j.apcata.2010.08.028.

[34] Park JY, Lee YJ, Karandikar PR, Jun KW, Ha KS, Park HG. Fischer-Tropsch catalysts deposited with size-controlled Co3O4 nanocrystals: Effect of Co particle size on catalytic activity and stability. Appl. Catal. A Gen. 2012; 411: 15-23. https://doi.org/10.1016/j.apcata.2011.10.010.

[35] Luo M, Hamdeh H, Davis BH. Fischer-Tropsch Synthesis: Catalyst activation of low alpha iron catalyst. Catal. Today. 2009; 140: 127-34. https://doi.org/10.1016/j.cattod.2008.10.004.

[36] Bian G, Mochizuki T, Fujishita N, Nomoto H, Yamada M. Activation and catalytic behavior of several Co/SiO_2 catalysts for Fischer− Tropsch synthesis. Energy & fuels. 2003; 17: 799-803. https://doi.org/10.1021/ef020236j.

[37] Li J, Xu L, Keogh R, Davis B. Fischer–Tropsch synthesis. Effect of CO pretreatment on a ruthenium promoted Co/TiO_2. Catal. Lett. 2000; 70: 127-30. https://doi.org/10.1023/A:1018833217001.

[38] Xiong H, Zhang Y, Liew K, Li J. Fischer–Tropsch synthesis: the role of pore size for Co/SBA-15 catalysts. J. Molec. Catal. A Chem. 2008; 295: 68-76. https://doi.org/10.1016/j.molcata.2008.08.017.

[39] Jalama K, Kabuba J, Xiong H, Jewell LL. Co/TiO_2 Fischer–Tropsch catalyst activation by synthesis gas. Catal. Commun. 2012; 17: 154-9. https://doi.org/10.1016/j.catcom.2011.10.029.

[40] Ma W, Jacobs G, Ji Y, Bhatelia T, Bukur DB, Khalid S, Davis BH. Fischer–Tropsch synthesis: influence of CO conversion on selectivities, H_2/CO usage ratios, and catalyst stability for a Ru promoted Co/Al_2O_3 catalyst using a slurry phase reactor. Topics Catal. 2011; 54: 757. https://doi.org/10.1007/s11244-011-9699-5.

[41] Bezemer GL, Radstake PB, Koot V, Van Dillen AJ, Geus JW, De Jong KP. Preparation of Fischer–Tropsch cobalt catalysts supported on carbon nanofibers and silica using homogeneous deposition-precipitation. J. Catal. 2006; 237: 291-302. https://doi.org/10.1016/j.jcat.2005.11.015.

[42] Liu JX, Su HY, Sun DP, Zhang BY, Li WX. Crystallographic dependence of CO activation on cobalt catalysts: HCP versus FCC. J. American Chem. Soc. 2013; 135: 16284-7. https://doi.org/10.1021/ja408521w.

[43] Borg Ø, Eri S, Blekkan EA, Storsæter S, Wigum H, Rytter E, Holmen A. Fischer-Tropsch synthesis over γ-alumina-supported cobalt catalysts: effect of support variables. J. Catal. 2007; 248: 89-100. https://doi.org/10.1016/j.jcat.2007.03.008.

[44] Bertole CJ, Mims CA, Kiss G. The effect of water on the cobalt-catalyzed Fischer-Tropsch synthesis. J. Catal. 2002; 210: 84-96. https://doi.org/10.1006/jcat.2002.3666.

[45] Rytter E, Borg Ø, Tsakoumis NE, Holmen A. Water as key to activity and selectivity in Co Fischer-Tropsch synthesis: γ-alumina based structure-performance relationships. J. Catal. 2018; 365: 334-43. https://doi.org/10.1016/j.jcat.2018.07.003.

CHAPTER 7: THE EFFECT OF ACTIVATION ATMOSPHERES ON THE PRODUCTION OF SYNTHETIC FUEL FROM FISCHER-TROPSCH SYNTHESIS OVER CO/SiO_2 AND $CO\text{-}RU/SiO_2$ CATALYSTS

This work has been prepared in a form of a paper for future publication in a journal.

Abstract

Syngas activation improved the selectivity of C_{5+} hydrocarbons and supressed the CH_4 formation for the Ru-promoted Co/SiO_2 catalyst. We present evidence of strong Co_2C fractions over the syngas reduced catalyst. It is postulated that the Co_2C transforms to Co(hcp) and enhances the production of long-chain hydrocarbons. Ru addition increased the degree of reduction remarkably which improved the %CO conversion for the H_2-treated catalyst. However, it also introduced excess H_2 on the catalyst surface which is detriment to the chain growth reaction and C_{5+} hydrocarbon selectivity. For the unpromoted catalysts, it was observed that syngas activation at 250 ˚C (1) gradually increases in the CO conversion due to further reduction of Co species under the syngas environment; (2) promoted the formation of paraffinic products; (3) led to higher CH_4 selectivity. Syngas reduction has the potential to eliminate the high costs H_2 reduction step, especially for small-scale FT plants. The catalyst pre-treated by hydrogenation-carburisation-hydrogenation (H-C-H) improved the %CO conversion by 40%.

7.1 Introduction

Many investigations are ongoing to test the suitability of syngas as a reducing agent for Fischer Tropsch synthesis (FTS) using traditionally employed catalysts [1-4]. The choice of catalyst for FTS is normally restricted to cobalt (Co) and iron (Fe) as they provide the best compromise between price and performance [5-6]. The use of CO and syngas as reducing agents has received much attention in Fe-based FTS, where they have been shown to enhance the catalytic activity by promoting the formation of iron carbides, which are believed to be the active phase [7-10]. Little attention has been paid to the effect of CO and syngas reduction on cobalt-based catalysts. Syngas/CO reduction is reported to promote the formation of cobalt carbides, which are believed to be inactive for FTS unlike iron carbides, thereby rendering these gases inefficient for the reduction of Co_3O_4 to active FTS catalysts [11-13]. However, positive effects on FT activity have been reported by de la Pena O'Shea et al. [14] who found the activity of a syngas-reduced Co/SiO_2 catalyst to be five times higher than that of an H_2-activated catalyst. Reduction was carried out at 500 °C for 2 hours for each reducing agent. Jalama et al. [4] reported higher catalyst activity and lower methane selectivity for a Co/TiO_2 catalyst reduced in syngas at temperatures between 250-400 ˚C compared to when reduced in H_2. This result was ascribed to the presence of CO in the reducing gas, which helped prevent the formation of Co-support compounds. The carbides formed during reduction were subsequently reduced to metallic Co(hcp) during reaction.

In contrast, Dai et al. [11] reported a decline in the activity of a syngas reduced Co/Al_2O_3 catalyst compared to H_2 reduction at 483 °C for 6.5 hours. This was attributed to the formation of inactive cobalt carbides and sintering of the metal particles. A few reports on activation with either syngas or CO-containing gas indicate high methane selectivity, which is related to the surface carbide phases formed under the syngas reduction atmosphere [12-15]. Nevertheless, cobalt carbide is reported to transform back to metallic Co(hcp) under an H_2 treatment at low temperatures [15-17,18-19], thus resulting in catalyst activity. These studies indicated that the consensus in the literature concerning the use of syngas as a reducing agent, is that the operating conditions or the gas composition affect the catalyst performance. The micro-environment conditions can significantly change the catalyst structure and a slight change in the structure of the catalyst could profoundly influence the catalytic performance. The best conditions for syngas reduction in Co-based FTS are still being investigated.

FTS is known to be a surface-catalysed and structure sensitive reaction. Its activity depends upon the metal particle size, metal structure, metal-support interaction, degree of reduction and dispersion [20-23]. The existence of metal-support interactions makes it difficult to precisely control the final structure of the surface-active component. The Co hexagonal closed packed(hcp) crystallographic structure has a high intrinsic activity for FTS compared to the face centred cubic(fcc) structure [24]. Therefore, it is of primary importance to disperse Co(hcp) on the support material to achieve better catalyst performance. The use of noble metal promoters, such as Ru and Pt, stimulates the formation of metallic Co by; (1) increasing the reducibility of the catalyst; (2) reducing metal-support interaction and (3) controlling the particle size by preventing agglomeration of the Co crystallites [25-29].

Noble metal-promoted catalysts typically exhibit a high Co site density and consequently, higher FTS rates and C_{5+} selectivity compared to unpromoted catalysts. The improved reducibility is ascribed to either the intimate contact between Co atoms and the noble metal or the supply of H_2 species spilled over from the more reducible noble metal to nearby Co oxides [29-32]. Iglesia and co-workers [33] reported a 3-fold increase in TOF and C_{5+} selectivity with the addition of small concentrations of Ru (<0.008) to Co/TiO_2. The increase in C_{5+} selectivity was ascribed to higher Co° site density, which promoted the re-absorption of α-olefins for further growth in hydrocarbon chain. Furthermore, the improved activity was ascribed to the synergy between Ru and Co atoms, with Ru atoms facilitating the removal of surface carbon and oxygen species on the surface of Co crystallites, thus preventing premature deactivation [33]. Hong et al. [31] also attributed the increase in the activity of a $0.2\%Ru\text{-}Co/SiO_2$ catalyst to the formation of bimetallic Co-Ru nanoparticles.

The success of an FTS process via the conversion of syngas depends on the ability of the catalyst to supress methane (CH_4) and carbon dioxide (CO_2) formation, while producing high fractions of C_{5+} hydrocarbons, olefins, or alcohols. The reduction atmosphere and operating conditions seems to be the major key to successfully reducing Co_3O_4 to metallic Co. In this paper, we demonstrate the effect of syngas reduction on the activity and selectivity of a Co/SiO_2 catalyst. We present evidence of Co_2C formation during syngas treatment and its transformation to Co(hcp) during reaction. Furthermore, since noble metals are costly, their speciation and chemical interaction with the base metal have seldom been studies in detail. We investigate the effect on FT activity of adding small quantities of Ru to the catalyst for different

syngas activation conditions. We demonstrate that the presence of Ru supresses the formation of CH_4 and improves the C_{5+} selectivity, for the syngas-reduced catalyst. The use of syngas as both reducing and reaction gas could potentially cut down the operating and start-up costs of a small-scale FTS plant, as syngas is readily available and can be obtained from renewable and cheap feedstock such as biomass. The capital costs of the FT plant would be considerably decreased if an H_2 plant is not needed for reduction, furthermore start-up would be simplified by using the same gas for reduction and reaction.

7.2 Experimental

7.2.1 Catalyst preparation

All the materials (SiO_2, Ru, Co (II) nitrate) were obtained from Sigma Aldrich. The catalysts were prepared using the incipient wetness impregnation technique where the support was mixed with an aqueous solution of $Co(NO_3)_2.6H_2O$ of an appropriate concentration to yield 15 wt% Co on a dry basis. For the Ru-promoted catalyst, co-impregnation was performed, where an aqueous solution of the Ru was impregnated in the support followed by an aqueous solution of the cobalt nitrate into the support containing Ru. All impregnates were dried at room temperature overnight followed by drying at 40 ˚C for 3h. Subsequently, the catalysts were dried at 110 °C for 6 h, to ensure the removal of any absorbed water, as per procedure described by Kababji et al. [34]. Lastly, the catalysts were calcined under flowing air at 350 °C for 8 h, in order to decompose the cobalt nitrate to cobalt oxide.

7.2.2 Catalyst characterisation

Specific surface areas of the catalyst were calculated by applying the Brunauer-Emmett-Teller (BET) method, measured at liquid nitrogen temperature using a Micrometrics Trista 3000 analyser. Samples were prepared prior to measurement by degassing them at 190 ˚C for 8h. The pore size distributions for each sample were evaluated from the desorption branches on the isotherms using the Barrett-Joyner-Halenda (BJH) method and the total pore volume was determined at a relative pressure of 0.99.

Temperature-programmed reduction (TPR) experiments were carried out in a Micrometrics 3000 apparatus by passing a mixture of 5 vol% H_2 in Ar through a 500 mg sample. The temperature was increased to 900 ˚C at a rate of 10 ˚C/min and the mount of H_2 consumed was determined using a TCD by passing the effluent gas through a cold trap in order to remove water from the exit stream. X-ray diffraction (XRD) patterns were obtained using a Phillips X'Pert Pro X-ray Diffractometer equipped with a monochromated CuKα X-ray source, flat plate geometry sample stage and pixel detector. To identify the crystalline phases present, the samples were scanned in the 2θ range from 20-80 ˚at a scan speed of 0.2 s/step. The mean crystallite size was estimated from the full width at half maxima of the diffraction peak using the Scherrer equation.

X-ray fluorescence (XRF) was used to measure the quantity of cobalt present in the fresh catalyst. The sample was first prepared by loading it into the pelletiser and pressurised to 10 KPa for a few minutes. The sample pellet was then placed in the XRF machine sample holder for analysis.

Transmission Electron Microscopy (TEM) was used to determine the distribution and morphology of cobalt atoms in each of the catalysts. TEM was performed using a JEOL 2010F instrument operating at 200 KV. Non-reduced catalyst particles were embedded in a resin and slices of nominal 50 nm thickness were prepared and used for the TEM measurement.

The in-situ powder X-ray diffraction (PXRD) measurements were carried out using an Anton-Paar XRK900 furnace under a flowing H_2 atmosphere (HP, 1 atm). The temperature was increased from 30 °C to 450 °C at a rate of 18 °C/min. For all PXRD data, the crystalline phase identification was done using DIFFRAC.EVA (Version 2. Release 2014) using the ICDD PDF2 database (Release 2016). Phase quantification was done using the Rietveld method as implemented in Bruker AXS TOPAS software (Version 5, 2014). Data collection was measured every 20˚ for every 2 hours of the isotherm at 450 °C.

X-ray photoelectron spectroscopy (XPS) was carried out in a custom built ultra-high vacuum(UHV) chamber with a base pressure of 1.5×10^{-10} Torr. The chamber was equipped with an Omicron EA 125 hemispherical electron energy analyser and a dual anode X-ray source. The MgK emission line (1253.6 eV) was used for XPS data acquisition, and the combined resolution of the X-ray/hemispherical energy analyser was 300 meV. The sample

was grounded and exposed to a 400-eV electron beam to avoid spurious charging. The chamber was also equipped with leak valves for gas (H_2) admission. A boron nitride heater was utilized to heat the sample in-situ and an optical pyrometer was used to monitor the sample remotely. In situ reduction consisted of timed exposures of the sample to 1.0×10^{-6} Torr of H_2 at 385◦Cand XPS spectra acquired after each exposure. The photoelectron binding energy was referenced to the C1s peak (284.7 eV) of adventitious carbon. The spectra were fitted using Igor Pro v6 (Wave Metrics)software using a Shirley background and Voigt functions. The same full width at half maximum (FWHM) was used for the two Co2p spins.

7.2.3 Catalyst activation

A fixed bed reactor was used in this work (inner diameter: 8mm). One gram of catalyst was loaded into the reactor for each experimental run. The catalysts were reduced to convert the cobalt oxide to the active species, such as Co^0 (metallic cobalt). In the current research three different reduction procedures were conducted for both the Co/SiO_2 and $Co/Ru/SiO_2$ catalysts:

(1) H_2 reduction: The samples (1 g of catalyst), reduced in-situ in pure H_2 at atmospheric pressure at a flowrate of 60 Nml/min. Reduction of the catalysts was done at a temperature of 350 °C. The reactor was maintained at the reduction temperature for 16 h.

(2) Syngas reduction: The catalyst was reduced using the same syngas ($60\%H_2/30\%CO/10\%N_2$) used for FTS at atmospheric pressure, a temperature range of 250 - 350 °C and flowrate of 60 Nml/min for 16 h.

(3) Hydrogenation-carburisation-hydrogenation (H-C-H) reduction: This reduction method was only conducted on the unpromoted Co/SiO_2 catalyst. The catalyst was firstly reduced in H_2 at 350 °C for 24 h, and then reduced in CO at 250 °C for 24 h, and lastly reduced in H_2 at 350 °C for 24 h. The flowrate of the gas (H_2 or CO) was set at 60 Nml/min at atmospheric pressure.

7.2.4 Catalyst testing

After the reduction step, the reactor was left to cool down to 180 °C. Thereafter, a typical FTS feed gas stream was introduced into the reactor, comprising 60 mol% H_2 and 30 mol% CO (H_2:CO ratio = 2:1) balanced in N_2, and flowing at 60 Nml/min. The pressure in the reactor was gradually increased to 20 bar, and thereafter the temperature of the reactor was also increased to the reaction temperature. Similar FTS conditions were used for all catalysts. The product analysis was conducted using an online Agilent gas chromatograph (GC). The gases were all supplied by African Oxygen (AFROX Ltd).

Table 7. 1*:* Catalyst reduction and reaction conditions for promoted and unpromoted Co/SiO_2 catalysts.

Catalyst	Reduction conditions					Reaction conditions				
	Agent	T °C	P Bar	FR Nml/min	Time H	Syngas	T °C	P bar	FR Nml/min	TOS h
15%Co/SiO_2	H_2	250	1	60	16	60%H_2/30%CO/10%N_2	210	20	60	0-128
	Syngas	250			16					0-130
		300								0-132
		350								0-122
	H_2-CO-H_2	350-250-350			H_2 for 24 h, CO for 24h, H_2 for 24 h.					0-131
15%Co-0.25%Ru/SiO_2	H_2	350	1	60	16	60%H_2/30%CO/10%N_2	210	20	60	0-124
	Syngas	350								0-127

7.3 Results and Discussions

7.3.1 Catalyst characterisation

The BET surface area and the average pore sizes for the catalysts are listed in Table 7.2. The mesoporous structure of the SiO_2 support was retained upon Co impregnation and it displayed

a large specific surface area, due to a smaller average pore size of about 6.78 nm. After impregnation, of the Ru catalyst, both the BET surface area and pore volume decreased significantly. The drop in the surface area could be due to pore filling with cobalt oxide crystallites or the effect of silica dilution due to the presence of cobalt oxide. However, the magnitude of the drop in surface area suggests that pore filling contributes more to the decrease in surface area than dilution. The pore volume decreased from 0.8 to 0.7 cm^3/g, which suggests that Co was deposited inside the pores. The same silica support was used to prepare both catalysts, however, modification of the catalyst with Ru broadened the pore size of the silica support significantly.

Table 7. 2: Physical properties for the unpromoted and Ru-promoted Co/SiO_2 catalysts

Catalyst	SiO_2 support	15% Co/SiO_2	15% Co-Ru/SiO_2
Catalyst BET pore size (nm)	6.8	6.2	7.7
Catalyst BET pore volume (cm^3/g)	0.8	0.7	0.7
Catalyst BET surface area (nm)	456.5	407.0	357.0
TEM average particle size (nm)	/	26.0	/
XRD crystalize size (nm)	/	17.0	26.0
XRD *d(Co˚) size (nm)	/	12.8	19.5
XRD dispersion (%)		7.5	4.9
XRF Co and Ru content (%) respectively		Co: 14.5 Ru: 0	Co: 15.1 Ru: 0.25
Reactor		Fixed bed reactor	
Reactor diameter (mm)	0.8	0.8	0.8
Catalyst weight loaded into the reactor (g)	1	1	1

*d(Co˚) = 0.75 x d(Co_3O_4)

The XRD patterns for the calcined and spent Co/SiO_2 and Co-Ru/SiO_2 catalysts are presented in Figure 7.1. For the calcined catalysts: (1) XRD characteristics of Co_3O_4 were hardly detected over the Co/SiO_2 catalyst, the Co/SiO_2 diffractogram presented extremely broad features, which suggests that the silica contained small Co_3O_4 nanoparticles and that the support is amorphous; (2) the addition of Ru increased the intensity of the Co_3O_4 peaks considerably on the silica support; (3) the Co_3O_4 crystallite size over the calcined Co/SiO_2 and Co-Ru/SiO_2 catalysts was about 17.0 nm and 26.0 nm, respectively, according to the Scherrer equation and

its metallic cobalt particle size estimated from $d(Co^{\circ}) = 0.75 \times d(Co_3O_4)$, was about 12.8 and 19.5 nm, respectively, see Table 7.2.

For the spent catalysts, the XRD patterns showed significant differences for different reducing temperatures and reducing agents. For the syngas-treated catalysts: (1) intense peaks located at 21.5˚ and 23.8˚ (marked by open kites) were clearly observed except for the Co/SiO_2 catalyst treated at 250 ˚C, these new characteristic peaks were assigned to deposited paraffinic wax ($(CH_2)_x$), as previously reported by Lin et al. [32]; (2) it should be noted that the appearance of these peaks differs with the reduction temperature from 250 ˚C to 350 ˚C, for the Co/SiO_2 catalyst, the Co/SiO_2-250 catalyst showed a weaker and broader peak around this area, which suggests that there is a lower paraffin deposition content than at 350 ˚C; (3) The Ru-promoted catalyst presented a third peak (Figure 7.1 B, marked by a black kite on the red graph) which is assigned to more $(CH_2)_x$ products; (4) all syngas treated samples presented additional new diffraction peaks around 37.0˚, 42.3˚ and 62.0˚C assigned to Co_2C diffraction (marked by black stars). The spent catalyst reduced at 250 ˚C showed stronger diffractions for Co_2C, indicating that more Co was transformed into Co_2C during syngas reduction at 250 ˚C than at 350 ˚C. The intensity of the diffraction peaks for Co_2C were even weaker for spent $Co\text{-}Ru/SiO_2$ than for spent Co/SiO_2, which suggests that the addition of Ru and higher temperatures supresses the formation of cobalt carbides.

For H_2 treated catalysts: similar $(CH_2)_x$ diffractions were observed, located at 21.5˚ and 23.8˚. However, the XRD-H_2 diffractions did not exhibit Co_2C formation, which suggests that the H_2/CO treatment following a high temperature reduction in H_2 is unfavourable for the carburisation of Co.

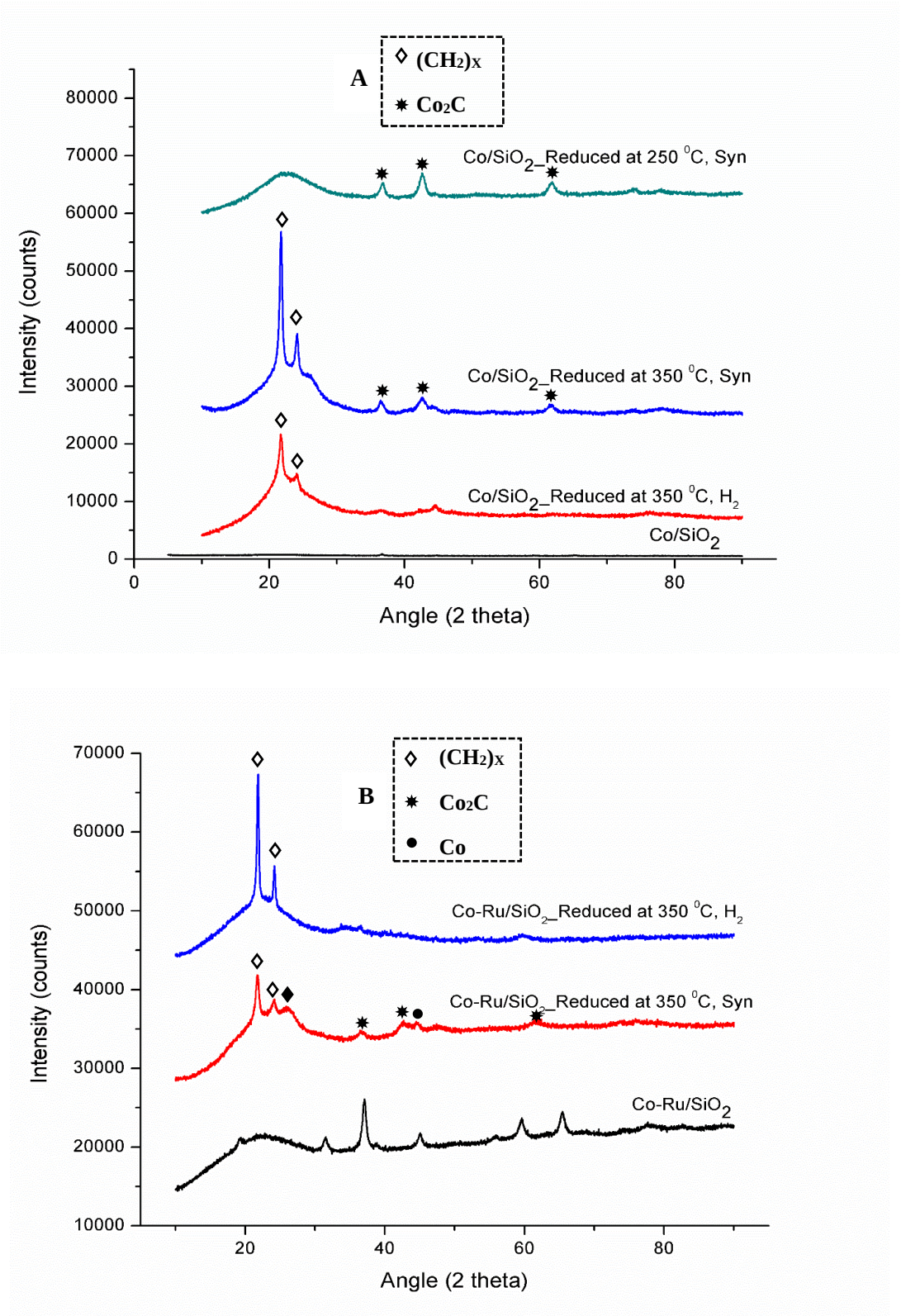

Figure 7. 1: XRD patterns for fresh and spent A. SiO_2 support B. Co/SiO_2 catalyst and C. $Co\text{-}Ru/SiO_2$ catalysts at different pre-treatment temperatures, reduced in either H_2 or syngas.

The effect of ruthenium addition on cobalt catalysts could be seen in the TPR profiles presented in Figure 7.2. The occurrence of multiple reduction peaks in both samples indicated the presence of several reducible cobalt species. The TPR profiles consisted of a two-step reduction of Co_3O_4 species ($Co_3O_4 \rightarrow CoO \rightarrow Co°$) in the temperature range 150-400 ˚C. The broad peak located at temperatures higher than 350 ˚C was assigned to the reduction of cobalt oxide species (Co^{2+}, Co^{3+}) which are interacting with the support. The TPR peaks of the Ru-promoted catalyst emerged earlier than the peaks of the monometallic catalyst, which indicated that the reducibility of Co_3O_4 species was significantly changed by the addition of Ru. Ru shifted the reduction temperature 50˚C lower, increasing the amount of Co species that could be reduced. The degree of cobalt reduction and mean particle size increased with an increase in the pore diameter of the silica support.

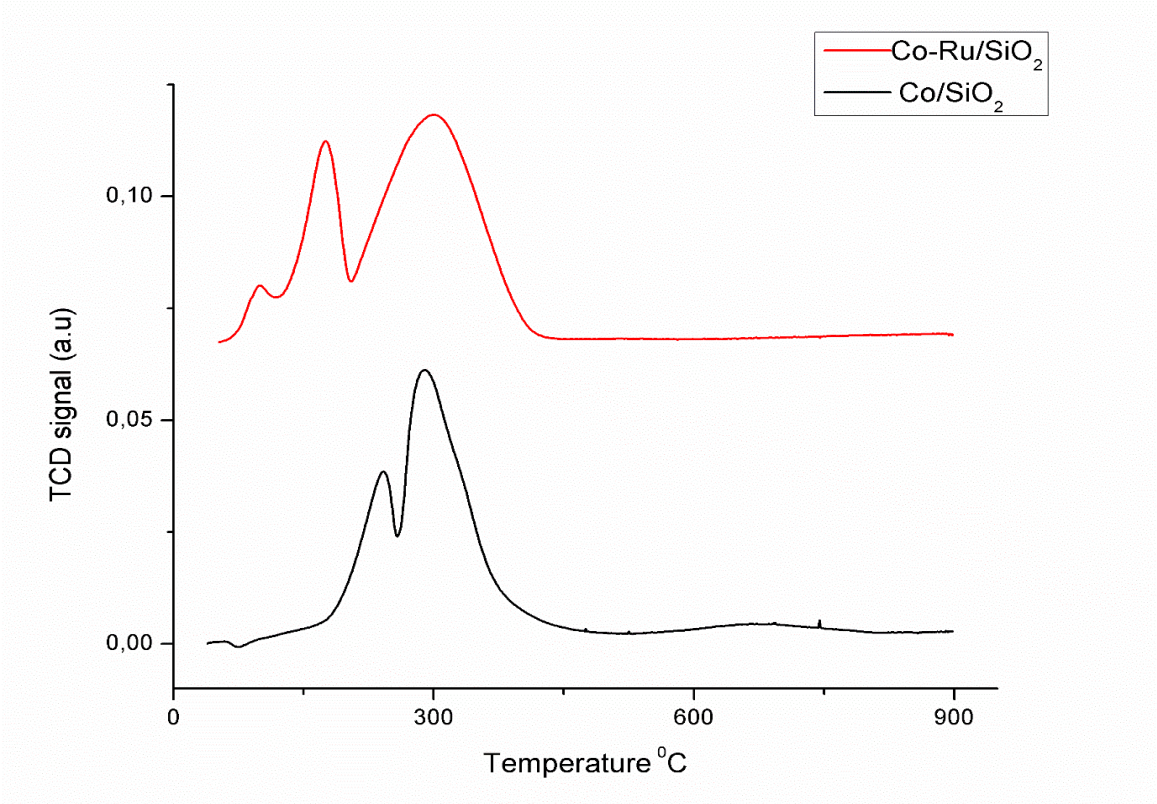

Figure 7. 2: TPR profiles for Co/SiO_2 (black line) and $Co\text{-}Ru/SiO_2$ (red line) catalysts

The TEM study of fresh and spent Co/SiO_2 catalysts showed good contrast between Co_3O_4 particles and silica, see Figure 7.3. Co_3O_4 particles exhibited a nearly spherical shape. The Co_3O_4 particles appears to be spatially dispersed on the unpromoted SiO_2 support, Figure 7.3A.

The Co particles seem to be much more dispersed in Figure 7.3B, which suggests that the number of Co particles deposited on the catalyst surface increased with Ru addition. Our findings are in line with Ma et al. [30] who reported that the addition of Ru, Re, Pd and Pt promoters to a Co/Al_2O_3 catalyst led to a higher Co dispersion compared to unpromoted catalysts.

Figure 7.3C and Figure 7.3D show the TEM images for spent $Co\text{-}Ru/SiO_2$ catalysts activated in syngas and H_2, respectively. The syngas activated catalysts show substantial structural differences with respect to the unreduced samples. The catalyst appears to have formed filamentous structures, which demonstrates the presence of other phases such as carbon nanoparticles that could have been deposited during the reduction or reaction. The H_2 reduced sample, Figure 7.3D, also shows a spatial Co clusters distributed on the SiO_2 support with a much lower Co distribution compared to the fresh catalyst.

The dispersion seems to be higher on the syngas-treated sample compared to the H_2 activated catalyst after the FT reaction. The cobalt reduction may be favoured by the presence of H_2 in the syngas and the formation of carbon nanostructures, which inhibit sintering and promote re-dispersion of Co particles. This is in line with the findings reported by de la Pena O'shea et al. [17]. They reported an increase in the number of Co active sites for samples activated in a syngas mixture compared to that activated in H_2, which led to a higher catalytic activity in FTS. In a newer study, de la Pena O'shea [35] reported the formation of carbon nanostructures under syngas activation, which prevented sintering of Co particles, thereby favouring their dispersion.

In addition, metal dispersion was calculated using the Co average particle size for the fresh catalyst and the results are reported in Table 7.2. The Ru-promoted catalyst exhibited a lower Co dispersion compared to the unpromoted catalyst, due to larger Co_3O_4 particles deposited on the support. In contrast, the TEM data indicated denser Co sites over the promoted catalyst compared to the catalyst without Ru. Furthermore, XRF analysis showed a Co loading of about 15 wt% for both catalysts as determined theoretically during preparation, see Table 7.2.

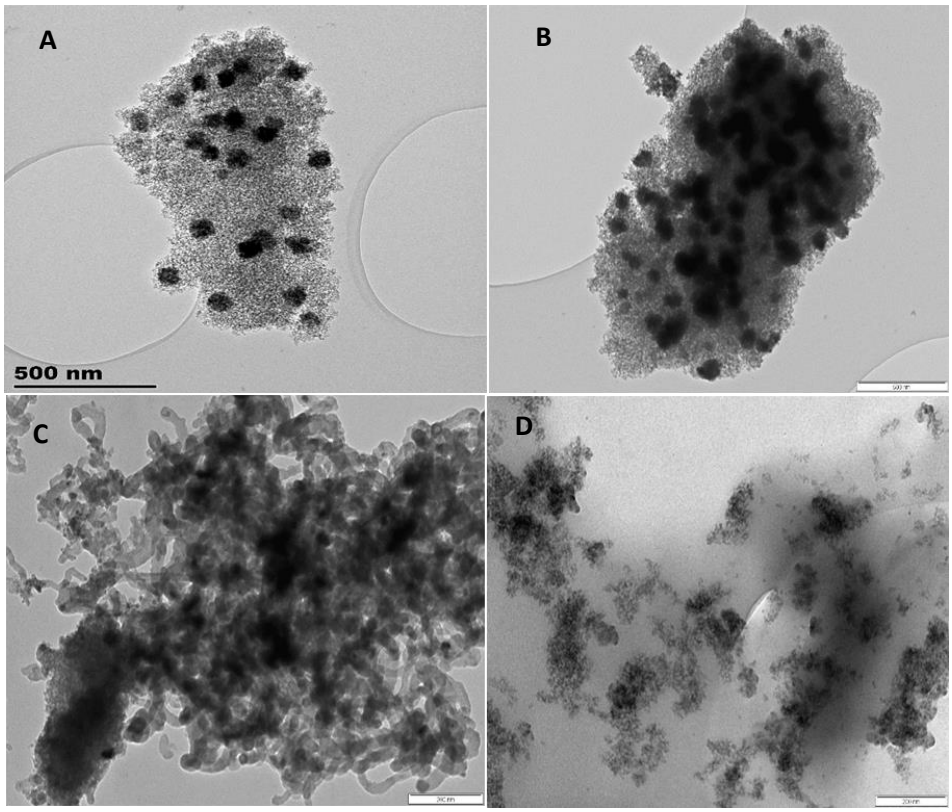

Figure 7. 3: TEM images for the fresh and spent catalysts A. fresh Co/SiO_2 sample B. fresh $Co-Ru/SiO_2$ sample C. spent $Co-Ru/SiO_2$ reduced in syngas at 350 ˚C D. spent $Co-Ru/SiO_2$ sample reduced in H_2 at 350 ˚C

Table 7. 3: XPS analysis for the unpromoted and Ru-promoted Co/SiO_2 catalysts

Catalyst	Co/SiO_2	$Co-Ru/SiO_2$	Co/SiO_2 250 ˚C		$Co-Ru/SiO_2$	Co/SiO_2	$Co-Ru/SiO_2$	Co/SiO_2
Treatment	Calcined		H_2	Syngas	H_2: 350 ˚C		Syngas: 350 ˚C	
Co2p3 Binding energy (eV)	781.2	780.8	781.8	780.9	781.1	781.0	781.2	782.3
Si2p atomic %	30.6	29.6	22.0	2.5	8.3	8.6	12.6	10.1
C1s atomic %	4.8	4.6	31.3	87.6	71.6	73.2	54.5	64.9

Table 7.3 summarises the XPS results obtained from the silica supported cobalt catalysts and their ruthenium promoted counterparts after calcination and after reaction, reduced at different temperatures in either H_2 or syngas. For the unpromoted catalysts (Co/SiO_2): (1) we observed an increase in the binding energy (BE) of the Co2p3 orbital from 781.2 to 781.8, 782.3 for the catalysts reduced at 250 ˚C in H_2 and 350 ˚C in syngas, respectively, and a decrease from 781.2 to 780.9 and 781.0 for the catalysts reduced at 250 ˚C in syngas and 350 ˚C in H_2, respectively. This suggests that stronger Co-support interactions will be present for the catalysts reduced at 250 ˚C in H_2 and at 350 ˚C in syngas than for their reduced counterparts in either H_2 or syngas; (2) we also observed a decrease in the Si2p atomic weight percent, for all the catalysts, which indicates that there is a lower probability to form Co silicates species on the catalyst surface; (3) also an increase in the atomic C1s percentage, with an extremely large amount of C1s found for the syngas-reduced catalyst at 250 ˚C, which indicates the likelihood to form cobalt carbide species. These results are in line with the findings of the XRD data (Figure 7.1A), whereby more intense Co_2C peaks were observed over the syngas-treated sample at 250 ˚C compared to 350 ˚C.

For the Ru-promoted catalysts: (1) the addition of Ru slightly shifted the binding energy (BE) of the Co2p3 orbital towards higher energies, see Table 7.3, at all reduction temperatures, and this could be taken as evidence of a strong interaction between the Co species on the surface and the support, however, the Si2p orbital atomic percentage significantly decreased for all the catalysts which suggests that Co silicates are less likely to be formed from these catalysts, with the lowest possibility being for the catalyst treated in H_2; (2) Additionally, we observed an increase in the C1s orbital atomic percentage from 4.6%, 54.5% and 71.6% for the $CoRu/SiO_2$, $Co\text{-}Ru/SiO_2$ treated in H_2 and the $Co\text{-}Ru/SiO_2$ treated in syngas catalysts, respectively. This suggests that the $Co\text{-}Ru/SiO_2$ catalyst treated in syngas at 350 ˚C would most likely form Co carbide species compared to the catalysts reduced in H_2. These results are in line with the XRD data, Figure 7.1B, which indicated the presence of cobalt carbide species in all the syngas treated samples.

In addition, the catalyst reduced in syngas, treated at 250˚C, exhibit the highest binding energy of all the catalysts, both the unpromoted and promoted catalysts. The catalyst reduced in syngas

at 350 ˚C showed a higher binding energy compared to its H_2-reduced counterpart, see Figure 7.4. Almost similar binding energies were obtained for the Co/SiO_2 catalysts treated at 350 ˚C. It can therefore be deduced that syngas activation promotes strong metal-support interactions compared to H_2 activation of cobalt-based catalysts. Furthermore, it is worth noting that the addition of Ru contributed to the formation of the Co_3O_4 crystalline phases, as higher fractions of Co_3O_4 were observed on the calcined $Co\text{-}Ru/SiO_2$ catalyst compared to Co/SiO_2. However, these Co_3O_4 fractions disappeared with treatment in either H_2 or syngas over the temperature range of 250-350 ˚C. As observed in Figure 7.4, the decrease in Co_3O_4 is much higher for the $Co\text{-}Ru/SiO_2$ catalyst reduced in H_2 than in syngas.

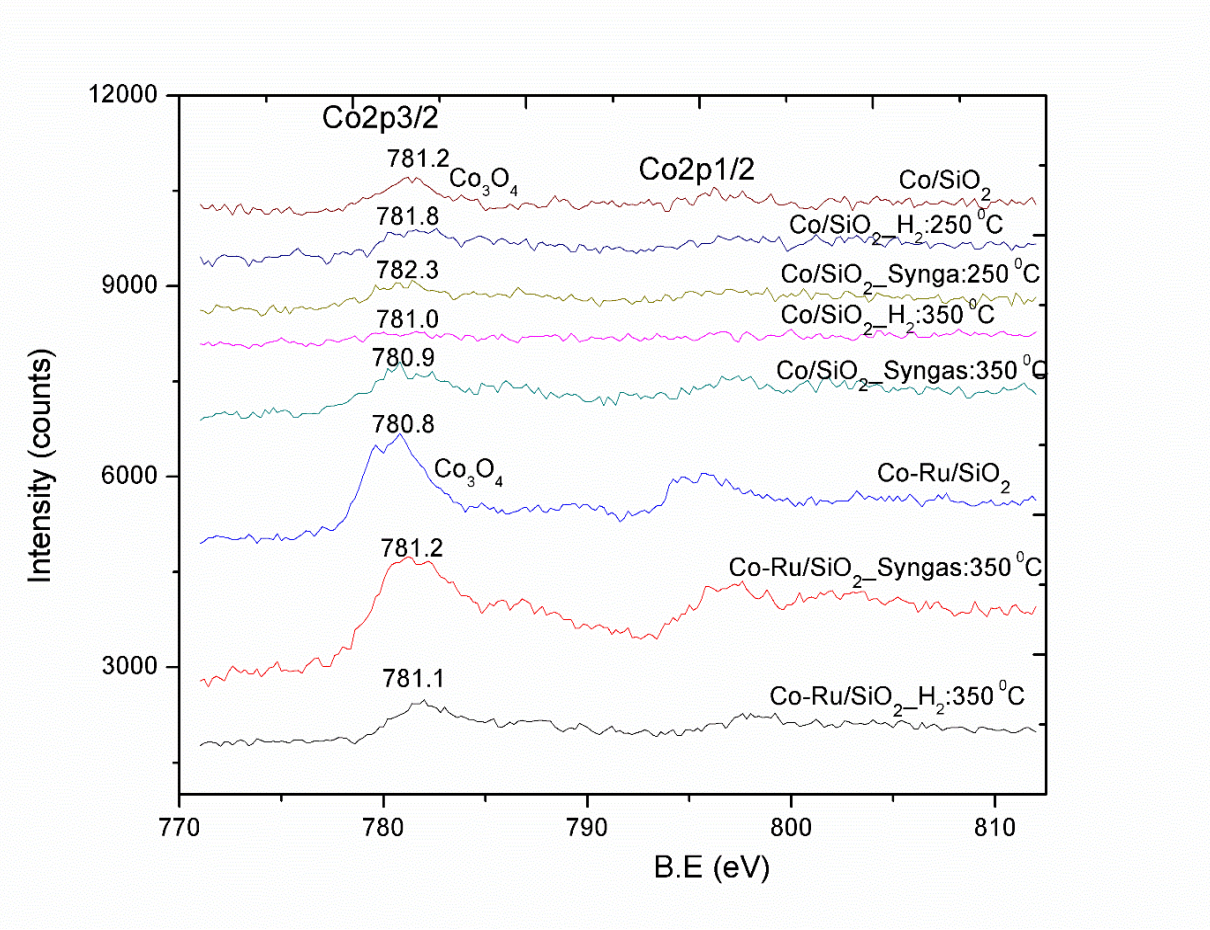

Figure 7. 4: Co2p XPS spectra for the supported cobalt catalysts

7.3.2 Catalyst testing

7.3.2.1 Unpromoted Co/SiO_2

Catalytic performance was evaluated at similar reaction conditions (210˚C, 20 bar, $H_2/CO = 2$) for the various catalysts that were reduced under different conditions as shown in Table 7.1. For the catalysts pre-treated with syngas: the Co/SiO_2 catalyst reduced at 350 ˚C exhibited the highest CO conversion compared to the catalysts reduced at either 250 or 300 ˚C. However, it afforded a lower activity than the catalyst activated in H_2, see Figure 7.5. Syngas activation at a low temperature (250 ˚C) led to no FTS activity for the first 40 h of the reaction, followed by a gradual increase in the CO conversion between 40 h to 120 h which then stabilised around 15%. The increase in activity observed at around 40 h might be due to: (1) the transformation of Co_2C species, as observed via XRD, Figure 7.1, to metallic Co in the presence of an H_2-rich syngas; (2) further reduction of cobalt oxide under the syngas atmosphere to an FTS active phase.

The catalyst activated at 300 ˚C showed a fairly constant activity with a %CO conversion around 5-7%, whereas a gradual decrease in the %CO conversion with time on stream (TOS) was observed over both the syngas and H_2 reduced samples at 350 ˚C. The XPS data indicated an increase in the atomic weight percentage for C1s with the reductive treatment at 350 for both H_2 and syngas, see Table 7.3. This suggests that there might be carbonaceous species deposited on the surface of the catalyst which are detrimental to the activity of the catalysts. The results for the H_2-treated catalyst could be taken as evidence that carbonaceous deposits also occur during the FT reaction.

All the catalysts (reduced both in H_2 and syngas) showed a high C_{5+} selectivity, in the range of 70-85%, yet further proof that Co-based catalysts are selective to long chain hydrocarbons, see Figure 7.5. The H_2-reduced catalyst has a slightly higher selectivity to C_{5+} hydrocarbons compared to syngas activated catalysts and displayed the lowest CH_4 selectivity, about 10%, compared to the syngas-reduced catalysts, which had a selectivity of CH_4 between 12-16%. The results are presented in Figure 7.5. For syngas pre-treated samples, the CH_4 selectivity was found to be highest for the catalyst reduced at 250 ˚C and lowest at 300 ˚C. The higher CH_4 selectivity for the catalysts reduced by syngas suggets experimental evidence that there may be another phase acting as a methanation site. In this case, the site for methanation could be either

Co_2C or surface carbon deposited during the reduction with syngas. No CO_2 was detected on any of the H_2 or syngas-activated samples. No catalyst deactivation was observed for the catalysts activated at either 250 or 300 ˚C by syngas. However, the catalysts activated both in H_2 and syngas at 350 ˚C deactivated with TOS before tending to a steady state.

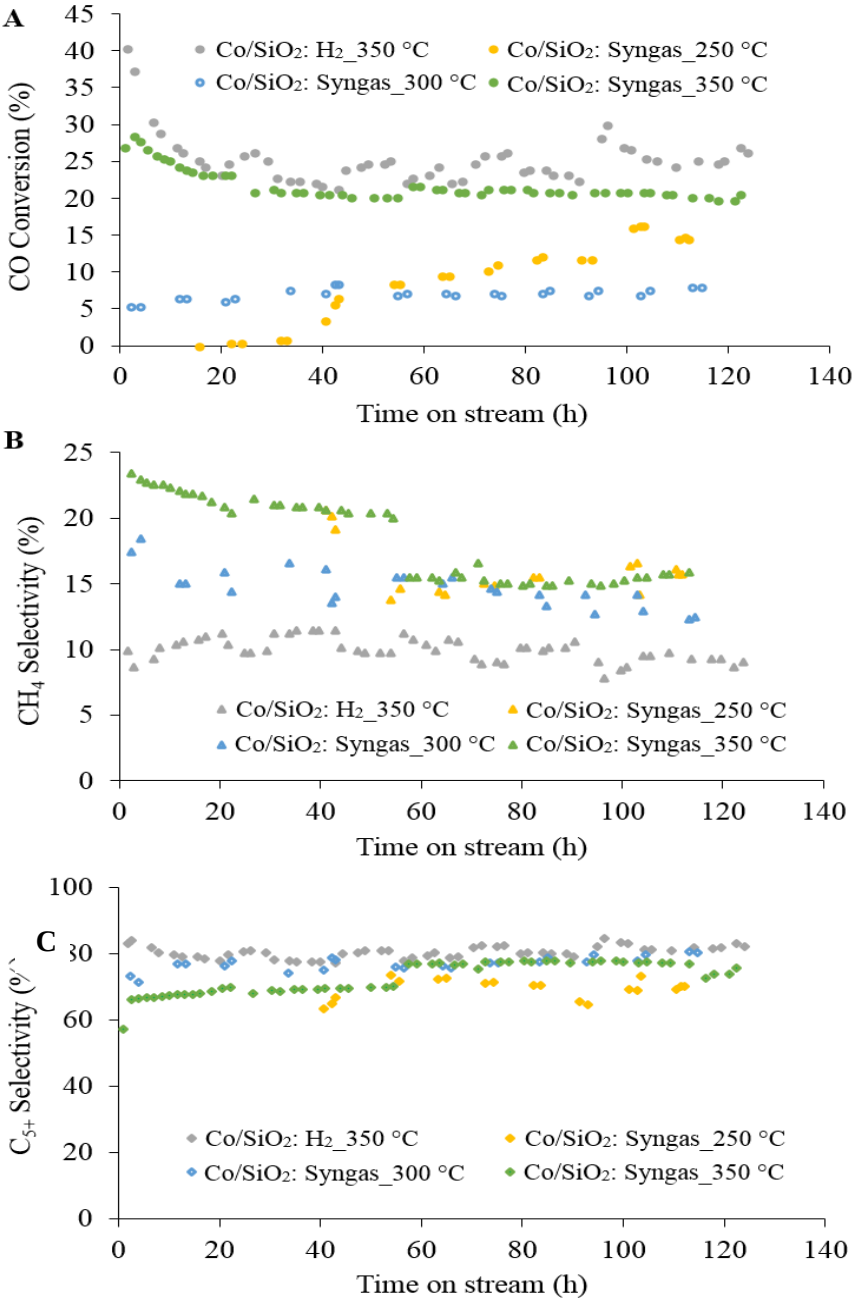

Figure 7. 5: CO conversion and product selectivity with time on stream for the Co/SiO_2 catalyst: (A) CO conversion; (B) CH_4 selectivity; and (C) C_{5+} selectivity. H_2_350 °C refers to the catalyst reduced with H_2 at 350 °C; Syngas_250 °C (300 °C or 350 °C) refers to the catalyst reduced with syngas at 250 °C (300 °C or 350 °C). Reaction conditions: 210˚C, 20 bar, 60 Nml/min and syngas: $H_2/CO = 2$.

The catalysts with standard H_2 treatment at 350 ˚C exhibited the highest %CO conversion and long chain hydrocarbon selectivity and the lowest CH_4 production compared to the syngas treated samples, thus indicating that H_2 is the better reducing agent. For the syngas treated catalysts, activation at 300 ˚C afforded the lowest activity, the highest initial C_{5+} selectivity and the lowest CH_4 selectivity compared to the samples reduced at either 250 or 350 ˚C. The catalyst activated at 250 ˚C showed the lowest initially activity (indeed no activity), due to lower Co_3O_4 reducibility and to the formation of Co_xC in the presence of CO in the reduction gas. This catalyst showed no activity for the first 40 h TOS, which suggest that the catalyst was not reduced and not active for FTS. However, after 40 h TOS the catalyst started gaining some activity which indicates that the catalyst reduced further under FTS environment. Two possible pathways for this reduction are: (1) the reduced oxide (CoO) decomposed to metallic Co thus leading to activity; (2) Co_xC acted as an intermediate to produce Co(hcp), the active phase for FTS.

De la Pena O'shea [35] reported that Co_3O_4 is almost completely converted to CoO under a syngas atmosphere at 300 ˚C, whereas reducing at a high temperature (350 ˚C) produced homogeneously dispersed Co(hcp) on carbon nanostructures. In agreement, Jalama et al. [4] detected metallic Co in the catalysts reduced at temperatures higher than 350 ˚C and found CoO only in the sample that was reduced at 250 ˚C in syngas. In this regard, we assume that the amount of Co(hcp) present in the 350 ˚C-syngas reduced sample is higher than the one found in the samples reduced at a lower temperature (250-300 ˚C). Hence the 350-activated sample showed a higher activity than the 250 ˚C - and 300 ˚C -activated samples. However, the 350-treated sample showed premature deactivation with TOS which could be due to wax product accumulation on the catalyst surface which may form a liquid layer thus affecting the adsorption of the gases.

The catalyst reduced with syngas at 350 ˚C exhibited the highest CH_4 selectivity, due to surface carbon that might have been deposited during the reduction of the catalyst, which might in turn have reacted with H_2 to produce CH_4. Lee et al. [36] reported that active carbon deposited via the reduction of Co/Al_2O_3 in CO reacts with H_2 to form CH_4 or oxygen to form CO_2. Jalama et al. [4] reported higher activity and CH_4 selectivity on the syngas reduced Co/TiO_2 catalyst at 250 ˚C compared to an H_2-reduced sample, which was related to reduction kinetics and residual cobalt carbide. Yang et al. [12] suggested that cobalt carbide inhibits the FTS and was

the source of CH_4 formation for a CO activated Co/TiO_2 catalyst. Therefore, we can relate the high CH_4 selectivity of the syngas-reduced sample to the presence of the Co_xC phase. The slight decrease in the C_{5+} selectivity of the syngas pre-treated catalysts can be attributed to low Co metal density obtained with syngas reduction, which suggests that C_{5+} hydrocarbons are generated on Co metal sites. Li et al. [13] reported that hydrocarbon products are produced on metallic sites, whereas CH_4 is produced on surface carbides.

Although the lowest conversion was obtained, the sample activated at 300 ˚C performed better in terms of selectivity than the samples reduced either at 250 and 350 ˚C. Activating at a lower temperature (250 ˚C) led to cobalt carbide (Figure 7.1) which supressed CO hydrogenation and promoted the formation of CH_4. Activating at a higher temperature (350 ˚C) led to the deposition of carbonaceous species which promoted premature deactivation and selectivity to shorter hydrocarbons.

7.3.2.2 Ru-promoted Co/SiO_2

The Ru-promoted Co/SiO_2 catalyst, reduced in H_2, showed higher initial and steady state CO conversion compared to the catalyst reduced in syngas, the results are presented in Figure 7.6. The addition of Ru increased the reducibility of the catalyst, which led to a higher Co˚ site density and consequently, higher FT activity. The Ru-promoted Co/SiO_2 catalyst reduced in syngas showed the lowest activity. However, it exhibited the highest C_{5+} and the lowest CH_4 selectivity compared to the catalysts reduced in H_2 as well as the unpromoted catalyst, see Figures 7.6 B and C. The low FT activity observed for the syngas-treated catalyst could be due to high metal-support interactions, observed by XPS, which inhibited the reduction of cobalt species.

Ru improved the selectivity to long chain hydrocarbons and supressed the CH_4 selectivity for the catalyst reduced in syngas. This can be attributed to the strong ability of Ru to introduce H_2 to the surface of the Co atoms, which further reduced the surface Co species and steadily increased the activity and selectivity of the catalyst as metallic sites were formed. The FTS

results are in agreement with the TEM data in Figures 7.3 C & D, where more metallic sites were observed over the syngas-treated catalyst compared to H_2 pre-treatment. The activity of the H_2-activated Ru-promoted catalyst decreased with TOS due to higher deposition of unreactive C1s species, see Table 7.3. An opposite effect was observed for the syngas reduced catalyst, which suggets evidence of Co_xC species being converted to Co(hcp) during the reaction or further reduction of CoO to metallic Co. These results are in line with the findings observed via XRD, Figure 7.1, which clearly shows the presence of Co_2C species in higher quantities for the syngas treated catalyst compared to those reduced in H_2.

Initially, the unpromoted Co/SiO_2 reduced at 350 ˚C exhibited higher activity than the Ru-promoted sample, pre-treated in syngas. However, with increasing TOS, the conversions of the catalyst with or without Ru reduced by syngas tended to the same value (Figure 7.6). No CO_2 was produced over the syngas reduced sample, while the H_2-activated Ru catalyst produced about 0.46% CO_2 (see Table 7.4), which might be due to a high-water partial pressure due to the high CO conversion.

The excess H_2 introduced by the Ru atoms on the surface of Co atoms enhanced CH_4 formation and supressed the chain grown reaction for the H_2-reduced $Co\text{-}Ru/SiO_2$ sample. In agreement, Tsubaki et al. [3] reported a lower chain growth probability for a catalyst promoted with Ru, which was attributed to the strong ability for the Ru to activate and introduce H_2 to the surface of the catalyst thus supressing the chain growth process. The activity of the syngas-reduced $Co\text{-}Ru/SiO_2$ catalyst at 350 ˚C gradually increased with TOS, which suggest a change in surface Co species, especially Co_xC to metallic Co. The presence of small amounts of Ru facilitated further reduction of cobalt carbides by supplying more H_2 to the catalyst surface. As the Co_xC is converted to Co˚, we observed a decrease in the CH_4 selectivity and an increase in the C_{5+} selectivity, see Figures 7.6.

Ru-promotion eliminates the high CH_4 selectivity associated with syngas reduction and promote chain growth through re-absorption of α-olefins resulting in long chain hydrocarbons, in agreement with literature [30,33]. Ma et al. [30] reported that the addition of small amounts of Ru promoter, increased the reducibility of the catalysts and consequently, increased the C_{5+} selectivity while decreasing the CH_4 selectivity by nearly the same extent. This was ascribed to the ability of Ru to supress secondary reactions of C_1-C_4 olefins, thus resulting in higher

molecular fractions. The increased degree of reduction was attributed to two main reasons: (1) noble metal dissociates H_2 resulting in a spillover to cobalt oxide sites; (2) the electronic effect from alloying (Co-noble metal) [30].

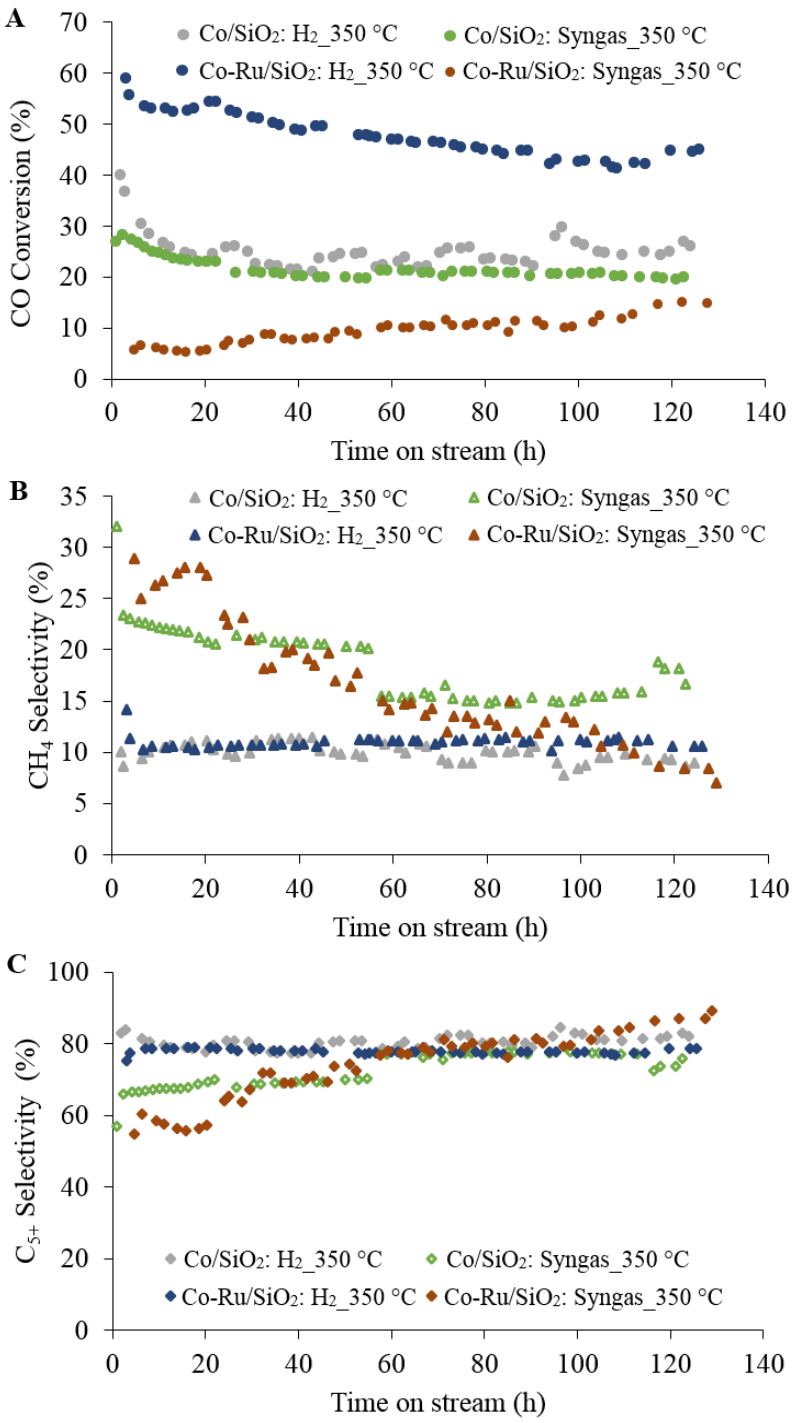

Figure 7. 6*:* CO conversion and product selectivity with time on stream for the Co/SiO_2 catalyst: (A) CO conversion; (B) CH_4 selectivity; and (C) C_{5+} selectivity. H_2_350 °C refers to the catalyst reduced with H_2 at 350 °C; Syngas_ 350 °C refers to the catalyst reduced with syngas at 350 °C. Reaction conditions: 210˚C, 20 bar, 60 Nml/min and syngas: $H_2/CO = 2$.

Table 7. 4: The activity and selectivity of the Co/SiO_2 and $Co\text{-}Ru/SiO_2$ catalysts activated by H_2 at 350 ˚C or by syngas at 250-350˚C, 60 Nml/min. Reaction conditions: 210 ˚C, 20 bar, 60 Nml/min, $H_2/CO = 2$.

Catalyst	Agent	Red. T(˚C)	FT activity and product selectivity (C%)							Alpha
			CO	CO_2	CH_4	C_{5+}	P_2/O_2	P_3/O_3	P_4/O_4	(α_{C3-6})
Co/SiO_2	Syngas	250	15	0	16	70	4.58	0.59	0.79	0.744
		300	7	0	13	80	0.94	0.34	0.41	0.746
		350	20	0	17	75	3.21	0.71	0.78	0.935
	H_2	350	26	0	9	82	3.68	*	0.56	0.832
$Co\text{-}Ru/SiO_2$	H_2	350	45	0.46	11	78	5.90	*	0.70	0.741
	Syngas	350	16	0	8	88	1.70	*	0.55	0.668

7.3.2.3 Paraffin to Olefin ratio

The product distribution for the catalysts reduced in both H_2 and syngas is presented in Figure 7.7. More paraffinic products were produced when the Co/SiO_2 catalyst was reduced at 250/350 ˚C in syngas compared to the catalyst reduced in H_2, see Figure 7.7 C&D. These findings agree with the XRD data, which showed stronger, more intense $(CH_2)_X$ peaks over the syngas treated catalyst and weaker peaks on the H_2-treated catalyst, Figure 7.1 A, suggesting that more paraffinic products are produced over syngas reduction. We observed an increase in the P/O ratio with TOS for the catalyst reduced at 250 ˚C, as the surface carbides were transformed under the syngas atmosphere and slowly converted to metallic Co. This surface restructuring favored the production of paraffinic products and led to a higher P/O ratio by the time steady state was achieved. The syngas pre-treated samples afforded a higher P_5/O_5 ratio compared to the unpromoted Co/SiO_2 sample reduced in H_2, see Figure 7.7 C&D.

The Ru-promoted catalyst reduced in H_2 displayed remarkably higher P/O ratios for the C_2-C_5 hydrocarbons fractions compared to the unpromoted catalyst or the syngas reduced catalyst,

Figure 7.7 A&B. The XRD data for the spent Co-Ru/SiO_2 treated in H_2 supports this as it showed more intense $(CH_2)_X$ peaks compared to the H_2-treated catalyst, suggesting that more paraffinic products are produced over the H_2 reduced catalyst. Furthermore, the Co-Ru/SiO_2 catalyst reduced in syngas achieved a higher P_5/O_5 ratio than the unpromoted catalyst reduced in H_2, see Figure 7.7 A&B. From these results, it can be deduced that syngas activation promotes more paraffinic products while H_2 produces more olefinic products, for unpromoted catalysts. However, Ru promotion enhances the formation of paraffinic products for the H_2-reduced catalysts, which may be due to an increase in the surface H_2 for secondary hydrogenation reactions. De la Pena O'shea et al. [14] studied the effect of syngas reduction on the Co/SiO_2 catalyst and similarly found that syngas activated catalysts exhibited a stronger hydrogenation activity and that they produced more paraffinic products than H_2.

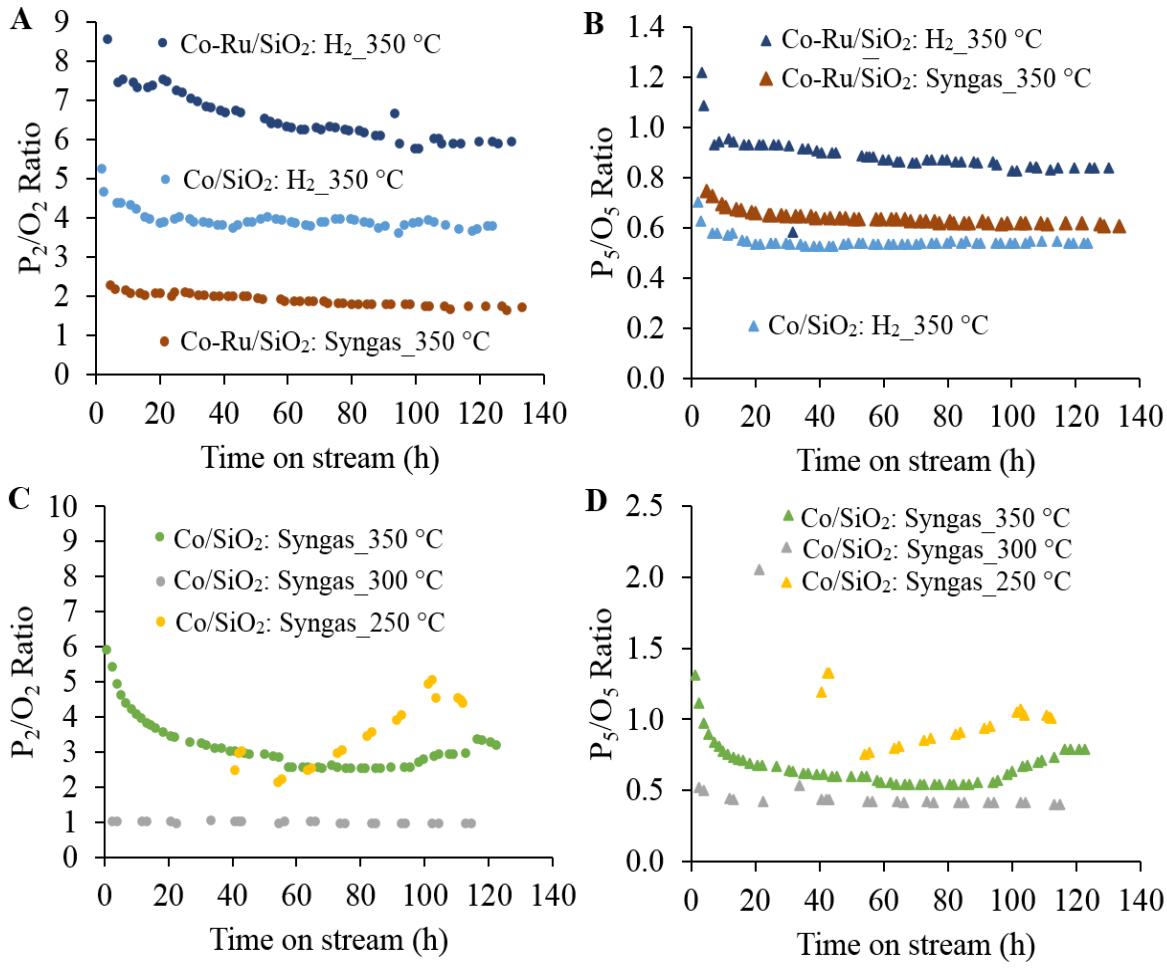

Figure 7. 7: Paraffin to olefin ratio (P/O) with time on stream for the Co/SiO_2 and Co-Ru/SiO_2 catalysts under different pre-treatment conditions: (A and C) P_2/O_2 (ethane/ethylene); (B and D) P_5/O_5 (pentane/pentene). H_2_350 °C refers to the catalyst reduced with H_2 at 350 °C; Syngas_250 °C (300 °C or 350 °C) refers to the catalyst reduced with syngas at 250 °C (300 °C or 350 °C). Reaction conditions: 210˚C, 20 bar, 60 Nml/min and syngas: H_2/CO = 2.

7.3.3 Hydrogenation-carburisation-hydrogenation (H-C-H) reduction procedure

We further investigated the use of CO and H_2 reduction agents in series instead of feeding a mixture of CO/H_2 (syngas) into the reactor for the CO hydrogenation of unpromoted Co/SiO_2. This reduction method is referred to as hydrogenation-carburisation-hydrogenation (H-C-H) method. Researchers reported that the H-C-H method has been shown to enhance the catalytic activity via the selective formation of metallic Co(hcp) which has a higher intrinsic activity compared to that of Co(fcc) obtained during the standard H_2 activation [15,37-39]. Gnanamani et al. [1] successfully prepared Co(fcc) and Co(hcp) supported on SiO_2 catalysts and investigated the effect of the Co metal phase on the catalytic activity.

The H-C-H activation of Co/SiO_2 resulted in a 40 % higher CO conversion compared to the standard H_2-activation at 350 °C, see Figure 7.8 A. The H-C-H method enriched the catalyst with Co(hcp) stacking resulting in superior activity. This is consistent with the observations made by Ducreux et al. [38] and Jongsomjit et al. [39] who reported an increase in the cobalt reducibility and dispersion on the catalysts treated by the H-C-H method that resulted in an improved FTS activity. The decomposition of the carbide to Co(hcp) was reported to facilitate the insertion of carbon atoms during the CO decomposition and extract then in the surface layer on hydrocarbon formation. Discussions were all based on the CO conversion and the effect of the H-C-H method on the selectivity of the hydrocarbons was not mentioned. The H_2 reduced catalyst has a higher C_{5+} selectivity and low CH_4 production compared to the H-C-H reduction route, Figure 7.8 B. This may be attributed to surface carbonaceous species deposited during the CO carburisation stage. Carbon deposited on the surface can exit in two forms namely: active carbon and/or graphitic carbon. Active carbon can react either with oxygen to form CO_2 or hydrogen to form CH_4. The graphitic carbon is non-reactive and can block the surface-active sites resulting in a detrimental effect on the activity. Lee [36] reported an increase in carbon deposition with an increase in temperature and that the atomic carbon deposited is either transformed morphologically into graphitic or polymeric carbon. The formation of CO_2 (reported in Table 7.5) and high CH_4 selectivity can be explained by the reaction between surface active carbon and the oxygen containing compounds.

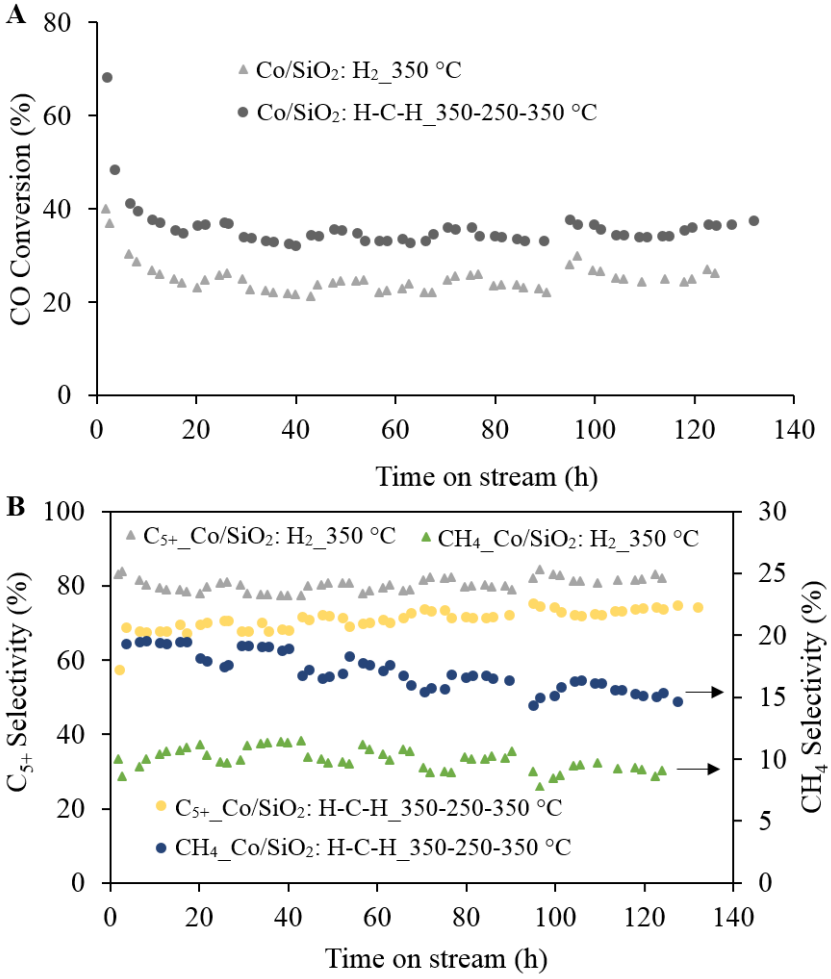

Figure 7. 8: CO conversion and product selectivity with time on stream for Co/SiO_2 and $Co\text{-}Ru/SiO_2$ catalysts under different pre-treatment conditions: (A) CO conversion; (B) CH_4 and C_{5+} selectivity; H_2_350 °C refers to the catalyst reduced with H_2 at 350 °C; H-C-H_ 350-250-350 °C refers to the catalyst reduced with H_2 at 350 °C, then with CO at 250 °C and then with H_2 at 350 °C. Reaction conditions: 210˚C, 20 bar, 60 Nml/min and syngas: $H_2/CO = 2$.

Table 7.5 presents the steady state data for FT catalytic tests performed after the different pre-treatment method. Reduction via H-C-H produced some CO_2 and the C_{5+} selectivity decreased slighly. The CH_4 selectivity for the H-C-H pre-treated sample is almost double that of the H_2 reduced sample. Yang et al. [12] suggested that Co_2C inhibits the FTS and is the source of CH_4 formation for a CO activated Co/TiO_2 catalyst. Recent studies indicate that Co_2C is converted to metallic Co under normal FT conditions [1,12,36]. In contrast, Karaca and co-workers [15] reported a decrease in the CO conversion from 60 to 20 % for a $CoPt/Al_2O_3$ catalysts comprised

of 80% Co(fcc) and 20% Co(hcp) due to the formation of Co_2C with prolonged TOS. These results present evidence that the Co_2C was converted to Co(hcp) during the H_2 decomposition step, resulting in enhanced CO conversion. The unreduced cobalt carbide could account for the high CH_4 selectivity.

Table 7. 5: The activity and selectivity of the Co/SiO_2 catalyst activated by H_2 at 350 ˚C and by H-C-H method (reduced by H_2 at 350 ˚C, then CO at 250 ˚C, and then H_2 at 350 ˚C), 60 Nml/min. Reaction conditions: 210 ˚C, 20 bar, 60 Nml/min, H_2/CO = 2).

Reducing Agent	**Conversion**	**Selectivity (%)**				**P/O**		**Alpha**
	%	%						**α**
	CO	CH_4	C_2-C_4	C_{5+}	CO_2	P_2/O_2	P_5/O_5	**C_{3-6}**
H_2	26	9	9	82	0	3.68	0.54	0.83
H-CO-H	37	15	11	74	0.83	2.35	0.43	0.83

7.3.4 Conclusion

Unpromoted Co/SiO_2 catalysts activated under syngas exhibited a high CH_4 selectivity, due to the formation of cobalt carbides during reduction, which favour the methanation reaction. The cobalt catalysts were selective to high molecular weight products with a selectivity between 70-85%. Ru-promotion led to a higher degree of reduction, Co dispersion and consequently, higher FT activity. The addition of Ru broadened the pore size of the silica support and resulted in larger Co_3O_4 particles being deposited compared to the unpromoted catalyst. The Ru-promoted catalyst activated under syngas exhibited the highest C_{5+} selectivity and lowest CH_4 selectivity compared to H_2-reduced sample, which is ascribed to the re-dispersion of Co particles, due to H_2 spillover from the Ru atoms to the surface of the catalyst which promoted further reduction of the cobalt oxide and cobalt carbide species. On the other hand, excess H_2 on the catalyst surface suppressed the chain growth reaction and enhanced the formation of CH_4 for the H_2-reduced sample. Higher P_5/O_5 ratios were observed with syngas activation

whereas pre-treatment with H_2 gives rise to olefinic products. Syngas has the potential to eliminate the high temperature reduction step and thereby decrease the costs associated with operation and start-up of a small-scale FT plants. The catalyst pre-treated by hydrogenation-carburisation-hydrogenation improved the CO conversion by 40%. We present evidence of inducing Co(hcp) via the Co_xC intermediate. However, the carbide acted as a source of CH_4 and CO_2 compromising the selectivity of higher hydrocarbons. Future studies may be necessary to improve the understanding of the role of the surface carbon on the activity of the catalysts as well as the effect of the reduction temperature.

7.4 References

[1] Gnanamani MK, Jacobs G, Keogh RA, Shafer WD, Sparks DE, Hopps SD, Thomas GA, Davis BH. Fischer-Tropsch synthesis: Effect of pretreatment conditions of cobalt on activity and selectivity for hydrogenation of carbon dioxide. Appl. Catal. A, Gen 2015; 499: 39–46. https://doi.org/10.1016/j.apcata.2015.03.046Get.

[2] Xu J, Bartholomew CH. Temperature-programmed hydrogenation (TPH) and in situ Mössbauer spectroscopy studies of carbonaceous species on silica-supported iron Fischer-Tropsch catalysts. J. Phys. Chem. B. 2005; 109: 2392-403. https://doi.org/10.1021/jp048808j.

[3] Tsubaki N, Sun S, Fujimoto K. Different functions of the noble metals added to cobalt catalysts for Fischer–Tropsch synthesis. J. Catal. 2001; 246: 236–246. https://doi.org/10.1006/jcat.2001.3163.

[4] Jalama K, Kabuba J, Xiong H, Jewell LL. Co/TiO_2 Fischer – Tropsch catalyst activation by synthesis gas. Catal. Comm. 2012; 17: 154–9. https://doi.org/10.1016/j.catcom.2011.10.029.

[5] Jahangiri H, Bennett J, Mahjoubi P, Wilson K, Gu S. A review of advanced catalyst development for Fischer-Tropsch synthesis of hydrocarbons from biomass derived syn-gas. Catal. Sci. Technol. 2014; 4: 2210–29. DOI: 10.1039/C4CY00327F.

[6] Martínez-Vargas DX, Sandoval-Rangel L, Campuzano-Calderon O, Romero-Flores M, Lozano FJ, Nigam KD, Mendoza A, Montesinos-Castellanos A. Recent advances in bifunctional catalysts for the Fischer–Tropsch process: one-stage production of liquid hydrocarbons from syngas. Ind. & Eng. Chem. Research. 2019; 58: 15872-901. https://doi.org/10.1021/acs.iecr.9b01141.

[7] Yang Y, Jia L, Meng Y, Hou B, Li D, Sun Y. Fischer–Tropsch synthesis over ordered mesoporous carbon supported cobalt catalysts: the role of amount of carbon precursor in catalytic performance. Catal. Lett. 2012; 142: 195-204. https://doi.org/10.1007/s10562-011-0747-3.

[8] Herranz T, Rojas S, Pérez-Alonso FJ, Ojeda M, Terreros P, Fierro JLG. Genesis of iron carbides and their role in the synthesis of hydrocarbons from synthesis gas. J. Catal. 2006; 243: 199–211. https://doi.org/10.1016/j.jcat.2006.07.012.

[9] Wezendonk TA, Sun X, Dugulan AI, van Hoof AJ, Hensen EJ, Kapteijn F, Gascon J. Controlled formation of iron carbides and their performance in Fischer-Tropsch synthesis. J. Catal. 2018; 362: 106-17. https://doi.org/10.1016/j.jcat.2018.03.034.

[10] O'Brien RJ, Xu L, Spicer RL, Davis BH. Activation Study of Precipitated Iron Fischer-Tropsch Catalysts. Energy & Fuels. 1996; 10: 921-6. https://doi.org/10.1021/ef9502315.

[11] Dai X, Yu C. Effects of pretreatment and reduction on the Co/Al_2O_3 catalyst for CO hydrogenation. J. nat. gas chem. 2008; 17: 288-92. https://doi.org/10.1016/S1003-9953(08)60066-3.

[12] Yang J, Jacobs G, Jermwongratanachai T, Anders DC, Burtron H. Fischer–Tropsch synthesis: Impact of H_2 or CO activation on methane selectivity. Catal. Lett. 2014; 144: 123–132. https://doi.org/10.1007/s10562-013-1099-y.

[13] Li J, Xu L, Keogh R, Davis B. Fischer–Tropsch synthesis. Effect of CO pretreatment on a ruthenium promoted Co/TiO_2. Catal. Lett. 2000; 70: 127–130. https://doi.org/10.1023/A:1018833217001.

[14] De la Peña O'Shea VA, Campos-Martı´n JM, Fierro JLG. Strong enhancement of the Fischer–Tropsch synthesis on a Co/SiO_2 catalyst activate in syngas mixture. Catal. Commun. 2004; 5: 635–638. https://doi.org/10.1016/j.catcom.2004.08.005.

[15] Karaca H, Safonova OV, Chambrey S, Fongarland P, Roussel P, Griboval-Constant A, Lacroix M, Khodakov AY. Structure and catalytic performance of Pt-promoted alumina-supported cobalt catalysts under realistic conditions of Fischer–Tropsch synthesis. J. Catal. 2011; 277: 14-26. https://doi.org/10.1016/j.jcat.2010.10.007.

[16] Claeys M, Dry ME, Van Steen E, Du Plessis E, Van Berge PJ, Saib AM, Moodley DJ. In situ magnetometer study on the formation and stability of cobalt carbide in Fischer–Tropsch synthesis. J. Catal. 2014; 318: 193–202. https://doi.org/10.1016/j.jcat.2014.08.002.

[17] Fischer N, Clapham B, Feltes T, Claeys M. Cobalt based Fischer-Tropsch activity and selectivity as a function of crystallite size and water partial pressure. ACS Catal. 2015; 5: 113–121. https://doi.org/10.1021/cs500936t.

[18] Kwak G, Kim DE, Kim YT, Park HG, Kang SC, Ha KS, Jun KW, Lee YJ. Enhanced catalytic activity of cobalt catalysts for Fischer–Tropsch synthesis via carburization and hydrogenation and its application to regeneration. Catal. Sci. Technol. 2016 ;6: 4594–4600. DOI: 10.1039/C5CY01399B.

[19] Pan Z, Parvari M, Bukur DB. Fischer–Tropsch synthesis on Co/Al_2O_3 catalyst: Effect of pretreatment procedure. Top. Catal. 2014; 57: 470-478. https://doi.org/10.1007/s11244-013-0203-2.

[20] Chen W, Lin T, Dai Y, An Y, Yu F, Zhong L, Li S, Sun Y. Recent advances in the investigation of nanoeffects of Fischer-Tropsch catalysts. Catal. Today 2018; 311: 8–22. https://doi.org/10.1016/j.cattod.2017.09.019.

[21] Saib AM, Claeys M, Van Steen E. Silica supported cobalt Fischer -Tropsch catalysts: Effect of pore diameter of support. Catal. Today 2002; 71: 395–402. https://doi.org/10.1016/S0920-5861(01)00466-7.

[22] Jacobs G, Ma W, Davis BH. Influence of reduction promoters on stability of cobalt/g-alumina Fischer-Tropsch synthesis catalysts. Catalysts. 2014; 4: 49-76. https://doi.org/10.3390/catal4010049.

[23] Carballo JMG, Yang J, Holmen A, García-Rodríguez S, Rojas S, Ojeda M, Fierro JLG. Catalytic effects of ruthenium particle size on the Fischer–Tropsch Synthesis. J. Catal. 2011; 284: 102–108. https://doi.org/10.1016/j.jcat.2011.09.008.

[24] Lyu S, Wang L, Zhang J, Liu C, Sun J, Peng B, Wang Y, Rappé KG, Zhang Y, Li J, Nie L. Role of active phase in Fischer−Tropsch synthesis: Experimental evidence of CO activation over single-phase cobalt catalysts. ACS Catal. 2018; 8: 7787–7798. https://doi.org/10.1021/acscatal.8b00834.

[25] Rytter E, Skagseth TH, Eri S, Sjastad AO, Cobalt Fischer-Tropsch catalysts using nickel promoter as a rhenium substitute to suppress deactivation. Ind. Eng. Chem. Res. 2010; 49: 4140–4148. https://doi.org/10.1021/ie100308f.

[26] Jacobs G, Das TK, Zhang Y, Li J, Racoillet G, Davis BH. Fischer–Tropsch synthesis: support, loading, and promoter effects on the reducibility of cobalt catalysts. Appl. Catal. A Gen. 2002; 233: 263–281. https://doi.org/10.1016/S0926-860X(02)00195-3.

[27] Jongsomjit B, Goodwin JG Jr. Co-support compound formation in Co/Al_2O_3 catalysts: Effect of reduction gas containing CO. Catal. Today 2002; 77: 191–204. https://doi.org/10.1016/S0920-5861(02)00245-6.

[28] Petersen AP, Claeys M, Kooyman PJ, Van Steen E. Cobalt-Based Fischer–Tropsch Synthesis: A kinetic evaluation of metal–support interactions using an inverse model system. Catalysts 2019; 9: 794. https://doi.org/10.3390/catal9100794.

[29] Diehl F, Khodakov AY. Promotion of cobalt Fischer-Tropsch catalysts with noble metals: A review. Oil Gas Sci. Technol. 2009; 64: 11–24. https://doi.org/10.2516/ogst:2008040.

[30] Ma W, Jacobs G, Keogh RA, Bukur DB, Davis BH. Fischer-Tropsch synthesis: Effect of Pd, Pt, Re, and Ru noble metal promoters on the activity and selectivity of a 25%Co/ Al_2O_3 catalyst. Appl. Catal. A Gen. 2012; 437–438: 1–9. https://doi.org/10.1016/j.apcata.2012.05.037.

[31] Hong J, Chernavskii PA, Khodakov AY, Chu W. Effect of promotion with ruthenium on the structure and catalytic performance of mesoporous silica (smaller and larger pore) supported cobalt Fischer–Tropsch catalysts. Catal. Today. 2009; 140: 135-141. https://doi.org/10.1016/j.cattod.2008.10.009.

[32] Lin Q, Liu B, Jiang F, Fang X, Xu Y, Liu X. Assessing the formation of cobalt carbide and its catalytic performance under realistic reaction conditions and tuning product selectivity in a cobalt-based FTS reaction. Catal. Sci. Tech. 2019; 9:3238-58. DOI: 10.1039/C9CY00328B

[33] Iglesia E, Soled SL, Fiato RA, Via GH. Bimetallic synergy in cobalt ruthenium Fischer-Tropsch synthesis catalysts. J. Catal. 1993; 143: 345-368. https://doi.org/10.1006/jcat.1993.1281.

[34] Kababji AH, Joseph B, Wolan JT. Silica-supported cobalt catalysts for Fischer–Tropsch synthesis: Effects of calcination temperature and support surface area on cobalt silicate formation. Catal. Lett. 2009; 130: 72-78. https://doi.org/10.1007/s10562-009-9903-4.

[35] De la Peña O'Shea VA, Homs N, Fierro JLG, De la Piscina PR. Structural changes and activation treatment in a Co/SiO_2 catalyst for Fischer–Tropsch synthesis. Catal. Today 2006; 114: 422–427. https://doi.org/10.1016/j.cattod.2006.02.065.

[36] Lee DK, Lee JH, Ihm SK. Effect of carbon deposits on carbon monoxide hydrogenation over alumina-supported cobalt catalyst. Appl. Catal. 1988; 36: 199-207. https://doi.org/10.1016/S0166-9834(00)80115-3.

[37] Gnanamani MK, Jacobs G, Shafer WD, Davis BH. Fischer–Tropsch synthesis: Activity of metallic phases of cobalt supported on silica. Catal. Today. 2013; 215: 13-7. https://doi.org/10.1016/j.cattod.2013.03.004.

[38] Ducreux O, Rebours B, Lynch J, Bazin D. Microstructure of supported cobalt Fischer-Tropsch catalysts. Oil Gas Sci Technol-Rev lFP 2009; 64: 49–62. https://doi.org/10.2516/ogst:2008039.

[39] Jongsomjit B, Goodwin JG Jr. Co-support compound formation in Co/Al_2O_3 catalysts: Effect of reduction gas containing CO. Catal. Today 2002; 77: 191–204. https://doi.org/10.1016/S0920-5861(02)00245-6.

[40] Graham UM, Jacobs G, Gnanamani MK, Lipka SM, Shafer WD, Swartz CR, Jermwongratanachai T, Chen R, Rogers F, Davis BH. Fischer–Tropsch Synthesis: Higher oxygenate selectivity of cobalt catalysts supported on hydrothermal carbons. ACS Catal. 2014; 4: 1662-72. https://doi.org/10.1021/cs400965t.

CHAPTER 8: Overall Conclusions

This chapter gives an overview conclusion of the study and prospects for future studies.

8.1 Conclusions

This work has provided a framework for analysing and improving the performance of cobalt-based FT GTL plants. FTS has a great potential to accomplish the energy insecurity brought by the depletion of fossil fuels and to utilise greenhouse gases to produce energy carriers. However, it faces the common bottleneck of low FTS activity and selectivity of targeted products, which could be due to external factors induced by catalyst pre-treatments, such as the active metal interaction with the support. Ongoing efforts devoted to excavating and accelerating the delivery of affordable, durable and highly active cobalt catalysts at a low cost to achieve a high selectivity towards valuable chemicals include the use of mild temperatures during catalyst pre-treatment, the use of promoters, and the use of different reducing agents in series. With that being the case, we investigated the role of cobalt species on the activity and selectivity of cobalt-based catalysts, by looking into the effect of support characteristics as well as the reduction temperature and the reducing agent.

We compared the catalyst activity and product selectivity from each set of catalysts that were tested at industrially relevant FTS conditions. We postulated that comparison of the catalyst's performance under similar FT reaction conditions, but different pre-treatments conditions might reveal novel generic rules that might provide avenue for future catalyst design and product-based FTS operations. The physicochemical properties of the catalysts were analysed by BET, XRD, TEM, XRF and XPS. Furthermore, additional in-situ PXRD and TPR measurements with special temperature programs were investigated to monitor the phase changes of the cobalt species on the support during catalyst activation. Based on the comparison between the characterization data and experimental results of the catalysts, possible new mechanisms and hypothesis could be used to explain the effect of the pre-treatment conditions subjected to the catalysts. In addition, it also provided prospects for future studies that would be pursued to optimise the FTS process and catalyst design to suit the targeted product.

We conducted several groups of FTS experiments in a gas-solid reaction regime with four different types of catalysts: Co/SiO_2, Co/TiO_2, Co/Al_2O_3, and $Co\text{-}Ru/SiO_2$, in a fixed-bed

reactor under typical low temperature FTS conditions. These catalysts were subjected to different pre-treatment conditions such as varying the reduction temperature in the range 220-350 ˚C and varying the reduction agent (using either H_2, syngas, or CO, respectively). The most important experimental findings are as follows:

(1) Catalyst activation by H_2:

In-situ PXRD results proved that Co_3O_4 could be reduced in H_2 to form CoO and/or Co^0 on the surface of the support; Increasing the reduction temperature, increased the amount of the Co^0, while the CoO content dropped; A multi-phase CoO-Co^0 was obtained for each cobalt-based catalyst, at a lower reduction temperature.

Increasing the reduction temperature from 250 ˚C to 350 ˚C, improved the catalytic activity of the FT reaction for both Co/ TiO_2 and Co/Al_2O_3, which could be attributed to an increase in the density of the Co^0 with increasing reduction temperature.

However, the Co/SiO_2 catalyst behaved differently than the Co/Al_2O_3 and Co/TiO_2 catalysts. The Co/SiO_2 catalyst showed a higher catalytic activity when reduced at 250 ˚C. The CoO-Co/SiO_2 catalyst demonstrated higher activity for both FT and WGS reactions. It was experimentally proved that the multi-phase of CoO-Co assisted the activation of CO and hydrogenation of R-CHx intermediates. This led to an increase in the CO hydrogenation activity and the selectivity to linear paraffinic products. A new mechanism, "CoO-Co H-assisted CO dissociation", was hypothesized.

The Co/TiO_2 catalyst exhibited the highest activity when treated at 350 ˚C in H_2 due to complete reduction of cobalt oxides to metallic cobalt, the intrinsic particle size (Co(fcc) = 8.7 nm) and higher Co metal dispersion compared to Co/SiO_2 and Co/Al_2O_3 catalysts. No WGS activity was observed for the TiO_2 supported catalysts, when reduced at a low temperature (220/250 ˚C). However, an increase in the reduction temperature led to the formation of a small amount of CO_2 due to a higher-water partial pressure and as a result, WGS activity. In addition, more paraffinic products were attained when the catalyst was reduced at 350 ˚C than at 250 ˚C due to enhanced secondary hydrogenation of olefins reaction.

(2) Catalyst activation by syngas:

All the catalysts (Co/SiO_2, Co/TiO_2, Co/Al_2O_3) could be reduced by syngas; and increasing the reduction temperature could increase the FT reactivity of the catalysts. Although the CO conversions were lower with these catalysts compared to the catalysts reduced by H_2, syngas activation afforded better product selectivity (low CH_4, high C_{5+}, high O/P) for the Co-catalysts reduced at lower activation temperature (250 ˚C). With syngas reduction, cobalt oxide could transform to cobalt carbide (Co_xC) species, which suppressed the hydrogenation reaction and resulted in the high selectivity of olefins excluding Co/SiO_2 reduced at 350 ˚C with syngas. Furthermore, we postulated that there is a synergistic effect between Co^0 and Co_xC that promotes the production of the long chain hydrocarbons and suppresses the formation of CH_4.

The Ru-promoted catalyst ($Co\text{-}Ru/SiO_2$) activated under syngas exhibited the highest C_{5+} selectivity and lowest CH_4 selectivity compared to H_2-reduced samples, which might be ascribed to the re-dispersion of Co particles, due to H_2 spillover from the Ru atoms to the surface of the catalyst. Unpromoted Co/SiO_2 catalysts activated under syngas at 350 ˚C exhibited a high CH_4 selectivity, which might be due to the formation of cobalt carbides during reduction, which favour the methanation reaction.

The Co/SiO_2 activated by H-C-H improved the CO conversion by 40% when compared to the catalyst reduced in H_2 at 350 ˚C. The increase of the FT activity might be due to the formation of the Co(hcp) via the Co_xC intermediate, which was introduced by the H-C-H treatment. However, the carbides transformed by catalyst carburization in CO acted as a source of methane and CO_2 compromising the selectivity of higher hydrocarbons.

8.2 Prospects for future study

(1) The Co/SiO_2 catalyst reduction at a lower temperature exhibited both high FT and WGS activity, making it suitable for converting H_2-lean syngas to liquid fuels. Furthermore, it eliminates the need for a high-temperature reduction step, which could be beneficial and cost-effective for commercial FT processes, such as a small-scale biomass to liquid process plant. More research work needs to be done to investigate the optimal catalyst pre-treatment conditions.

(2) Syngas activation is recommended for the production of olefins which can be used as building blocks in the chemicals industry and H_2 activation is recommended for the production of long chain hydrocarbons. However, in order to conduct a better prediction through these experiments, additional data needs to be obtained. Therefore, we recommend more activation studies using syngas for catalyst reduction to potentially cut-down operation costs for the FTO process.

(3) We recommend more studies on the effect of the reduction temperature to rank the activity of CoO versus that of Co and CoO/Co mixture.

(4) We recommend in-situ XRD studies to determine both the phase change and phase abundance during syngas reduction and reaction.